Elite Sport as a Unique Test Arena for Printed Wearable Technology

Andrew Claypole BEng

Submitted to Swansea University in fulfilment of the requirements for the Degree of Engineering Doctorate

Swansea University

2020

Summary

A Graphite nanoplatelet enabled, flexible, printed heater has been developed to help maintain muscles temperature in elite athletes, to provide a competitive advantage. The heaters had to conform to the body to maximise heat transfer whilst minimising disruption to athletic effort. The heat output had to remain uniform even while flexed and stretched.

The impact of formulation on the rheology and printability of Graphite nanoplatelet based stretchable conductive inks was investigated. Plasma functionalised Graphite nanoplatelets were dispersed in a low viscosity Thermoplastic Polyurethane resin. Established suspension rheology models were fitted to the experimental data and a best fit found using the Krieger-Dougherty model.

Ammonia plasma functionalised Graphite nanoplatelets were proved to form a more stable ink than un-functionalised Graphite nanoplatelets.

Graphite nanoplatelets were hybridised with carbon black to improve the electrical properties of the coatings. The carbon black coated the Graphite nanoplatelets, improving interplatelet contact. At the highest carbon black concentrations, increases in viscosity and elasticity prevented the ink from relaxing to form a consistent layer. An optimum ink formulation produced coatings with a sheet resistance of 177Ω/□.

The stretchable carbon ink had superior electromechanical properties than a stretchable silver ink. The carbon ink maintained electrical conductivity up to substrate break and showed a repeatable electromechanical response to cyclic straining to 100% nominal strain.

The stretchable inks were constructed into a printed heater and thermoformed onto Lycra. The heaters produced uniform heat output up to 20% nominal strain, during cyclic loading to 10% nominal strain and while compressed.

The optimised inks were used to create heaters for a stretchable, prototype base-layer garment for cold chamber testing, which better maintained muscle temperature and the athlete's perception of warmth than an unheated control. An optimised design was used to produce garments for outdoor winter training 2018/2020 in preparation for the Tokyo Olympics.

Contents

Declarations

This work has not previously been accepted in substance for any degree and is not being concurrently submitted in candidature for any degree.

Signed 

Date.....4th August 2020.....

This thesis is the result of my own investigations, except where otherwise stated. Other sources are acknowledged by footnotes giving explicit references. A bibliography is appended.

Signed 

Date.....4th August 2020.....

I hereby give my consent for my work, if relevant and accepted, to be available for photocopying and for inter-library loans **after expiry of a bar on access approved by the University.**

Signed 

Date.....4th August 2020.....

Acknowledgements

I would firstly like to thank M2A and my industrial sponsor Haydale as their financial support made this project possible. The M2A project has been supported by the European Social Fund through the Welsh Government. A special mention must go to everyone at the M2A office whose hard work has made the EngD a much easier and enjoyable experience for myself.

I would like to thank my supervisor, Professor. Liam Kilduff, for your support and guidance throughout the process. As a keen sportsman myself, the opportunity to work within elite sport during my project has really been a dream come true. I would also like to thank Professor. David Gethin for the time and care you have shown this thesis over the last few months.

I would like to thank all of the staff at the Welsh Centre for Printing and Coating who have helped to make my EngD an enjoyable experience. Special thanks must go to Chris Phillips, who helped me pull together the early drafts; Christine and Glyn for their advice, support and laughs; James, Alex, Jon and Ben who have always been willing to provide a helping hand. I would also like to thank Sarah-Jane Potts for her support and help in generating the SEM images.

Last but not least, I would like to thank my family who have provided endless support and care throughout this process. To my Mum and Dad, thank you for always encouraging me to follow my dreams and creating a loving and supportive environment to do so. To Dad and James, thank you for all your help, hard work and support throughout; without you, this thesis wouldn't have been possible. Thank you to my brothers, James, Robert and Christopher who have always been there to support me in all I have done, and who are always available to provide a light-hearted and welcome break from work. Finally, to my girlfriend Sophie, thank you for always being there for me.

List of Figures

Figures

Tables

Equations

Nomenclature

Symbols

°C = Degrees Centigrade

Tm = Muscle Temperature

W = Watts

V = Volts

GPa = Gigapascal

MPa = Megapascal

σ *= Shear Stress*

γ *= Simple Shear*

$\dot{\gamma}$ *= Shear Rate*

η *= Shear Viscosity*

δ *= Deformation*

F = Force

V = Velocity

A = Area

h = Gap height

a = the radius of the particle

$\Delta\rho$ *= The density difference between the particle and the suspending fluid*

g = Acceleration due to gravity

η_0 *= Continuous Phase Viscosity*

η/η_0 *= Suspension Viscosity (Relative Viscosity)*

G' = Elastic Shear Modulus

G" = Viscous Shear Modulus

δ *= Phase Angle*

η^* *= Complex Viscosity*

ω *= Angular Frequency*

ϕ *= Phase Volume*

ϕ_m *= Maximum Packing Fraction*

$[\eta]$ *= Intrinsic Viscosity*

μm *= micrometres*

nm = nanometres

Ra = Average Surface Roughness

Rz = Peak-peak Surface Roughness

Ω = *Ohms*

*K*Ω = *Kilo-ohms*

*M*Ω = *Mega-ohms*

Ω/□ = *Ohms/square*

Ω·*cm = Ohms centimetre*

wt% = Weight Percent

N = Newtons

Ar = Aspect ratio

Acronyms

PHM = Passive Heat Maintenance

CON = Control

WU = Warm-up

ATP = Adenosine Triphosphate

PPO = Peak power output

NH_3 = Ammonia

CF_4 = Tetrafluoromethane

O_2 = Oxygen

GNP = Graphite Nanoplatelets

CB = Carbon Black

CNTs = Carbon Nanotubes

SWCNTs = Single-Walled Carbon Nanotubes

MWCNTs = Multi-Walled Carbon Nanotubes

CNFs = Carbon Nano-fibres

GO = Graphene Oxide

NH_3 GNP = Ammonia Plasma Functionalised Graphite Nanoplatelets

O_2 GNP = Oxygen Plasma Functionalised Graphite Nanoplatelets

R1 GNP = Un-functionalised Graphite Nanoplatelets

TPU = Thermoplastic Polyurethane

PVC = Poly(vinyl-chloride)

PDMS = Polydimethylsiloxane – Silicones

EC = Ethyl Cellulose

COC = Cyclic Olefin Copolymers

PC = Polycarbonate

EBA = poly(ethyl-butyl-acrylate)

PET = Polyethylene terephthalate

DAA = Diacetone alcohol = 4-Hydroxy-4-methyl-2-pentanone

ITO = Indium Tin Oxide

SAOS = Small amplitude oscillatory shear

LVR = Linear Viscoelastic Range

vdW = van der Waals

DLVO = Derjaguin, Landau,Verwey, Overbeek theory

E-B = Einstein-Batchelor Model

K-D = Krieger-Dougherty Model

M-P = Maron-Pierce Model

RMSE = Root Mean Square Error

WLI = White Light Interferometry

SEM = Scanning Electron Microscope

CVD = Chemical Vapour Deposition

WCPC = Welsh Centre for Printing and Coating at Swansea University

A-STEM = Applied Sports Technology Exercise and Medicine group at Swansea University

EIS = English Institute of Sport

Chapter 1: Introduction

1.1 Background

In elite sport where the margins between success and failure can come down to hundredths of a second or a few millimetres, wearable technology has the potential to give athletes the critical edge. Muscle temperature maintenance is an area in which wearable technology has the potential to have a performance impact. Muscle temperature has a significant effect on muscle function, force and power production [1][2]. Muscle temperature in humans is often elevated in one of two ways, namely an active warm up or through passive heat maintenance devices [2]. An active warm up which involves exercises that induce increases in muscle temperature through increases in metabolic rate, with just 15 minutes of active warm up shown to increase muscle temperature by 3-4°C at a depth of 2-4cm [2]. There is a well-established link between warming up and sports performance with a recent study showing that 79% of research has demonstrated an improvement in physical performance following a warm-up [3]. Passive heat maintenance involves the use of an external heat source to add heat to the desired muscles to elicit an increase in muscle temperature [2]. Muscle temperature (Tm) drops immediately following the cessation of exercise with the rate at which Tm declines exacerbated by environmental conditions [1][3], with colder ambient conditions leading to a faster decline in muscle temperature, owing to a larger temperature gradient between the muscle, skin and the ambient air [1]. These losses in muscle temperature have been shown to be greater closer to the surface of the skin [2], with the superficial muscle temperature being more susceptible to environmental heat exchange [1]. It is not uncommon for elite athletes to experience periods of inactivity while competing, whether this be between the end of a warm up and the start of competition, during a half time interval or between rounds of activity and in these periods it is possible that muscle temperature may drop below an optimal level which may have a detrimental effect on performance, particularly in power based sports like weightlifting, jumping and sprinting [1][2][3]. A drop in muscle temperature of just 0.3°C at a depth of 2cm into the muscle has been linked to a decline in sprint cycling performance [1]. These periods of inactivity are often important as they allow for acid-base homeostasis, phosphocreatine restoration, muscle potentiation and give an opportunity for the athlete's to receive tactical instruction therefore, a passive method of maintaining muscle temperature may be a prudent option than a further active warm up [3]. If

muscle temperature can be artificially maintained following a warm-up using either insulating clothing or external heating it may yield a benefit in subsequent activities that require high levels of power [2]. Therefore, there is a clear demand for a heat maintenance device capable of maintaining body temperature [4].

1.2 Passive Heat Maintenance Strategies

Passive heat maintenance strategies have been shown to attenuate the declines in muscle temperature following a post warm up recovery period better than an athletes standard training attire [1] with these attenuated losses linked to improved power output in sprint cycling [1]. Strategies for maintaining body temperature are currently available for the sport, medical and leisure market. Warm water immersion and heated blankets have been shown to be beneficial to power-based performance however these passive heat maintenance methods have been shown to be difficult to implement outside of a laboratory environment limiting their practical use [1]. Therefore, it is important that more portable and practical passive heat maintenance techniques and devices are developed to further the use of passive heat maintenance devices in a practical environment [1]. Chemical Heat Packs can also be used to for body heating [5] however these are typically single use or require submersion in boiling water to reverse the chemical change therefore their practical use is limited.

Aluminium foil jackets, such as the Blizzard Jacket (Fig. 1a), act to maintain temperature by clinging to the body and trapping warm air within cells which acts as an insulating layer to reduce convective heat losses, while their reflective surface reduces radiative heat losses [3] These blizzard jackets have been shown to attenuate losses in core temperature gained during the warm up better than their normal training attire leading to improved peak power output in a counter movement jump and improved repeated sprint performance in professional rugby league players [3]. However, using the Blizzard jacket did not completely maintain core temperature following warm up and given the relationship between core temperature and performance additional post warm up strategies need to be investigated to further attenuate or to prevent post warm up losses in core temperature [3].

Wire heating elements can be sewn into fabric inserts to create soft, flexible heating system (Fig. 1c) which can then be integrated into clothing. An example of this is the Adipower heat pants (Fig. 1b) worn by the British Track Cycling team in the London 2012 Olympics. These trousers combined 7.5W electrical heating elements with

insulative pants to reduce muscle temperature losses. Faulkner et al tested the performance of these electrically heated and insulated pants and found that they attenuated muscle temperature losses better than insulation alone and standard training attire, relating to an improvement in peak power output during a sprint cycle, however muscle temperature still decreased at all muscle depths following the 30 minute recovery period, even in a 15.9±0.3°C environmental chamber [2]. Therefore, further work is required to further attenuate or prevent losses in muscle temperature, especially as these losses would be expected to be greater in colder environmental conditions, where heat losses to the environment would be greater. Wires are typically used as heating elements however they have disadvantages such as non-uniform heating, weight, oxidative corrosion, high manufacturing costs and short lifetime as wires can break [6][7]. As the wire is the only component that generates heat and that typical garment fabrics are poor thermal conductors, wire heaters typically show poor heat uniformity (Fig. 1d). Wire heaters are also susceptible to the creation of hot spots, with any local change to the resistance of the wire, through damage or strain, causing local increases in the resistance associated with increases in temperature. This poor heat uniformity and susceptibility to the creation of hot spots limits the potential maximum temperature of wire heating elements.

Printing offers a promising alternative to create a thin, flexible, low power heater. DuPont have successfully printed a flexible heater, consisting of silver tracks for carrying the current and small carbon blocks as the resistors used to generate the heat (Fig. 1e). This heating panel was incorporated into a jacket that was worn in the opening ceremony of the 2018 Winter Olympics by members of the USA Olympic team (Fig. 1f). Although the DuPont Intexar heater proves the viability of the commercialisation of a printed heater for wearable technology, the actual heated area, denoted by the areas covered by the carbon resistor, is relatively small compared to the amount of silver current conductor.

a) [8]

b) [9]

c) [10]

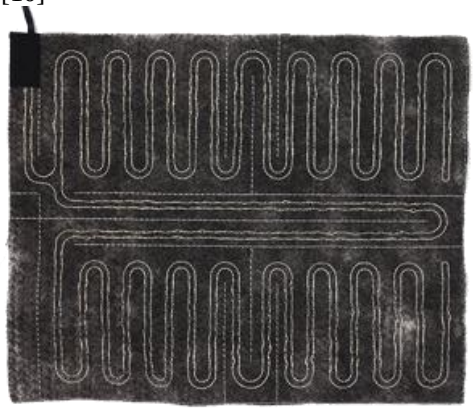

d) [10]

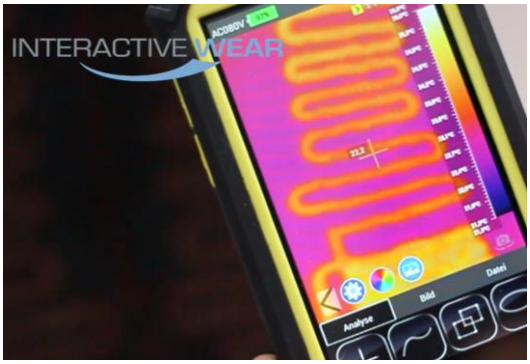

e) [11]

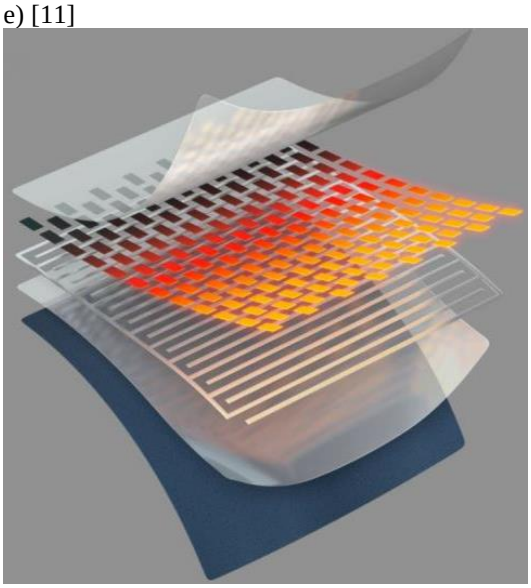

f) [12]

Figure 1.2.1 - Passive heat maintenance devices; a)Blizzard aluminium foil jacket, b) Adidas Adipower heat pants, c) Interactive wear flexible wearable heating element, d) Thermal image of the flexible wearable heat output, e) Structure of DuPont Intexar Heat printed heating element, f) Ralph Lauren-DuPont Team USA Heated Jacket

More importantly the printed heater was attached to a non-stretchable piece of outerwear for comfort heating. For the printed heaters to be used in training the

printed heaters will have to be attached to more stretchable fabrics and will need to be more mechanically and chemically robust to withstand the rigours of use in training.

The author developed a flexible plane heater using a graphene enabled ink that could be screen printed directly onto textile (Fig. 1.2.2c) and was subsequently granted a patent relating to graphene enabled printed heaters for wearable technology WO2017129663A1 [13]. The heater consisted of a printed square of graphene enabled ink that was used as the resistor to uniformly generate heat while silver busbars were printed along two parallel edges of the heater in order to facilitate a constant potential across the busbars, giving an even heat distribution. The 5x5cm^2 heater could reach temperatures of 56.6°C from a 3V power supply (Fig. 1.2.2b). This heater was directly screen printed onto a non-stretch textile and then encapsulated using a two-part silicone in order to protect it from mechanical strains. The best performing heater suffered only a 1.1°C drop in temperature performance following 200 curls around an 8cm diameter steel cylinder.

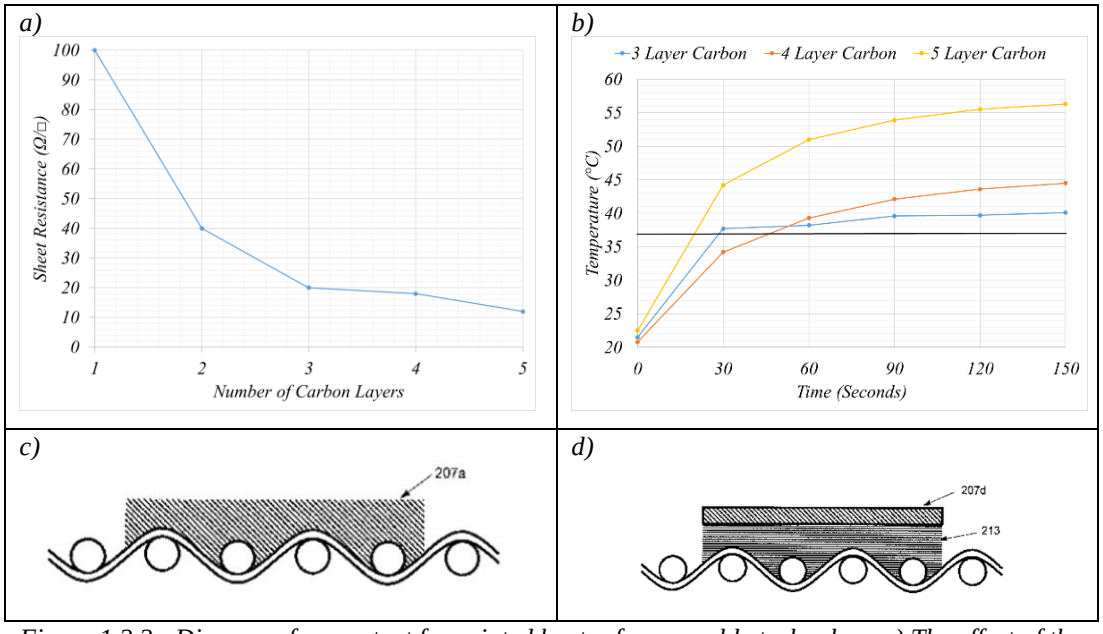

Figure 1.2.2 - Diagrams from patent for printed heater for wearable technology a) The effect of the number of layers carbon conductive ink on the sheet resistance of 5x5cm heaters, b) the heater performance of 5x5cm heaters printed onto various fabric substrates with varying layers of carbon at 3v, c) the original heater design with the carbon heater ink (207a) coated directly onto the fabric, d) An alternative design where the conductive carbon heater ink (207d) is printed onto a polymer (213) which is then attached to the fabric. All images from patent WO2017129663A1 [13].

Although the heater showed good resistance to being flexed around a set radius, when it was printed onto a stretchable fabric, such as those used in performance clothing, the heater began to crack underneath the encapsulant. Further work is

required to improve the mechanical properties of the ink formulation to allow these heaters to be printed onto softer, more flexible substrates that can be utilised in performance clothing for use during training. These inks could then lead to the development of larger, more mechanically robust printed heaters, with improved heat uniformity, that can be attached to stretchable fabrics, to create heaters that better conform to the body. The focus of this project is to develop and integrate a flexible and stretchable heater that can be printed onto soft flexible substrates to create a product that will improve athletic performance. To do this will require the development of new conductive inks with improved flexibility allowing the devices to comfortably conform to the body providing minimal disruption to the athlete while being mechanically strong enough to withstand the rigours of elite sport.

1.3 Thesis Outline

Chapter 2 reviews the current literature, starting with passive heat maintenance

Chapter 3 outlines the materials and methods used.

Chapter 4 assesses the viability of Graphite Nanoplatelets (GNPs) as the main conductive filler in a stretchable carbon ink. Shear and Oscillatory rheology are used to characterise the effect of loading on dispersion and particle interactions. The effectiveness of plasma functionalisation on maintaining the dispersion of GNPs is assessed. The inks are then screen-printed, and an optimum GNP loading for electrical conductivity and print roughness identified.

Chapter 5 examines the effectiveness of Carbon Black (CB) in improving the electrical conductivity of GNP inks and studies the effect that the addition of CB has upon the rheological properties of the ink and therefore the printability of the screen-printing conductive ink.

Chapter 6 examines the electrical performance of the stretchable carbon ink under various nominal strains, cyclic and compressive loading and compares it to that of a stretchable silver. The effect of layering the carbon ink on the electrical and mechanical performance of the composite coating is studied. These inks are then utilised to create a novel stretchable, flexible, printed GNP heater, that was thermoformed onto clothing, and the performance of the heater under tensile strains measured.

Chapter 7 summarises the key findings of this work and suggests potential future work.

References are given at the end of every chapter.

1.4 References

[1] S. Faulkner, R. Ferguson, S. Hodder and G. Havenith, "External muscle heating during warm-up does not provide added performance benefit above external heating in the recovery period alone," *Eur J Appl Physio,* pp. 2713-2721, 2013b.

[2] S. Faulkner, R. Ferguson, N. Gerret, M. Hupperets, S. Hodder and G. Havenith, "Reducing Muscle Temperature Drop after Warm-up Improves Sprint Cycling Performance," *Official Journal of the American College of Sports Medicine,* pp. 359-364, 2013.

[3] L. Kilduff, D. West, N. Williams and C. Cook, "The influence of passive heat maintenance on lower body power output and repeated sprint performance in professional rugby league players," *Journal of Science and Medicine in Sport,* pp. 482-486, 2013.

[4] M. Raccuglia, A. Lloyd, D. Filingeri, S. Faulkner, S. Hodder and G. Havenith, "Post-warm-up muscle temperature maintenance: blood flow contribution and external heating optimisation," *European Journal of Applied Physiology,* vol. 2, no. 116, pp. 395-404, 2015.

[5] Hothands, "Hothands," Hothands, [Online]. Available: https://hothands.com/. [Accessed 8 January 202].

[6] H. K. Park, S. M. Kim, J. S. Lee, J.-H. Park, Y.-k. Hong, C. H. Hong, Kim and K. Kang, "Flexible plane heater: Graphite and carbon nanotube hybrid composite heater," *Synthetuc Metals,* vol. 203, pp. 127-134, 2015.

[7] H. K. Park, S. M. Kim, J. S. Lee, Y.-K. Hong, C. H. Hong and K. K. Kim, "Flexible plane heater: Graphite and carbon nanotube hybrid nanocomposite," *Synthetic Metals,* pp. 127-134, 2015.

[8] Mountain Safety, [Online]. Available: http://www.mountainsafety.co.uk/Products-Blizzard-Survival-Jacket-Orange-aspx. [Accessed 19 11 2019].

[9] Loughborough University, [Online]. Available: https://www.lboro.ac.uk/microsites/enterprise/enterprise-awards/2013/knowledge-transfer/adipower.html. [Accessed 19 11 2019].

[10] Interactive Wear, "Heat Applications," Interactive wear, [Online]. Available: http://interactive-wear.de/solutions/9-enabler/33-heat. [Accessed 19 11 2019].

[11] Du Pont, Du Pont, [Online]. Available: http://electronicmaterials.dupont.com/intexar-heat. [Accessed 19 11 2019].

[12] In style, [Online]. Available: https://www.instyle.com/news/team-usa-opening-ceremony-olympic-uniforms-ralph-lauren. [Accessed 19 11 2019].

[13] D. Deganello, Y. Mouhamad and A. Claypole, "Heatable garment, fabrics for such garments, and methods of manufacture". WO Patent WO2017129663A1, 3 8 2017.

Chapter 2: Literature Review

2.1 Introduction

The physiological benefits of passive heat maintenance and some of the currently available techniques are first reviewed. The demands of wearable technology are then described. Printing as a potential manufacture method for wearable technology is then reviewed with a focus on screen printing. The components of functional inks are then described with a focus on carbon conductive materials as the functional component. The benefits of using rheology to characterise the dispersion of the nanocarbons are reviewed alongside the effect of these rheological characteristics upon print performance. The performance of carbon-based printed plane heaters is reviewed alongside the original patented heater developed by the author that led to the current project. Finally, a closure section details the main findings from the literature review and the subsequent focus of the experimental work.

2.2 The Role of Passive Heat Maintenance in Elite Sport

There is a well-established link between muscle temperature and sporting performance [1][2][3]. The physiological and metabolic benefits of an increased muscle and core temperature include increases in neural transmission rates, increased speed of muscle contraction, increased anaerobic metabolism, increased oxygen delivery to muscles [2][3][4]. Muscle temperature begins to decrease immediately following the cessation of exercise, with these declines exacerbated by the environment, which would be expected to have a detrimental effect on performance [2]. Elite athletes commonly experience periods of inactivity while competing, whether this is between the end of a warm-up and the start of competition or during a half time interval [2][4]. These periods of inactivity during or before performance are important as they allow for acid-base homeostasis as well as an optimal balance between phosphocreatine restoration and muscle potentiation [2] as well as tactical delivery [5]. Attenuating the decline in core temperature, and more importantly muscle temperature, after a warm-up is important to maintain the up regulation of the physiological pathways that are responsible for improving sports performance [3]. Passive heat maintenance typically requires the use of heated clothing, outdoor survival jackets and/or heated pads [5].

West *et al (2013)* studied the effect of post-warm-up recovery time on core temperature and the swim performance of international swimmers [2]. Following a standardised warm-up, the athletes recovered for either 20 or 45 minutes in ambient conditions of 28.2°C. Core temperature declined under both conditions with decreases in core temperature of 0.3 and 0.7°C in the 20 and 40-minute conditions respectively. The greater decline in core temperature over 40 minutes was associated with a 1.5±1.1% decrease in 200m swim performance compared to the 20-minute recovery period. Given the strong link between temperature and optimal performance in swimming alternative strategies for the maintenance of or even elevation of core or muscle temperature should be examined with one avenue of potential research the use of heat maintenance garments between the cessation of warm up and the start of competition.

Mohr *et al (2013)* studied the effect of inactivity on core and muscle temperature and its subsequent effect on sports performance during a simulated 15-minute half time period in soccer players [4]. During a 15-minute simulated half-time period muscle temperature dropped by 2°C (Fig 2.2.1a) and this correlated with a 2.4% decrease in sprint performance. This lower muscle and core temperature subsequently explains the decline in the performance of soccer players at the start of the 2nd half. Performing an 8-minute active re-warm-up during half-time helped to maintain muscle temperature and this was associated with maintenance of repeated sprint performance (Fig 2.2.1b) [4].

Kilduff *et al (2013)* explored the effect of employing a post-warm-up passive heat maintenance strategy on core temperature, peak power output and repeated shuttle sprint ability in professional rugby league players [3]. The passive heat maintenance strategy employed was the Blizzard Survival Jacket, which is a multi-layer aluminium foil jacket designed to cling to the body trapping warm, still air, providing insulation that limits convective heat loss. The performance of the Blizzard jacket was compared to that of a control, consisting of the athletes normal training attire, worn during a 15-minute post-warm-up recovery period in a 19.5°C indoor sprint track.

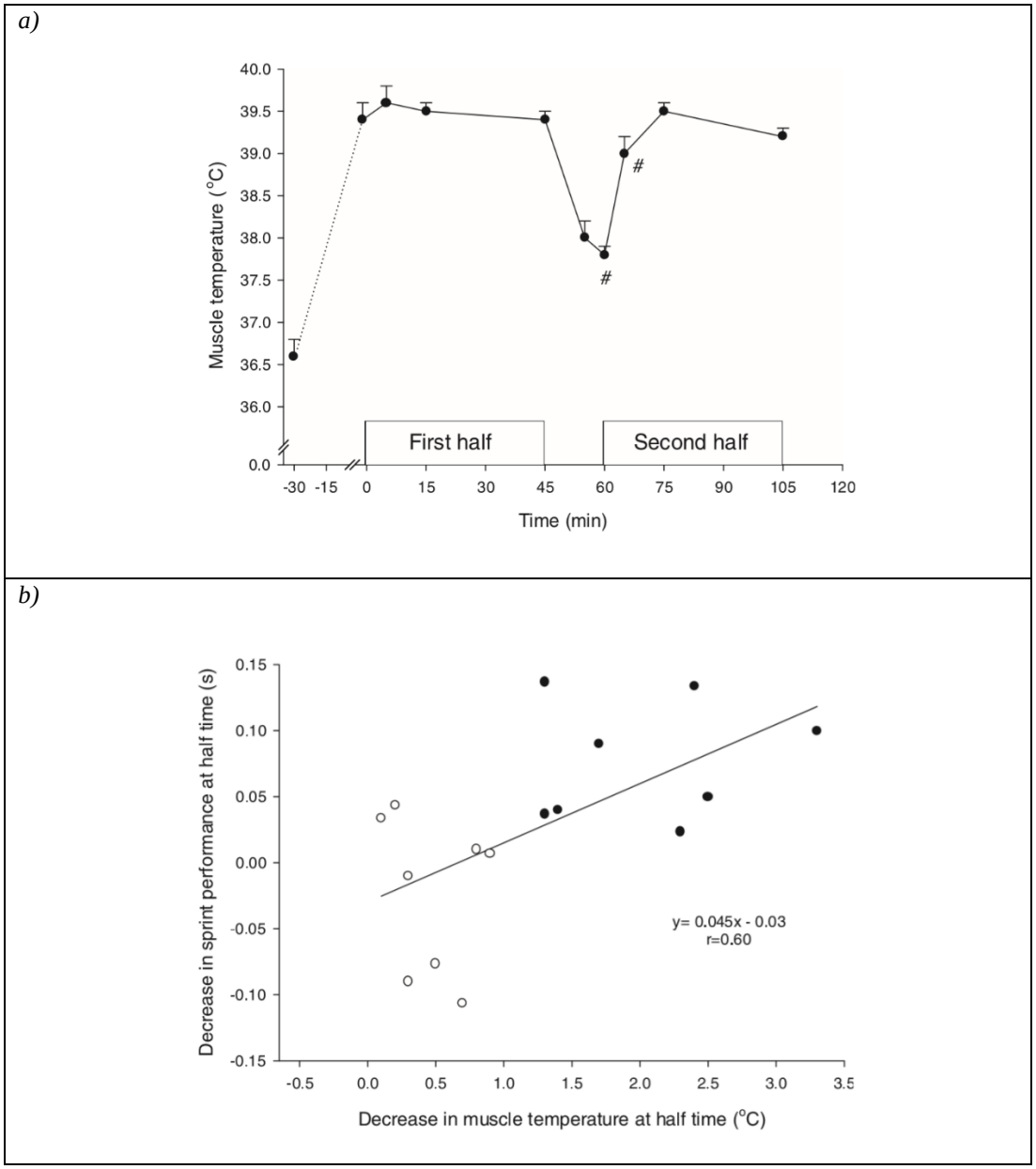

Figure 2.2.1 - Mohr et al (2013) The effect of muscle temperature on sprint performance of soccer players a) Muscle temperature of field players during a soccer match (n=8). Means± standard error measurement. #: denotes significant difference between the first and second halves. b) Individual relationship between decrease in muscle temperature at half-time (x-axis) and decrease in sprint performance at half-time (y-axis). Players both in re-warm-up (RW) (open circles) and control (CON) (closed circles) are included. The correlation coefficient for the relationship was 0.60 (n=16). [4]

Core temperature decreased in both conditions following the 15-minute recovery period (Fig. 2.2.2a). However, decreases in the core temperature were lower in the passive heat maintenance condition, 0.19±0.08°C, than in the control condition, 0.55±0.1°C, and this was associated with smaller declines in repeated sprint performance (Fig. 2.2.2b) and peak power output in the passive heat maintenance condition following the 15 minute recovery period than seen in the control. However, the use of the Blizzard survival jacket did not completely maintain the

increases in core temperature post warm up and given the relationship between core temperature and performance additional post warm up strategies need to be investigated [3].

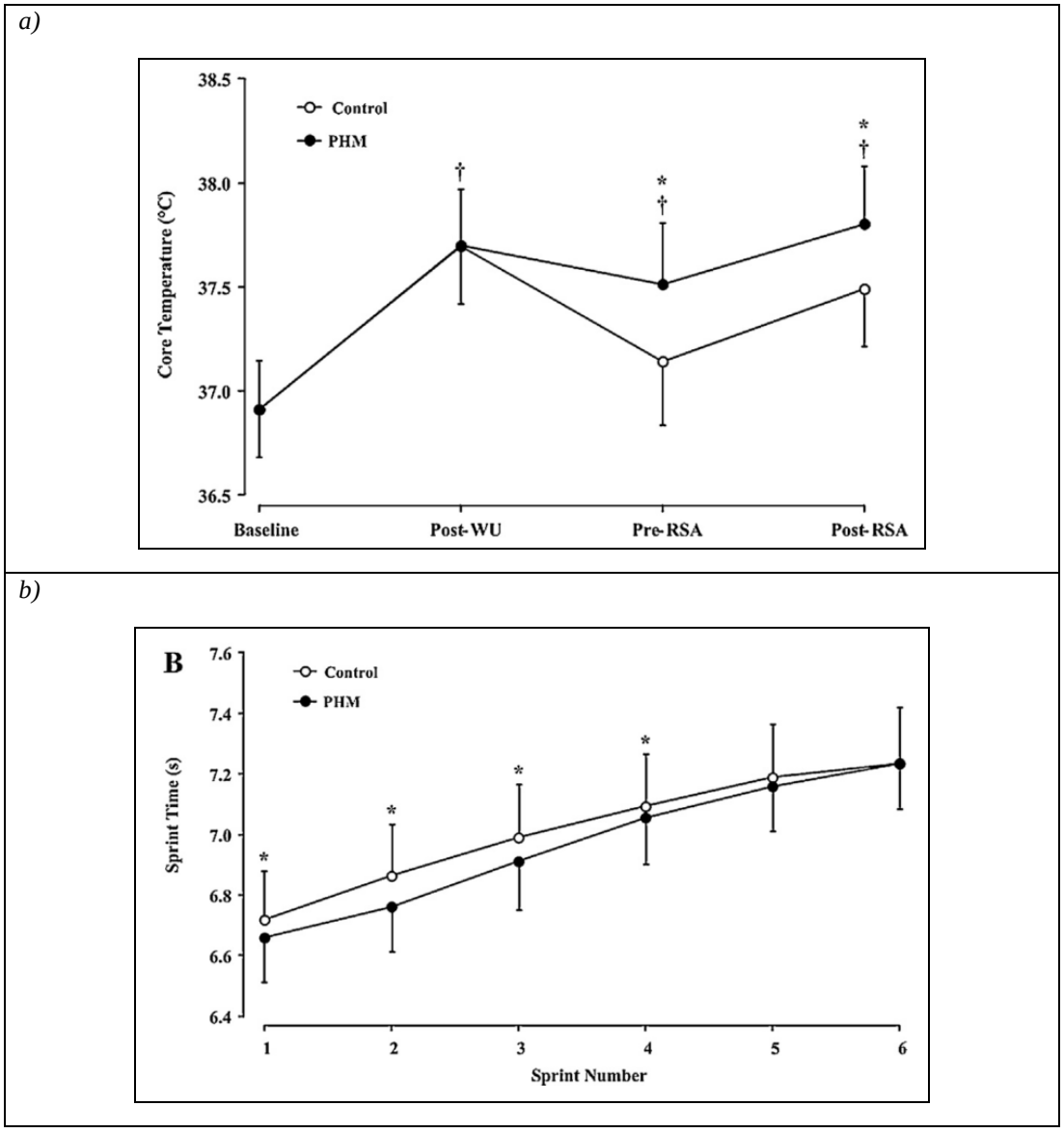

*Figure 2.2.2 - Kilduff et al (2013) the effect of passive heat maintenance jacket on core temperature and repeated sprint performance. a) Core temperature responses to the control and passive heat maintenance (PHM) conditions after completion of a standardised warm-up (WU). Data presented as mean±SD. † Indicates difference from baseline under both conditions ($p<0.05$). * Indicates conditional difference ($p<0.05$)* [3]. *b) sprint times during the repeated sprint ability test (B), under the control and passive heat maintenance (PHM) conditions. Data presented as mean±SD. * Indicates conditional difference ($p<0.05$)* [3].

Russel *et al (2017)* compared the effectiveness of active heat maintenance, passive heat maintenance and a combination of the two in attenuating half time losses in core temperature and its subsequent effect on the repeated sprint ability of professional rugby union players [5]. The 20 athletes performed a standardized warm-up

followed by a 15 minute recovery period during which they adopted one of four interventions namely; a Control consisting of their standard kit and rest, Passive consisting of a blizzard survival garment and rest, Active which consisted of 7 minutes of rest followed by 8 minutes of re-warm-up and a Combined intervention which consisted of 7 minutes of rest while wearing the blizzard survival garment followed by 8 minutes of re-warm up. This was done in an indoor facility where the air temperature was 20.5°C. The combined intervention better preserved core temperature than the active and passive methods, with all methods better at preserving muscle temperature than the control (Fig 2.2.3a). The active and passive methods both maintained a similar level of core temperature higher than that of the control. Compared to the control all interventions improved peak power output in a counter movement jump and initial sprint performance, but the best results were found in the combined intervention. Heat maintenance strategies decreased the drop in core temperature following a simulated half time and therefore protected counter movement jump and sprint performance at the start of the second half.

Another method of passive heat maintenance is by using electrically heated clothing. In this an external heat source is applied directly to the skin in order to attempt to maintain muscle temperature. For example, electrically powered heaters are used in heated car seats, military clothing and as mobile heaters. Joule heating dictates that at a fixed low voltage (e.g. 12V) low resistance is critical when electrical energy is converted into thermal energy. Metal alloy wires are typically used as heating elements however they have disadvantages such as non-uniform heating, weight, oxidative corrosion, high manufacturing costs and short lifetime as wires can break [6].

Faulkner *et al (2013)* investigated the effect that passive heat maintenance strategies, including electrically heated clothing, had upon the muscle temperature and subsequent athletic performance of sprint cyclists following a 30-minute passive recovery period [1]. Three methods of passive heat maintenance were used: 1) Control (CONT) where participants wore commercially available tracksuit bottoms, 2) Insulation (INS) where participants wore a pair of insulated athletic pants and 3) Insulation plus Heating (HEAT) where participants wore the same insulated trousers but with the addition of external heating pads located around the thigh. The heating

elements could reach temperatures of 40-43°C and were powered by a 14.8V battery that generated 7.5W to each heating pad.

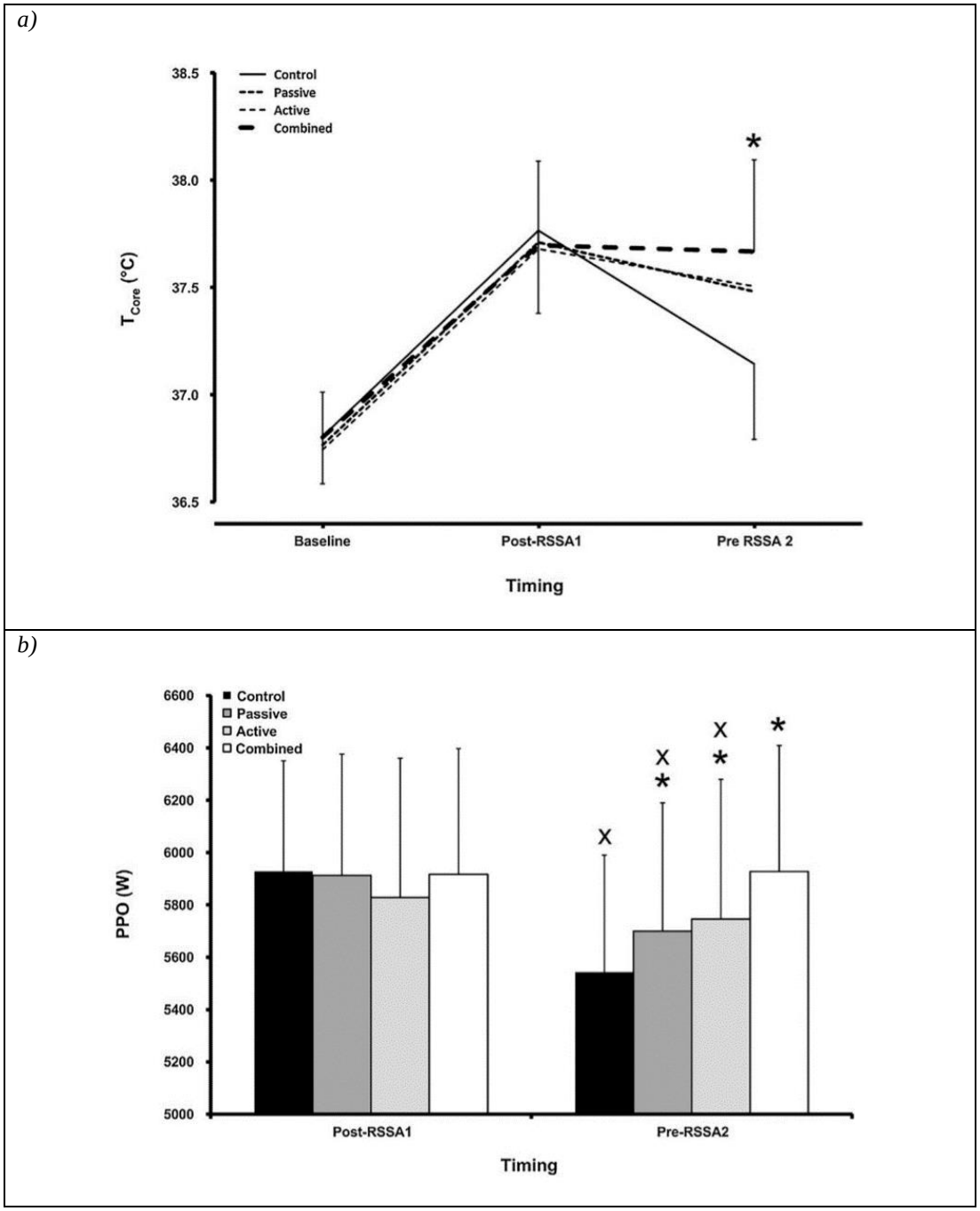

Figure 2.2.3 - Russel et al (2017) The effect of different heat maintenance strategies on core temperature and peak power output. a) Core temperature (T_{core}) responses throughout the control, passive, active and combined trials where RSSA represents Repeated Shuttle Sprint Ability. b) Peak power output (PPO) in a counter movement jump for the control, passive, active and combined trials

Muscle temperature still decreased in all conditions, however muscle temperature remained higher in the HEAT pants at all times compared to INS and CONT (Fig. 2.2.4). Use of an insulated garment combined with internal heating elements around

the thigh attenuated losses better than insulation alone. Use of the heated garment led to a muscle temperature that was approximately 1°C higher at a depth of 1cm, and 0.4°C higher at 3cm after a 30-minute recovery period when compared to CONT and INS. This was associated with a greater peak power output (~9%) during a 30s maximal sprint test in the HEAT compared to the CONT. The increase in power output after HEAT is probably due to an elevated rate of ATP turnover because of the higher muscle temperature.

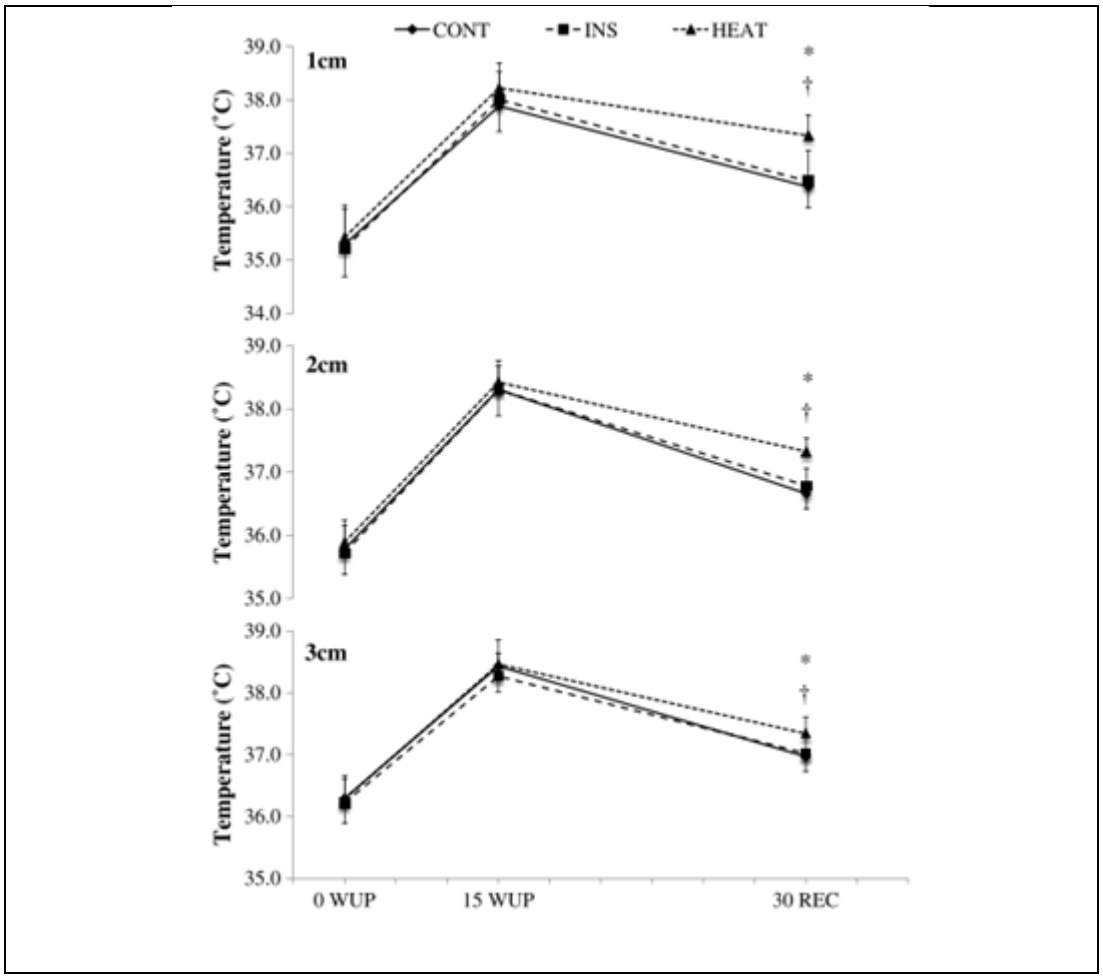

*Figure 2.2.4 - Faulkner et al (2013) The effect of electric passive heat maintenance device on muscle temperature. Muscle temperature at 3, 2, and 1 cm depth measured before the warm-up (0WUP), immediately after the warm-up (15WUP), and after 30 min seated recovery (30REC) in the control (CONT), insulation only (INS), and insulation + heating (HEAT). *P G 0.0005, HEAT 9 CONT. †P G 0.0005, HEAT 9 INS. From [1].*

Raccuglia *et al (2016)* noted that despite there being a significant attenuation in the muscle temperature in Faulkner's [1] study when athletes used the HEAT trousers, participants still experienced a significant 1.5°C drop in muscle temperature [7]. Raccuglia suggested the micro-climate between the heater and the skin could be a

contributing factor to reductions in leg muscle temperature. The electrically heated trousers used by Faulkner [1] were limited to a maximum temperature of 40°C, to avoid the risk of skin burns at 45°C, as the maximum temperature output of the heaters varied when flexed. It was suggested that 40°C was not a high enough temperature to passively maintain the muscle temperature gained during the warm-up. To investigate this Raccuglia [7] looked at the changes in deep, mid and superficial muscle temperature following a 30 minute recovery period after an active warm up using three different passive heat maintenance strategies; 1) Water Perfused Trousers (WPT) at 43°C, 2) Electrically Heated Trousers (ELEC40) at 40°C and 3) Control which was a non-heated piece of clothing. The study showed that an optimised heating procedure where the external heating element produced a temperature of 43°C instead of 40°C could maintain leg muscle temperature better than electrically heated trousers at 40°C and a non-insulating control.

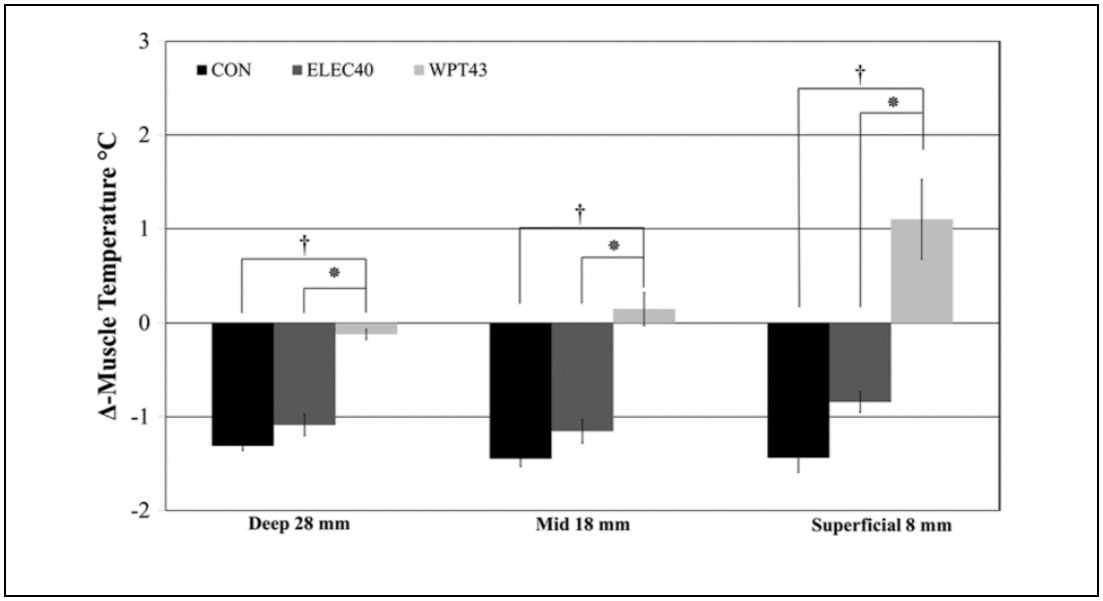

*Figure 2.2.5 – Racuglia et al (2016) The effect of different passive heat maintenance strategies on Muscle temperature loss following a recovery period. Normalised muscle temperature (difference from post-warm- up) recorded after 30 min of passive recovery following a standardised sprint cycling warm-up in CON (tracksuit bottoms), ELEC40 (electrically heated trousers at 40 °C) and WPT43 (trousers per- fused with water at 43 °C) at deep (28 mm)-, mid (18 mm)- and superficial-Tmvl (8 mm) depths. †Significant effect ($p < 0.001$) of WPT43 on post-warm-up Tmvl compared to CON. *Significant difference ($p < 0.001$) between the two heating procedures: ELEC40 and WPT43 [7]*

It was found during piloting of the study that external heating at 40°C led to a skin temperature of only 37°C and that this temperature was not high enough to maintain the increase in muscle temperature gained during warm-up.

However external heating using the WPT at a heating temperature of 43°C produced a skin temperature of 38°C which led to increases in the superficial and mid temperature as well as severely attenuated the depth following the 30-minute recovery period. Therefore skin temperature has a large impact upon maintaining leg muscle temperature. An optimal skin temperature is thought to be 39°C with an upper threshold of 43°C as above this there are impairments to muscle function.

There is a clear link between muscle temperature maintenance and athletic performance. No passive heat maintenance method has been able to completely maintain the muscle temperature gained during warm up. Given the link between body temperature and performance this should be a key research avenue. There is a need for a heating device capable of maintaining skin temperature, and therefore muscle temperature, at 39-43°C that is portable, practical and can safely give a consistent heat output even when flexed. All of the garments tested have been of the don-doff nature, where they are worn during a recovery period and removed before any practical effort, however there has been no studies on an electrically heated passive heat maintenance device for use in training. This would bring about extra challenges as the device would have to provide minimum disruption to technique and athletic effort. All the passive heat maintenance strategies have been tested in a thermo-neutral environment, however losses of body temperature to the environment would be expected to be greater in colder environmental conditions, with the effectiveness of these devices not tested under this kind of thermal stress.

2.3 Nanocomposites for Wearable Technology

Polymer composites with improved electrical conductivity can be utilized for electric heating materials and devices [8]. Flexible nanocomposites created by dispersing an electrically conductive nanoparticle within an elastomeric polymer could provide a means to create a new passive heat maintenance device capable of maintaining skin temperature even while flexed, bent or stretched.

Wearable electronics, such as fitness trackers, are increasingly being used within the sports and fitness industries to improve sporting performance. For widescale uptake

of these devices in elite sport they must provide minimum disruption to athletic effort or technique. To successfully integrated devices into clothing requires these devices to conform to the shape of the body, to give the garment an overall good fit. In order to conform with the human body the components of wearable electronics should be highly flexible/stretchable, lightweight, mechanically robust and aesthetically pleasing [9]. In humanoid robot applications where large deformation is experienced, such as in the knee or elbow region, it is imperative that wearable devices have stretch-ability [10]. Stretch-ability improves the conformity of electronics with the body as well as facilitating flexibility and thus improves the reliability of the measurement of several health parameters in wearable systems [10]. In textile applications about 15-20% strain occurs through the life cycle of the product [11].

Metals alone are not sufficiently stretchable to be used as heaters or interconnects as they have an elastic modulus of approximately 100GPa in comparison with elastomers which have elastic moduli of approximately 1MPa. Stretchable interconnects that act as rubber, stretching and regaining their shape and electrical properties offer an interesting alternative to metals [10].

To achieve flexible/stretchable electronics two main strategies have been employed namely; (a) utilization of deformable structures (b) using rubber like intrinsically flexible/stretchable materials [9][10]. Wires laid in serpentine patterns with optimised design regarding their wave amplitude, curvature and width can be stretched up to 90% with negligible effect on its electrical properties [10].

Intrinsically flexible materials can be formulated as conductive nanocomposites, typically consisting of conductive fillers dispersed within an elastic polymer matrix (Fig. 2.3.1a, b) with the electrical conductivity tuned by varying the loading of the filler material, with electrical conductivity typically increasing with filler content as the percolation path through the composite becomes increasingly well developed. In general, the electrical conductivity of the composite will increase as loading ratio of filler increases, however, increases in filler loading ratio will also increase the elastic modulus, therefore there is a trade-off between electrical conductivity and elastic modulus [10]. Various materials have been explored for use in wearable electronics including advanced carbon materials, metals and conductive polymers [9].

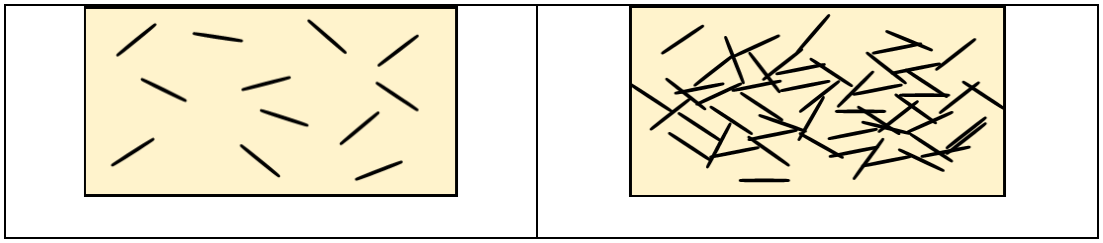

Figure 2.3.1) Diagram representing the microstructure of a nanocomposite with a) low filler concentration b) high filler concentration

The elastic moduli and electrical conductivity of various polymers and filler materials can be seen in Figure 2.3.2. The global conductivity of the percolated network within the polymer matrix is a function of the conductivity of the filler, the contact resistance between filler particulates and conductivity induced by tunnelling effects between adjacent non-contacting particles [10]. Interaction between the stretchable interconnects and the substrate must also be considered as large differences in the elastic modulus will lead to high stress concentrations at the interface leading to unreliable performance [10].

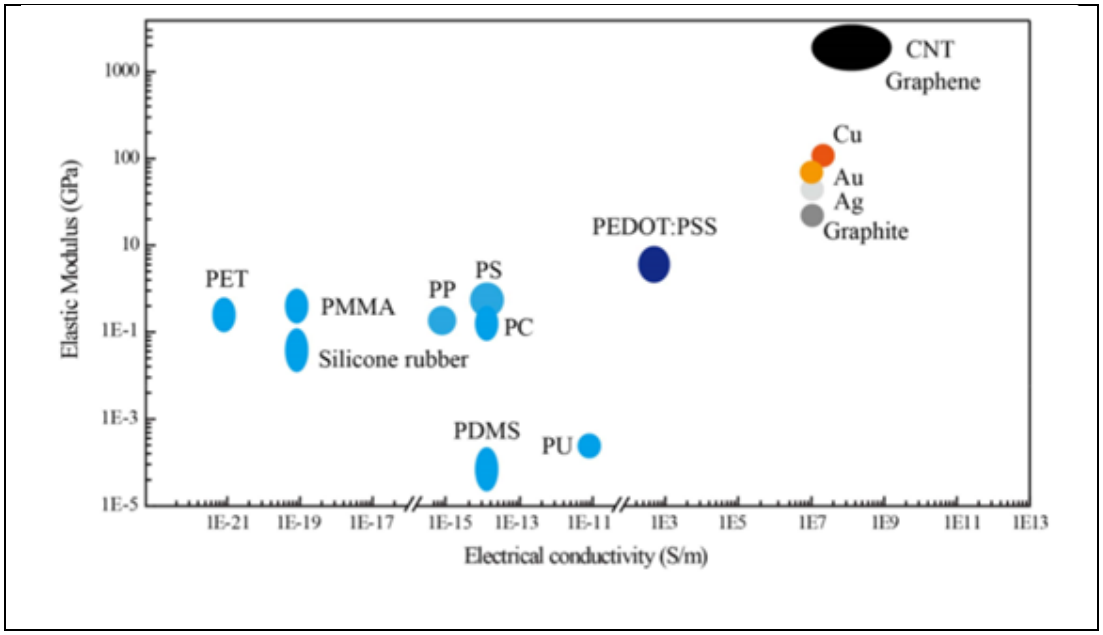

Figure 2.3.2 - Dang et al (2017) Comparison of the elastic properties of various materials for stretchable interconnects with electrical conductivity [10]

2.4 Formulating Conductive Inks

2.4.1 Using Printing to Manufacture Wearable Electronics

Printing can be used to accurately deposit these nanocomposites to create a wearable device. Printing offers a scalable method to produce thinner, more flexible, stretchable and environmentally friendly devices produced by higher throughput processes with reduced production costs [10][12][13]. To do this requires these

nanocomposites to be formulated into inks with the composition of printing inks and their physical properties are determined greatly by the nature of the printing process [14].

2.4.2 Components of a functional ink

A simple functional ink contains three key components;

1. Functional component;
    - Imparts a desired functionality into the coating
        i. Pigment – Adds colour
        ii. Conductive Particle – Determines electrical properties
2. Resin/binder;
    - Gives coating much of its mechanical properties
    - Binds the coating to the substrate
3. Solvent;
    - Dissolves the polymer before being evaporated off during curing to leave a solid coating

Inks transfer mechanism and the type of drying of the ink on the substrate principally determine the structure of a printing ink [15]. The components selected and interactions between each of these components will have a profound effect on processability of any ink as well as the properties of the final coating.

A fundamental function of the ink is to adhere to the substrate [14]. The ink must have good adhesion to the substrate, whether it mechanically anchors to the substrate by penetrating into pores in the substrate [15].

The following segment of the literature review will examine each of the different components individually.

2.4.3 Functional Component

2.4.3.1 Metal Based Fillers

Metal based materials, such as silver flake, are often used in conductive inks owing to their relatively higher bulk electrical conductivity than alternatives such as carbon [10][13]. Silver is an attractive material for use in conductive inks owing to its excellent electrical properties, however, it has a high cost and has shown a tendency to migrate into other layers of multilayer devices. Copper has good electrical conductivity, but it oxidises rapidly under ambient conditions reducing conductivity

due to poor interparticle electrical contact. Metallic inks often require high temperature sintering following printing which limits their use on paper and other low temperature flexible substrates [13], however nanoparticle silvers have been developed that have low sintering temperatures of 150°C making them suitable for plastic and paper where higher temperatures could be tolerated [16].

Silver nano-wire composites have been shown to be capable of maintaining conductivity up to 115% strain [10]. Suikkola *et al (2016)* characterised the electrical response to applied strain of a commercially available stretchable silver ink screen printed onto Thermoplastic Polyurethane (TPU) substrates and found a break in electrical conductivity at 74% nominal strain together with increase in the resistance with the number of repeat cycles to 10, 15 and 20% strain [11]. However, it was noted that after 100s the samples recovered to values 1.3, 1.4 and 1.7 times their initial resistance, with this time dependency attributed to the structural properties of the TPU substrate [11]. The strain response of Silver flake/TPU and Silver flake/polychloroprene composites at 91wt% (56% vol) was examined by Araki et al [17], who found that as the conductive wires were strained, the electrical contacts were gradually reduced as the initially densely packed silver flakes were pulled away from one another and micro-crevices appeared between the flakes, although electrical contact was maintained up to 400% strain [17].

2.4.3.2 Carbonaceous Fillers

Carbon materials are often used as conductive fillers because of their widespread availability, high electrical conductivity and low cost [10]. Carbonaceous material such as Carbon Black (CB), Carbon Nanotubes (CNTs), Graphite, Graphene or their hybrids have been added to polymers to improve their thermal, mechanical and electrical properties [6][18][19]. Consequently carbon-based pastes and inks are extensively used in a wide range of printed electronic devices, including resistive heater panels, electrochemical sensors, pressure sensors, printed batteries and supercapacitors. Advantages of carbon inks include their relatively low cost, disposability, ease of use, chemical inertness, the ability to be modified or functionalised and their controllable electronic properties [9][20][21][22]. Carbon inks offer ease of use and economic advantage over other commercially available conductive materials, such as silver, graphene and CNTs [22]. Compared to metal

nanoparticles, carbon Nanomaterials have the virtues of good flexibility, high stability which benefit their application in wearable strain sensors [9].

Carbon Black

Disperse systems of carbon black are used in many industrial applications including printing inks, organic coatings, polymer processing and cable coating [23]. Carbon black is a sub-micron scale, high surface area particle that is roughly spherical in shape [20].

Carbon black is largely used due to its low cost, simplicity of preparation and overall good performance [6][8][18]. However, high loading levels are required to reach the percolation threshold for electron conduction compared to other carbon materials as a result of the large contact resistance between carbon blacks caused by the point contact in the matrix as well as the low crystallinity of carbon black itself [6][8].

Graphite

Graphite flakes offer a low-cost carbon material with superb thermal and electrical conductivity as well as superb mechanical strength due to their strong sp^2 C-C bond [6]. Graphite has a layered planar structure, typically tens of microns in length and is conductive along its planes [20]. Delocalization of electrons in the π-electron system results in high electronic conductivity in the plane parallel to the graphene plane, while there is no conductivity between adjacent graphene layers [12].

Graphite nanocomposites typically have weak mechanical strength. Utilisation of graphite flakes within a polymer matrix is limited as graphite has no reactional groups existing in the basal plane leading to poor interaction with the polymer, leading to a nanocomposite with weak mechanical strength. Graphite can be modified to expanded graphite, reduced graphite oxide or a graphite intercalation compound in order to improve interaction with a polymer, however the modified graphite suffers many defects in the basal plane during chemical treatment and therefore, disturbed electron conduction at these sites [6].

Park *et al (2015)* observed relatively small amounts of polymer on the graphite flakes, meaning the polymer doesn't adhere to the graphite flakes as the basal plane of the graphite does not have a functional group to interact with the polymer. The Graphite/epoxy nanocomposite also had voids caused by the poor packing of graphite [6].

Kasgoz *et al (2014)* dispersed several carbonaceous fillers into cyclic olefin copolymer (COC) using a twin-screw extrusion method. SEM images of the composites revealed the size of the graphite flakes to be approximately 14um with a thickness of 3.5um. At 30wt% the graphite composites showed large holes/voids, where the flakes packed inefficiently. This was attributed to the extrusion method not being sufficient to exfoliate the plates and the low affinity of the flakes to the polymer [19].

Graphite Nano-platelets

GNPs (Graphite Nano Platelets) are high aspect ratio graphitic nanocarbons, with typical thickness 0.05um and diameter 2.6um [24]. Exfoliated GNPs are short stacks of graphene sheets that can be added to polymers to produce electrically conductive composites [25]. Exfoliated Graphite nanoplatelets offer an alternative to CNTs as they combine low cost and conductivity properties [25][26]. The high aspect ratio and large surface area of GNPs offers a much lower electrical percolation threshold than that of conventional CB [10][26]. However, GNPs agglomerate readily due to strong interplatelet van der Waals forces and high surface energy making dispersing them within a composite difficult [26].

Graphene

Graphene, a two-dimensional Nano-carbon with a honeycomb carbon structure has received tremendous attention due to its excellent thermal, electrical and mechanical properties [13][27]. Graphene boasts excellent electrical properties as well as outstanding thermal conductivity [27][28][29] with a thermal conductivity in the range of 3080-5150 W/mK [27]. Graphene's outstanding thermal properties have been attributed to a combination of factors such as its high aspect ratio, two-dimensional geometry, stiffness and its low thermal interface resistance. Graphene's outstanding thermal properties allow it to be utilised to produce composites with substantially improved thermal conductivity [27].

Graphene can be obtained by either top-down or bottom up strategies. Bottom-up strategies based on the growth of carbon atoms into 2-D layers, using processes such as CVD, is limited by the process' high cost, complexity in the transfer process and difficulties in scale up. Top-Down approaches involve the exfoliation of graphitic material towards graphene, reduction of graphene oxide or carbonization of other

fillers. These methods are widely used owing to their numerous advantages such as high yield, low cost and solution processability [13].

In graphite parallel layers of graphene are stacked due to van der Waals forces, these attractive forces must be overcome to create single graphene sheets. Stabilising graphene sheets against agglomeration remains challenging. Under high shear rate, shear forces have the potential to peel of adjacent graphene layers from graphite. After being exfoliated into individual sheets graphene relies on the stabilization effects of solvents and surfactants to minimize the intermolecular attraction, thus, to improve the stability of its dispersion [13].

Carbon Nanotubes

Carbon Nanotubes (CNTs) offer a high aspect ratio, high crystallinity, strong interaction with the polymer due to their large surface area [6] and much improved electrical conductivity, thermal conductivity and mechanical strength to the nanocomposite than carbon blacks [6][8]. However, CNTs are relatively high cost and tend to bundle and entangle together to give inhomogeneous conductivity due to the high van der Waals forces between the carbon nanofillers [6][10].

CNT production methods often produce two types of CNTs, metallic and semiconductor, with a major challenge being how to separate the two [30].

SWCNT-PDMS composite films embedded in PDMS have shown uniaxial and biaxial straining of 70-100% without electrical or mechanical damage [10].

Graphite and Carbon Black

Hybridizing Carbon Nano-fillers has been shown to be an efficient method to improving the properties of composites. Carbon conductive screen-printing inks typically use Graphite as the more conductive component and the relatively smaller Carbon Black (CB) particles to create denser films with enhanced interplatelet connectivity [31]. Planar graphite platelets typically tens of microns in length are typically combined with smaller sub-micron spherical carbon black particles. The spherical CB particles have been shown to improve electronic transport by improving the interparticle contact between graphite particles. Orientation and size of graphite platelets strongly affects the conductivity of carbon prints [12]. Since conductivity is mainly provided within the graphite particle, electrical conductivity is dependent on particle-particle contact. The correct balance between carbon black and

graphite must be found to achieve suitable conductivity while maintaining film processability and integrity [31]. Graphite/CB inks have been shown to be capable of achieving coatings with sheet resistances between 8-130Ω/□ [31]. Works have examined the performance of Graphite/CB paste inks for screen printing focussing on total carbon content [31], the ratio of Graphite to Carbon black [20], the effect of ink composition [12] and the effect of post processing [22].

Graphite Nano-platelets and Carbon Black

Fan *et al (2009)* added CB to GNP/Epoxy composites at <5 wt%. The CB was well dispersed and attached to GNP edges and surface as well as filling the voids between the platelets producing large increases in the electrical conductivity of the composites. They propose that the mechanism for this improvement is that the addition of CB helped prevent the GNPs from agglomerating during processing due to van der Waals forces, improving their dispersion and forming an excellent conductive network through the matrix owing to due to the existence of multiple electronic pathways (Fig. 2.4.3.2.1) [26].

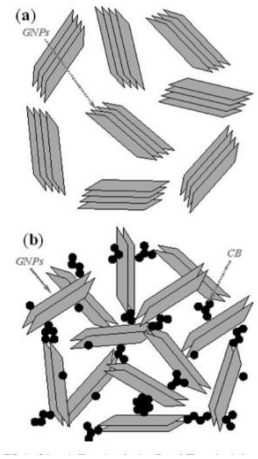

Figure 2.4.3.2.1 - Fan et al (2009) The effect of hybridising GNPs with CB [26]

Oxfall *et al (2015)* examined the effect that the addition of carbon black had upon the rheological properties of GNP poly(ethyl-butyl-acrylate) (EBA) composites mixed by solution processing at <18 vol%. In this work the effect of high and low structured carbon black on the electrical and rheological properties of GNP/EBA composites was studied. High structured Carbon Black particles were seen homogenously dispersed between the graphite nanoplatelets, to provide a physical bridge between the GNP stacks increasing the electrical conductivity. This is because

the CB is far smaller and lower aspect ratio and as such can disperse in a more efficient manner [18].

2.4.3.3 Dispersion of nanocarbons

Dispersion of Nano-fillers is a key issue in governing the properties of composites [27][29]. Graphene agglomerations can be the initiation site for the formation of cracks or pinholes in the composite [29]. Challenges regarding uniform dispersion and good filler to matrix interfacial wetting must be resolved in order to see benefits in mechanical reinforcement from GNPs [32][33]. However, achieving good dispersion of nanocarbons within a fluid has been proved difficult as a result of the inert, hydrophobic, ultra-high interfacial area per volume and highly agglomerated nature of carbon nanomaterials [32][34][35][36]. Atomic motions in neighbouring particles drive carbon nanomaterials together, and if not counteracted, the van der Waals forces cause particles to adhere upon contact [37][38]. Repulsive forces arising from like charges or a protecting moiety on the surface of particles can be large enough and of long enough range to counteract the van der Waals forces to give a stable colloidal suspension [37].

2.4.3.4 Nano-Carbon Functionalisation

Altering the surface chemistry of the carbon Nanomaterials is an efficient method for helping to overcome these problems [34]. The chemical functionalization of graphene may lend further advantages to the polymer nanocomposite due to the nanoscale structures enhanced dispersion and interaction with the polymer matrix [28].

Acid treatments have been used with the aim of adding carboxyl and hydroxyl groups to the surface of CNTs to improve solubility with common solvents and epoxy resins [32][39]. However, with chemical functionalisation there is an enhancement in the number of defects in graphene due to functionalisation [27][28]. Surfactants have been shown to improve the dispersion of CNTs in polymers and solvents [32] and have been used to promote steric repulsion, which forces CNTs far enough apart to prevent agglomeration [39]. However, the addition of any polymer to the surface of a particle must be accounted for by increasing the effective particle radius [37][40].

Amino functionalisation of CNTs improved the interaction between the CNTs and the polymer assisting in creating a good dispersed distribution in the epoxy polymer

matrix [6]. The amino functionalised CNTs exhibited a high interfacial adhesion with the epoxy polymer due to the high surface area of the CNTs as well as the presence of the amine groups to give a nanocomposite with improved mechanical strength compared to Graphite [6].

2.4.3.5 Plasma Functionalisation

Plasma functionalisation offers a dry, scalable, non-polluting, fast, one step method of surface modification with the aim of making carbon Nanomaterials more hydrophilic by adding polar groups to aid dispersion [32][34][35][41]. A wide variety of plasma treatments have been used including O_2, NH_3, CF_4 [34][41] with a view to increasing the polarity of the surface of CNTs and the overall adhesion of CNTs to the surrounding polymer matrix [34][35][41]. Ammonia plasma treatment has been shown to increase the surface nitrogen content on CNTs [32][34][35], in the form of amine, imine, nitrile and imide groups [34][35]. Plasma treated CNT's showed higher free surface energy and smaller contact angles with water, attributed to the additional polar hydroxyl, carboxyl and amide groups on their surface [32], with this increased surface polarity leading to chemical affinity to polar resins and solvents and with-it dispersion. Amine groups attached to CNT walls has even been shown to lead to the formation of covalent bonds with an epoxy resin, improving the interface between the nanotubes and the epoxy [42].

2.4.4 Resin/Binder

The resins should form a stable solution in acceptable solvents [14].

The resin system in the ink largely determines the adhesive properties [15]. Resin selection is the most important factor for providing the ink with good adhesion to the substrate. The resins also are required to give the film adequate flexibility, with inadequate flexibility resulting in poor adhesion. Ink formulation can be based on resins that show similarity to the substrate to give improved adhesion [14]. On non-absorbent substrates, such as films or foils, adhesion is primarily affected by the film forming ability of the ink, and the molecular affinity for the substrate. The choice of resin for a specific substrate is therefore important [14].

Pigments are dispersed within the binder with the pigment enclosed by a binder "shell". This shell prevents finely dispersed particles from associating into agglomerates and subsequently being deposited. Binders harden on the substrate and thereby bind the pigments to the substrate [15].

2.4.4.1 Thermoplastic Polyurethane

Thermoplastic polyurethanes (TPUs) are an important performance thermoplastic block copolymer and provide a broad platform for the development of multifunctional materials. TPUs are alternating block co-polymers consisting of polar hard segments and non-polar soft segments that form a two-phase microstructure. The hard segments composed of polar materials can form carbonyl to amino hydrogen bonds and thus tend to agglomerate or cluster into hard domains, whereas the non-polar soft segments form amorphous domains [43].

TPUs offer a combination of favourable properties such as excellent elongation, high impact strength, good elasticity and biocompatibility. They are widely used in creating flexible electronic composites such as flexible displays, wearable electronics, sensors, flexible energy storage, thin film transistors [44]. Higher thermal and enhanced mechanical properties have been reported for polyurethane nanocomposites [28], with carbon materials having been previously been utilised in TPU composites to give improved electrical conductivity and tensile properties.

2.4.4.2 PVC

Poly (vinyl chloride) (PVC) plays an important role in the plastic industry but must be combined with a number of additives before processing. The addition of plasticisers to a PVC formulation decreases many of the mechanical properties of PVC such as tensile strength and hardness but increases the low temperature flexibility, elongation and ease of processing. The mechanical properties of PVC are dependent upon the degree of dipolar interaction between molecules and any disruption to these harms the properties of the PVC [45].

2.4.5 Solvent

Solvents should not evaporate so quickly on the press that they cause instability in the printing process but are able to dry quickly once on the substrate. Solvents can also affect ink adhesion. Solvents can assist the wetting and flow out of ink to give a continuous film which is essential for good adhesion. Solvents can also penetrate the substrate to cause softening of the surface to aid adhesion. Printing workshops, such as screen-printing shops, are also often not well ventilated therefore health and safety considerations are of vital importance when selecting a solvent [14].

2.4.6 Additives

These are often added to inks to influence drying, flow behaviour and abrasion resistance [15].

2.4.6.1 Surfactant Systems

Surfactant systems are typically used in inks and coatings to help improve the dispersions of pigments and filler materials within the resin. Surfactants are typically molecules with one part of the molecule having a high affinity for the particle surface and the other end of the molecule having a high affinity for the liquid media.

Trappe and Weitz *(2000)* used a double tailed surfactant with a more polar amine group that attaches to the surface of the carbon black allowing the two hydrocarbon tails to act as steric stabilisers [46].

The only report on polymeric surfactants stabilising graphene dispersions is by Stankovich *et al*, where poly(sodium-4-styrene sulfonate) (PSS), a well-known amphiphilic polymer, was used as a surfactant to stabilize dispersions of rGO, with the dispersion showing excellent stability for up to a year. Non-ionic surfactants have the hydrophobic tail adsorbed onto the graphene surface and the hydrophilic end in the suspending fluid creating a barrier between the particles [13].

Surfactants however can remain as a residual component in the final printed structure that can negatively affect the electrical properties of the composite. Polymers have been established as an interesting alternative to surfactants in stabilising Graphene in liquid media, since they can form emulsion systems that hinder graphene flakes from aggregation. The combination of different polymers and solvents gives a variety of options for formulating graphene inks. PVA, PVP, PMMA, EC have been used in a variety of solvents to create stable graphene dispersions. The search for a suitable polymer solvent combination is ongoing and attracts a great deal of attention [13].

2.5 Conductive Inks and Coatings

In the manufacture of printing inks, the pigment is dispersed in a resin consisting of the binder and the solvent [15]. Conductive inks typically contain silver, carbon, gold or copper as the conductive element within a polymer/solvent blend with the choice and the ratios of these materials being dependent on conductivity requirements, adhesion, ease of processing, economics substrate flexibility and the curing conditions [47].

The pigments are then usually dispersed throughout the binder using a dispersion process such as three roll milling, before this final ink is homogenised once more [15]. Three roll milling has been shown to be an effective method of dispersing graphite and amino functionalised CNTs in an epoxy matrix [6].

Use of metal-based inks is also not very environmentally friendly and may cause water toxicity, cytotoxicity and genotoxicity [13]. Therefore, for human application there is a critical need for a low cost, stable and environmentally friendly conductive ink [13].

Potts *et al (2019)* Screen printed a 22.5wt% graphite ink and found that the inks had high surface roughness, Ra=2.8um, with signs of mesh marking, agglomeration and pinholes. SEM imaging showed that the graphite flakes were randomly oriented with large gaps between the flakes and only small amounts of contact with neighbouring flakes [22]. A 22.5wt% GNP only ink printed thinner, smoother layers than a graphite only ink, with measured surface roughness values Ra=0.8um, with this decreased roughness attributed to the relatively smaller size of GNPs. SEM imaging showed the GNPs were also randomly oriented with some voids present.

Graphite is one of the most widely used materials for stretchable and conformable electrodes [10]. In order to achieve the desired electrical conductivity typically large amounts of filler are used, which also leads to the degradation of stretch-ability in graphite-based nanocomposites [10].

Tran *et al (2018)* published a review into the use of graphene-based ink formulations [13]. Recent research has focussed on the direct exfoliation of graphene in liquid media which can then be directly used in printing. Exfoliation of graphite into graphene in liquid media has advantages of low cost and solution processability. The development of proper graphene conducting inks for printing on flexible substrates still faces challenges including the aggregation of graphene sheets in suspension, the unsuitable viscosity and surface tension and a lack of adhesion to the substrate. The major challenge with graphene inks is to overcome the van der Waals forces between adjacent graphene layers for successful exfoliation into a stable dispersion. Graphene inks should be stable against precipitation to provide steady performance and uniform conductive patterns. The simplest way to reduce intermolecular van der Waals forces between graphene sheets is liquid immersion, where the attraction

between layers in reduced by the presence of the suspending medium. Due to its outstanding mechanical, electrical graphene ink is promising for printing of flexible conductive circuits.

Hatala *et al (2019)* changed the ratio of G:CB at 20wt% in EC and found optimum electrical conductivity at a ratio of G:CB of 3:1 and a trend for decreasing roughness with increasing CB content owing to the CB relatively smaller size [12].

Phillips *et al (2019)* compared the effect of changing ratio G:CB on the performance of screen- printed carbon conductive inks at 21.7 and 29.4 wt% [20]. Roughness increased with Graphite content as the large graphite particles had an increasingly large effect on the surface of the prints. At high concentrations the graphite particles were close to one another and coated in CB, at lower concentrations the graphite particles were far away from one another with the polymer/CB matrix forming the bulk of the ink and heavily coating most of the particles. Increasing CB increases the concentration of CB in the CB/polymer matrix spaced between the graphite particles to give increased conductivity. Greater distances between conductive graphite particles gave decreased conductivity for the lower concentration carbon inks.

2.6 Characterising the material properties of the ink

2.6.1 Benefits of using Rheology.

When developing conductive inks much of the focus is often on the material properties of the ink, with little consideration given to how changes in formulation affect the ink's rheological properties and subsequent printability.

Depending on the printing process, inks have largely variable flow properties ranging from extremely thin, through highly viscous, up to dry powder like consistencies. The "Consistency" of a printing ink has a decisive influence on the productivity and quality of a print job. "Consistency" can be classified into various individual properties that should be adjusted to match specific printing presses, substrates, printing subjects, speed etc as optimally as possible [15].

The rheological properties of the ink play an important role in the features of printed specimens [13][48]. Unsuitable ink characteristics may result in defects and short circuits of the conductive patterns [13]. However, literature highlights no simple correlation between printing ink viscosity, mesh characteristics and quality and quantity of conductive ink deposit [31]. Therefore, further work is required to

examine how changing ink formulation effects the rheological properties of the ink and the print performance as well as the material properties of the inks themselves.

The ability to characterise the microstructure and flow properties of dispersion is essential for understanding and controlling their rheological properties [49]. The interaction of the various components in a paint/ink formulation results in a non-Newtonian system with complex rheological behaviours [48]. The rheology of dispersions is an important processing parameter and the ability to characterize and understand the effect of functional particle on the fluid viscosity of resin systems is essential in manipulating flow properties to create optimised ink formulations [49]. The addition of a dispersed phase can lead to the introduction of all kinds of non-Newtonian behaviour [49] [50] with suspensions of colloidal particles exhibiting a wide range of rheological behaviours ranging from simple viscous fluids to highly elastic pastes [46].

2.6.2 Suspension Rheology

A good introduction to shear and viscoelastic rheology can be found in Barnes [37] [51], with further information given in the methods section. However, for the purpose of this literature review we will focus on aspects of suspension rheology, with a specific focus on Nanocarbon rheology. The viscosity of a particle suspension is largely a function of particle volume fraction, ϕ, particle shape, interactions between particles, particle size distribution, suspension structure, surface properties, adsorbed species and the hydrophilic/hydrophobic nature of the particles/polymer [36][37][38][39][50].

For suspensions of colloidal particles non-hydrodynamic forces such as Brownian, electrostatic and London-van der Waals forces become significant [37][49][50][52] [53].

There are three main types of forces acting on a particle in suspension [51];

1. Colloidal forces arising from particle interactions; Colloidal forces interact to produce either an attractive or repulsive force between particles. Examples of this include the ever-present van der Waals attraction forces or electrostatic repulsion originating from like charges on particle surfaces.

2. Brownian Randomising Force; Causes constant randomisation of the spatial arrangement of particles as well as their orientation. Brownian forces are strongly size dependent and play a significant role for particles <1um.
3. Viscous forces acting on a particle; These are proportional to the viscosity difference between the particles and the surrounding fluid.

According to Derjaguin, Landau,Verwey, Overbeek (DLVO) theory the stability between two surfaces in suspensions is dependent on the net sum of the electric double layer, steric repulsion (steric) and van der Waals (vdW) attraction [13]. Aggregation occurs due to vdW attraction, while the electric double layer, which creates a net charge when two particles are within close contact to one another, and steric stabilization provide powerful tools to enhance dispersion by preventing two particles from forming attractive vdW interactions (Fig. 2.6.2.1) [13].

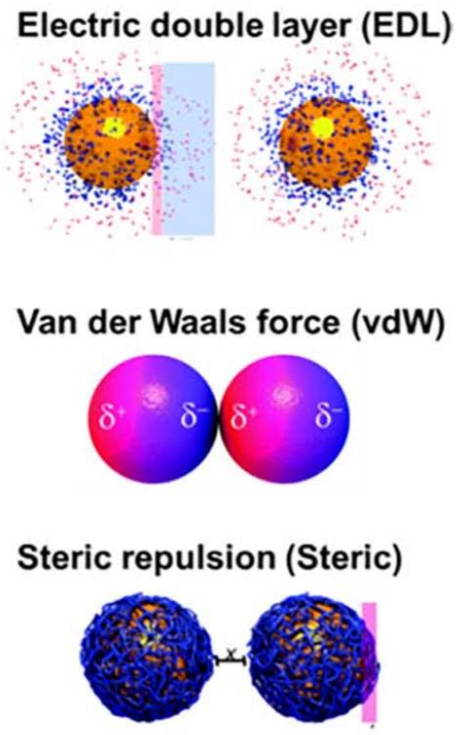

Figure 2.6.2.1 - Tran et al (2018) Colloidal particle-particle interactions within a fluid [13]

Barnes, Hutton and Walters *(1989)* describe the way in which flow affects the viscosity of suspensions of particles [51]. When discussing the shear properties of non-Newtonian suspensions shear rate is an important parameter as flow also has a large effect on the fluid microstructure and therefore the viscosity of suspensions. When particles are introduced to a structure, they assume a state of thermodynamic

equilibrium where Brownian motion dominates corresponding to a random disordered state. When a relatively unaggregated, concentrated suspension, in which the Brownian forces dominate, flows at very low shear rates, the particles necessarily have to move around each other or "bounce off each other for overall flow to occur, this involves a large resistance and the resulting viscosity is high (Fig. 2.6.2.2). The distribution of particles remains essentially undisturbed because the effect of Brownian motion dominates the shear motion and restores the randomness of the rest-state distribution and the viscosity remains essentially constant. At slightly higher shear rates, the imposed velocity gradient induces an orientation of the particle structure, which is not restored by the Brownian motion. This orientation enables particles to move past each other more freely than at very low shear rates and hence the viscosity is lower [51]. At even higher shear rates, the structure is so grossly orientated that the particles form layers separated by clear layers of the continuous phase. The viscosity is then at its minimum value.

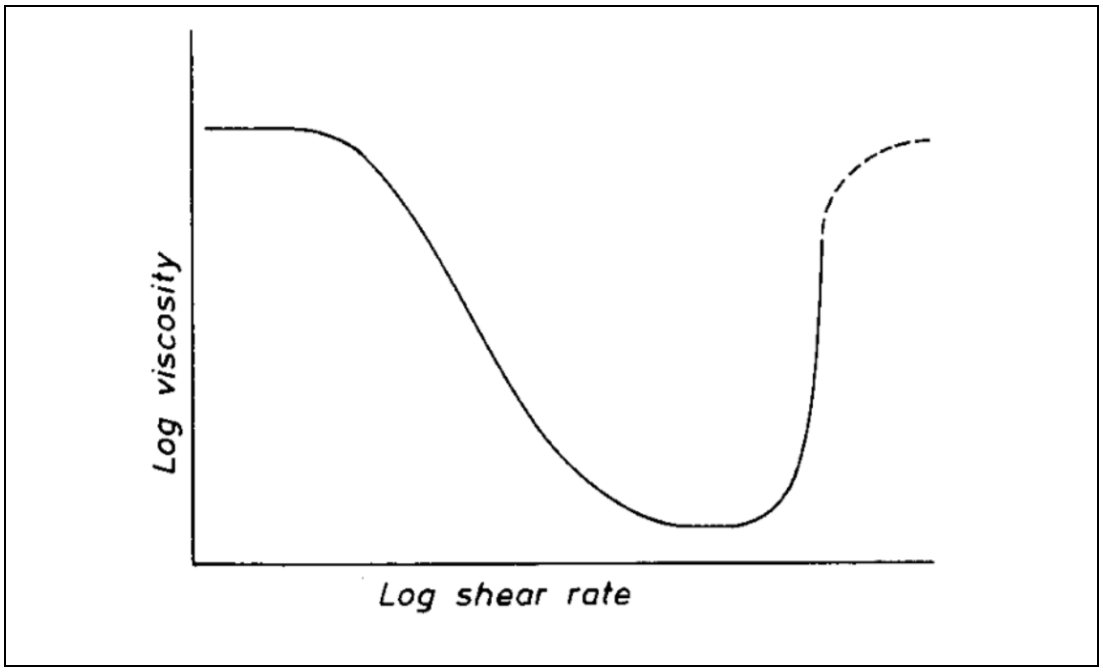

Figure 2.6.2.2 - Barnes, Hutton and Walters (1989) Typical representation of the effect of shear rate on the viscosity on a high concentration, unaggregated suspension [51]

Barnes, Hutton and Walters *(1989)* also describe the effect of concentration of particles on fluid microstructure and suspension viscosity [51]. Fluid microstructure plays a large role in the measured viscosity. Increasing the concentration of particles has a large effect upon the viscosity of suspensions. The presence of individual particles means the diversion of streamlines and hence higher viscosity. At higher

concentrations resistance rises as particles must move out of one another's way to align with the flow. At the highest concentrations even more resistance is encountered as flocs form that trap the continuous phase and stop it deforming at the same rate as the rest of the microstructure.

Willenbacher and Georgieva *(2013)* describe the effect of particle phase volume (ϕ) on the viscosity of a suspensions of hard spheres at various shear rates, with the inset diagrams representing the various phase structures formed, from liquid to gel-like, as phase volume increases (Fig. 2.6.2.3) [49]. At low concentrations, $\phi<0.5$, suspensions are in a liquid state with a low-shear rate Newtonian plateau observable as particles can diffuse freely as well as there being no long-range order within the fluid. Viscosity in the low shear rate Newtonian plateau depends only on the volume of the fluid occupied by the particles and not the size of the particles. The low shear rate viscosity and shear thinning behaviour increase with increasing particle volume. As concentration increases, $0.5<\phi$, more crystalline type structures develop, and shear thinning is seen over the whole measured shear range. At higher concentration the probability of particle interactions increases, and hydrodynamic interactions become more dominant [53].

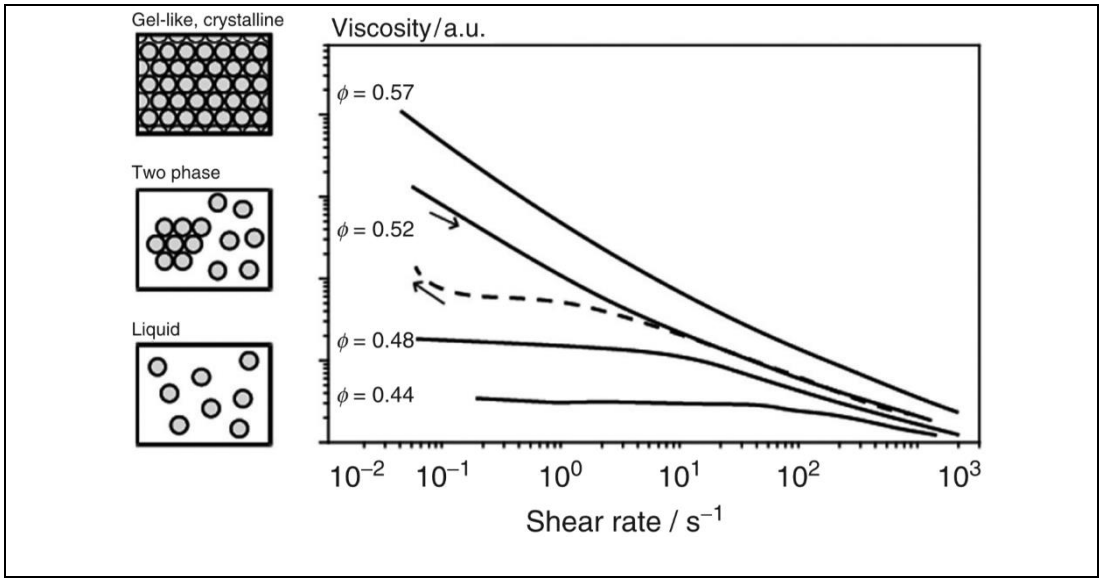

Figure 2.6.2.3 - Willenbacher and Georgieva (2013) The effect of concentration on the shear rate viscosity relationship [49]

Much research in particle suspension rheology has focussed on spherical particles, however particle anisotropy introduces several additional affects [50]. Particle anisotropy can cause the enhanced diversion of flow around non-spherical particles

[37][50] and enhanced particle interaction between high aspect ratio particles than would be expected for spherical particles [50]. Viscosity increases more rapidly, and yield stresses and shear thinning behaviour develop at much lower volumes as anisotropy increases [50]. The contribution of high aspect ratio particles on the viscosity of a suspension is affected by orientation to the flow [50].

Particle interactions in which the particles form loose flocculates can have a large effect on the microstructure and therefore shear properties of the fluid. The structure of the dispersion is highly dependent on the process of formation of the flocs, the size of the dispersed particles, wettability to the dispersing medium, and the strength and nature of attractive forces [23]. Loose flocs with fractal structure can form immobilising part of the continuous phase [49]. Above a critical concentration a sample spanning gel like network forms capable of elastically storing energy [49]. Yield stress has been attributed to the formation of a network of articles that deforms elastically in response to an applied stress by transmitted by direct particle to particle contact [50].

There are four main ways a suspended particle can interact with polymer molecules that are also suspended in the continuous phase [51];

1. Neutrally; The polymer merely acts as a thickener for the continuous phase.
2. For specific polymers, such as block co-polymers some part of the molecule can adsorb onto the particle while the other protrudes into the continuous phase. This can have the effect of hindering any flocculation that may take place, especially for very small particles, and prevent any sedimentation or creaming.
3. Bridging flocculation where polymer molecules can anchor two particles together.
4. Depletion flocculation where the polymer molecules are excluded from the gap between particles, creating an osmotic pressure difference that draws solvent from between the particles pulling them together.

Phase volume, ϕ, is used instead of wt% as the rheology of suspensions is largely dependent on the hydrodynamic forces that act on the surface of particles or aggregates of particles generally irrespective of particle density [51].

Most of the models for the viscosity of suspensions are derived from Einstein's equation for the viscosity of dilute suspensions of hard spheres (Equation 2.6.2.1). This equation is typically only valid for very dilute suspensions, ϕ>0.01 of hard spheres, as it assumes the flow around a particle does not influence the velocity field of any other particle [37][49] and therefore the flow around each particle can be described by the hydrodynamic equations of motion, with inertia neglected [52]. The suspension viscosity is directly proportional to the viscosity of the continuous medium, η_0, and is affected by the shape of the particles, represented by the intrinsic viscosity, $[\eta]$, and the volume of the dispersion, ϕ;

$$\frac{\eta}{\eta_0} = (1 + [\eta]\phi)$$

Equation 2.6.2.1- Einstein Equation

Increases in viscosity with particle loading come from the hydrodynamic disturbance of the flow field as it is diverted around the particles [37][53]. When a sphere is pulled out towards a rod or squashed down to a disk, giving higher aspect ratio particles, the diversion of the streamlines increases and with it the viscous energy dissipation and therefore the viscosity [37] [38]. In Einstein's equation this increase in aspect ratio is represented by an increase in $[\eta]$.

At higher concentrations hydrodynamic interactions between particles become increasingly important [49]. Batchelor adapted Einstein's equation to account for hydrodynamic interactions by adding a second order correction [54] (Equation 2.6.2.2),

$$\frac{\eta}{\eta_0} = 1 + 2.5\phi + 6.2\phi^2$$

Equation 2.6.2.2- Einstein-Batchelor Equation

The Einstein-Batchelor equation has been validated for suspensions of hard sphere ϕ>0.1 [49]. Above this point, multi-particle interactions become increasingly important with increasing concentration [49] and the above equations tend to fit poorly for concentrated regimes as they assume a finite value for viscosity as $\phi \rightarrow 1$. However, this is unrealistic as the typical maximum packing for monodisperse hard spheres is ϕ=0.74 [50].

The more successful models for predicting the viscosity of concentrated dispersions tend to include ϕ_m as a variable [50]. For calculating the viscosity of medium to high concentrations of particles the Krieger-Dougherty (K-D) equation (Equation 2.6.2.3) has been found to be more useful [37];

$$\frac{\eta}{\eta_0} = (1 - \frac{\phi}{\phi_m})^{-[\eta]\phi_m}$$

Equation 2.6.2.3 - Krieger-Dougherty Equation

Maximum packing, $\phi_{m,}$ is the point where enough particles have been added for the viscosity to appear infinite [51] [50]. The Krieger-Dougherty model is often fitted to experimental data with ϕ_m and $[\eta]$ used as the fitting parameters to derive information about the maximum packing factor and the particle aspect ratio [53]. Experimentally derived values of ϕ_m and $[\eta]$ can be found in Table 2.6.2.1.

Maximum packing is a function of particle factors such as particle shape and particle size distribution, with higher aspect ratio particles and narrow particle size distributions being related to lower maximum packing fractions [37][49][51]. Maximum packing increases with particle polydispersity as the smaller particles can fit in the gaps between the bigger ones [51][52]. This effect of particle size distribution is more pronounced in the concentrated regime, ϕ>0.50 for spheres, where particle interactions become increasingly important [40][51].

Particle asymmetry has a strong effect on $[\eta]$ and ϕ_m and hence on the viscosity concentration relationship [51]. The zero shear $[\eta]$ increases with particle aspect ratio as the high aspect ratio particles occupy a greater volume in the flow [49]. Higher aspect ratio particles lead to higher values of $[\eta]$ and lower values of ϕ_m as the particles pack poorly producing greater increases in viscosity for higher aspect ratio particles than spheres at the same phase volume [36][51].

Flow also effects the maximum packing fraction, especially with high aspect ratio particles, with the flow aligning the particles into a more favourable arrangement, allowing them to pack more effectively causing an increase in maximum packing with increasing shear rate [37][39][51].

Table 2.6.2.1 The effect of particle morphology on the intrinsic viscosity, $[\eta]$ and maximum packing factor ϕ_m

Particle	Dimensions (μm)	Aspect Ratio, Ar	Intrinsic Viscosity, $[\eta]$	Maximum Packing factor, ϕ_m	Reference
Oblate – Polyacrylic Glitter	31.2x236	0.136	3.17	0.621	Mueller et al [50]
Spherical – Glass Bead	108	1	3.27	0.641	Mueller et al [50]
Prolate A - SIC grit	206x121	1.75	3.77	0.542	Mueller et al [50]
Prolate B - Woolastonite	96.3x24.5	4.69	5.39	0.454	Mueller et al [50]
Prolate C - Woolastonite	353x28.1	9.17	6.07	0.343	Mueller et al [50]
Glass Fibre	-	7	3.08	0.374	Barnes et al [51]
Glass Fibre	-	14	5.03	0.26	Barnes et al [51]
Glass Fibre	-	21	6.0	0.233	Barnes et al [51]
Quartz Grain	53-76	-	5.8	0.371	Barnes et al [51]
Glass Plates	100x400	4	9.87	0.382	Barnes et al [51]
Carbon Black	0.04x0.05	1	22.16	0.637	Kasgoz et al [19]
Carbon Fibres	3000x8	375	4.88	0.209	Kasgoz et al [19]
Graphite	14x3.5	10	5.40	0.189	Kasgoz et al [19]
Expanded Graphite		25	29.47	0.320	Kasgoz et al [19]

It has previously been found experimentally that the product of $\phi_m[\eta]$ is often around 2 [37], and the K-D model is often simplified to the Maron-Pierce model (Equation 2.6.2.4).

$$\frac{\eta}{\eta_0} = (1 - \frac{\phi}{\phi_m})^{-2}$$

Equation 2.6.2.4- Maron-Pierce Equation

This model has previously been found to be useful for predicting the viscosities of suspensions of fibrous or otherwise irregular particles [40], with Metzner [38] describing it as “the best empirical expression for the effect of filler on viscosity”.

Barnes [51] proposes a simple model relating the intrinsic viscosity of very high aspect ratio disks to the particle aspect ratio (Equation 2.6.2.5)

$$[\eta] = \frac{3 \times (Aspect\ Ratio)}{10}$$

Equation 2.6.2.5- Relationship between aspect ratio and intrinsic viscosity from Barnes [51]

2.6.3 Nano-Carbon Rheology

Rheology has been suggested as a method for assessing the dispersion of carbon Nanomaterials in a fluid with well dispersed nanoparticles will show different rheological behaviour compared to their agglomerated or flocculated counterparts [23][39][53]. Nanoparticles in a suspension are subject to particle-particle forces, particle-fluid interactions, viscous forces under flow, and Brownian forces [53]. For suspensions of colloidal particles non-hydrodynamic forces such as Brownian, electrostatic and London-van der Waals forces become significantly important [37] [52]. A physically stable ink would be expected to show no change in its rheological properties over 6 months in storage [48], this can be examined by using shear Rheometry to measuring the flow curves, or oscillatory rheology to measure the elastic storage modulus at various intervals in time [48].

Nanoparticles can’t achieve high filler values due to the ultra-high interfacial area per volume, which leads to difficulties dispersing the nanoparticles, leading to fractal networks that dramatically reduce ϕ_m [36]. Flocculates lead to lower maximum packing fractions as in general flocs are not tightly packed [51], giving a larger effective particle radius [37][39] and leading to a larger effective filler volume [36], as well as trapping polymer within these flocs which then can’t deform at the same rate as the rest of the matrix, leading to higher viscosities [37].

Much of the work on the effect of particles on suspension viscosity has focussed on non-interacting particles in Newtonian Fluids [37][50][51][52]. The fundamental work into the effect of particle aspect ratio on suspension viscosity, such as the work by Mueller and Llewelyn [50], focussed on non-interacting, macro sized particles

such as glass beads and glitter [50], with aspect ratios much lower than those typically found in carbon nanomaterials. Previous works on the dispersion of carbon Nano-materials using rheology have focussed on Carbon Black (CB) [19][23] [46], Carbon Nanotubes (CNTs) [19][39][53], Carbon Nano-fibres (CNFs) [19][54], GNPs [18] [25], Graphene oxide (GO) [53] and Expanded Graphite (EG) [19] typically at low volumes and in high viscosity resin systems used in composite manufacture.

The addition of Carbon black, carbon fibres, graphite and exfoliated graphite to cyclic olefin copolymers (COC) increased the low shear viscosity of the unfilled COC polymer, with viscosity and the low shear rate shear thinning behaviour increasing with increasing concentration. The addition of CB had the highest effect on the low shear viscosity and low shear thinning behaviour. They found that $[\eta]$ was greatest in EG>CB>G>CF and that ϕ_m was CB>EG>CF>G [19].

Amari, Uesugi & Suzuki *(1997)* studied the effect of increasing carbon black content on the viscoelastic properties of melt polymers in the molten state at 130°C and in the solid state at 25°C [23]. They found that both storage, *G'*, and loss modulus, *G"*, increased with increasing carbon black concentration, with the moduli becoming increasingly frequency independent with increased loading. At low concentrations the CB exists as isolated small clusters, however with increasing concentration these clusters flocculate into a 3D network.

King *et al (2011)* characterised the effect of increasing concentration exfoliated GNPs had on the electrical, mechanical and rheological properties of a xGNP/Polycarbonate (PC) composite [25]. Increasing the concentration GNP increased the viscosity at all shear rates but especially at low shear rates.

Exfoliated fillers such as Graphene have long-range connectivity that arises from physical interparticle interactions. Due to the high specific area, these particles form a network of connected interacting particles in the suspending fluid. Macroscale agglomeration of GO in PDMS suspensions showed up as $G'>G''$ at low frequencies, with this macro scale aggregation/agglomeration driven by Brownian motion in the low viscosity PDMS suspension [53].

Oxfall *et al (2015)* examined the effect of the addition of carbon black upon the rheological properties of GNP poly(ethyl-butyl-acrylate) (EBA) composites mixed

by solution processing at <18 vol%. In this work the effect of high and low structured carbon black on the electrical and rheological properties of GNP/EBA composites was studied. Increasing concentration GNP and CB increased the *G'* with *G'* becoming increasingly frequency independent especially at low volumes. The orientation in the flow direction of anisotropic conductive fillers will influence their conductive properties [18].

Trappe and Weitz *(2000)* found that increasing the phase volume of carbon black created an increasingly dense network of particles, represented by an increase in *G'* with loading with *G'* becoming more frequency independent [46]. At the highest phase volume ϕ=0.147, *G'>G"* and *G'* was nearly frequency independent. At intermediate volumes, ϕ=0.097, a crossover frequency was seen at intermediate frequencies, and imagery had shown a dense network had formed. At the volumes ϕ=0.064, *G"* increased nearly linearly with frequency and *G">G'* at all frequencies, imaging with less dense network formed. At the lowest concentration, ϕ=0.033, *G">>G'*, with *G'* increasing linearly with frequency, and a barely measurable G, which is characteristic of a Newtonian fluid as would be expected for a dilute suspension. They proposed that the Carbon black forms a solid but tenuous purely elastic network, with G' independent of frequency, which grows in magnitude with increasing ϕ. This network is interspaced by the purely viscous suspending medium, with *G"* increasing linearly with frequency and independent ϕ.

When suspensions of CNTs in PDMS are well dispersed they show a viscoelastic response like that of the unfilled PDMS, a liquid-like behaviour with *G">G'* at all frequencies. Following aggregation, the suspensions showed a more solid like response with *G'>G"* at low frequency as a CNT network formed. Adding functional groups to the surface of CNTs is one of the most effective ways to improve dispersion and prevent agglomeration in a suspending medium [53].

2.7 Screen Printing

2.7.1 Screen Printing

Screen printing is a process in which ink is forced through the open areas of a stencil supported on a mesh of synthetic fabric supported by a frame an onto the substrate underneath by drawing a squeegee over the stencil [14]. This thesis will focus on flatbed screen printing, in which both the printing bed and substrate are both flat and the screen is transferred through the mesh by movements of the squeegee [15].

Screen printing is the dominant deposition method in printed electronics due to its relative simplicity, cost-effectiveness, reproducibility, versatility and maturity in the sector. Screen printing offers the ability to accurately deposit thick layers of a wide range of inks, including viscous slurries with high functional component loading, with minimum pressure over a wide area at economical production rates offering scalability to large scale manufacture [13][20][21][31].

Disadvantages of screen printing include relatively low digital resolution, dry out of the ink in the screen affecting resolution and contact between the squeegee and the substrate can cause distortion of soft substrates [13].

The screen-printing process can be subdivided into four segments (Fig. 2.7.1.1) [15];

1) Filling Zone; Volume of ink on the screen is moved like a tidal wave, with the ink underneath the tidal wave penetrating the screen
2) Contact Zone; Ink in front of the squeegee edge in the contact zone passes through the screen and makes contact with the printing substrate
3) Adhesion Zone; Behind the edge of the squeegee in the adhesion zone the ink ensures that the printing form adheres to the substrate
4) Release Zone; The Screen's pulling strength pulls ink fibres out of the ink film in the release zone meaning that the ink remains in the mesh and an even layer of ink is deposited on the substrate.

However, in practical use, the screen is often "Flooded" prior to each print stroke. This is when the ink is first spread evenly over the screen with virtually no pressure and there is no contact between the screen and the substrate, cleaning the ink residues remaining in and on the screen from preceding print processes [15].

As screen printing is often used to produce very thick inks, drying of these inks often takes a relatively long time [15].

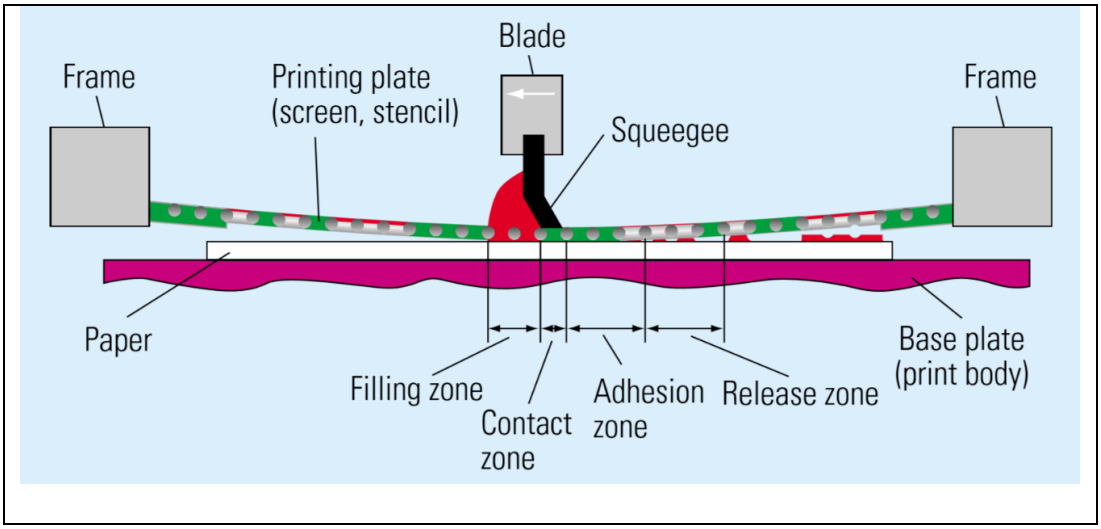

Figure 2.7.1.1 - Kipphan (2001) The screen-printing process [15]

The quality of screen-printed patterns is generally dependent on the ink rheology, printer hardware (screen, squeegee, substrate) and the printing process [13]. The resolution of screen printing is limited by the mesh size of the screen, the viscosity of the ink, the surface energy of the substrate, the speed of the process [10]. Control of the conductivity of screen-printed features is vital for achieving the correct performance and is governed by the inherent conductivity of the deposited material as well as the thickness and depth of the printed features [20].

The flow of the ink through the mesh or the stencil is significant since it determines the uniformity of printed surface which is an important feature of conductive circuits [13]. Surface topography of the final coating impacts on the electrical properties of the film as the topological variations provide a significant barrier to efficient charge transfer [31][47]. As a conductive pathway is only as conductive as it's least conductive part, variations in the thickness of the ink because of print defects such as mesh marking can cause thinner less conductive areas of the print, therefore it is important to control the ink and the printing process to create smooth prints of an even thickness. The topography of the surface of a printed feature are the underlying topography of the print which is a consequence of the print process as well as the ink rheology and the roughness due to the size and morphology particles [20][31][47]. and substrate roughness. Surface topography is also important in multi-layer devices where the incumbent surface topography influence the lay down of subsequent layers with this difference in topography having the potential to impact overall device performance [31].

Material rheology impacts subsequent ink transfer to the film and the geometry and conductor density in the cured film [31]. The more viscous an ink, the less easily it flows through the screen and the more difficult it is for the ink to spread into an even film [15]. The ideal ink should have a high rest state viscosity and a low viscosity at high shear rate, and a fast recovery time [13]. It is important that the ink shear thins as it passes through the screen before recovering following the removal of shear to ensure print quality [12]. Higher low shear viscosities and steeper shear profiles gave higher print roughness owing to the inability of the ink to slump following release from the screen [20][22] to leave a relatively rough surface with mesh marking [22]. Increased resin content in the lower carbon content inks resulted in smoother more consistent printed films without mesh marking seen at higher concentrations [20]. The thickness of ink deposited is a function the open screen area and the stencil thickness (Fig. 2.7.1.2) [15]. Coarser screens deposit thicker films due to higher available screen volume in the mesh [47].

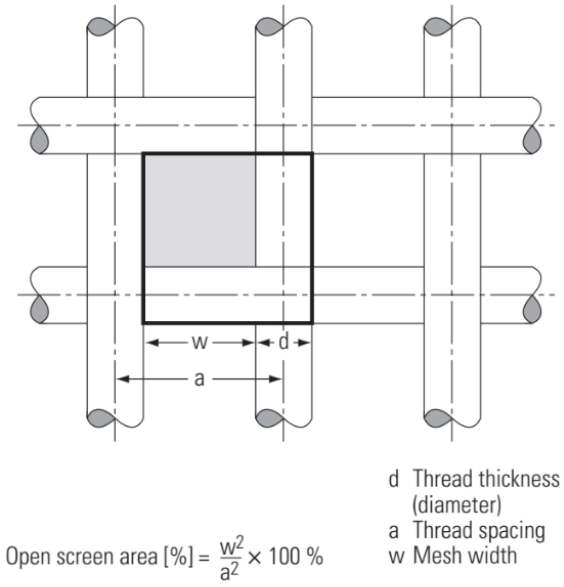

Figure 2.7.1.2 - Kipphan (2001) - The screen geometry [15]

As screen printing is open to the atmosphere solvents must not be so volatile that there is excessive solvent loss during printing, and the solvents do not cause the squeegee to swell or crack or remove the stencil [14].

Drying methods are dependent on the substrate and ink. Many drying methods involve the physical removal of volatile solvents in the ink, leaving the resin and

other materials to bind the pigments to the substrate. The rate of drying is affected by the evaporation rate if solvents, the affinity and retention of the solvents by resins and the ambient and additional means of applying energy to evaporate the solvents [14]. Thicker films also require longer drying times [47].

Screen printing can be used to print onto a wide variety of substrates; however, the thick ink film is often less flexible than the substrate in which it is printed leading to poor adhesion [14]. Therefore, when printing onto very flexible and even stretchable substrates it is imperative that the inks also have similarly mechanical properties to ensure good adhesion between the ink and the substrate.

A large variety of ink types are available for screen printing. The viscosity of the ink must be matched to the desired ink, layer thickness and fineness of mesh [15]. An ink must have sufficiently low viscosity for it to pass through the screen but must not be so low as to cause “slurred” printing. The inks need to remain coherent on the mesh before printing, transfer through the mesh without sticking it to the substrate, flow to make the ink film continuous and so avoid the pattern of the mesh but maintain the image and then dry rapidly when applied to the substrate . Mesh marking is when a pattern of the mesh appears in the dry film and is always due to poor flow or over-pigmentation [14].

During screen printing, pastes are run at various shear rates, therefore, to understand the effect of rheology on printing it is important to discuss the rheology at various shear rates [21]. At the start of a printing cycle, ink is in a low shear rate rest condition where it is at high viscosity. The ink is then pushed by the squeegee over the screen surface, at an intermediate shear rate before being forced through the mesh at a high shear rate at which point the ink is at its lowest viscosity. The shear rate then reduces and the ink recovers its structure and hence viscosity. This recovery will determine the degree of slumping in the print [20].

High carbon content inks gave less consistent line widths and line thicknesses over the whole line width. As the viscosity of the inks were reduced the inks were better able to slump to form a consistent line [20]. Reduction in line width for the higher solids content and therefore higher viscosity inks is a function of the reduced leakage at the screen substrate interface and a reduction in the “slumping” of the high viscosity fluid as the ink is released from the screen [31].

The highest resolution widely achievable with screen printing is 50μm [10]. Lower solids content and therefore lower viscosity inks were able to render the finest details attributed to the lower viscosity of the fluids allowing easier transit through the screen and easier flow into the line to create a continuous feature [31]. Lower viscosities allow printed lines to slump more readily [20]. Lower viscosity inks create thicker prints as more ink flows through the screen under the shear provided by the squeegee [21].

The viscoelastic behaviours of inks at low shear rates has been postulated to as a key indicator of the material transfer process in screen printing [31]. Jewell *et al (2013)* Examined the effect that increasing carbon content between 38-43wt% had upon the rheological and print performance of Graphite/Carbon Black screen-printing inks [31]. Increasing the carbon content of the inks increased the ink viscosity, elasticity, dry film thickness and electrical conductivity of the films, however, the lower carbon films were able to render the smallest feature size as the less viscous and elastic inks could more easily flow through the screen to create a continuous feature. Increasing solid content increased the deposited wet film thickness indicating that increasing the viscous and elastic properties of the formulation aids ink transfer. This supports a pull transfer mechanism as material removal from the screen is enhanced by the higher elasticity of the material which maintains the integrity of the material filament between the substrate and the screen.

Phillips *et al, 2019* compared the effect of changing ratio G:CB on the performance of screen- printed carbon conductive inks at 21.7 and 29.4wt% [20]. All inks showed shear thinning behaviour, with higher amounts of CB associated with higher low shear rate viscosity with the higher CB content inks more readily shear thinning. This effect was attributed to the smaller higher surface area CB having smaller interparticle distance leading to increased interparticle interactions. These weak particle-particle interactions were easily broken down by shear. More consistent thicknesses and roughness's in lower carbon inks are a consequence of greater slumping following mesh release from the substrate during snap off. Saw tooth edge and mesh effects visible in printed lines with highest viscosity ink, high concentration highest CB content ink. Higher carbon black content gave higher rest viscosity, greater shear thinning and a lower high shear viscosity. Association

between low shear rate viscosity, with stiffer inks giving and higher ink film thickness and retaining mesh markings.

As the electrical properties of the coating are dependent on the quality and consistency of the print as well as the inks material properties it is imperative that inks are developed to be compatible with the final printing process to ensure optimisation of the inks for electrical performance. The matching of the ink's rheological properties to the process conditions is often overlooked in the lab scale development of conductive nanocomposites which tend to focus on the composite's material properties.

2.8 Nanocomposite Heating Films

Flexible electrothermal heaters are attracting a growing interest because of their broad applications in wearable electronics, including warming garments and as flexural warmers for medical devices and vehicles [6][55].

Metal wire heaters provide non-uniform heating, are heavy, rigid, high cost, suffer from oxidative corrosion, have low heating efficiency and have a short lifetime on account of broken wires [6][8][55]. Indium Tin Oxide (ITO) is often used to create transparent plane heaters; however, the high cost and slow thermal response and rigidity makes them unsuitable for wearable applications [55][56].

Nanocomposite heaters could provide a route to production at scale and reduced weight; however, performance still needs improving with respect to cost, simplifying production and improving the electrical properties [6]. Metal nanostructure heaters have low sheet resistance, therefore, can be operated at low driving voltages, however oxidation at the junction of nanowires at high temperatures and their high material costs limit their practical use [55]. Single-walled Carbon Nanotube (SWCNT) heaters have been shown to have rapid thermal response and better heating performance than ITO, however dispersion often requires strong acid treatments and surfactants that affect the conductivity of SWCNT based films in addition to the difficulty in removing semi-conducting SWCNTs [56].

Polymer composites containing carbon Nano-fillers have advantages such as being lightweight, corrosion resistance, easy processing and lower manufacturing costs for electric heating applications [8]. Graphene based heaters often show fast heating rates and homogenous heat distribution [56]. Graphene based heaters typically suffer

from large sheet resistance and therefore require high input voltages for applications where higher temperatures are required. High running voltage poses a risk to human health, therefore a low resistance heater that can run at low voltages is preferable to reduce human risk [55].

Park *et al (2015)* hand screen-printed inks of different ratio Graphite: amino functionalised CNTs/ epoxy resin at 50wt% onto a Polyethylene terephthalate (PET) to form a printed heater (Fig. 2.8.1) and compared its heater performance to that of a carbon black/graphite heater and a copper wire heater [6]. The performance of the heater was tested at 12V in a 20°C room and it was found the 40:10 Graphite/a-MWNT heater had the best heater performance, reaching close to 60°C and showing good uniformity even when bent.

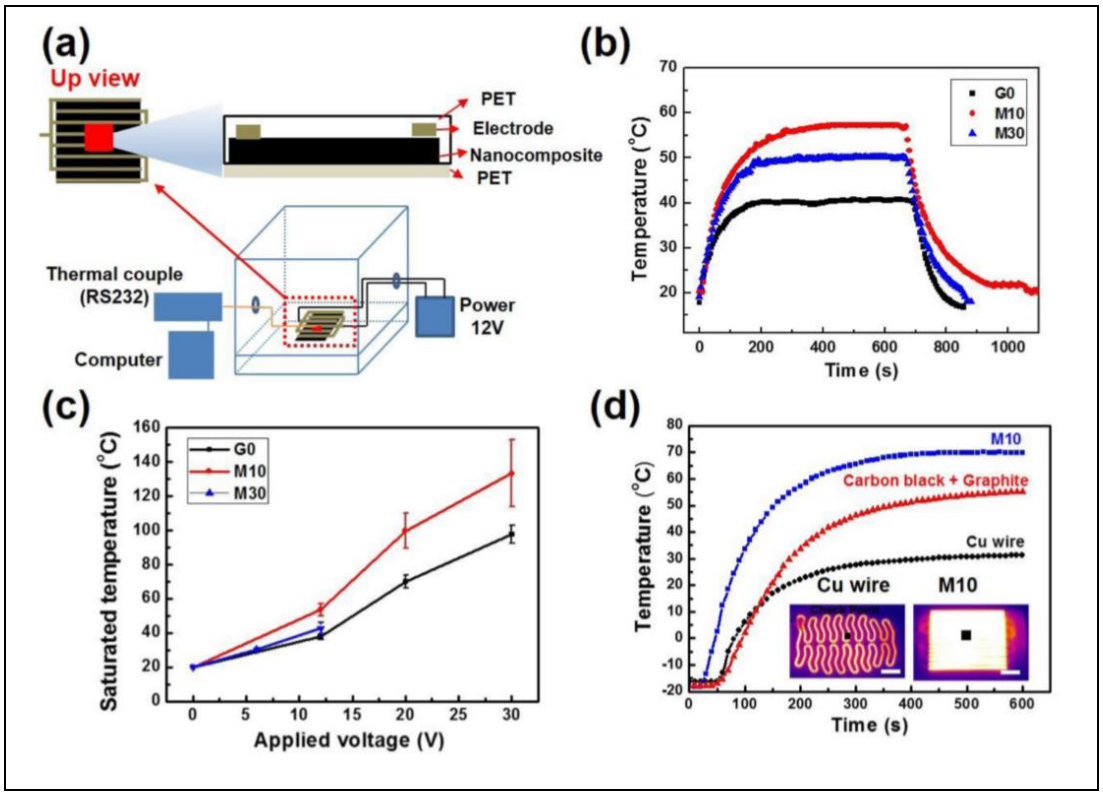

Figure 2.8.1 – Park et al (2016) The performance of a Graphite/a-MWNT heater. a) the design of the Graphite/a-MWNT heater, b) the time-temperature time response of the G0 (Graphite) heater, M10 (Graphite: a-MWNT 40:10) and M30 (Graphite: a-MWNT (30:10), c) The effect of increasing voltage on the saturated temperature, d) Comparison of M10 heater to a carbon black/ graphite heater and a copper wire heater where the black square represents a 5x5cm area [6]

Lin *et al 2017* created a flexible plane heater from a mix of laser reduced graphene oxide (LRGO) and silver particles which was dispersed in deionised water and then drop cast onto polyimide film [55]. The Graphene oxide was then reduced by laser. The heater showed good uniformity of temperature output even when flexed. The

best performing heater was capable of achieving 229°C at 18V. They compared this performance to other heaters in the literature with the results displayed in Figure 2.8.2. The heater was bent 150 times at 2Hz and showed a temperature deviation of 8°C. This was developed into an elbow patch for alleviating arthritic suffering and could achieve 70°C from a 15V power supply (Fig. 2.8.3).

Table 1 A comparison of previous flexible heaters with the ones prepared in this research

Material	Sheet resistance ($\Omega\ \square^{-1}$)	Driving voltage (V)	Response time (s)	Steady-state temperature (°C)
Ag-doped LRGO	158.7	18	5	229
TRGO	641	60	10	206
Doped graphene	43	12	80	97
Electrochemically exfoliated graphite	159	30	20	139
Ag nanowires	33	7	200	53
Ag mesh	32.5	6	150	85
Multi-walled CNTs	349	12	50	65
Single-walled CNTs	580	12	60	95
CNTs and Ag nanowires	50	15	30	110
Ag mesh and ITO	300	12	43	10
Ga doped ZnO	10.7	12	48	88
ITO nanoparticles	633	20	110	163
Fluorine-doped tin oxide	253	12	700	39

Figure 2.8.2 - Lin et al (2017) Table comparing the performance of flexible plane heaters in the literature [55]

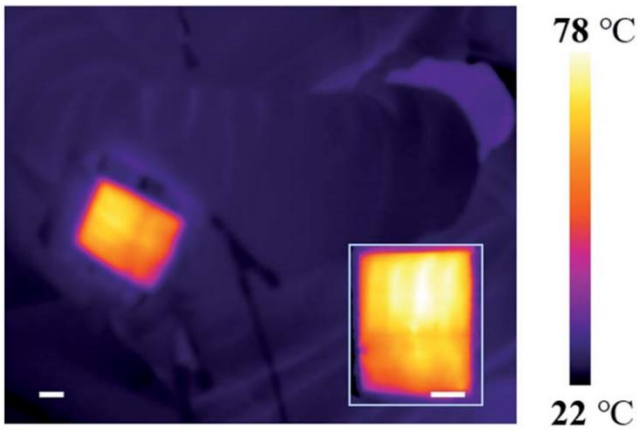

Fig. 6 Prospective application of the heater. Utilizing the LRGO/Ag particle heater to treat arthritis of the elbow (scale of the ball is 2 cm).

Figure 2.8.3 - Thermal image showing the performance of the printed heater developed by Lin et al (2017) [55]

Kang *et al (2011)* transferred chemical vapour deposition (CVD) graphene sheets onto PET. The 4x4cm heaters had a sheet resistance of 43Ω/□ and were capable of reaching approximately 100°C from a 12V power supply [56]. They measured the temperature response of the heater and found that the temperature output decreased by 9% at bending strains of up to 4%

An and Jeong *(2013)* solution cast Graphene/epoxy composite with varying Graphene contents between 0-10 wt% onto a polyimide film and measured their electric heating performance between 1-100V [8]. Above 2 wt% Graphene the electrical resistance of the composites decreased rapidly as an increasingly interconnected network of Graphene sheets formed within the epoxy resin. At 10wt% the composites were capable of reaching 126°C at 30V.

Pahalagedara et al *(2017)* CB/PU has been screen printed directly onto fabric for wearable heating applications, with these heaters capable of reaching 65°C from 15V power supply, however this was done by hand screen printing 3 layers over a small 4x3cm area, and the performance of these coatings under strain was not measured [57]. Therefore, further work is required to create larger area heaters with more established techniques and temperature performance under strain should be monitored.

The heaters typically studied in this literature review have largely been coated using lab scale techniques such as drop casting and hand screen printing and the heaters produced have typically been small area, therefore one challenge is to create and test consistently create larger heaters with larger scale more scalable techniques. The heaters are also typically coated onto rigid films such as PET and not the softer more stretchable substrates used in wearable sports clothing such as thermoplastic polyurethane (TPU). As the thick film inks are often less flexible than the substrate this would mean that the inks would experience further mechanical challenges when printed onto soft substrates. To conform to the body to give better heat transfer and to be used on the stretchable base-layers used in sports clothing the heaters need to be able to stretch. Due to the rigid nature of the substrates, although bend testing has been performed, the thermal response of the heater to strain has not been calculated. This thesis looks at creating a mass manufacture stretchable printed heater.

2.8 Closure

A link has been established between body temperature and sporting performance. Several strategies, both passive and active, have been developed to help attenuate losses in muscle temperature following a period of inactivity, however no method has been found to prevent these drops in muscle temperature completely. The effectiveness of these techniques in maintaining muscle temperature has largely been done in thermoneutral environments, however, there has been little research into the

performance of these garments in colder environments where heat losses would be expected to be greater. Most of the garments tested have been designed to be worn during periods of inactivity, no garment has been developed specifically for use during training or physical effort. To do this requires the heaters to be integrated into more stretchable fabrics and with this requires the heaters themselves and the electronics to be increasingly flexible and stretchable to improve the conformability of the heaters to the muscles to avoid disruption to the athlete during athletic efforts.

Wearable printed heaters offer a thinner, more flexible heating solution that has yet to be assessed as a potential method for attenuating heat losses in elite sport. Flexible plane heaters have been developed but many of these heaters are printed onto non-stretchable substrates such as PET and polyimide, therefore their heating performance has been assessed under bending conditions but not under strain. To be attached to a stretchable base-layer garment requires the heaters to be printed onto a soft substrate that easily deforms, such as the polyurethanes used in heat transfer graphics typically used in the sports textile industry, the ink will be subject to larger tensile strains. The heater needs to be able to stretch conform to the body to give a closer fit to the muscle to improve conductive heat transfer to the skin requires the heaters. A strain resistance of 15-20% has been suggested to be suitable in the clothing industry. To do this requires the development of new stretchable and flexible inks specifically for wearable heating applications.

When designing an ink, it is important that the inks rheological properties are matched to the printing process to create smooth, highly electrically conductive prints. Good interaction between the ink and the substrate and the formation of a smooth consistent film are important for adhesion between the ink and the substrate. Creating a smooth print has also been linked to improving the conductivity of prints and being significant in the overall performance of multi-layer printed devices. The ability of the ink to flow through the screen and then level out to form a smooth layer is critical for adhesion. Therefore, the inks in this thesis will be optimised for rheological properties and print performance as well as material properties.

Graphene inks typically suffer from large sheet resistance, limiting their use in wearable technologies where low resistances are required to achieve higher temperatures off lower voltages [55]. Therefore, there is a requirement to create a

low sheet resistance, flexible and stretchable graphene-based ink capable of reaching sufficiently high temperatures from a low voltage source for use within wearable technology.

Graphene nanoplatelets are a promising material for conductive inks, however due to their high aspect ratio and inert surface they typically agglomerate under van der Waals forces. Therefore, plasma functionalisation can be used to improve interaction with polymer to prevent agglomeration. Rheology is a promising method for assessing the dispersion of the GNPs, modelling and controlling their behaviour.

Therefore, this thesis aims to develop new stretchable conductive inks, optimise their properties for mass screen printing, characterise their response to strain, before building a stretchable heater for testing as a passive heat maintenance device in elite sport.

2.9 References

[1] S. Faulkner, R. Ferguson, N. Gerret, M. Hupperets, S. Hodder and G. Havenith, "Reducing Muscle Temperature Drop Post Warm-up Improves Sprint Cycling Performance.," *Medicine and Science in Sport and Exercise,* vol. 45, no. 2, pp. 359-365, 2013.

[2] D. West, B. Dietzig, R. Bracken, D. Cunningham, B. Crewther, C. Cook and L. Kilduff, "Influence of post-warm-up recovery time on swim performance in international swimmers," *Journal of science and medicine in sport,* vol. 16, no. 2, pp. 172-176, 2013.

[3] L. Kilduff, D. West, N. Williams and C. Cook, "The influence of passive heat maintenance on lower body power output and repeated sprint performance in professional rugby league players," *Journal of Science and Medicine in Sport,* vol. 16, no. 5, pp. 482-486, 2013.

[4] M. Mohr, P. Krustup, L. Nybo, J. Nielsen and J. Bangsbo, "Muscle temperature and sprint performance during soccer matches - beneficial effect of re-warm up after half time," *Scandinavian journal of medicine and science in sports,* vol. 14, no. 3, pp. 156-162, 2004.

[5] M. Russel, R. Tucker, C. Cook, T. Giroud and L. Kilduff, "A comparison of different heat maintenance methods implememnted during a simulated half time period in professional Rugby union players," *Journal of science and medicine in sport,* vol. 21, no. 3, pp. 327-332, 2018.

[6] H. K. Park, S. M. Kim, J. S. Lee, J.-H. Park, Y.-k. Hong, C. H. Hong, Kim and K. Kang, "Flexible plane heater: Graphite and carbon nanotube hybrid composite heater," *Synthetic Metals,* vol. 203, pp. 127-134, 2015.

[7] M. Raccuglia, A. Lloyd, D. Filingeri, S. Fulkner and G. Havenith, "Post-warm-up muscle temperature maintenance: blood flow contribution and external heating

optimisation," *European Journal of Applied Physiology,* vol. 116, no. 2, pp. 395-404, 2016.

[8] J. An and Y. Jeong, "Structure and electrical heating performance of graphene/epoxy composite films," *European Polymer Journal,* pp. 1322-1330, 2013.

[9] C. Wang, K. Xia, H. Wang, X. Liang, Z. Yin and Y. Zhang, "Advanced Carbon for Flexible and Wearable Electronics," *Advanced Materials,* vol. 31, 2019.

[10] W. Dang, V. Vinciguerra, L. Lorenzelli and R. Dahiya, "Printable Stretchable Interconnects," *Flexible and Printed Electronics ,* vol. 2, 2017.

[11] J. Suikkola, T. Bjorninen, M. Mosallaei, T. Kankkunen, P. Iso-Ketola, L. Ukkonen, J. Vanhal and M. Mantysalo, "Screen-Printing Fabrication and Characterisation of Stretchable Electronics," *Scientific Reports,* vol. 6, pp. 1-8, 2016.

[12] M. Hatala, P. Gemeiner, M. Hvojnik and M. Mikula, "The effect of ink composition on the performance of carbon-based conductive screen printing inks," *Journal of Materials Science: Materials in Electronics,* vol. 30, pp. 1034-1044, 2019.

[13] T. S. Tran, N. K. Dutta and N. R. Choudry, "Graphene Inks for Printed Flexible Electronics: Graphene dispersions, ink formulations, printing techniques and applications," *Advances in colloid and interface science,* vol. 261, pp. 41-61, 2018.

[14] R. Leach and R. Pierce, The Printing Ink Manual: Fiffth Edition, AA Dordrecht: Springer, 1993.

[15] H. Kipphan, Handbook of print media: Technologies and production methods, Springer Science & Business Media, 2001.

[16] D. Gethin, *Private Communication. David Gethin,* 2020.

[17] T. Araki and Nogi, "Printable and Stretchable Conductive Wirings Comprising Silver Flakes and Elastomers," *IEEE Electron Device Letters,* vol. 32, no. 10, pp. 1424-1426, 2011.

[18] H. Oxfall, G. Ariu, T. Gkourmpis, R. Rychwalski and M. Rigdahl, "Effect of carbon black on the electrical and rheological properties of graphite nanoplatelets/ poly(ethyl-butyl-acrylate) composites," *eXPRESS Polymer Letters,* vol. 9, no. 1, pp. 66-76, 2015.

[19] A. Kasgoz, D. Akin, A. I. Ayten and A. Durmus, "Effect of different types of carbon fillers on mechanical and rheological properties of cyclic olefin copolymer (COC) composites," *Composites Part B: Engineering,* vol. 66, pp. 126-135, 2014.

[20] C. Phillips, A. Al-Ahmadi, S.-J. Potts, T. Claypole and D. Deganello, "The effect of graphite and carbon black ratios on conductive ink performance," *Journal of Materials Science,* vol. 52, pp. 9520-9530, 2017.

[21] C. Hua, X. Li, L. Shen, H. Lei, X. Guo, Z. Liu, Q. Kong, L. Xie and C.-M. Chen, "Influence of co-solvent hydroxyl group number on properties of water-based conductive carbon paste," *Particuology,* vol. 33, pp. 35-41, 2017.

[22] S.-J. Potts, Y. C. Lau, T. Dunlop, T. Claypole and C. Phillips, "Effect of photonic flash annealing with subsequent compression rolling on the topography, microstructure and electrical performance of carbon-based inks," *Journal of Materials Science,* vol. 54, pp. 8163-8176, 2019.

[23] T. Amari, K. Uesugi and S. Hiroaki, “Viscoelastic properties of carbon black suspension as a flocculated percolation system,” *Progress in Organic Coatings,* vol. 31, pp. 171-178, 1997.

[24] Haydale Graphene Industries, “HDPlas Technical Data Sheet,” [Online]. Available: https://www.graphene-info.com/files/graphene/HDPlas-GNP-Technical-Sheet-2.03.pdf. [Accessed 14 2 2018].

[25] J. King, M. Via, M. FA, K. Wiese, E. Beach, M. Cieslinski and G. Bogucki, “Characterization of exfoliated graphite nanoplatelets/ polycarbonate composites: Electrical and thermal conductivity, and tensile, flexural, and rheological properties,” *Journal of composite materials,* vol. 46, no. 9, pp. 1029-1039, 2011.

[26] Z. Fan, C. Zheng, T. Wei, Y. Zhang and G. Luo, “Effect of Carbon Black on the electrical property of Graphite Nanoplatelet/Epoxy resin composites,” *Polymer Engineering and Science,* pp. 2041-2045, 2009.

[27] S. Chatterjee, J. Wang, W. T. N. Kuo, C. Salzmann, L. W.L, R. Hollertz, F. Nuesch and B. Chu, “Mechanical reinforcement and thermal conductivity in expanded graphene nanoplateles reinforced epoxy composites,” *Chemical Physics Letters,* pp. 6-10, 2012.

[28] S. Yadav and J. Cho, “Functionalized graphene nanoplatelets for enhanced mechanical and thermal properties of polyurethane resin,” *Applied Surface Science,* pp. 360-367, 2013.

[29] S. Kim, Y. Noh and J. Yu, “Thermal conductivity of graphene nanoplatelet filled composites fabricated by solvent free processing for the excellent filler dispersion and a theoretical approach for the composites containing the geometrized fillers,” *Composites: Part A,* pp. 219-225, 2015.

[30] T. Tanaka, Y. Urabe, D. Nishide and H. Kataura, “Continuous Separation of Metallic and Semiconducting Carbon Nanotubes Using Agarose Gel,” *Applied Physics Express,* vol. 2, no. 12, p. 125002, 2009.

[31] E. Jewell, S. Hamblyn, T. Claypole and D. Gethin, “The impact of carbon content and mesh on the characteristics of screen printed structures,” *Circuit World,* vol. 39, no. 1, pp. 13-21, 2013.

[32] J. Williams, W. Broughton, T. Koukoulas and S. S. Rahatekar, “Plasma treatment as a method for functionalising and improving the dispersion of carbon nanotubes in epoxy resins,” *Journal of Materials Science,* pp. 1005-1013, 2013.

[33] R. J. Zaldivar, P. M. Adams, H. I. Kim, J. P. Nokes and D. N. Patel, “Strength Improvements in Toughened Epoxy Composites Using Surface Treated GNPs,” *Journal of Applied Polymer Science,* 2014.

[34] A. Felten, C. Bittencourt, J. Pireaux, G. Van Lier and J. Charlier, “Radio-frequency plasma functionalisation of carbon nanotube surface O_2, NH_3, and CF4 treatments,” *Journal of Applied Physics,* vol. 98, 2005.

[35] C. Saka, “Overview on the Surface Functionalization Mechanism and Determination of Surface Functional Groups of Plasma Treated Carbon Nanotubes,” *Critical Reviews in Analytical Chemistry,* vol. 48, no. 1, pp. 1-14, 2018.

[36] M. R. Rueda, M.-C. Auscher, R. Fulchiron, T. Perie, G. Martin, P. Sonntag and P. Cassagnau, “Rheology and applications of highly filled polymers: A review of current understanding,” *Progress in Polymer Science,* pp. 22-53, 2017.

[37] H. A. Barnes, A Handbook of Elementary Rheology, Aberystwyth: University of Wales Institute of Non-Newtonian Fluid Mechanics, 2000.

[38] H. A. Barnes, "A Review of the Rheology of Filled Viscoelastic Systems," *Rheology Review,* pp. 1-36, 2003.

[39] D. Litchfield and D. Baird, "The rheology of high aspect ratio nano-particle liquids," *Rheology Review,* pp. 1-60, 2006.

[40] A. Metzner, "Rheology of Suspensions in Polymeric Liquids," *Journal of Rheology,* vol. 29, pp. 739-775, 1985.

[41] Z. Utegulov, D. Mast, P. He, S. Donglu and R. Gilland, "Functionalization of single-walled carbon nanotubes using isotropic plasma treatment: Resonent Raman spectroscopy study," *Journal of Applied Physics,* vol. 97, 2005.

[42] F. Gojny, J. Nastalczyk, Z. Roslaniec and K. Schulte, "Carbon nanotube-reinforced epoxy-composites: enhanced stiffness and fracture toughness at low nanotube loading," *Composites Science and Technology,* vol. 64, pp. 2363-2371, 2004.

[43] H. Qi and M. Boyce, "Stress-strain behaviour of thermoplastic polyurethanes," *Mechanics of Materials,* vol. 37, pp. 817-839, 2005.

[44] S. Ansari and M. Muralidharan, "Electronic Applications of Polyurethane and Its Composites," in *Flexible and Stretchable Electronic Composites,* Switzerland, Springer, 2016, pp. 87-135.

[45] V. Pita, E. Sampaio and E. Monteiro, "Mechanical properties evaluation of PVC/plasticizers and PVC/thermoplastic polyurethane blends from extrusion processing," *Polymer Testing 21,* pp. 545-550, 2002.

[46] V. Trappe and D. Weitz, "Scaling of the viscoelasticity of weakly attractive particles," *Physical Review Letters,* vol. 85, no. 2, pp. 449-452, 2000.

[47] B. Phillip, E. Jewell, P. Greenwood and C. Weirman, "Material and process optimization screen-printing carbon graphite pastes for mass production of heating elements," *Jornal of Manufacturing Processes,* vol. 22, pp. 185-191, 2016.

[48] T. F. Tadros, Colloids in Paints, Weinheim: WILEY-VCH Verlag GmbH & Co. KGaA, 2010.

[49] N. Willenbacher and K. Georgieva, "Rheology of disperse systems," in *Product Design and Engineering,* 2013, pp. 7-49.

[50] S. Mueller, E. Llewellin and H. Mader, "The rheology of suspensions of solid particles," *Proceedings of the Royal Society A,* vol. 466, pp. 1201-1228, 2010.

[51] H. A. Barnes, J. F. Hutton and K. Walters, An Introduction to Rheology, Amsterdam: Elsevier Science Publishers, 1989.

[52] D. Jeffrey and A. Acrivos, "The rheological properties of suspensions of rigid particles," *AIChE Journal,* vol. 22, no. 3, pp. 417-432, 1976.

[53] P. Cassagnau, "Linear viscoelasticity and dynamics of suspensions and molten polymers filled with nanoparticles of different aspect ratios," *Polymer,* vol. 54, pp. 4762-4775, 2013.

[54] J. Xu, S. Chatterjee, K. W. Koelling, Y. Wang and S. E. Bechtel, “Shear and extensional rheology of carbon nanofibre suspensions,” *Rheological Acta,* vol. 44, pp. 537-562, 2005.

[55] S. Lin, T. Zhang, Q. Lu, D. Wang, Y. Yang, X. Wu and T. Ren, “High-performance graphene-based heater for wearable applications,” *RSC Advances,* vol. 7, no. 43, pp. 27001-27006, 2017.

[56] J. Kang, H. Kim, K. Kim, S. Lee, S. Bae, J. Ahn, Y. Kim, J. Choi and B. Hong, “High-performance graphene-based transparent flexible heaters,” *Nano letters,* vol. 11, no. 12, pp. 5154-5158, 2011.

[57] L. Pahalagedara, I. Siriwardane, N. Tissera, R. Wijesena and N. d. Silva, “Carbon black functionalised stretchable conductive fabrics for wearable heating applications,” *RSC Advances,* vol. 7, pp. 19174-19180, 2017.

Chapter 3: Materials and Methodology

3.1 Introduction

This chapter outlines the experimental techniques used within this thesis while demonstrating the statistical robustness of the work. Specific analysis of methods and materials will be assessed at the beginning of each chapter.

3.2 Materials

3.2.1 GNP selection

GNP was selected as the main conductive particle owing to its highly electrically and thermally conducting graphitic structure, but with its Nano-scale size, high aspect ratio, high surface area, it was hypothesised that this would provide better interaction with the polymer than the larger graphite particles, by having greater surface area in contact with the polymer. GNPs also have the potential to be functionalised to change the surface chemistry of the particles to improve interaction with the polymers.

Plasma functionalisation was used to treat the surface of the GNPs to improve their interaction with the polymer resin. Several different plasma functionalisation treatments are available, including but not limited to O_2, NH_3, and CF_4. Initial experiments compared the time stability of O_2 and NH_3 plasma functionalised GNPs to that of an un-functionalised control (R1), with these plasma treatments selected as it was hypothesised that this would improve the polarity of the surface of the GNPs to improve their interaction with the TPU resin. To identify a potential plasma functionalisation treatment for further research 22.5wt% of NH_3, O_2 and R1 GNPs were dispersed using three roll milling into a 9.7wt% thermoplastic polyurethane (TPU)/ Diacetone alcohol (DAA) carrier system. To measure the time stability of these suspensions an equilibrium shear ramp was taken over 31 days and changes to the equilibrium viscosity measured. Further information on the time stability measurements is given in section 3.3.5. The viscosity of the resin/solvent system was measured over the same time period to ensure that any changes in viscosity in time were due to changes to the particles and not the resin/solvent system (Fig. 3.2.1). The viscosity of the unfilled TPU resin system was stable over a 31-day period, indicating that the resin/solvent system is stable over this time period.

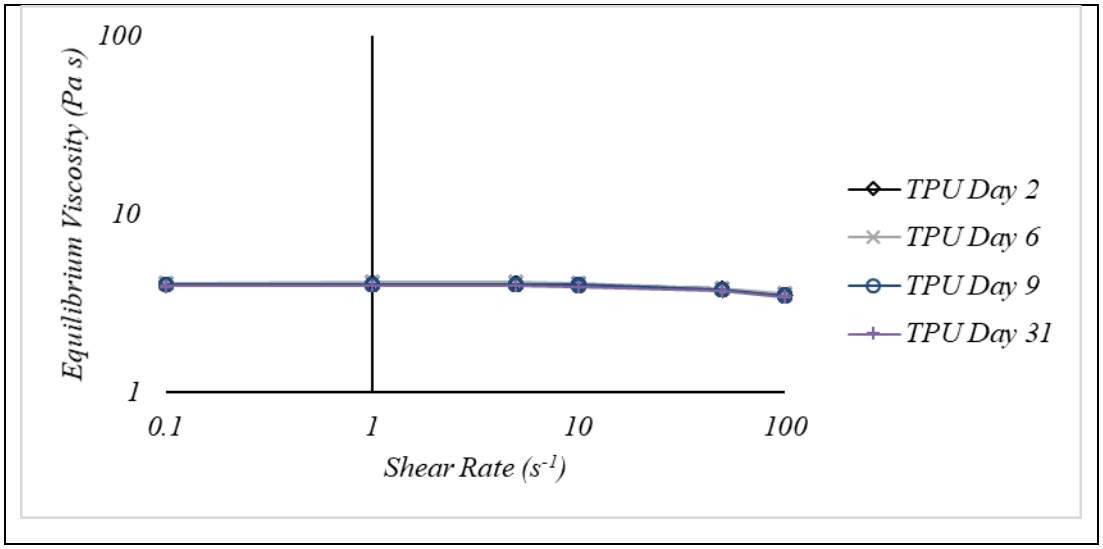

Figure 3.2.1 - Changes to the shear dependent equilibrium viscosity of the TPU/DAA resin system over a 31-day time period

The viscosity of the ammonia functionalised GNP (NH_3) and the unfilled resin (TPU) remained stable over 31 days while the viscosity of oxygen functionalised GNP (O_2) and unfunctionalized GNPs (R1) decreased (Fig. 3.2.2). Following this NH_3 was identified as the optimal plasma treatment for GNP in a TPU/DAA system and therefore, going forward the performance of NH_3 GNPs was compared to that of unfunctionalized R1 GNPs as a control.

3.2.2 Carbon Black

Conductex SC Ultra (Birla Carbon) is a commercially available carbon black used in conducting coatings [1].

3.2.3 Resin Selection

To be used in wearable applications requires the nanocomposite coatings to stretch to between 15-20%. As the resin provides much of the coating's mechanical properties such as the flexibility, an elastomer resin was selected. As the resin properties largely dictate ink adhesion, a thermoplastic polyurethane was selected owing to its similarity to the thermoplastic polyurethane transfer materials used within the sports textile industry. Thermoplastic Polyurethane (TPU) (Huntsman Irostic S7614-12) was selected as the resin for the flexible inks owing to its combination of favourable properties such as excellent elongation, high impact strength, good elasticity and biocompatibility, and use within wearable technology. This specific resin was selected as it shows high adhesion to a variety of substrates, is recommended for textile applications and has an elongation at break of 940-1300% [2]

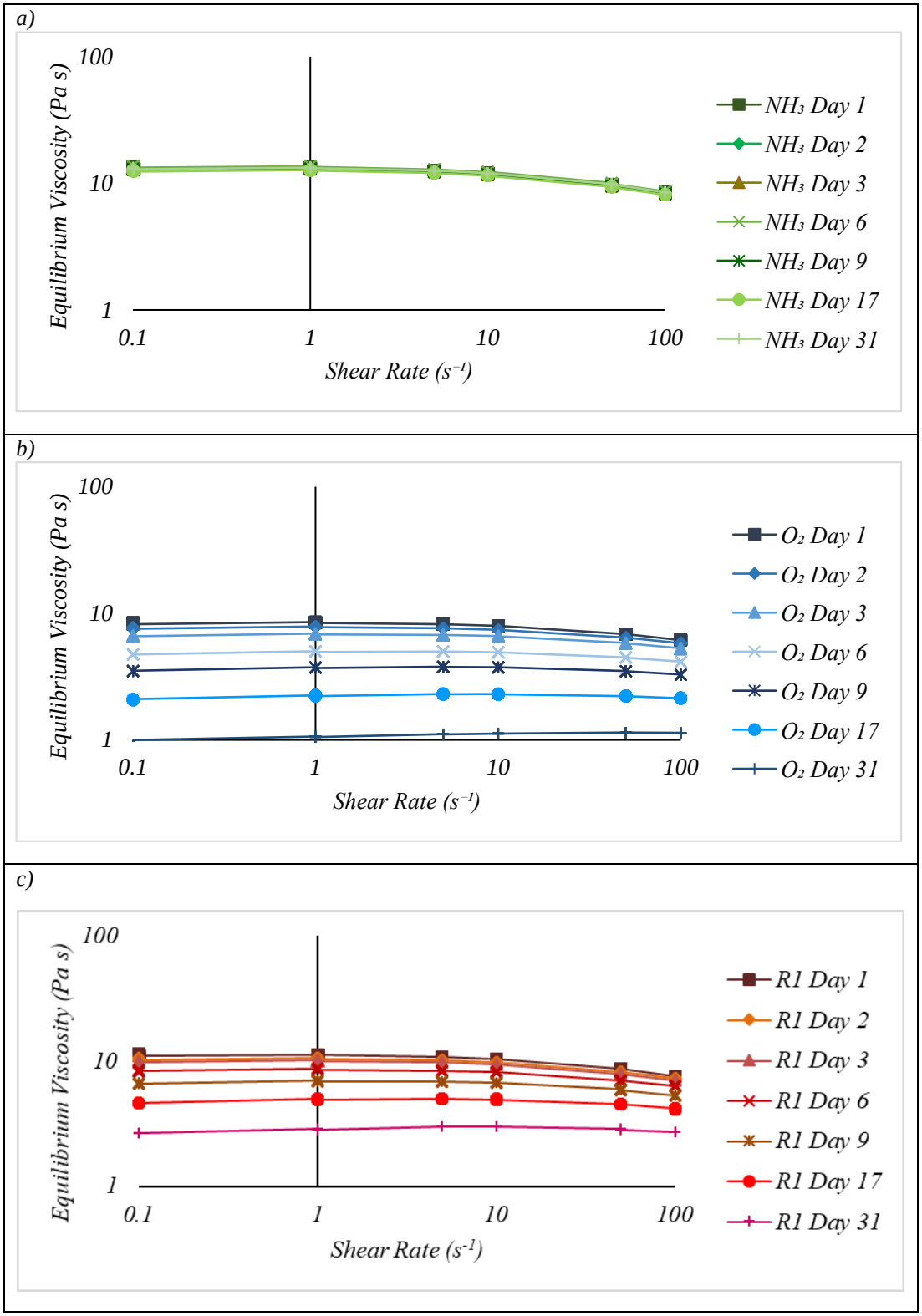

Figure 3.2.2 - The effect of time on the equilibrium viscosity of 22.5 wt% GNP dispersions in a 12.5 wt% TPU/DAA suspension with different pre treatments. a) Ammonia Plasma Functionalisation, b) Oxygen Plasma Functionalisation c) Un-functionalised GNPs

3.2.4 Solvent Selection

Diacetone Alcohol was selected as the solvent due to its ability to dissolve the resin system, it's high boiling point, giving long life on the screen, it's current use in

commercial formulations and it's low toxicity making it suitable for mass production in a screen-printing facility where the screen-printing floor is often poorly ventilated.

3.2.5 Substrate

Polyethylene Tetrephalate (PET) was selected for the initial experimentation into the dispersion of GNPs and the electrical properties of the ink as its low surface roughness, relative to the thermoplastic polyurethane substrates, would allow for easy determination of the dispersion of the particles within the coating.

A heat transfer Thermoplastic Polyurethane was selected for the determination of the electromechanical properties of the ink as well as the heater performance under strain. TPU was selected as this is a soft stretchable substrate commonly used within the sports textile industry.

3.3 Ink Synthesis

3.3.1 Resin System Synthesis

Thermoplastic polyurethane pellets were dissolved in 4-Hydroxy-4-Methyl-2-Pentanone (DAA) (99% Sigma Aldrich) by overhead mixing the pellets in the solvent while the solution was heated to 70-100°C using a hot plate (Fig. 3.3.1). The weight of all of the components used within the process were weighed before and after mixing, with any weight loss assumed to be due to solvent evaporation.

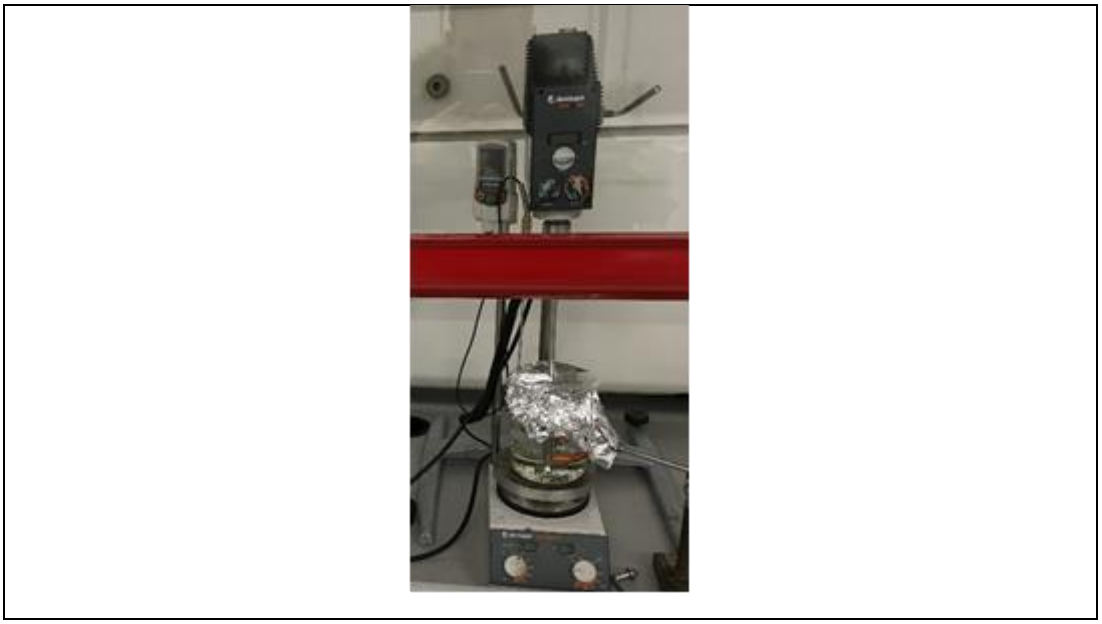

Figure 3.3.1 - Resin synthesis using an overhead stirrer and hot plate

This amount of solvent was then added back into the varnish system and mixed for a further 10 minutes using an overhead stirrer until visibly mixed. A sample of the ink

was then taken and measured using the rheometric procedure described below to ensure consistency before any particles were added.

3.3.2 Particle Wetting

Nanocarbon particles are often agglomerated in powder form owing to their high surface area and inert surface. Therefore, work needs to be done to break down these agglomerates to reduce the particles to primary particles to allow their surface to be wet by the polymer and the solvent.

The nanocarbons used in the inks were weighed directly into their pots. Correct quantities of the TPU/DAA resin were then added to the dry nanocarbons, these were stirred by hand and left for 24 hours to allow the particles to wet. These were then further dispersed using a paint shaker (Minimix MK 4, Merris Development Engineering Ltd, Maidenhead, UK) to ensure good dispersion of the mill base. This procedure was a proven dispersion method for carbons developed within the Welsh Centre for Printing and Coating [3].

3.3.3 Three-roll milling

The mill base of all the inks were stirred to ensure the particles were evenly distributed throughout the mill base then dispersed using a three-roll mill (EXACT advanced technologies GmbH) using the same procedure outlined by Phillips et al [4] and shown in Table 3.3.3, with the mill cleaned between passes 3 and 4.

Table 3.3.3 - Three roll milling procedure

Pass	Back Gap (um)	Front Gap (um)	Speed (rpm)
1	60	15	200
2	40	10	200
3	20	5	200
4	20	5	200

Figure 3.3.3 - Exact Triple Roll Mill

3.4 Rheometry

3.4.1 Stress Controlled Rheometry

A stress-controlled rheometer (Malvern Kinexus Pro) was used to assess the rheological properties of the dispersions. A 40mm diameter roughened parallel plate geometry was used to negate the risk of wall slip due to the heavily filled nature of the fluids. A gap of 0.5mm was found experimentally to minimise wall slip and prevent particles jamming. The temperature was kept constant at 25°C using a Peltier plate system.

3.4.2 Shear Rheology

In flow, elements of a liquid are deforming and adjacent points in the liquid are moving relative to one another [5]. There are two main types of flow, shear flow where particles are flowing past or over one another (Fig. 3.4.2.1a) and extensional flow where particles are moving away from one another (Fig. 3.4.2.1b) [5].

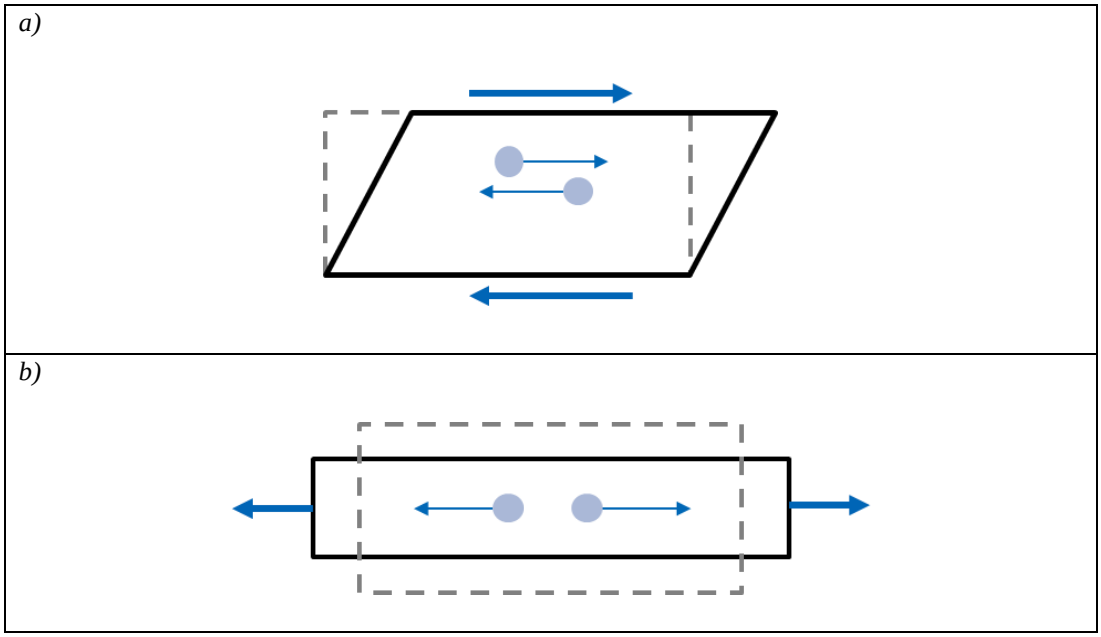

Figure 3.4.2.1 – Particles in flow a) Particles moving past one another in shear flow, b) Particles moving away from one another in extensional flow

Figure 3.4.2.2 demonstrates the situation when a force, F, (N), is applied to the top surface of a fluid of area, A, (m^2) a height, h, (m) from a stationary edge. The shear stress, σ, (Pa) represents the (F) per unit area (A) creating or produced by the flow (Equation 3.4.2.1).

$$\sigma = \frac{F}{A}$$

Equation 3.4.2.1 – Shear Stress

The simple shear, γ, is calculated by dividing the deformation, δ, by the height from the stationary edge, h (Equation 3.4.2.2).

$$\gamma = \frac{\delta}{h}$$

Equation 3.4.2.2 – Simple Shear

Where the velocity, V, is calculated from the change in deformation, δ, in time, t, (seconds) (Equation 3.4.2.3).

$$V = \frac{d\delta}{dt}$$

Equation 3.4.2.3 - Velocity

The shear rate, $\dot{\gamma}$, measured in reciprocal seconds, s^{-1}, represents the change in velocity, V, with increasing distance, h, from the stationary edge (Equation 3.4.2.4).

$$\dot{\gamma} = \frac{dV}{dh}$$

Equation 3.4.2.4 – Shear Rate

From this the viscosity, η, (Pa s) which gives the ratio of shear stress to shear rate, often used to describe a fluids resistance to flow can be calculated (Equation 3.4.2.5).

$$\eta = \frac{\sigma}{\dot{\gamma}}$$

Equation 3.4.2.5 – Shear Viscosity

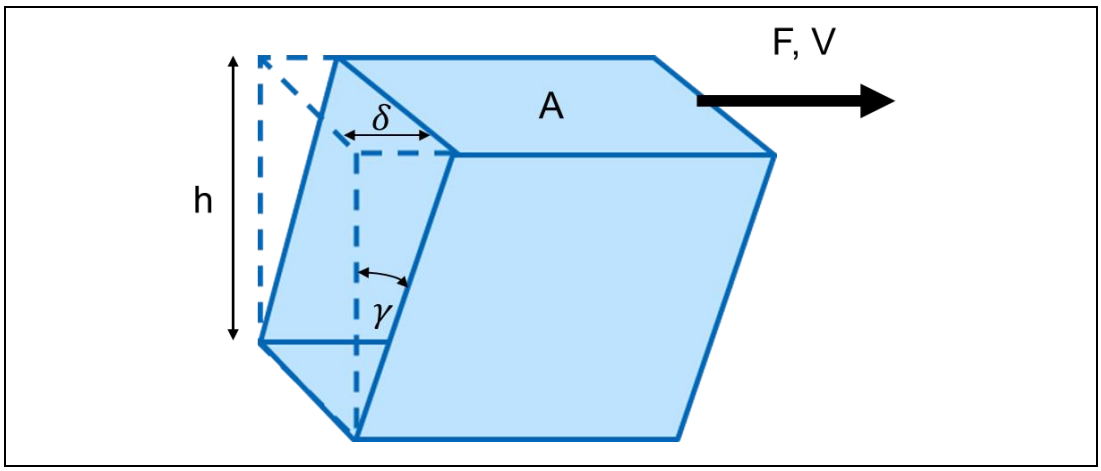

Figure 3.4.2.2 - The effect of force being applied to the top surface of a fluid while the bottom edge remains on a stationary plate

Shear Rheometry with a stress controlled parallel plate rheometer (Fig. 3.4.2.3) works by applying a force, F, over the known area of the plates, A, to calculate the shear stress, σ (Pa) (Equation 3.4.2.1). The geometry velocity, V, is then measured, with a gap of known height, h, set before testing, to calculate the $\dot{\gamma}$ (s^{-1}) (Equation 3.4.2.4). From these two parameters η (Pa s) can be calculated.

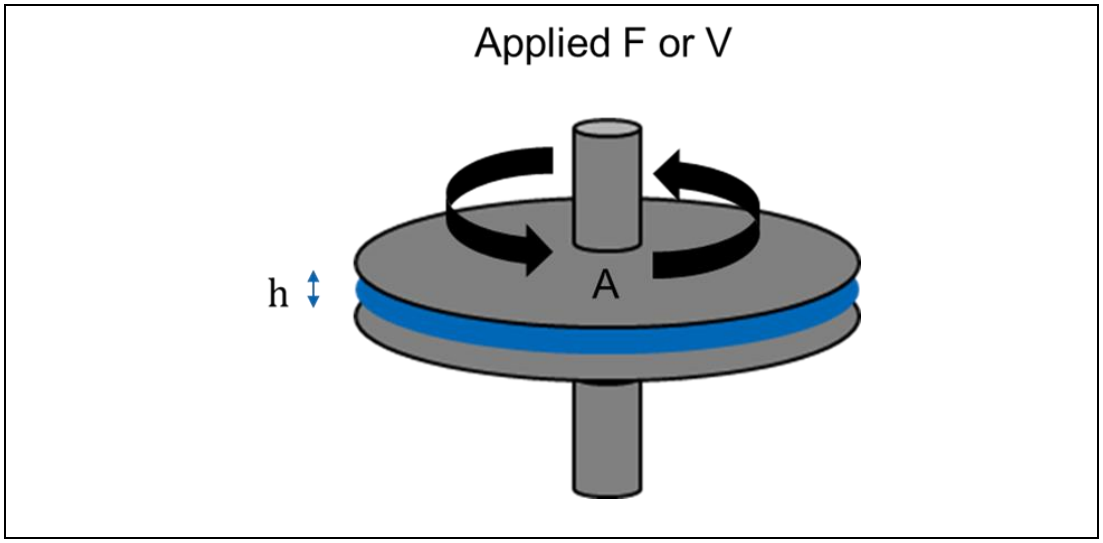

Figure 3.4.2.3 - Shear Rheometry with a stress-controlled rheometer and parallel plate geometries

3.4.3 Experimental Procedure

The phase volumes of GNP can be calculated using a density of 2.2, 1.2 and 0.93g/cm^3 for the GNPs, TPU and DAA respectively and Equation 3.4.3.1.

$$\phi_{GNP} = \frac{\left(\frac{M_{GNP}}{\rho_{GNP}}\right)}{\left(\left(\frac{M_{GNP}}{\rho_{GNP}}\right) + \left(\frac{M_{TPU}}{\rho_{TPU}}\right) + \left(\frac{M_{DAA}}{\rho_{DAA}}\right)\right)}$$

Equation 3.4.3.1 How to calculate phase volume GNP

Where;

ϕ = *Phase volume*

M = Mass (g)

P = Density (g/cm^3)

Table 3.4.3.1 – Mass, volume and phase volume of GNP inks

Mass (g)			Volume (cm^3)			Phase Volume (ϕ)		
GNP	TPU	DAA	GNP	TPU	DAA	GNP	TPU	DAA
0	12.5	87.5	0	10.417	94.086	0	0.100	0.900
15	10.625	74.375	6.818	8.854	79.973	0.071	0.093	0.836
20	10	70	9.090	8.333	75.269	0.098	0.090	0.812
25	9.375	65.625	11.364	7.813	70.5650	0.127	0.087	0.786
30	8.75	61.25	13.636	7.292	65.860	0.157	0.084	0.759

Wall slip occurs when the dispersed phase close to the wall is depleted as particles are driven away from the wall, creating an effective lubricating layer at the wall where particle concentration is zero [5]. This results in the material at the wall being essentially different from the bulk. A roughened plate was used to minimise the effect of wall slip. Slip is highly gap size dependent, since the slip layer becomes more important as gap size decreases. Therefore, changes to the viscosity of the measurement with changes to the measuring gap, h (Fig. 3.4.2.3) gap could be indicative of slip. To examine this the viscosity of suspensions at various gap sizes was measured Figure 3.4.3.1.

Between ϕ=0.071 and 0.127 the viscosity is largely independent of gap size indicating the absence of slip over the shear rate measured. Slip can be seen in the highest concentration at $100s^{-1}$, however, using a measuring gap of between 0.4-0.5mm minimised the dependence of the measurement on gap size, especially at shear rates $<80s^{-1}$. From this a gap of 0.5mm was selected to minimise slip over the whole concentration range.

The materials were first subjected to an up-down shear ramp with the measurement of instantaneous viscosity taken from the down ramp (Fig. 3.4.3.2). By first shearing the inks to $100s^{-1}$ before measurement to ensure that all samples had been consistently pre-sheared before measurement. The time between step changes in the shear rate was approximately 6s. Thixotropy is a change in the viscosity of the inks with time of shearing rather than rate of shearing and arises as a result of the time taken for any shear induced change in the microstructure to take place. The up-down shear ramps are sometimes used as a measure of thixotropy, however as thixotropy is a function of both shear rate and time it cannot be accounted for in experiments where both these variables are changed simultaneously [5].

a) 15wt% (ϕ=0.071)

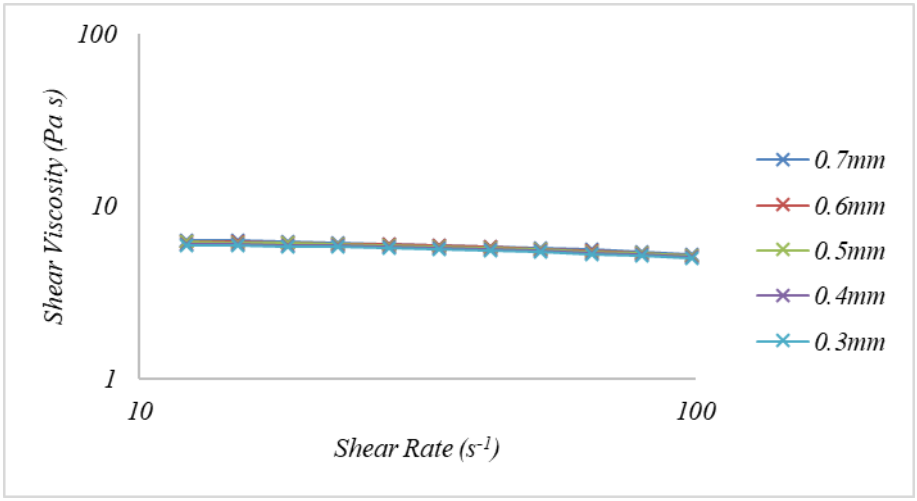

b) 25wt% (ϕ=0.127)

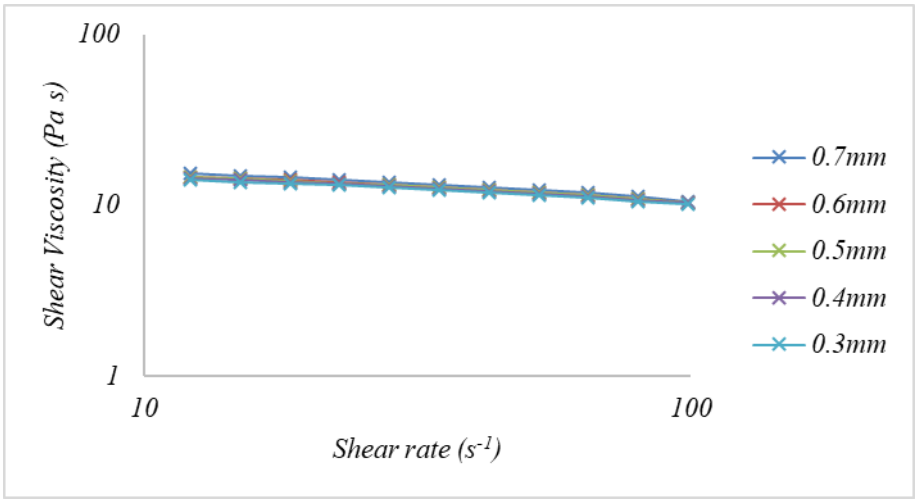

c) 30wt% (ϕ=0.157)

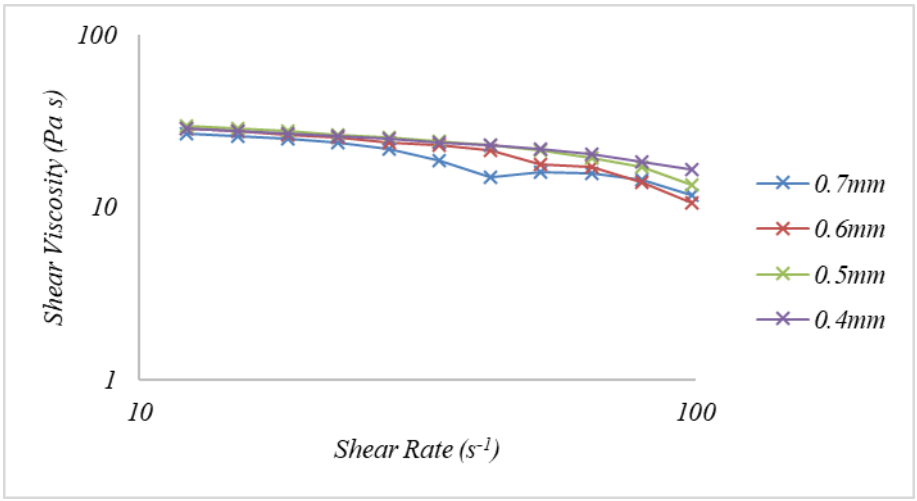

Figure 3.4.3.1 - The effect of measurement gap on the shear dependent viscosity of GNP suspensions at a) 15wt% (ϕ=0.071), b) 25wt% (ϕ=0.127), c) 30wt% (ϕ=0.157)

a) 0wt% (ϕ=0)

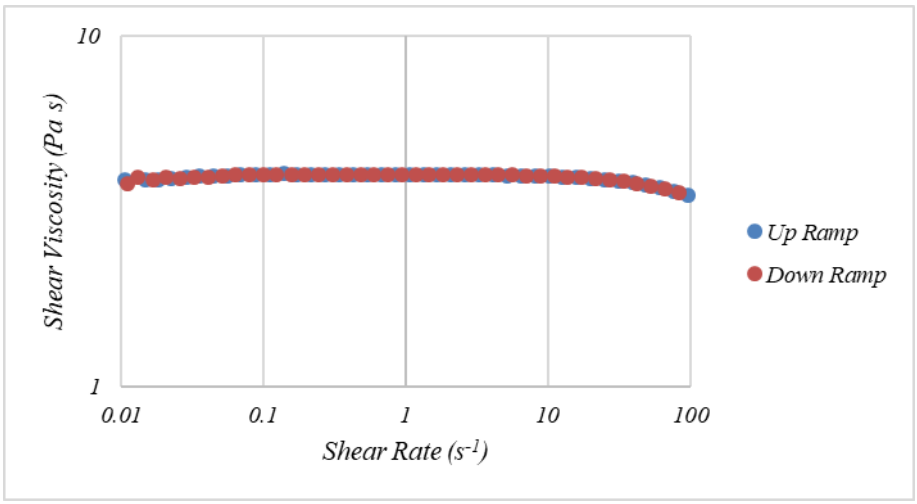

b) 25wt% (ϕ=0.127)

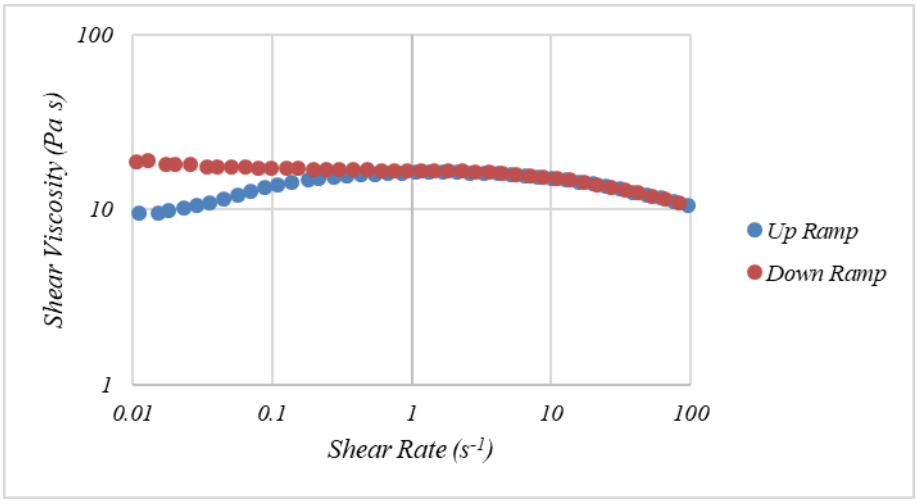

c) 30wt% (ϕ=0.157)

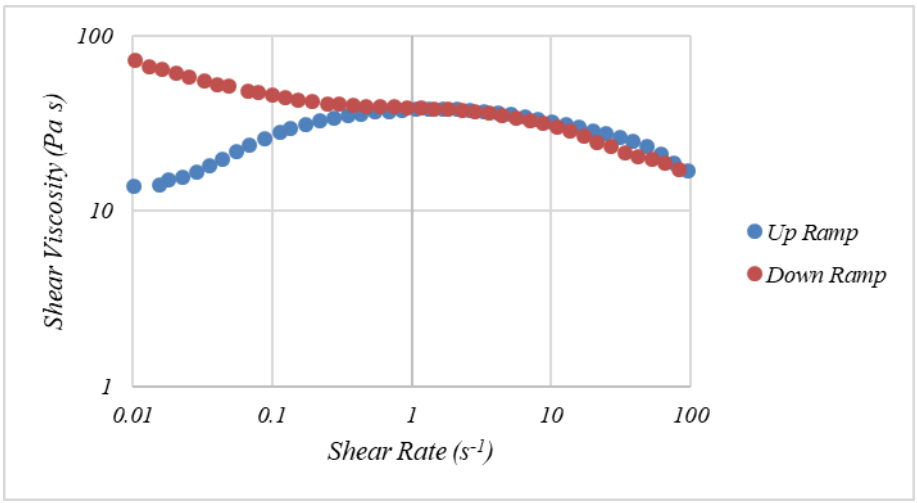

Figure 3.4.3.2- The effect of the initial Up and Down shear ramps on the instantaneous viscosity of NH_3-GNP suspensions a) The unfilled TPU resin (ϕ=0), b) 25wt% (ϕ=0.127), c) 30wt% (0.157)

To examine whether any of the inks had any thixotropic effects equilibrium viscosity measurements were taken by shearing the inks at reducing shear rates between 100-0.1s^{-1} for a period of 150 seconds (Figure 3.4.3.3). Between 15 and 25wt% the inks show little thixotropic effects, with viscosity relatively constant with time of shearing (Figure 3.4.3.3a, b). At the highest concentration of 30wt% there are some thixotropic effects at 0.1,10 and 50s^{-1} as the microstructure of the fluid takes time to build as the shear rate is stepped down (Fig. 3.4.3.3c). At 100s^{-1} there is a decrease in the viscosity of the fluid in time, however, this is likely an artefact of the measurement technique as a result of the 5.9s gap between the downwards shear ramp ending at 0.01s^{-1} and the 100s^{-1} starting being too short, as the increase in shear rate has to break down the structure formed at 0.01s^{-1} in the previous test.

A comparison of the instantaneous viscosity values from the shear ramp and the equilibrium viscosity at 150s^{-1} for the NH_3 GNP inks in the 12.5wt% TPU resin can be seen in (Figure 3.4.3.4). That there is little difference between the instantaneous viscosity values and the equilibrium viscosity values suggests that the time of shearing and rate of ramp have little effect on the measured viscosity for these inks over the shear range measured. The highest concentration, ϕ=0.157, GNP ink shows deviation from the viscosity measured from the shear ramp at the highest shear rates of >50s^{-1}, however, the equilibrium viscosity value is still lower than that of the lower concentration which could be a result of the sample slipping at the highest shear rate 100s^{-1} as seen in Figure 3.4.3.1c. As the shear ramp has a greater number of shear related data points and showed good match with the equilibrium data the shear ramp was used to describe the viscosity.

a) 15wt% (ϕ=0.071)

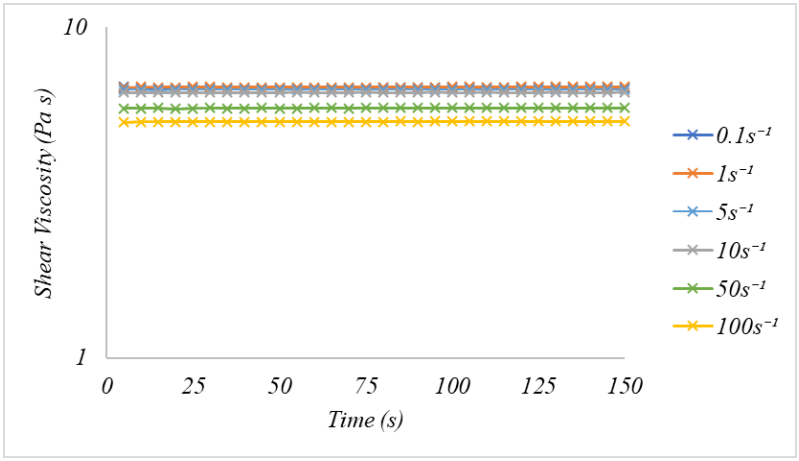

b) 25wt% (ϕ=0.127)

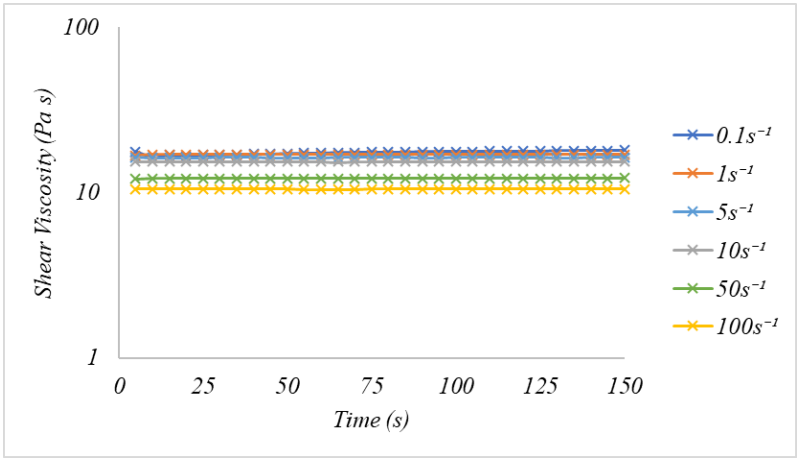

c) 30wt% (ϕ=0.157)

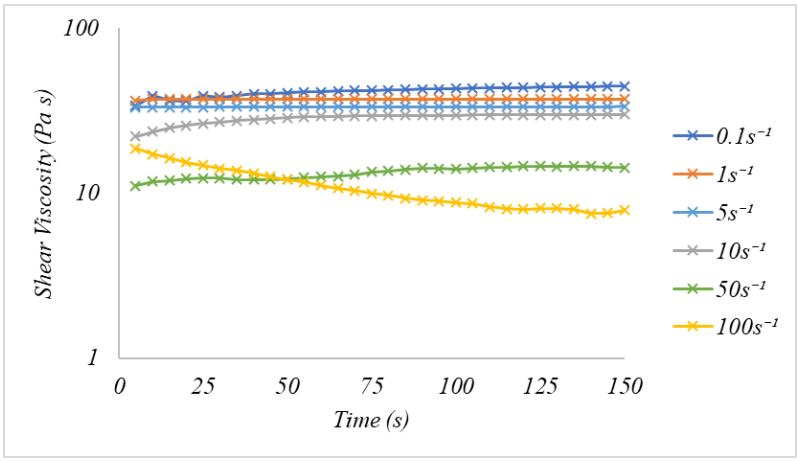

Figure 3.4.3.3 - The effect of time of shearing on the viscosity of NH_3 GNP suspensions at a concentration of a) 15wt% (ϕ=0.071), b) 25wt% (ϕ=0.127), c) 30wt% (ϕ=0.157)

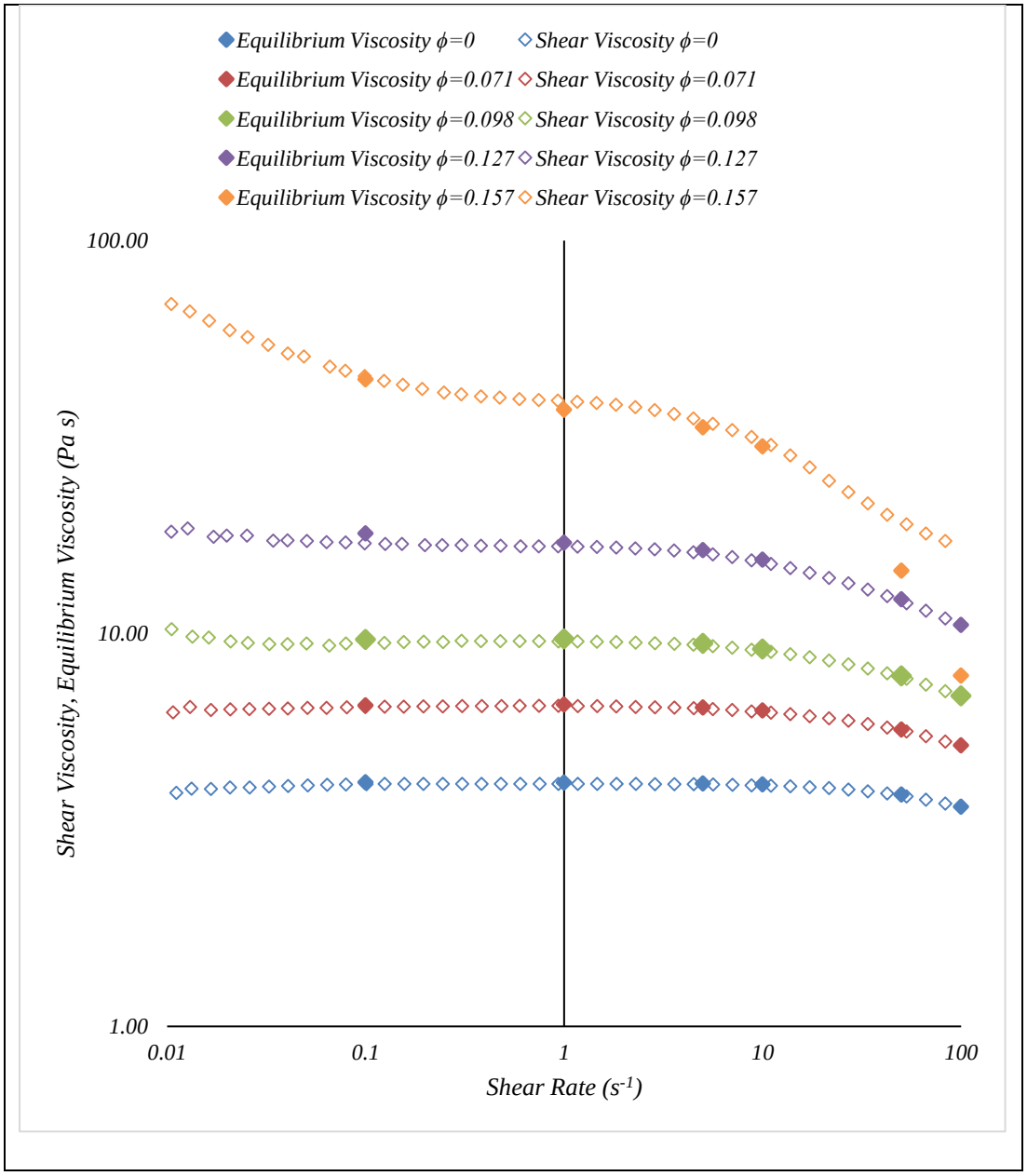

Figure 3.4.3.4 - The effect of shear rate on the viscosity from the shear ramp (open symbols) and the equilibrium viscosity at 150s (filled symbols) of GNP inks at ϕ=0 (Blue), 0.071 (Red), 0.098 (Green), 0.127 (Purple), 0.157(Orange)

Three measurements of each of the GNP inks was performed, with standard deviations of >0.19 Pa s at 1.17s^{-1}, found for all concentrations. By comparing the instantaneous viscosity at all measured shear rates for the unfilled, the lowest filled and the most concentrated GNP suspensions the consistency of the measurement at all shear rates can be visualised (Fig. 3.4.3.5). Therefore, for the shear measurements the results displayed are the mean of the 3 inks and error bars were not used on the rheological graphs.

a) 0wt% (ϕ=0)

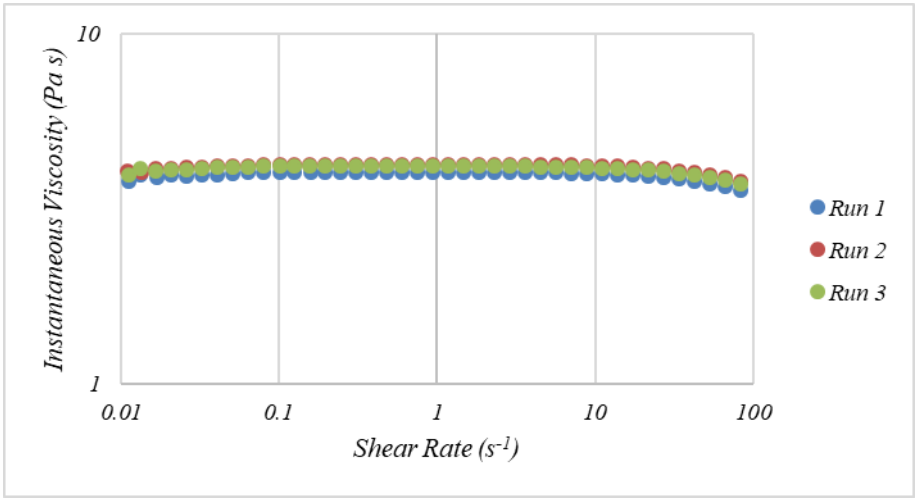

b) 15wt% (ϕ=0.071)

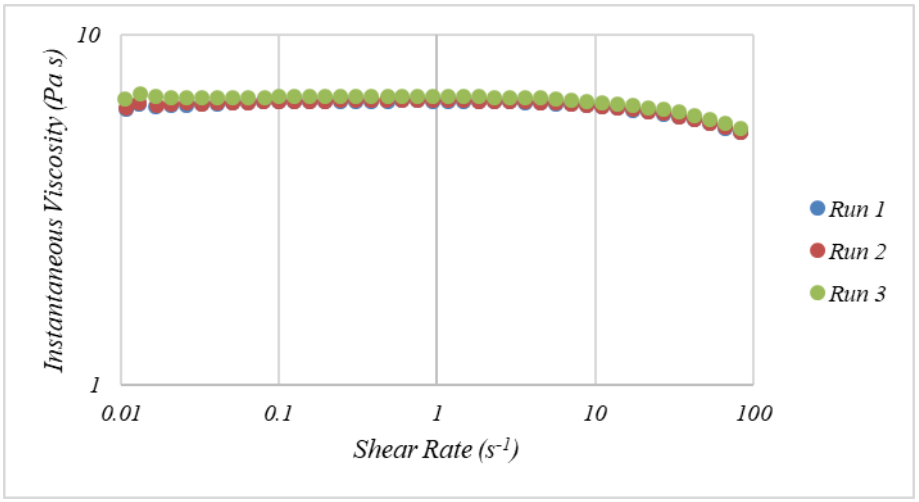

c) 30wt% (ϕ=0.157)

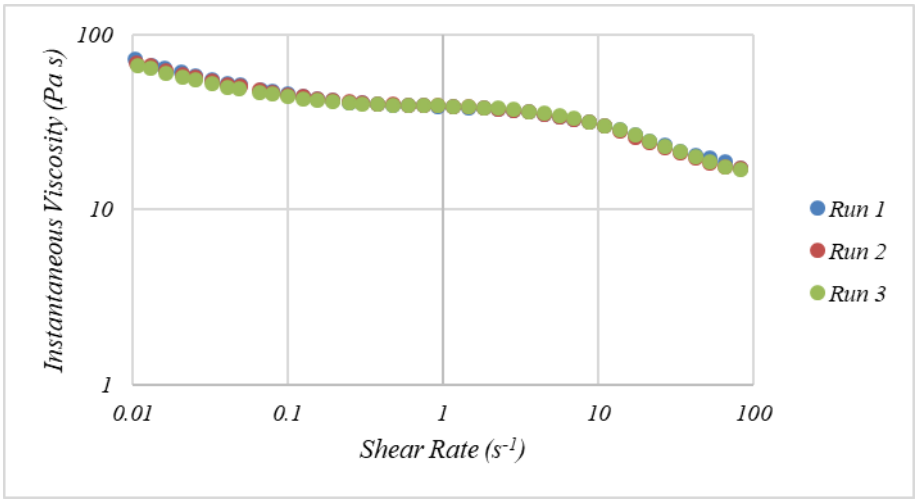

Figure 3.4.3.5 - The effect of shear rate on the shear viscosity of 3 consecutive measurements of NH_3-GNP suspensions in a TPU/DAA resin a) 0wt% (ϕ=0), b) 15wt% (ϕ=0.071), c) 30wt% (ϕ=0.157)

3.4.4 Viscoelasticity

Viscoelasticity is when a material shows both viscous, fluid, behaviours as well as an elastic, solid-like, behaviours. Viscoelastic behaviour at low shear has been postulated as a key indicator of the material transfer process in screen printing, with higher ink elasticity increasing the wet film thickness suggesting the elastic nature of the inks aids ink transfer as increased material is pulled from the screen by the higher elasticity of the material which maintains the integrity of the material filament between the substrate and the screen [6]. There is still a lack of understanding in the processes regarding flow-out and levelling of coatings, however there may be some correlation between elastic recovery and surface irregularity during levelling [7]. This increased elasticity maintains ink integrity as filaments are pulled from the ink film by the screen and could also lead to longer fibres which are unable to relax following printing to leave an uneven surface topography.

Small Amplitude Oscillatory Shear (SAOS) is a non-flow technique that can be used to examine the viscoelastic properties of a material. As a non-flow technique, SAOS measurements must be performed within the linear viscoelastic range (LVR) to ensure that the measurement is not breaking down the microstructure of the fluid. In the LVR *G'* and *G"* are independent of strain amplitude [8]. LVR can be identified using a Strain amplitude sweep.

Before quiescent viscoelastic measurements were made the linear viscoelastic range (LVR) was assessed by taking strain amplitude sweeps at the measured frequencies. In the LVR the viscoelastic parameters, such as *G'*, are independent of strain or strain amplitude [8], demonstrating that the microstructure of the fluid responds without changing [5]. Outside of this region the microstructure is broken down or built up by the flow. The LVR decreased with increasing ϕ as suggested by Barnes [9] (Fig. 3.4.4.1). From this a complex shear strain of 1% was selected as the strain in the viscoelastic measurements.

A frequency sweep was conducted to get the time related Viscoelastic response of materials, with high frequencies corresponding to short times and low frequencies corresponding to long times [5]. A complex shear stress amplitude sweep was taken at the lowest and highest frequencies for the lowest and highest filled systems to ensure that the whole measured frequency range was within the LVR (Fig 3.4.4.2).

From this a frequency of 1% complex shear strain was selected as the strain amplitude for the SAOS measurements.

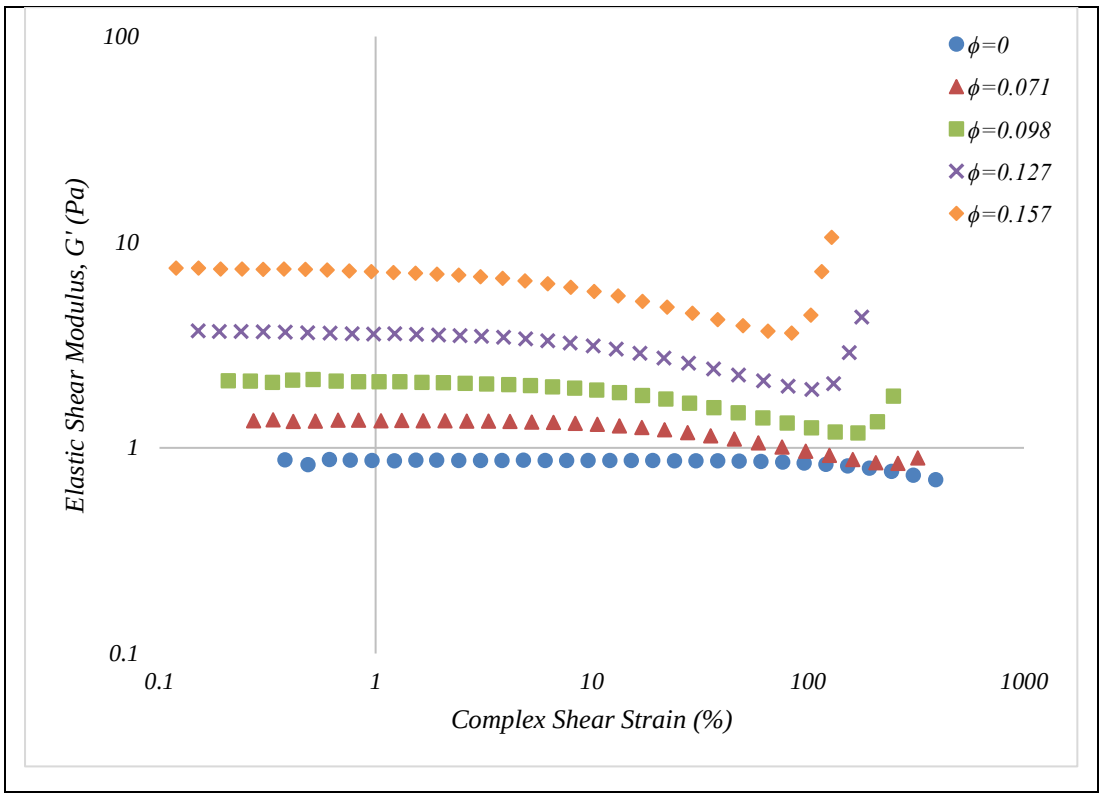

Figure 3.4.4.1 - The effect of complex shear strain on the elastic storage modulus at increasing concentration of NH_3-GNP in a TPU/DAA resin system

SAOS involves imposing a shear stress of known frequency and amplitude within the LVR of the fluid and measuring the strain response of the fluid. This strain response of the material can be split into an in-phase elastic response, *G'*, and a 90° out of phase viscous response, *G"* [5][10][11]. *G'* is a measure of the energy stored by the material during a cycle of deformation and represents the elastic behaviour of the material, while *G"* is a measure of the energy dissipated or lost as heat during the shear cycle and represents the viscous nature of the material [10].

Phase Angle is the ratio of viscous to elastic behaviour of a viscoelastic material, with a theoretically pure Newtonian fluid having a phase angle of 90° and a purely Hookean elastic material having a phase angle of 0° [10][11].

Frequency sweeps are used to identify the time dependent response of a material [10], with high frequencies corresponding to short times and low frequencies corresponding to long times. Elastic behaviour dominates at high frequencies, and therefore short times, and viscous behaviour dominant at lower frequencies and longer times [10].

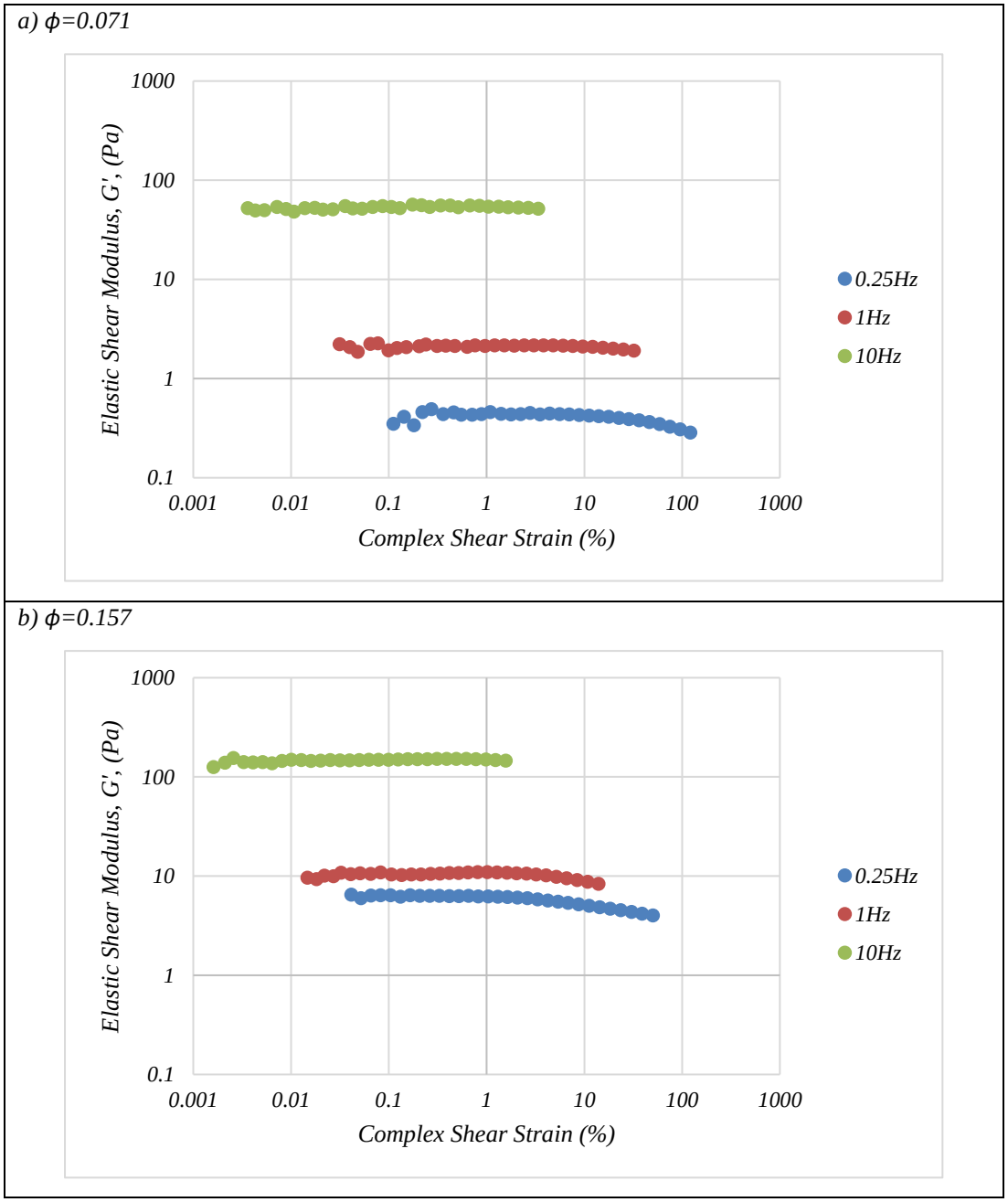

Figure 3.4.4.2 - The effect of complex shear strain at various frequencies on the elastic shear modulus G' for a) 15wt% NH_3 GNP, b) 30wt% NH_3 GNP

3.4.5 Time Stability Measurement Procedure

To assess the time-stability of the suspensions the rheological properties of the inks were sampled at 4-week interviews to identify any changes to the rheological profiles of the inks. The inks were only opened for rheological sampling to reduce the effects of solvent evaporation and to ensure a consistent phase volume of particles within the sample. It was hypothesised that any changes to the dispersion of the particles could be identified by changes to the rheological profiles of the fluids as the particles agglomerated to form particles of a new shape. The GNPs would be expected to show sedimentation owing to the density difference between the

particles and the suspension medium, with any particle agglomeration enhancing sedimentation [12] and is governed by Stokes Law (Equation 3.4.5.1).

$$V = \frac{2\Delta\rho g a^2}{9\eta}$$

Equation 3.4.5.1 – Stokes Law

Where;

a = the radius of the particle

Δρ = The density difference between the particle and the suspending fluid

η = The viscosity of the suspending liquid

g = Acceleration due to gravity

The suspensions were lightly stirred by hand with a flat tipped spatula to re-distribute any sedimentation of particles to ensure a sample representative of the whole ink was extracted for measurement. This process was chosen over mechanical stirring with these low shear rates unlikely to re-disperse any agglomerated particles, while re-distributing any larger particles. There was little resistance provided to the spatula upon stirring and any sediment was readily re-dispersed confirming that no hard cake had formed at the bottom of the pot [13]. The first shear ramp is up to $100s^{-1}$ and therefore would be a greater force than that applied during hand mixing therefore the level of hand mixing had little effect on the consistency of the measurement.

3.4.6 Ink Rheology Modelling

Rheology has been suggested as a means for assessing the dispersion of particles within a suspension. Conducting inks often consist of a semi-dilute or concentrated dispersion of conductive particles within a resin/solvent solution. Established models used to describe the viscosity of semi-dilute and concentrated suspensions, such as the Krieger-Dougherty model, use consist of terms related to particle morphology, namely the intrinsic viscosity, $[\eta]$, and the maximum packing fraction, ϕ_m. The intrinsic viscosity $[\eta]$ increases with particle aspect ratio, with higher aspect ratio particles having a higher intrinsic viscosity. Maximum packing fraction ϕ_m is also a function as aspect ratio as maximum packing factor decreases with increasing aspect ratio as high aspect ratio particles pack less efficiently than spherical ones, however

maximum packing factor is also a function of particle size distribution, particle flocculation, flow and particle size distribution. By fitting of these rheological models to experimental data using the intrinsic viscosity and maximum packing fraction as fitting parameters the work aimed to gain information about the particle shape and aspect ratio. The Solver add on in Microsoft excel was used to fit a curve to the experimental data for the instantaneous viscosity at $1.17s^{-1}$. Non-linear least squares fitting was used to fit the suspension rheology models to the experimental data. $1.17s^{-1}$ was selected as the shear rate to allow for comparison with other suspensions within the literature. The Generalised Reduced Gradient (GRG) non-linear curve fit algorithm was selected with 100000 iterations using the intrinsic viscosity, $[\eta]$ and maximum packing (ϕ_m) as the fitting parameters as suggested by Mueller et al [14]. Sensible starting values for the fitting parameters were identified and constraints of $50>[\eta] > 0$ and $0.157 < \phi_m < 0.64$ set. Goodness of fit was assessed using root mean square error (RMSE). Using equations such as those proposed by Barnes, the intrinsic viscosity can then be used to estimate the aspect ratio of the particles. As the GNPs are high aspect ratio nano-particles prone to agglomeration it was hypothesised that any change to the aspect ratio of the particles as a consequence of poor dispersion quality or agglomeration of the particles could be seen as a change in the intrinsic viscosity.

3.5 Printing

The inks were printed on a DEK 248 semi-automated flatbed screen printing press with a polyester mesh with 61 threads per cm, 64um thread diameter a 13um emulsion, 2.5mm snap off, 130mm length diamond squeegee a 12kg squeegee force and 70mm/s flood/print speed. These settings were used to allow for direct comparison of the electrical and print performance of the new flexible inks with the Haydale conductive ink (IGSC02002) used in the original heater patent. The screen design included a 4.5mm square patch for bulk thickness and sheet resistance measurements along with a set of 25mm lines of different thickness to assess the ability to print fine features (Fig. 3.5.1).

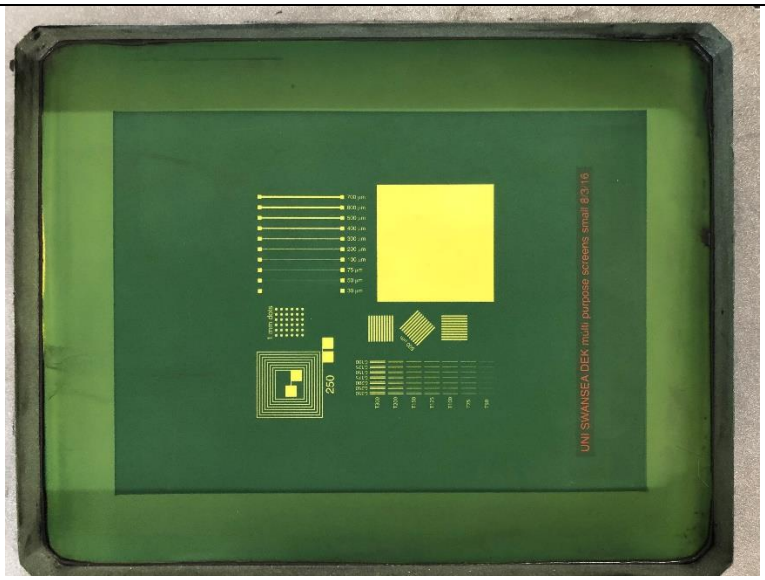

Figure 3.5.1 - Polyester test screen design consisting of a block area and 25mm long lines

The inks were printed onto PET DuPont Melinex (HiFi Films) to allow for assessment of the electrical and surface properties of the inks and to give a direct comparison with the Haydale ink. The first four prints were ignored as they could be contaminated by the cleaning fluid used to prepare the screen and may have been subject to any initial process transients [6]. Diacetone Alcohol was used as the solvent within the ink, with the prints dried in an SC technical dryer at 70°C for a residence time of 10 minutes and left for a further 24 hours on drying racks before any characterisation. This drying procedure was selected as it was observed that the coatings had a visual change when dry.

To assess the tensile properties of the inks they were printed onto a Stretchable TPU Substrate (Greenstik Materials) using the same process settings. This print used a 54-70 mesh polyester mesh to give a thicker ink deposit to reduce the number of layers required to produce the prototype heating garments. The screens consisted of 15x5 and 20x5 rectangular patches that were to form the heater elements. These were also used as samples for the electromechanical testing using a Hounsfield material tester.

3.6 Surface Characterisation

To calculate the printed thickness 4 measurements were taken from the edges of each of 4.5x4.5mm squares using white light interferometry (NT9300, Veeco Instruments, Inc., Plainview, NY, USA). This was done using a 5x Lens and a 1.00x Field of View. Surface topography of the ink has been linked to substrate adhesion, electrical

properties and performance in multi-layer devices. Therefore, as the printed heater is required to be a conductive multi-layer device it is imperative that the process lays down smooth consistent films. The average surface roughness, Ra, was taken away from the edge of the square to avoid any edge effects. The microstructure of the prints was examined using a Scanning Electron Microscope at 6000x magnification. To characterise the stretchable inks and the heaters

The printed thickness of the coatings for the heaters and mechanical testing was calculated by measurements the step height between the edge of the coating and the substrate on 5 of the prints for each ink (Fig. 3.6.1a). The roughness for the heaters and mechanical testing was calculated by taking 3 measurements from the centre of the 3 heaters away from any edge affects (Fig. 3.6.1b).

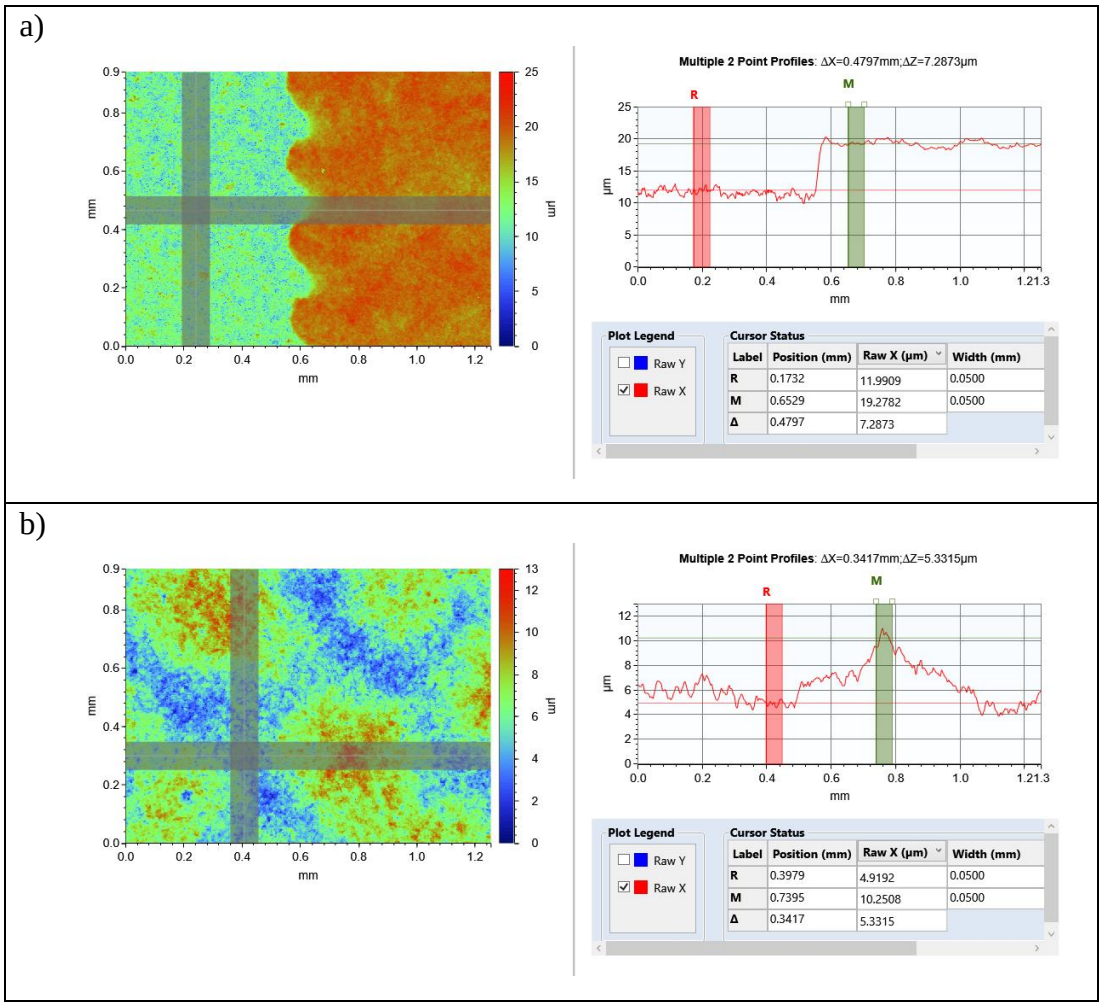

Figure 3.6.1 - Example of white light measurement from a) The edge of a single layer carbon print, b) The centre of a single layer carbon print

3.7 Resistivity Measurements

The literature review identified the need for low resistivity carbon-based inks that could work at low voltages allowing them to be safely used in wearable heating applications. As the new inks were designed to be a flexible replacement for the Haydale IGSC2002 ink used in the original patent it had a targeted resistance of <100Ω/□ normalised at 25.4um. As this ink is to be used in heater applications where the direct heat output is influence by the resistance of the coating it is important that the ink shows consistency over a print run.

For the characterisation of the ink's electrical performance in Chapters 4 and 5 the sheet resistance of the 45mm square was measured using the four-point probe method. A SDKR-13 probe (NAGY Messsysteme GmbH) with a tip distance of 1.3mm was used with a Keithley 2000 multimeter. A correction factor of 4.5 was used as proposed by Smits [15].

To calculate the electrical properties of the samples for electromechanical testing a two-point method was used to calculate the resistance using a Keithley 2000 multimeter. The path length of the measurement was 14x0.5cm. Resistivity of the sample was also calculated from this method to give greater information about the material properties of the coating. The bulk resistivity for the samples was calculated from the two-point resistance measurements along the 14x0.5cm path length using the formula;

$$R = \frac{\rho L}{A}$$

Equation 3.7.1 – Electrical Resistance

Where;

R = Resistance (Ohms)

ρ = Resistivity (Ohm·cm)

L = Length (cm)

A = Cross sectional area (cm^2)

3.8 Mechanical Testing

The inks were screen-printed onto the thermoplastic polyurethane substrate (TPU) and cured using the method described in Chapter 3.4. British Standards for the

determination of tensile properties of plastics, BS EN ISO 527-1:2012, and films and sheets, BS EN ISO 527-3:1996, were used to guide the measurement of the tensile properties of the coatings [16] [17]. Three 15x0.5cm test strips were cut from the prints using a sharp knife, with the edges of the samples inspected for any notches or tears. The samples were then carefully removed from the TPU backing plastic taking care not to strain the sample. Adhesive copper tape was attached 0.5cm from opposing ends of the test sample to leave a 14cm electrical path length. Clips were then attached to ensure good electrical contact between the wires and the flat printed samples. Resistances were measured continuously during tensile testing using a source meter (Keithely). Tensile testing was performed using a Hounsfield Tensile Tester with a 100N load cell, a gripping distance of 10cm and an extension speed of 50mm/min (Fig 3.8.1a). The samples were tested in a controlled lab environment (18±1°C, 50±10% relative humidity). The nominal strain used for testing was calculated from the measured gripping distance. Three samples were tested to extension at break and cycled to 10% nominal strain. Compression tests were also performed using a 10kN load cell and a 200N compressive force on 3 of the carbon samples (Fig 3.8.1b). The samples were compressed with the ink on the outside radius initiating large tensile strains, to simulate the inks being creased during use. The heat performance of the samples was tested by measuring the temperature output of the 15x5cm heaters, described later, while being strained to 10, 20, 40 and 60% tensile strain until failure of the heaters using a 10KN load cell.

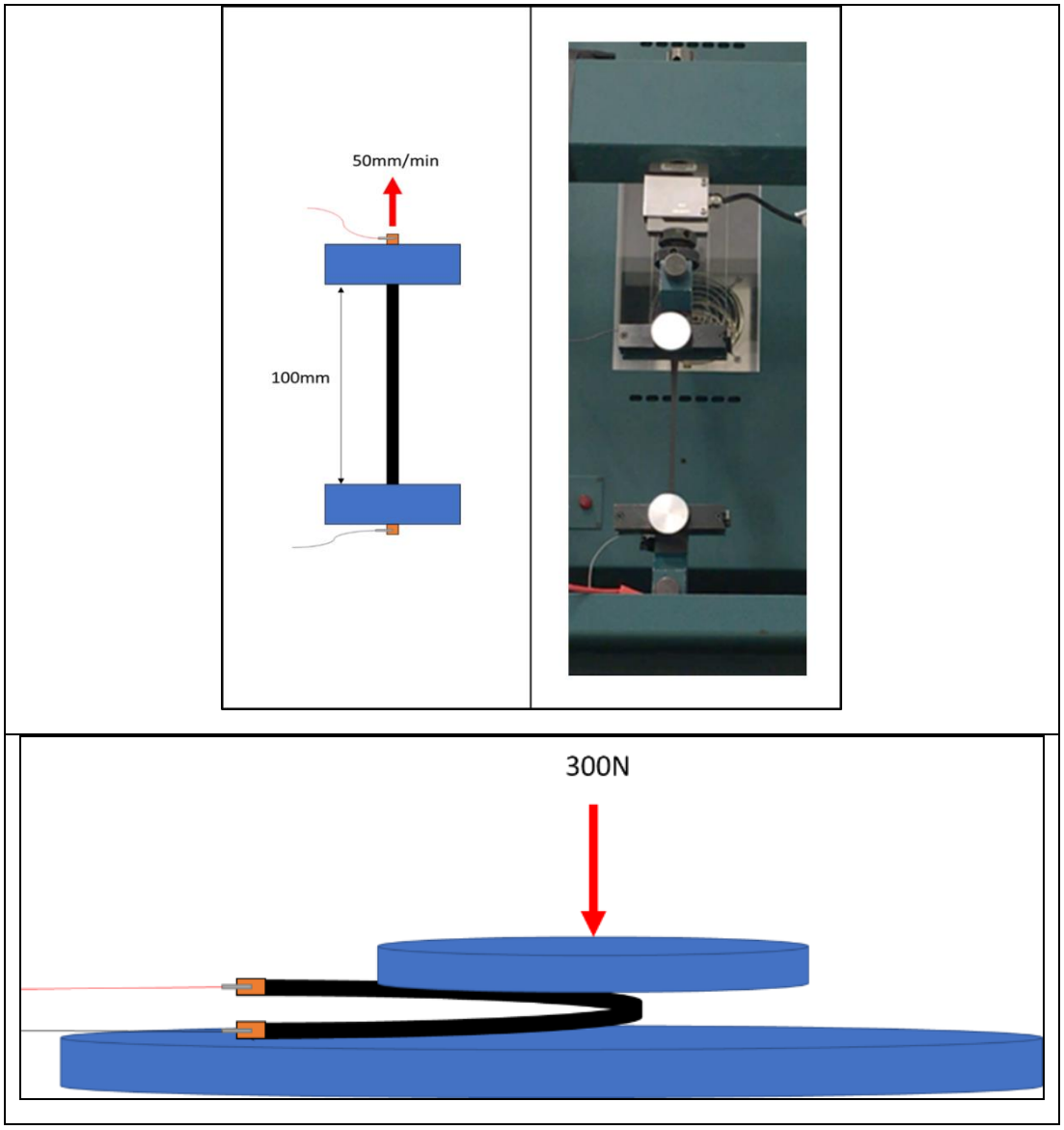

Figure 3.8.1 a) Simultaneous measurement of electrical and extensional tensile properties b) Simultaneous compression and electrical properties

3.9 Heater Fabrication

The stretchable inks were screen-printed (DEK 248) using a 54-70 mesh onto the stretchable TPU substrate to create stretchable printed heaters. The heaters consisted of two 15x5cm layers of flexible GNP/CB, with a 15x0.5cm third layer of flexible silver ink on parallel sides of the heater. Increasing the number of printed layers has been shown to increase the temperature output of the heaters [19]. Two layers of carbon were printed for the electro-mechanical testing of the heater as initial experimentation showed that a two-layer carbon heater could reach >40°C from a 15V power supply. Further information on the effect of the number printed carbon layers on the temperature output of the heaters can be found in section. These heaters were then heat pressed at 160°C and 5bar for 15 seconds onto lycra using a t-shirt

press (Stahls Hotronix Fusion) to create a printed, stretchable, wearable heater system. Copper tape and clips were used to attach the conventional wiring to the flat heater elements.

3.10 Heater Performance

An infrared thermal imaging camera (Optris PI Precision Line) was used to assess the heater performance. The heaters were suspended in the grips of the Hounsfield mechanical testing rig, with only air behind them ensuring that no heat was being transferred to any object. A measure area was taken from the centre of the heaters, and an emissivity of 0.98 used for the filled carbon surface [18]. This same technique was used to measure heat output during the tensile testing, with the measure area focussed on the lower half of the heater near to the stationary grip.

3.11 Closure

Ammonia plasma functionalisation has been hypothesised to be the optimum plasma treatment for enhancing the stability of GNPs in a TPU/DAA resin system and therefore further research in this thesis will largely focus on comparing the performance of ammonia plasma functionalised GNPs (NH_3 GNP) to that of a control. Thermoplastic polyurethane (TPU) and Diacetone Alcohol (DAA) have been identified as creating a compatible binder/solvent system, with the TPU selected for its excellent elongation at break and adhesive properties as well as its compatibility with the TPU substrate to be used in the final application. Diacetone Alcohol was selected for its high boiling point and current use within the screen-printing industry.

A rheological procedure has been set out that shows good reproducibility and low measurement error. The inks have been identified as having low thixotropic properties as identified by their similar instantaneous and equilibrium viscosities. The linear viscoelastic range of the materials has been identified for different concentrations and frequencies, with a complex shear strain of 1% selected as the amplitude for the measurement of the viscoelastic properties.

The procedure for screen-printing as well as for the characterisation of the final prints has been set out to allow for comparison of the inks across the development and important measurement characteristics identified.

3.12 References

[1] Birla Carbon, “Speciality Carbon Blacks,” Birla Carbon, 2017. [Online]. Available: https://birlacarbon.com/wp-content/uploads/2017/02/Specialty-Blacks-Product-Portfolio-Brochure.pdf. [Accessed 23 01 2020].

[2] Huntsman Corporation, “Huntsman Adhesives Irostics,” Huntsman Corporation, [Online]. Available: http://www.huntsman.com/polyurethanes/Media%20Library/a_MC1CD1F5AB7BB1738E040EBCD2B6B01F1/Products_MC1CD1F5AB8081738E040EBCD2B6B01F1/Adhesives_former_MC1CD1F5B06E31738E040EBCD2B6B01F1/Literature1_MC1CD1F5B093D1738E040EBCD2B6B01F1/files/a_irostic_4pg.pdf. [Accessed 23 01 2020].

[3] C. Phillips and D. Beynon, “Private communication with Chris Phillips and David Beynon,” Swansea, 2015.

[4] C. Phillips, A. Al-Ahmadi, S.-J. Potts, T. Claypole and D. Deganello, “The effect of graphite and carbon black ratios on conductive ink performance,” *Journal of Materials Science,* vol. 52, pp. 9520-9530, 2017.

[5] H. A. Barnes, A Handbook of Elementary Rheology, Aberystwyth: University of Wales Institute of Non-Newtonian Fluid Mechanics, 2000.

[6] E. Jewell, S. Hamblyn, T. Claypole and D. Gethin, “The impact of carbon content and mesh on the characteristics of screen printed structures,” *Circuit World,* vol. 39, no. 1, pp. 13-21, 2013.

[7] T. F. Tadros, Colloids in Paints, Weinheim: WILEY-VCH Verlag GmbH & Co. KGaA, 2010.

[8] H. A. Barnes, J. F. Hutton and K. Walters, An Introduction to Rheology, Amsterdam: Elsevier Science Publishers, 1989.

[9] H. A. Barnes, “A Review of the Rheology of Filled Viscoelastic Systems,” *Rheology Review,* pp. 1-36, 2003.

[10] N. Willenbacher and K. Georgieva, “Rheology of disperse systems,” in *Product Design and Engineering*, 2013, pp. 7-49.

[11] J. Claypole, Application of advanced rheometric tecniques to printing fluids, Swansea University Thesis, 2015.

[12] D. J. Shaw, Introduction to Colloid and Surface Chemistry, Oxford: Butterworth-Heinemann, 1992.

[13] T. C. Patton, Paint Flow and Pigment Dispersion, New York: John Wiley and Sons, 1979.

[14] S. Mueller, E. Llewellin and H. Mader, “The rheology of suspensions of solid particles,” *Proceedings of the Royal Society A,* vol. 466, pp. 1201-1228, 2010.

[15] F. Smits, “Measurement of sheet resistivities with the four point probe,” *Bell Syst Technical J,* vol. 37, pp. 711-718, 1957.

[16] British Standards Institution, “BS EN ISO 527-1:2012 Plastics - Determination of Tensile Properties Part 1 General Principles,” 2012. [Online]. [Accessed 05 02 2020].

[17] British Standards Institution, “BS EN ISO 527-3:1996 Plastic - Determination of tensile properties - Part 3: Test conditions for films and sheets,” 1996. [Online]. [Accessed 05 02 2020].

[18] Engineering Toolbox, “Emissivity Coefficients Materials,” Engineering Toolbox, 2003. [Online]. Available: https://www.engineeringtoolbox.com/emissivity-coefficients-d_447.html. [Accessed 7 10 2019].

[19] D. Deganello, Y. Mouhamad and A. Claypole, “Heatable garment, fabrics for such garments, and methods of manufacture”. WO Patent WO2017129663A1, 3 8 2017.

Chapter: 4 Using Graphite Nanoplatelets as the functional component of conductive Inks in an elastomeric binder

Graphite nano-platelets were identified as a candidate for the main conductive filler to create a new flexible conductive ink, combining the in-plane electrical conductivity of graphitic carbon with a high surface area and potential to be functionalised to improve compatibility with the thermoplastic polyurethane (TPU) resin system. Experiments in Chapter 3 identified Ammonia plasma functionalised Graphite Nano-platelets (NH_3 GNP), creating more stable inks compared to oxygen functionalised GNPs (O_2 GNPs) and unfunctionalized GNPs (R1 GNPs).

This chapter initially looks to examine the effect that varying concentrations of NH_3 GNPs has upon the rheological properties of the TPU/DAA resin system. The effect of plasma functionalisation on the print performance and time stability of GNP/TPU/DAA inks is then examined by comparing the print characteristics and rheological properties of the NH_3 GNPs over time to an Un-treated control (R1 GNPs). Finally, as the main purpose of the GNPs is to provide a smooth, conductive surface to give improved adhesion and electrical conductivity, the sheet resistance and topography of the NH_3 GNP inks is compared at varying concentrations and a maximum GNP loading concentration for optimised topography and conductivity identified.

4.1 Using Rheology to Quantify the dispersion of GNPs

4.1.1 Introduction

Increasing the conductive carbon content within the ink is often seen as a method to increase the electrical conductivity, however increasing the carbon content will also increase the viscosity and elasticity of the inks [1]. The quality of screen-printed patterns is generally dependent on the ink rheology, printer hardware (screen, squeegee, substrate) and the printing process [2], therefore, any changes to the rheological properties of the inks will impact subsequent print quality. The flow of the ink through the mesh or the stencil is significant since it determines the uniformity of printed surface which is an important feature of conductive circuits [2].

Fluid microstructure plays a large role in the measured viscosity. Increasing the concentration of particles has a large effect upon the viscosity of suspensions. The presence of individual particles means the diversion of streamlines and hence higher viscosity. At higher concentrations further resistance arises as particles must move

out of one another's way to align with the flow. At the highest concentrations even more resistance is encountered as flocs form that trap the continuous phase and stop it deforming at the same rate as the rest of the microstructure [3].

Dispersion of Nano-fillers is a key issue in governing the properties of composites [4][5]. However, achieving good dispersion of nanocarbons within a fluid has been proved to be difficult as a result of the inert, hydrophobic, ultra-high interfacial area per volume and highly agglomerated nature of carbon nanomaterials [6][7][8][9]. Atomic motions in neighbouring particles drive carbon nanomaterials together, and if not counteracted, the van der Waals forces cause particles to adhere upon contact [10][11].

Rheology has been suggested as a method for assessing the dispersion of carbon nanomaterials in a fluid, with a suspension of well dispersed nanoparticles having different rheological behaviour to that of their agglomerated or flocculated counterparts [12][13][14].

The ability to model suspensions is a powerful tool that allows for prediction of the properties of a fluid, guiding future formulation work using GNPs. The fitting of these models to the experimental data can also be used to gain information about the particles suspended within the fluid. The Krieger-Dougherty model can be fitted to experimental data with ϕ_m and $[\eta]$ used as the fitting parameters to derive information about the maximum packing factor and the particle aspect ratio [14]. Particle asymmetry has a strong effect on $[\eta]$ and ϕ_m and hence on the viscosity concentration relationship [3]. The zero shear $[\eta]$ increases with particle aspect ratio as the high aspect ratio particles occupy a greater volume in the flow [15]. Higher aspect ratio particles lead to higher values of $[\eta]$ and lower values of ϕ_m as the particles pack poorly producing greater increases in viscosity for higher aspect ratio particles than spheres at the same phase volume [3][9].

This initial work aims to use shear and oscillatory rheology to study the effect of increasing NH_3 GNP concentration on the rheological properties of the fluid. Suspension rheology models are then fitted to the experimental data to allow for prediction of the effects of the particles on viscosity and to gain information about the aspect ratio of the particles within the fluid.

4.1.2 Materials and Methods

4.1.2.1 Materials

Ammonia plasma functionalized GNPs (NH_3 GNP) (Haydale Ltd) and a commercially available thermoplastic polyurethane (TPU) (Huntsman Irostic S7614) were used. The TPU was dissolved in Diacetone Alcohol (Sigma Aldrich) at 70°C to create the low viscosity (≈4 Pa.s) resin system.

4.1.2.2 Ink Synthesis

Densities of 2.2g/cm^3 was used to calculate the volume of the NH_3 GNPs, with the composition of the various inks available in Table 4.1.2.1 [16]. Four phase volumes (ϕ), ϕ=0.071, 0.098, 0.127, 0.157 of NH_3 GNP were wet in the TPU resin system for 24 hours. Phase Volume represents the volume of the dispersion occupied by the dispersed phase instead of weight fraction as in the suspension viscosity models based upon Einstein's model for particle dispersion [10].

The inks were then further dispersed using the procedure described in Chapter 3. Directly following milling the suspensions were then again mixed with the paint shaker as a further distributive mixing step.

Table 4.1.2.1 Composition of GNP inks

	wt %		
Name	GNP	TPU	DAA
ϕ=0	0	12.5	87.5
ϕ=0.071	15	10.625	74.375
ϕ=0.098	20	10	70
ϕ=0.127	25	9.375	65.625
ϕ=0.157	30	8.75	61.25

4.1.2.3 Method

The shear and viscoelastic properties of the unfilled resin and the four concentrations of NH_3 GNP were tested using the rheological test method described in Chapter 3. The inks were then screen-printed onto PET (HiFi Films) using the method outlined in Chapter 3. Scanning electron microscope (SEM) images were taken to study the dispersion of the GNPs in the final print. The measurement tool within ImageJ [17] was used to estimate the GNP diameter and thickness.

4.1.3 Particle Characterisation

There was a wide particle size distribution of the GNPs with platelet diameter ranging from ≈1-8μm (Fig. 4.1.3.1). The platelets have generally aligned to form a paved type structure, however within this structure there are large gaps where the high aspect ratio platelets are unable to pack efficiently, with GNPs at various angles relative to the substrate.

a) 3000x magnification

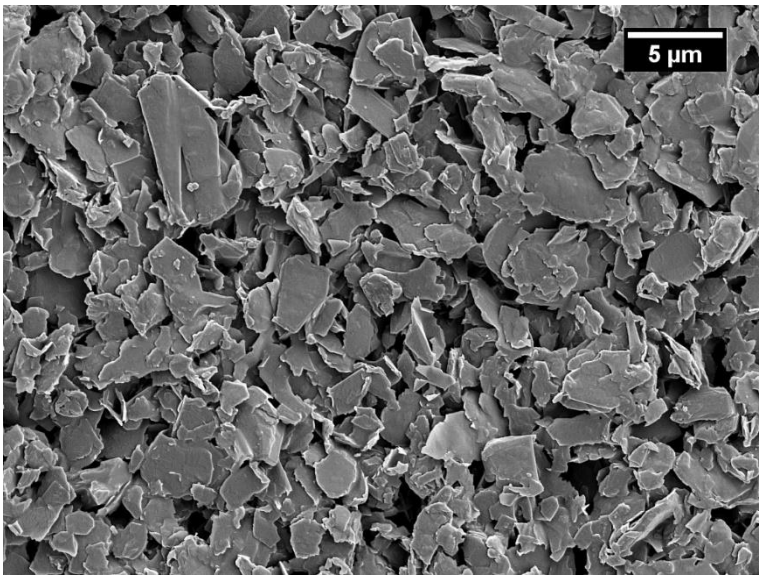

b) 6000x magnification

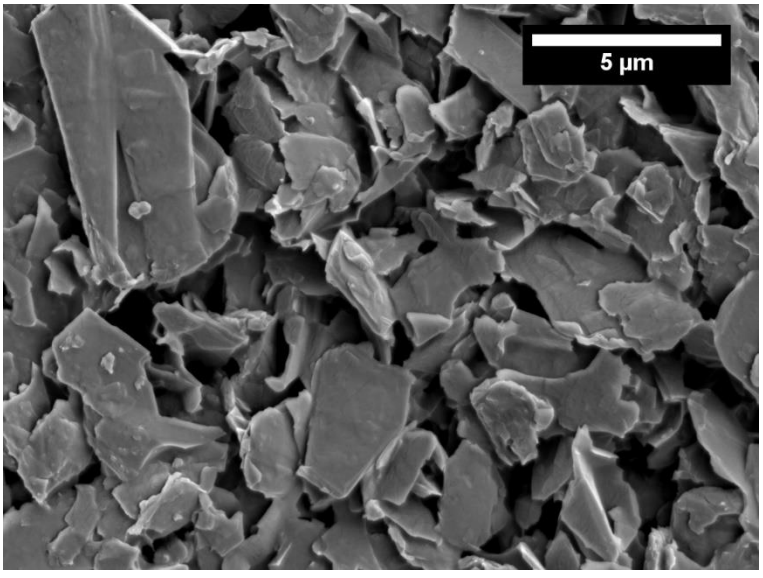

Figure 4.1.3.1 - SEM images at a)3000x and b)6000x magnification of the ϕ=0.098 GNP suspensions

This is in good agreement to the work on GNP based inks by Potts et al [18] and the work on Graphite composites by Kasgoz et al [19]. The thickness of these platelets

can be estimated to be ≈0.075-0.1um from the platelets which haven't fallen flat, and whose edges are visible. The absence of any large agglomerates in the final print suggests that the GNPs were initially well dispersed.

4.1.4 Rheological Characterisation

The effect of concentration on the dynamic viscosity at different shear rates is shown in Fig. 4.1.4.1. Increasing the concentration of NH_3 GNPs increased the viscosity and the amount of shear thinning behaviour, producing an upwards shift in the viscosity-shear rate curves with the onset of shear thinning behaviour moving to lower shear rates in good agreement with the works in the literature on macro scale particles [11][20][21] and the work on exfoliated GNPs in high viscosity melt polymers by King et al [22].

At ϕ=0.071, 0.098, 0.127 the GNP suspensions show a similar shear profile to the unfilled TPU resin system (Figure 4.1.4.1). At low shear rate, a Newtonian plateau is visible as Brownian forces overcome shear to maintain a random distribution and orientation of the GNPs despite the increasing shear. This indicates the absence of structure within the fluid with the GNPs well dispersed and particle interactions minimal allowing liquid like behaviour to dominate.

At ϕ=0.157 there is a large increase in the low shear viscosity with increases in shear thinning behaviour across the whole shear range measured, with shear thinning behaviour seen at low shear rates. At higher concentrations as there is a reduction in the typical minimum interparticle distance with increasing concentration, increasing the probability of particle-particle interactions, as shear rates decrease interactions between the high aspect ratio, Nano-scale GNPs increase, causing increased disruption to flow, increasing viscosity. The introduction of structure to the fluid that disrupts the random orientation and dispersion of the particles, with Brownian motion less significant for these larger groups of interacting particles it is therefore unable to restore the random distribution of the particles and the low shear rate Newtonian plateau is replaced by low shear rate shear thinning behaviour.

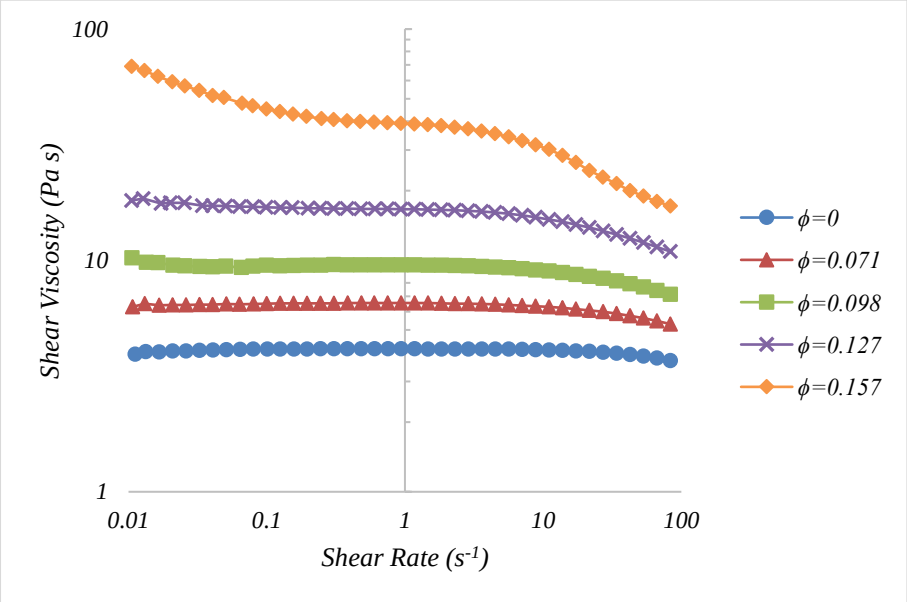

Figure 4.1.4.1 - The effect of increasing phase volume of NH_3-GNP on the shear viscosity at varying shear rates

At higher shear rates, shear forces overcome the random spatial dispersion and orientation of particles to orient the particles and particle structure with the flow, reducing flow line distortion and allowing particles to move more freely over one another reducing the viscosity [3].

All the suspensions show a zero intercept on the shear stress axis indicating the absence of a yield stress (Figure 4.1.4.2).

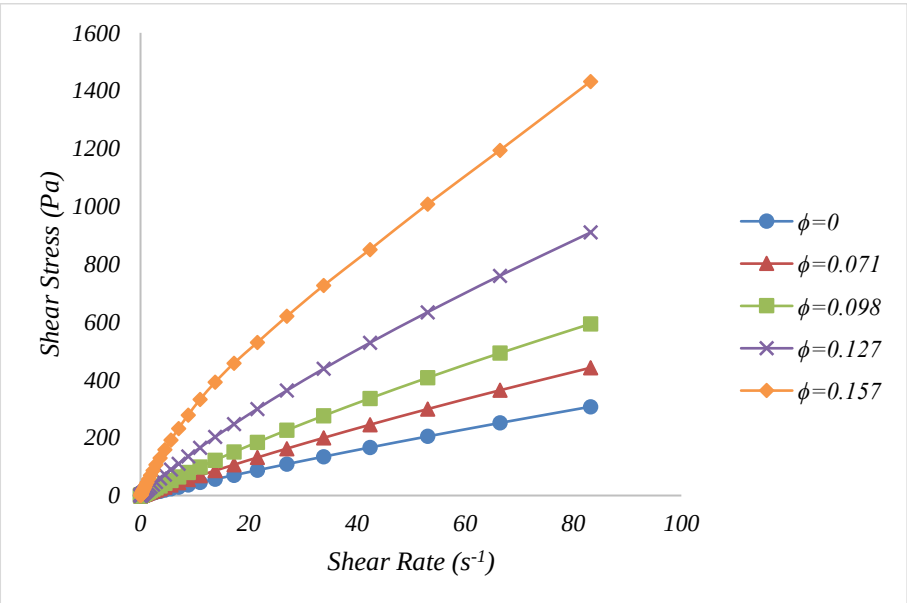

Figure 4.1.4.2 - The effect of increasing concentration NH_3 GNP on the low shear rate shear stress response

Yield stress has previously been attributed to the formation of a dense 3D network of particles capable if elastically storing energy [5]. The ϕ=0, 0.071, 0.098 show a near straight line through the origin indicating near-Newtonian behaviour.

Small Amplitude Oscillatory Shear (SAOS) [3][15] is a measure of the viscoelastic properties of a material, that allows examination of the microstructure of the fluid. This viscoelastic response can be split into an in-phase elastic response, *G'*, and a 90° out of phase viscous response, *G"* [10][23]. Frequency sweeps are used to identify the time dependent response of a material [15]. In a frequency sweep, high frequencies correspond to short times and behaviour is dominated by the elastic response, and low frequencies correspond to long times and the viscous behaviour dominates [10].

A strain amplitude sweep was used to identify the linear viscoelastic range (LVR) of the materials with the results at 1Hz shown in (Figure 4.1.4.3). Strain amplitude sweeps at 0.25 and 10Hz can be found in Chapter 3. In the LVR *G'* and *G"* are independent of strain amplitude [15]. From this a complex shear strain of 1% was selected as it was within the LVR for all the concentrations tested.

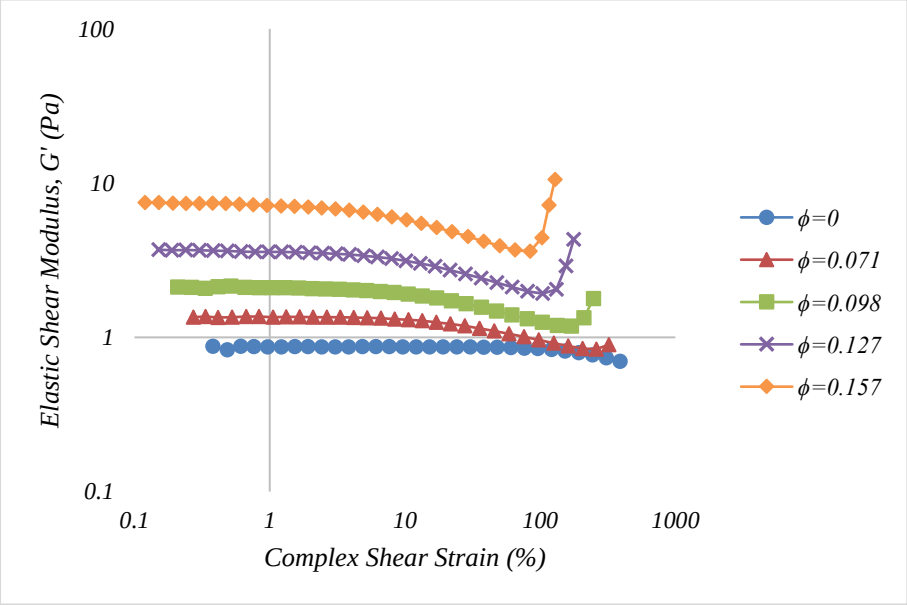

Figure 4.1.4.3 - The effect of increasing concentration of the strain amplitude response of GNP inks at 1Hz

Figure 4.1.4.4 presents the effect of frequency on the elastic shear modulus for the NH_3 GNP inks at a complex strain of 1%. Increasing GNP concentration increases *G'* at all measured frequencies, as the particles occupy a greater volume within the

fluid, increasing particle-polymer interactions as the particle surface area in contact with the suspending fluid increases and increasing particle-particle interactions capable of elastically storing energy as interparticle distance decreases. *G'* becomes increasingly frequency independent with a low frequency plateau developing. This is in good agreement with the works on Carbon black [12][24]. This low frequency plateau has previously been attributed to increased network type particle-particle interactions capable of elastically storing energy as interparticle distances decrease [24]. This suggests the formation of increased network type interactions [13] under periods of slower flow (Figure 4.1.4.4). This shows good agreement with the shear data (Figure 4.1.4.1) where shear thinning behaviour was observed at low shear rates as a network began to form.

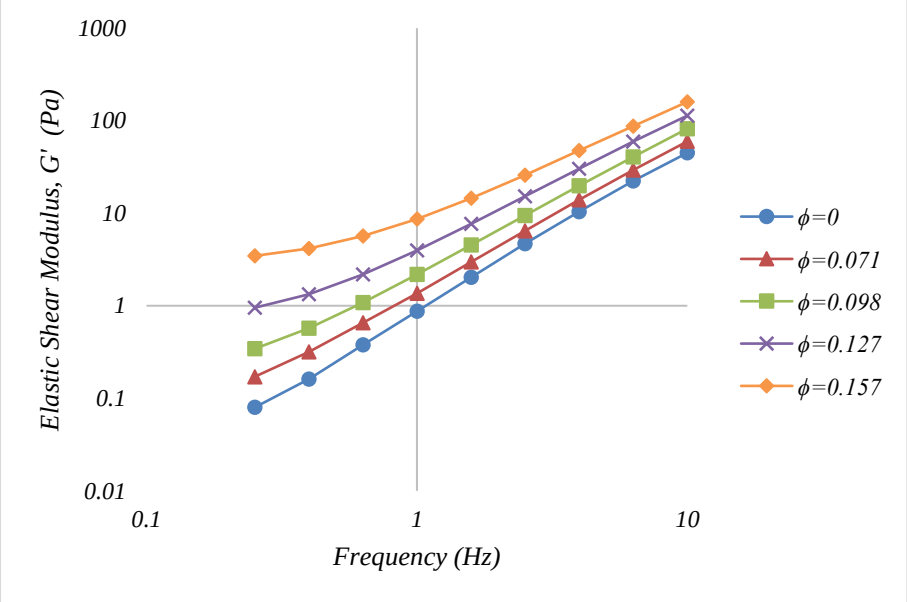

Figure 4.1.4.4- The effect of concentration NH_3 GNP on the frequency dependent response of the elastic shear modulus, G', of GNP inks at a complex shear strain of 1%

Figure 4.1.4.5 illustrates the effect of frequency on the viscous shear modulus of the NH_3 GNP suspensions at a complex shear strain of 1%. *G"* also increases with ϕ at all concentrations as seen in the literature [12], however, the increases are more frequency dependent with linear increases in G". For all phase volumes G">G', $G' \propto \omega^2$ and $G'' \propto \omega$ and viscous liquid like behaviour dominates. The fluids are in the terminal/viscous zone and have not flocculated to form a dense 3D network. For the lowest phase volumes G">>G', with a very low measured G' with this behaviour characteristic of a Newtonian fluid as would be expected for a dilute suspension [24].

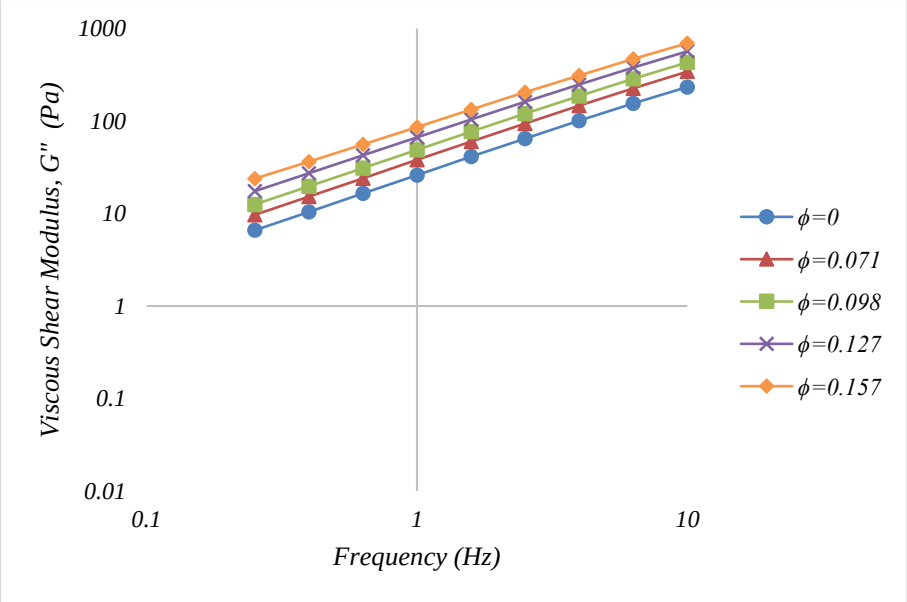

Figure 4.1.4.5 - The effect of concentration NH_3 GNP on the frequency dependent response of the viscous shear modulus, G", of GNP inks

These results show good agreement with the proposed qualitative model by (Trappe and Weitz, 2000) for the effect of increasing ϕ on network development in carbon black suspensions [24] as increasing ϕ increases the magnitude of *G'* with *G'* becoming increasingly frequency independent while *G"* continues to increase linearly with frequency. They proposed that increasing phase volume increases the magnitude of a purely elastic network, with a frequency independent *G'*, interspaced by a purely viscous suspending fluid, where *G"* is linearly dependent on frequency. This suggests an elastic network of GNP particles are forming interspaced by the viscous TPU resin system.

This is further reinforced by the phase angle, δ which represents the ratio of viscous to elastic forces within the fluid, with a theoretically pure Newtonian fluid having δ=90 and a Hookean elastic solid having δ=0. Increasing concentration decreases the phase angle at all measured frequencies as the number of particle-particle and particle-polymer particles capable of elastically storing energy increase (Figure 4.1.4.6).

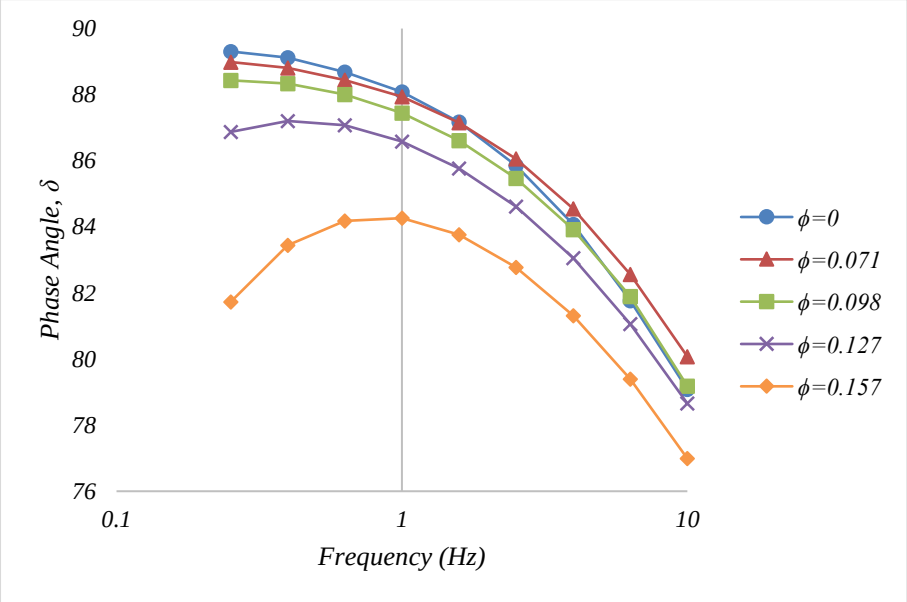

Figure 4.1.4.6- The effect of increasing phase volume GNP on the frequency dependency of the phase angle

All inks show phase angles >76 over the measured frequency range, showing that in this range viscous behaviour dominates and liquid like behaviour prevails indicating the absence of structure within the fluid.

At ϕ=0.127 and 0.157 there is a decrease in phase angle with this decrease starting at approximately 1Hz for the ϕ=0.157 ink. *G'* became increasingly frequency independent with increasing concentration with a low frequency plateau developing. This can be attributed to network type particle interactions (Figure 4.1.4.4). This network formation causes the ink to show more solid like behaviour at low frequencies.

At higher frequencies the phase angle, and as such the proportion of elastic forces of all the inks ϕ<0.157 begin to converge while the ϕ=0.157 ink maintains a higher proportion of elastic behaviour even at the highest frequencies and therefore shortest times.

The complex viscosity, η*, as a function of angular frequency, ω, can be related to the shear viscosity, η, as a function of shear rate, $\dot{\gamma}$, using the Cox-Merz rule (Equation 4.1.4.1)

$$\eta(\dot{\gamma})|_{\dot{\gamma}=\omega} = |\eta^*(\omega)| = \sqrt{\eta'^2(\omega) + \eta''^2}$$

Equation 4.1.4.1 The Cox-Merz Rule [25]

The Cox-Merz rule is used for the GNP suspensions in Figure 4.1.4.7. At low phase volumes, $\phi<0.098$, the complex viscosity shows good correlation with the shear viscosity. However, with increasing GNP concentration the shear viscosity curve increasingly deviates from that of the complex viscosity, which has previously been suggested to be due to the formation of a solid-like structure within the suspension [25].

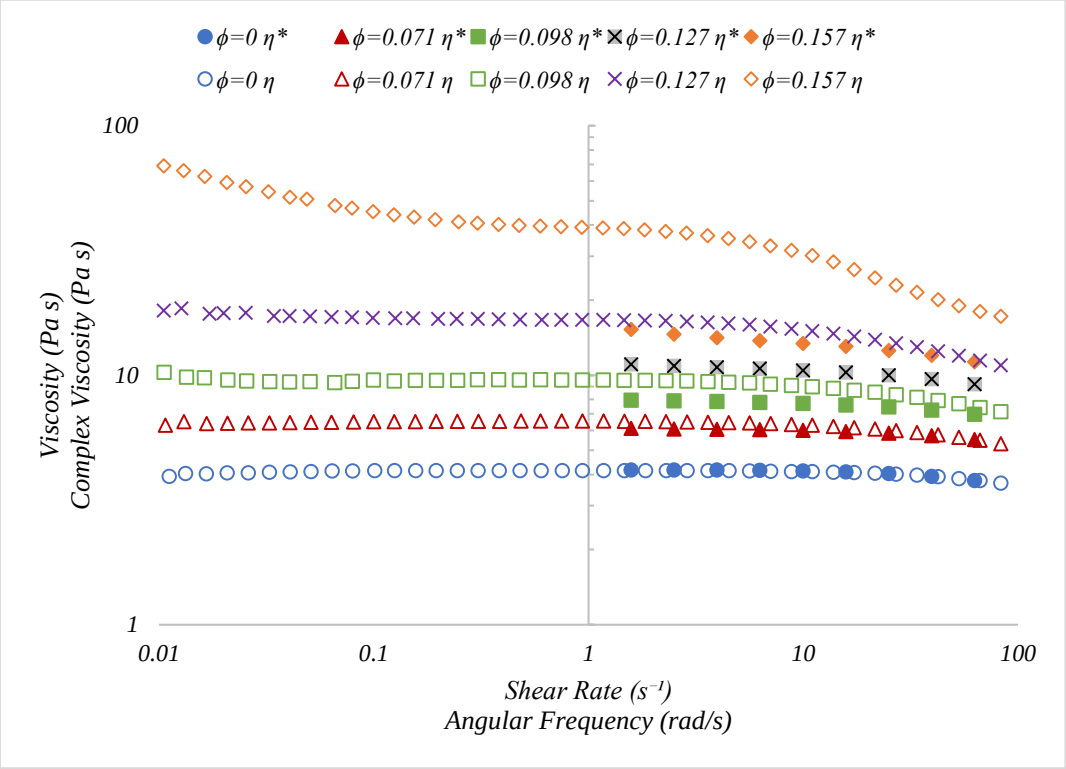

Figure 4.1.4.7) The effect of GNP concentration on the Cox-Merz relationship. Unfilled symbols represent the shear viscosity while filled symbols represent the Complex viscosity

The established rheology models described in Chapter 2 were fitted to the experimental data for the NH_3 GNP suspensions to model the effect of increasing GNP concentration on the rheology of a low viscosity resin. The Krieger-Dougherty model (Equation 2.6.2.3) can be fitted to experimental data to identify the intrinsic viscosity, $[\eta]$ and the maximum packing fraction, ϕ_m (Figure 4.1.4.8). The intrinsic viscosity can be related to the particle aspect ratio to give an insight into the particle morphology. The maximum packing fraction is the point where enough material is added for the viscosity to become infinite, therefore identifies the maximum amount of any material that can be added to a suspension. This is especially important in conductive inks where increasing amounts of conductive material are added to achieve the required electrical properties. This information can then be used to help

guide future GNP-based ink formulations. A best fit (RMSE=0.117) was found by fitting K-D model to the experimental data using an intrinsic viscosity $[\eta]$=6.33 and maximum packing fraction ϕ_m=0.184 (Figure 4.1.4.8), with an especially good fit found at higher phase volumes in agreement with the work on CNFs of Xu et al [13][26]. The K-D model slightly overpredicts the viscosity for the most dilute concentration, ϕ=0.071, as had been previously seen by Mueller et al [21], but overall a good fit is obtained.

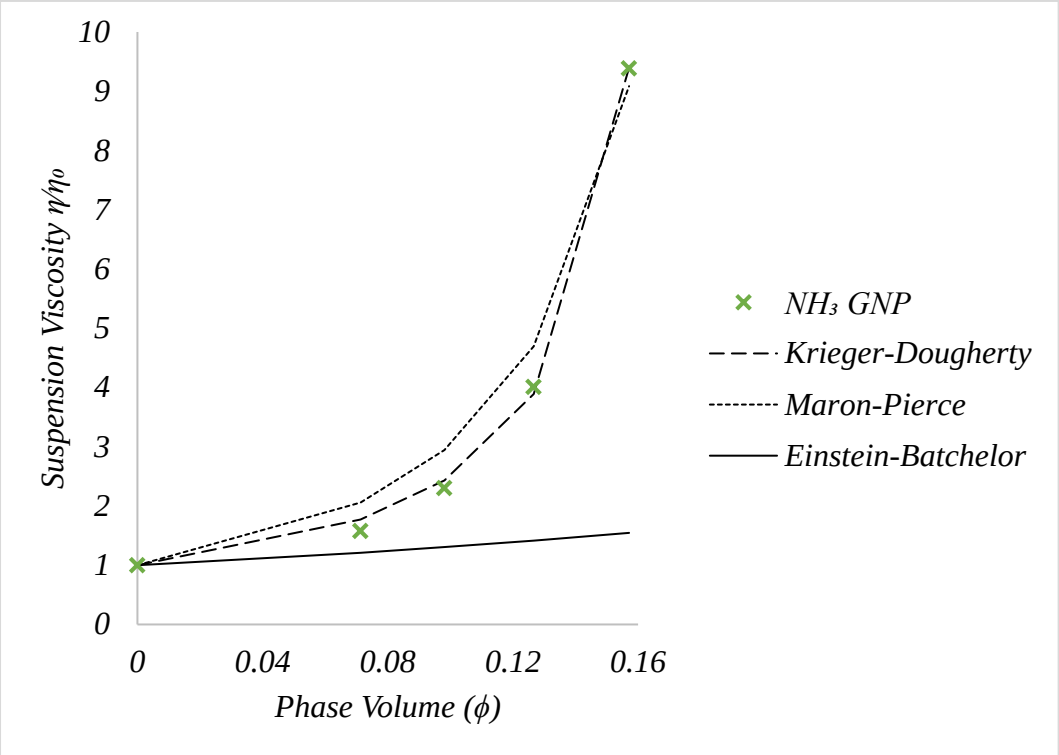

Figure 4.1.4.8- Fitting the Krieger-Dougherty (K-D), Maron-Pierce (M-P) and Einstein-Batchelor (E-B), to the relative equilibrium viscosity data at 1.17^{s-1}

The intrinsic viscosity $[\eta]$=6.33 is significantly higher than that for submicron spheres $[\eta]$ =2.7 [3], in agreement with the literature as $[\eta]$ increases as a sphere is squashed to a disk or elongated to a rod to give higher aspect ratio particles [10]. There is good agreement with the $[\eta]$=5.40 and ϕ_m=0.189 found for graphite by Kasgoz et al [19] with the slightly higher $[\eta]$ and lower ϕ_m for the GNPs likely a consequence of the GNPs Nano-scale high aspect ratio particles occupy a greater volume in the flow, causing enhanced flow line distortion and particle-particle interaction.

Barnes [3] proposes a simple model relating the intrinsic viscosity of very high aspect ratio disks to the particle aspect ratio (Equation 4.1.4.2)

$$[\eta] = \frac{3 \times (Aspect\ Ratio)}{10}$$

Equation 4.1.4.2 Relationship between aspect ratio and intrinsic viscosity from Barnes [3]

Using $[\eta]$=6.33 for GNPs gives a particle aspect ratio of 21.12. This shows good agreement with the technical data sheet where the aspect ratio of the GNPs was in the range of 26-96 and the SEM images where aspect ratio was seen to be approximately 10-100.

The maximum packing fraction ϕ_m=*0.184* of the GNPs is like the ϕ_m=*0.189* found for graphite by Kasgoz et al [19], however this figure is lower than the ϕ_m=0.233 found for glass fibres with a similar intrinsic viscosity, $[\eta]$=6.0, [3] and the ϕ_m=0.343 found for prolate Woolastonite particles, $[\eta]$=6.07, by Mueller et al [21]. This disagrees with the trend for lower ϕ_m with increasing particle aspect ratio $[\eta]$ [20] as non-spherical particles typically occupy a greater volume in the flow at the same ϕ, therefore the minimum separation at a given ϕ is lower, and hence ϕ_m is also lower [21].

The Maron-Pierce equation also provides a good fit (RMSE=0.49) using a ϕ_m=0.235 and is a simpler single variable fit. The ϕ_m calculated is far lower than the ϕ_m=0.680 for smooth spheres, and ϕ_m=0.44 for rough spheres [20], and closer to the value of ϕ_m=0.18 found for carbon fibres (Ar =7) by Kitano et al [20]. While the Maron-Pierce provides an acceptable fit, it uses the assumption that $[\eta]\phi_m$=*2*. Using ϕ_m=0.235 this estimates a $[\eta]$=8.51. This is significantly higher than the $[\eta]$=6.33 predicted by the Krieger-Dougherty and explains why the Maron-Pierce overestimates the viscosity at low loading when increases in viscosity are largely due to the diversion of streamlines around particles. The Maron-Pierce equation also predicts a higher ϕ_m and therefore underpredicts the effect of filling on viscosity at the higher loading levels of ϕ=0.157, where particle interactions become increasingly important as $\phi \rightarrow \phi_m$.

The Einstein-Batchelor (E-B) model provides a poor fit (RMSE= 3.72) especially at higher concentrations, as it assumes ϕ_m=1 and therefore underestimates the exponential effect of particle additions as $\phi \rightarrow \phi_m$ predicted in the literature [21]. Therefore, it can be noted that to model the effect of high aspect ratio nanocarbons it

is important to use the two component Krieger-Dougherty model as it can account for the relatively low maximum packing factor of nanocarbons for their aspect ratio.

The Krieger-Dougherty model was used to gain information about the particle aspect ratio which when combined with imaging techniques could be used to identify dispersion within the fluid. The polydisperse nature of the GNP suspensions must be considered as it would lead to lower measured relative viscosities than would be expected for a monodisperse suspension [3]. Therefore, the values of $[\eta]$ and ϕ_m must be considered as an average and not an exact value, as a monodisperse suspension would be expected to have higher viscosity leading to higher $[\eta]$ and lower ϕ_m.

The nanoscale dimensions of the GNPs lead to decreased interparticle distances than would be found for larger particles. The high particle aspect ratio, Ar=21.12, indicated by the high intrinsic viscosity $[\eta]$=6.33, mean that the GNPs occupy a large volume within the flow. These factors combine to mean that particle interactions increase rapidly as $\phi \rightarrow \phi_m$, causing rapid increases in viscosity. These increased particle interactions are shown by the large increases in viscosity, the development of low shear rate shear thinning and the development of the low frequency plateau in G' in the ϕ=0.157 suspension, as the GNPs begin to interact to form a network of particles. These high levels of particle interactions lead to lower maximum packing fractions as in general flocs are not tightly packed, giving a larger effective particle radius [13]. These flocs pack less effectively leading to relatively low values of ϕ_m considering the particle aspect ratio. This poor packing ability can be seen in the SEM images where particles are lying at various angles relative to the substrate with GNP free gaps visible within the coating.

The effect of increasing concentration GNP on the viscosity of a low viscosity TPU resin system has been studied. The rheological, flow, properties of the ink play an important role in the features of printed specimens [2][27]. The ability to characterise and predict the effect of GNP on the rheological properties of this low viscosity resin system gives essential information that will help understand and control the rheological properties of GNP based conductive inks to improve ink performance.

4.2 The Effect of Plasma Functionalisation on GNP Stability

4.2.1 Introduction

Achieving good dispersion of nanocarbons within a fluid has been proved difficult as a result of the inert, hydrophobic, ultra-high interfacial area per volume and highly agglomerated nature of carbon nanomaterials [6][7][8][9]. Plasma functionalisation offers a non-destructive method of changing the surface chemistry of the nanocarbons to improve their affinity for the polymer matrix and with it improve the dispersion of the nanocarbons in the polymer solutions, preventing their re-agglomeration.

A physically stable ink would be expected to show no change in its rheological properties over an extended period in storage [27]. A suspension in which the particles have agglomerated to form pairs, or agglomerates of higher numbers, can be considered a suspension of single particles of new shape and as such must be expected to have rheological properties different from a suspension in which the particles remain well dispersed no matter how low the phase volume [50].

By comparing changes in time to the shear and complex rheology of suspensions of Ammonia Plasma Functionalised Graphite Nano-platelets (NH_3 GNP) and Un-functionalised Graphite Nano-platelet (R1 GNP), this part of the study aims to establish whether plasma functionalisation provides an effective means of maintaining particle dispersion.

4.2.2 Materials and Method

4.2.2.1 Ink Composition

The same TPU resin used in Chapter 4.1 was used for this study. Ammonia plasma functionalised GNPs (NH_3-GNP) and an oven dried (130°C) un-functionalized GNP (R1-GNP) were supplied by Haydale Ltd. These were used to compare the effect of plasma functionalisation on GNP dispersion. Ammonia plasma functionalisation has been shown to increase the polarity and surface Nitrogen content of the CNTs and it is hypothesised that a similar effect on GNPs [6] will lead to increased compatibility to the polar hard segments of the thermoplastic polyurethane. The R1-GNPs were oven dried to simulate the pre-treatment of the GNPs before plasma functionalisation. Three phase volumes (ϕ), ϕ=0.071, 0.098, 0.127 of each type of GNP were used to create the inks using the methods detailed in the methods and materials section Chapter 3.

4.2.2.2 Method

The rheological properties of the inks and the time stability of these suspensions was studied using the method outlined in Chapter 3. The time stability comparison in was done over 3 phase volumes, ϕ=0.071, 0.098, 0.127 (15, 20, 25wt%), with the theory that if it were a particle agglomeration effect then increasing the particle concentration would decrease the interparticle distance and increase the likelihood of particle-particle interaction. A sample of the resin was measured over the same time period to ensure that any changes to the rheological profile of the filled suspension was not a result of changes to the resin. The inks were then screen printed onto PET and their surface characteristics analysed using the procedures set out in Chapter 3.

4.2.3 Results

Similar increases in viscosity with increasing concentration were found for both the NH_3 and R1 GNP suspensions (Fig. 4.2.3.1), with the viscosity of the R1 GNP suspensions showing good fit (RMSE=0.329) to the model developed for NH_3 GNP. That the particles have a similar affect upon the diversion of flow represented by similar increases in viscosity with concentration suggests that initially following dispersion the particles are of a similar size, shape and quality of dispersion irrespective of plasma functionalisation treatment.

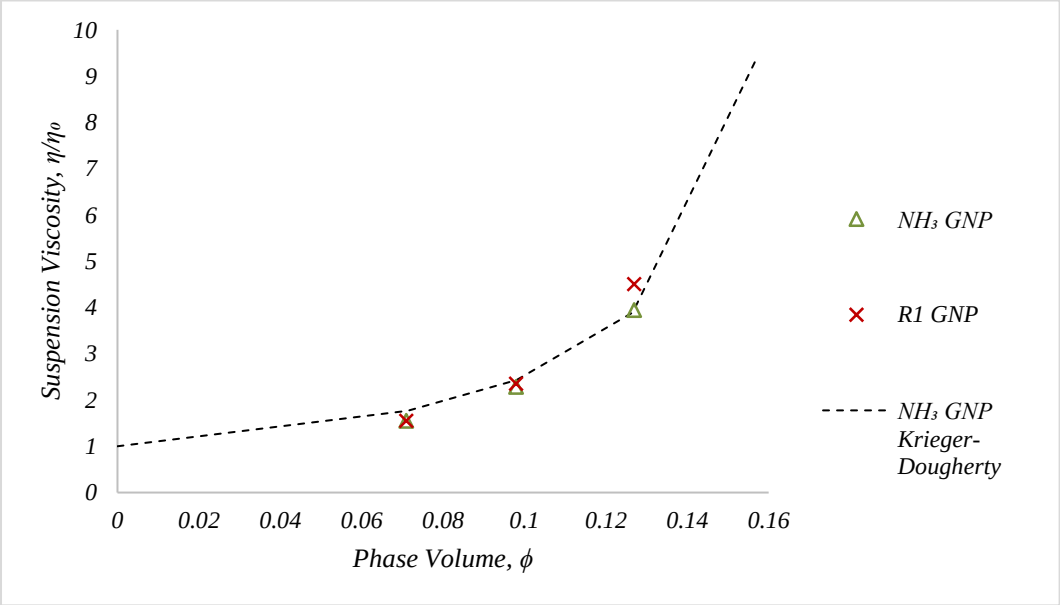

Figure 4.2.3.1 - The effect of increasing phase volume, ϕ, GNP on the suspension viscosity at a shear rate of 1.17s^{-1}

The flow behaviour of the two suspensions is also very similar (Fig. 4.2.3.2) owing to their similar particle morphology and dispersion quality.

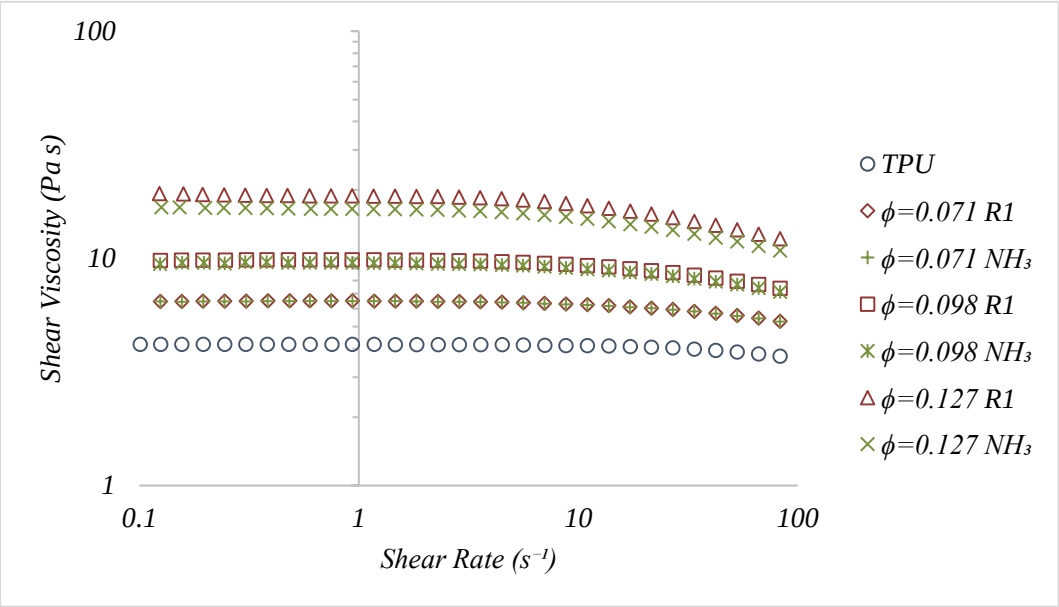

Figure 4.2.3.2 - The effect of increasing phase volume GNP on the shear rate viscosity curve for ammonia functionalized NH_3 and unfunctionalized R1 GNPs

Increasing concentration of GNP similarly increases both the viscous and elastic forces for both the NH_3 and R1 inks (Fig. 4.2.3.3). G”>>G’ for all inks as viscous properties dominate elastic forces to give largely liquid like behaviour. This is in good agreement with the shear data. There is very little difference between both the G’ and G” of the plasma functionalised and unfunctionalized GNPs indicating the particles are of a similar size, shape and dispersion giving fluids with a very similar microstructure. Increasing concentration of GNP caused increases in G’ as the interparticle distance between GNPs decreased increasing GNP-GNP interactions, as well as the increased particle-polymer interactions. Increases in G” with increasing concentration result from increased energy loses in the fluid as particles move to new equilibrium positions.

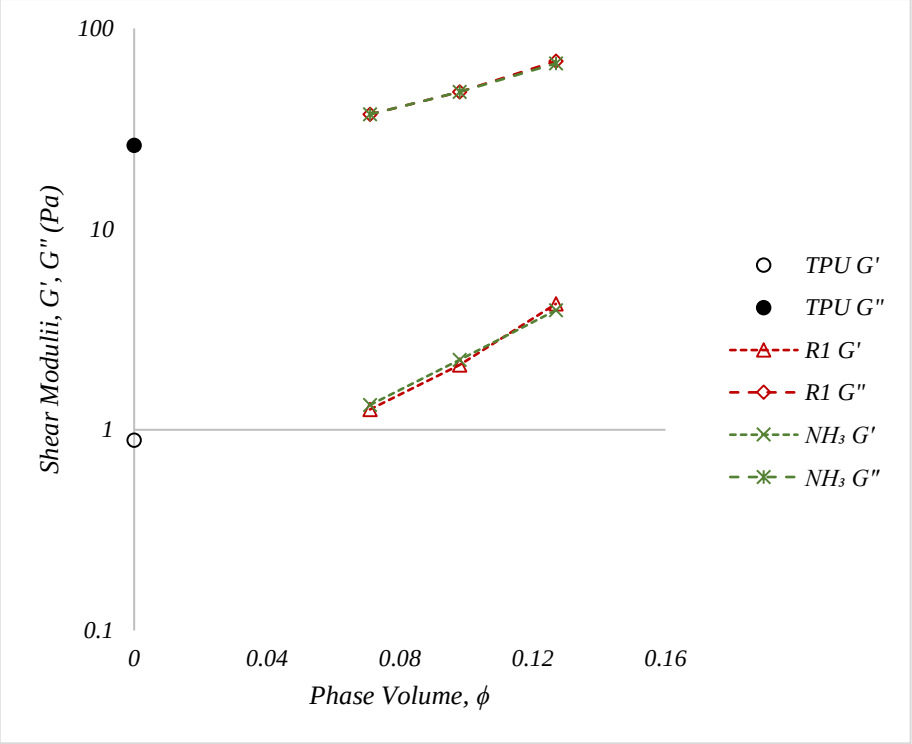

Figure 4.2.3.3 - The effect of increasing concentration GNP on the elastic, G', and viscous, G'', shear moduli at various phase volumes, ϕ, for Unfunctionalized R1 GNP and Ammonia Functionalized NH_3 GNP

The inks were then screen printed onto a smooth substrate and their surface analysed using white light interferometry. The print performance can be seen in Fig. 4.2.3.4. As well as the similarities in the rheological data when screen-printed the two coatings show similar surface roughness and electrical properties irrespective of plasma functionalisation. This reinforces that the GNPs are of similar size and shape following plasma functionalisation and that the plasma functionalisation has not damaged the structure of the GNPs and therefore their electrical properties. Increasing the volume of GNP increased the conductivity of the inks, as a greater volume of conductive material meant an increased number of conductive pathways and therefore increased conductivity.

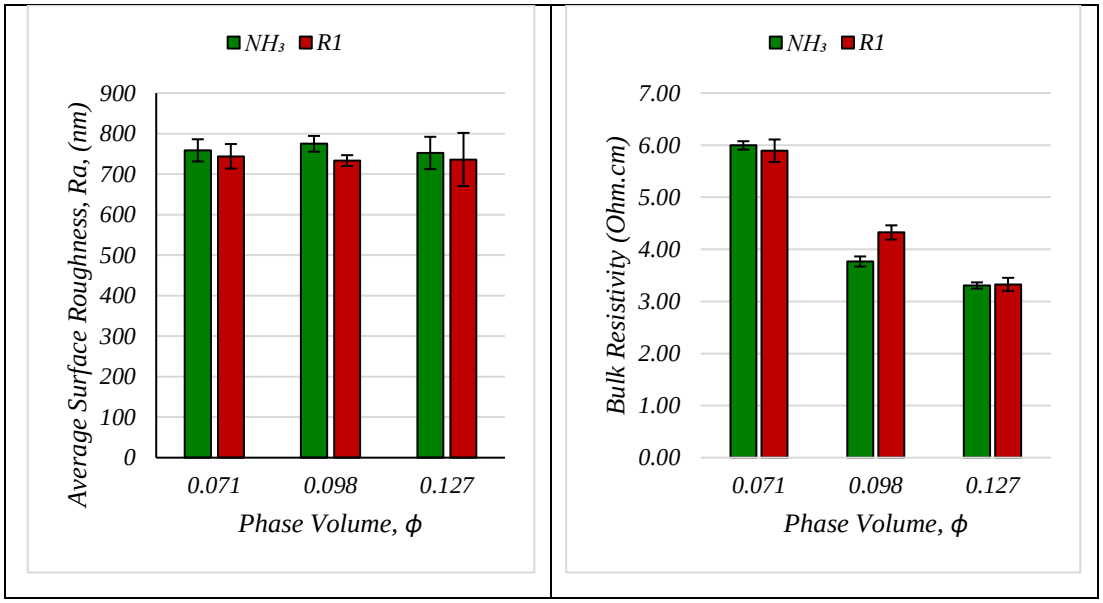

Figure 4.2.3.4 - The effect of plasma functionalisation on a) Average surface roughness, b) Bulk resistivity, of three different volumes of Ammonia plasma functionalised, NH_3, and unfunctionalized, R1, GNPs

A physically stable suspension would be expected to maintain its rheological properties over an extended period [27]. Studying changes to the flow curves was used to understand how the microstructure of the suspensions has changed in time. The changes to the equilibrium viscosity of the suspensions at $1s^{-1}$ can be seen in Figure 4.2.3.5. The viscosity of the thermoplastic polyurethane resin increases slightly over the 12-week period as solvent evaporates to leave a higher polymer concentration resin while the viscosity of the R1 GNP suspensions decreases in time, with the highest concentration inks showing the fastest decrease in their viscosity (Fig 4.2.3.5a). Over the same time period the plasma functionalised NH_3 GNPs follow a similar trend to the thermoplastic polyurethane and maintain their viscosity at all concentrations (Fig 4.2.3.5b). The unfilled thermoplastic polyurethane resin maintains its viscosity and its near-Newtonian rheological properties over 12 weeks and therefore can be considered stable over the measured time frame. Slight increases in the viscosity are likely a consequence of solvent evaporation increasing the polymer concentration within the resin system. This leads to increased interaction between neighbouring polymer chains and associated with this an increased resistance to flow.

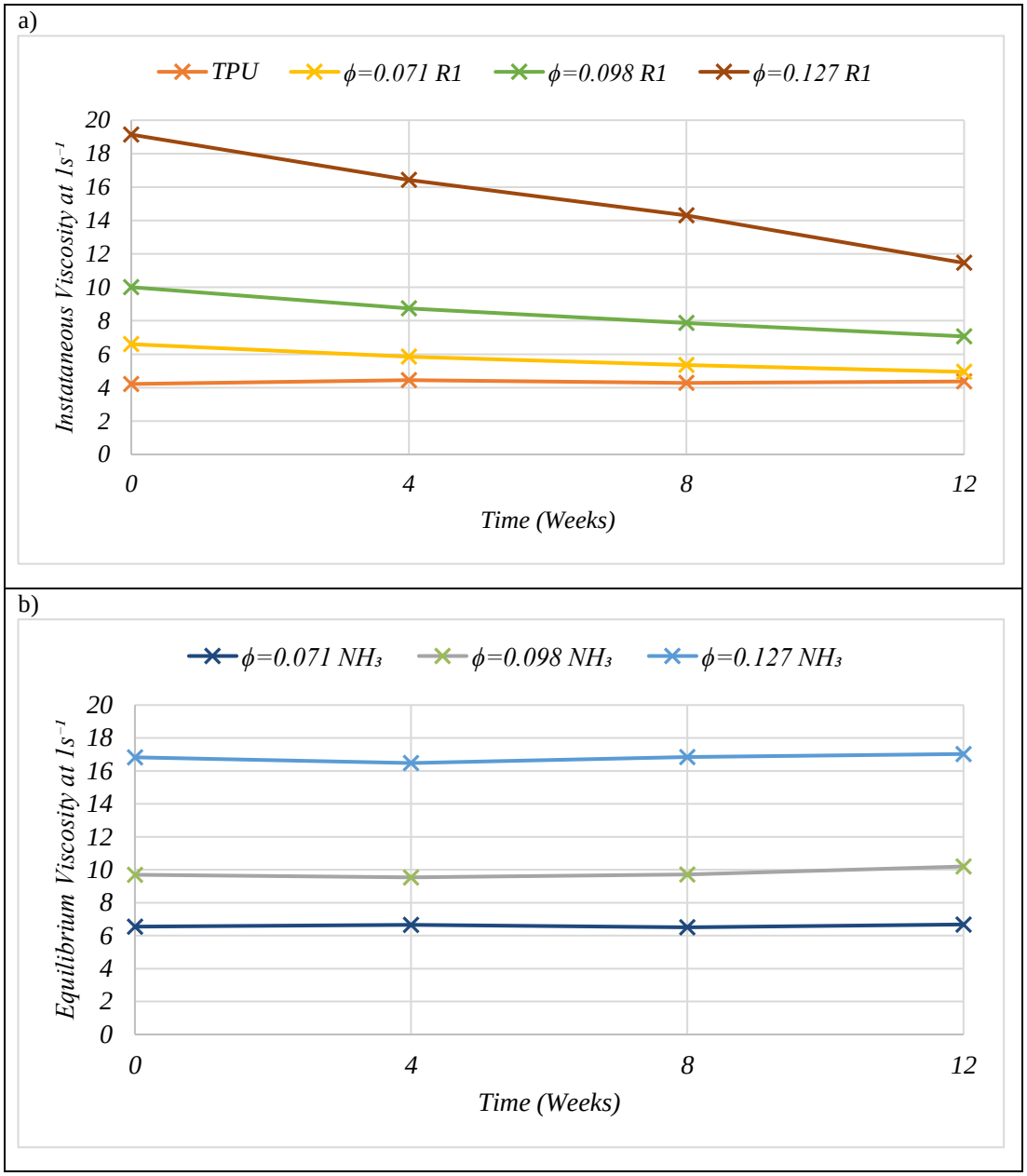

Figure 4.2.3.5 - changes to the equilibrium viscosity over a 12-week period for a) R1 GNPs and the unfilled thermoplastic polyurethane, b) NH_3 GNPs

Changes to the shear viscosity profile of the NH_3 and R1 GNPs can be seen in Figure 4.2.3.6. The viscosity of the R1 GNP suspensions decreases over time at all measured shear rates and volumes (Fig. 4.2.3.6a, c, e) with the non-Newtonian behaviour of the suspensions also decreasing in time. These decreases in viscosity in time are most significant for the higher concentration suspensions, with percentage decreases in viscosity at $1.17s^{-1}$ over 12 weeks at ϕ=0.071, 0.098, 0.127 of -23.98, -29.72, -39.44% respectively. Over the same time period the NH_3 GNP suspensions maintain their rheological properties at all shear rates and concentrations, with slight increases in viscosity due to solvent evaporation (Fig. 4.2.3.6b, d, f). The contrast

between the NH_3 GNP and unfunctionalized R1 GNPs is especially evident at the highest concentration where the NH_3 GNPs have maintained their high volume in the flow and with it their higher viscosity and non-Newtonian behaviour, while the R1 GNPs have become both less viscous and more Newtonian.

The increases in viscosity and shear thinning behaviour with concentration were associated with the increased concentration of GNP occupying a larger volume within the flow, increasing distortion of streamlines and increasing particle-polymer and particle-particle interactions. Both behaviours have decreased in time for the R1 GNPs implies the particles are now occupying a smaller volume within the flow, decreasing both the particle-polymer and particle-particle interactions. However, agglomerated particles would also sediment under the action of gravity faster owing to their larger size. The pots were initially stirred to ensure that any large sedimented particles were re-distributed throughout the mixture and a consistent sample taken, however in the time between the pots being lightly stirred and the measurement taking place any very large particles could've sedimented towards the bottom of the pot to leave a sample of an effective lower concentration.

The viscoelastic response of the materials shows good agreement with the shear measurements with both the elastic, G', and viscous, G", shear moduli of the unfunctionalized R1 GNP inks decreasing over time (Fig. 4.2.3.7a, c) while the G" of the NH_3 GNP inks remain consistent in time (Fig. 4.2.3.7d). The G' of the NH_3 GNP inks and the unfilled TPU resin increases as solvent evaporates to leave an ink of higher solids content, increasing particle-particle, particle-polymer and polymer-polymer interactions (figure 4.2.3.7 b). The reduction in G' reinforces a decrease in the volume that the particles occupy in the fluid, reducing the surface area in contact with the fluid and therefore particle-polymer interactions, while by occupying a smaller volume in the flow any particle-particle interactions capable of storing energy will also decrease. G" is a measure of the viscous energy lost as heat or friction during the oscillatory measures also decreases in time.

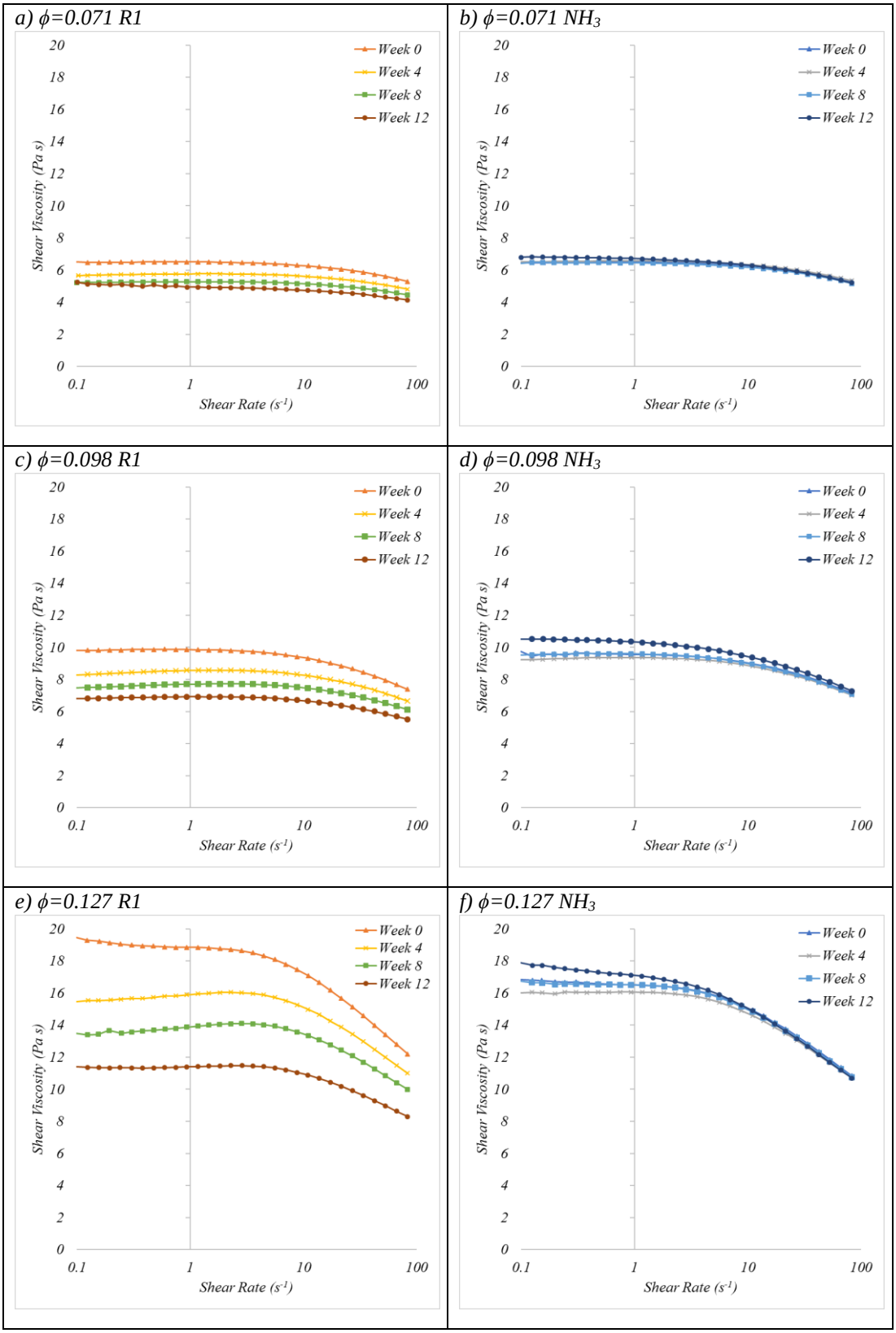

Figure 4.2.3.6; The effect of storage time on the flow curves for GNP inks at various phase volumes. a) c) e) Unfunctionalised R1 GNP. b), d), f) Ammonia functionalised NH_3 GNP

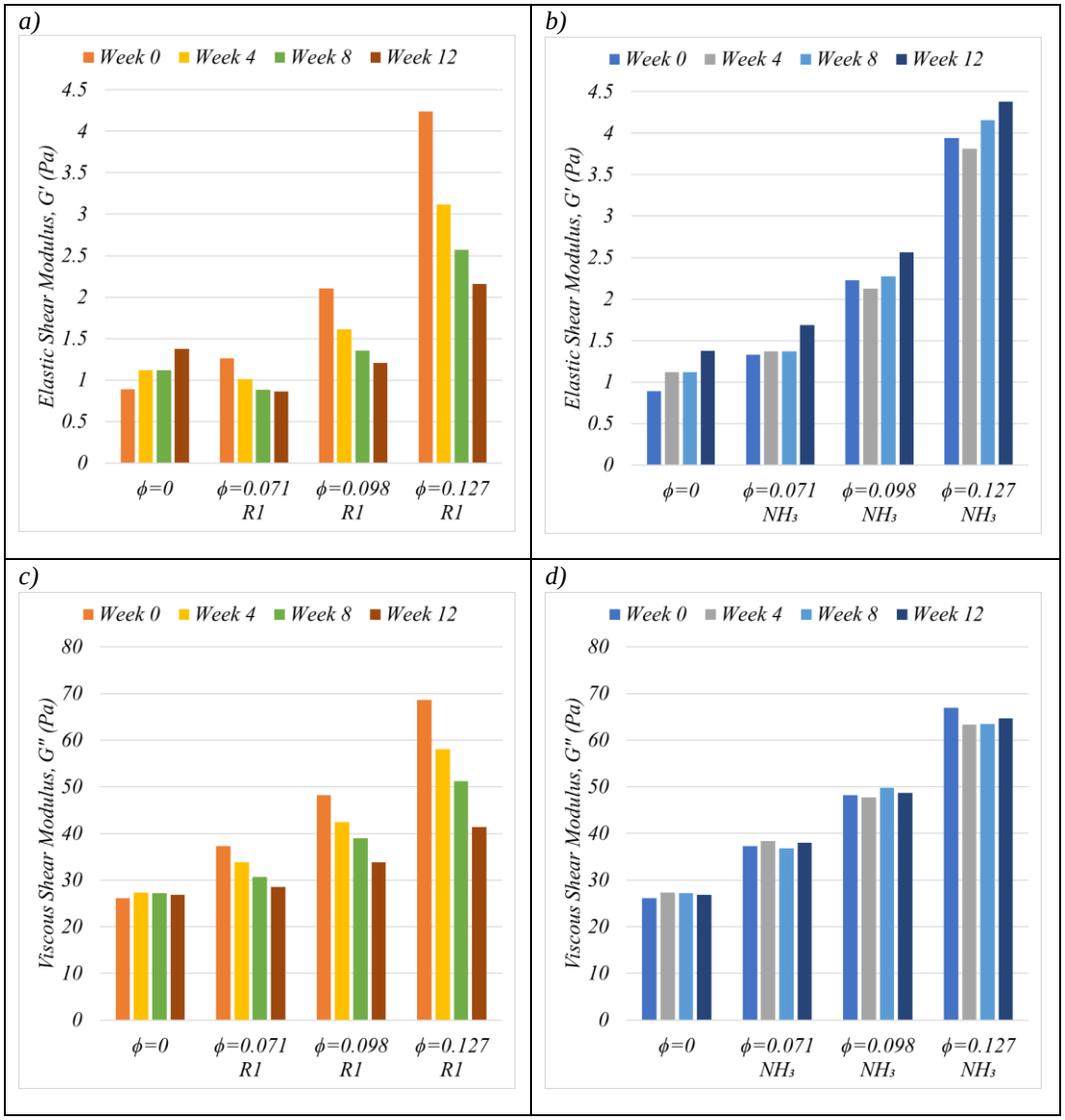

Figure 4.2.3.7) Changes to the elastic and viscous shear moduli at 1Hz for different concentrations in time. a, c) Unfunctionalized R1 GNP and b, d) Ammonia functionalised NH_3 GNP

The unfunctionalized R1 GNP suspensions saw a decrease in the viscosity, shear thinning behaviour and the viscoelasticity of the fluids in time associated with a decrease in the volume in which the particles occupy within the flow, therefore reducing particle-polymer and particle-particle interactions.

As nanocarbon particles in a low viscosity fluid, interparticle colloidal forces such as Brownian motion, van der Waals forces, electrostatic and steric stabilization effects would be expected to play a significant role. In time the relatively chemically inert, high surface area, unfunctionalized R1 GNPs approach one another under the action of Brownian motion and agglomerate due to van der Waals forces to form larger particles of a decreased aspect ratio. A suspension in which the particles have formed pairs, or higher multiples, can be considered a suspension of single particles of new

shape and as such must be expected to have properties different from a suspension in which the particles remain well dispersed no matter how low the phase volume [28]. Agglomeration to form larger, lower aspect particles would lead to increased typical minimum separation between particles and therefore a reduction in particle-particle interactions, while also reducing particle surface area in contact with the fluid and therefore reduce particle-polymer interactions. A reduction in particle aspect ratio caused by the agglomeration of particles would lead to reduced viscous energy dissipation around the particles, especially at low shear rates when the particles are randomly oriented with the flow. The decreases in viscosity, non-Newtonian behaviour and the viscoelastic properties are greatest for the highest concentration R1 GNP suspensions where particle-particle and particle-polymer interactions would be most prevalent supports the theory that the decline in viscosity is particle related. However, this decrease could also be the result of the particles agglomerating to form larger particles, that sediment between the ink being redistributed to the ink being measured to reduce the effective concentration of the ink.

The ammonia plasma functionalised NH_3 GNPs maintain their viscosity, shear thinning behaviour and viscoelastic properties over the same twelve-week period, indicating that the GNPs have maintained their size, shape and aspect ratio. NH_3 plasma functionalization has previously been shown to increase the surface Nitrogen content of nanocarbons, increasing surface polarity. Addition of the polar N groups to the surface of the NH_3 GNPs would provide improved chemical affinity for the polar segment of the TPU, allowing the TPU to better wet the GNPs, to create a steric barrier that helps to hold the GNPs far enough apart to prevent agglomeration. This allows the GNPs to maintain their dispersion and with it their rheological properties. The plasma functionalisation and enhanced wetting did not affect upon the electrical properties of the GNPs suggesting that the polymer is not fully covering the GNP and therefore there is still direct carbon-carbon contact between the GNPs in the dry coating to allow electrical pathways to form.

Overcoming the inherent tendency of the Nano-carbon to agglomerate to form a stable dispersion of nanocarbons is important if nanocarbons are to be taken from the lab scale to industrial production where an ink must have sufficient shelf life for them to become an economically viable competitor for existing carbon inks such as Graphite and Carbon Black based inks largely used in industry. Ammonia Plasma

functionalisation has been shown to improve the dispersion and time stability of GNPs in a low viscosity TPU resin for use printing inks, while not negatively affecting its electrical properties, giving it an advantage over other methods of chemical functionalisation.

Ammonia plasma functionalisation has been shown to improve the suspension stability of GNP inks compared to an unfunctionalized control. This is the first-time rheology has been used to examine the effect of plasma functionalisation on the stability of GNP suspensions. This increased stability could be a result of increased particle-polymer interaction preventing agglomeration through steric stabilisation. The rate of decrease in the viscosity of the inks is related to particle concentration, with the viscosity of higher concentration inks changing at a faster rate than their lower concentration counterparts. This relationship between concentration and change to the rheological properties could be a consequence of the decreased interparticle distance causing increased particle interaction, leading to the agglomeration of particles to form particles of a new shape, giving suspensions of new rheological properties.

4.3 Print Performance of NH_3 GNP inks

4.3.1 Introduction

Carbon inks often require high loading levels to achieve the required conductivity for use in printed electronic devices, however these high loading levels often affect the rheological properties and therefore the processability of the inks. At the start of this chapter it was demonstrated that increasing the concentration of GNPs increased the interparticle interactions to cause large increases in the viscosity and elasticity of the inks, this part of the chapter looks to investigate the effect of these changes to the rheological parameters on the processability of the inks and their subsequent electrical properties.

4.3.2 Materials and Methods

The ink used was as per Chapter 4.1. The inks were Screen printed onto PET (Hifi films) and their topography and electrical properties were measured using the procedure outlined in Chapter 3.

4.3.3 Results

White light Interferometry (WLI) was used to assess the dispersion of the particles following screen printing. The thickness of the coatings exponentially increased with

ϕ from 3.94±0.27 to 11.12±0.64µm. Increased viscosity and elasticity has been linked to increased ink transfer as more material is drawn from the ink [1]. However, this increase in thickness could also be due to an increase in the solid content of the ink with increased carbon loading.

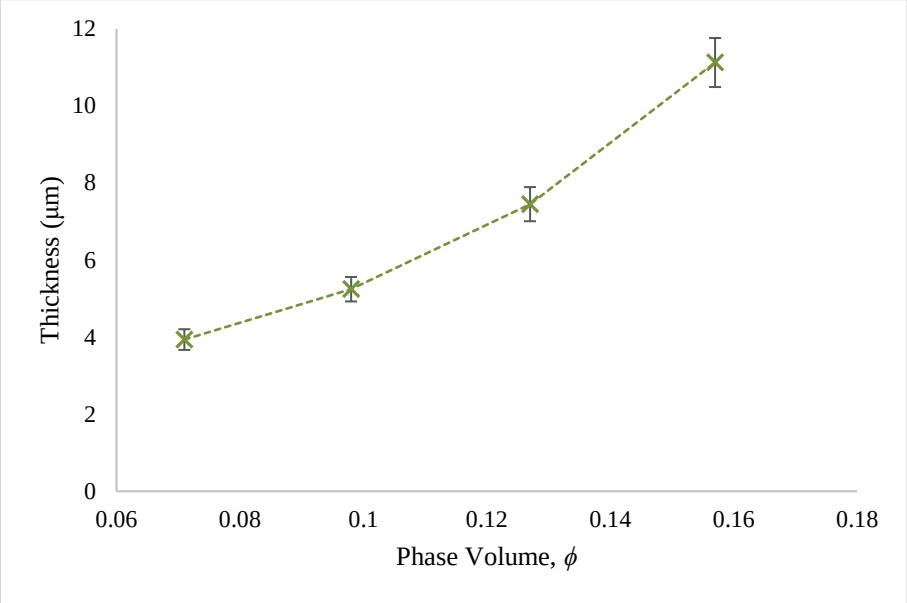

Figure 4.3.3.1) The effect of increasing concentration GNP on the printed thickness

Average roughness (Ra) of the coatings was <775nm for the $\phi \leq 0.127$ GNP suspensions indicating the absence of any large agglomerates (Figure 4.3.3.2a). These inks show good agreement in surface roughness to the 800nm found by Potts et al [18] for GNP screen printing inks, which was substantially lower than the 2.8um roughness of graphite inks, owing to the GNPs smaller size [18]. Rz compares the highest and lowest consecutive peaks (Figure 4.3.3.2b). Variance in Rz increases with ϕ as the thicker inks are less able to settle to form a consistent print as ink viscosity and elasticity increases, preventing them from relaxing to form a smooth layer. At ϕ=0.157 there is a large increase in the surface roughness and the variance in roughness of the prints.

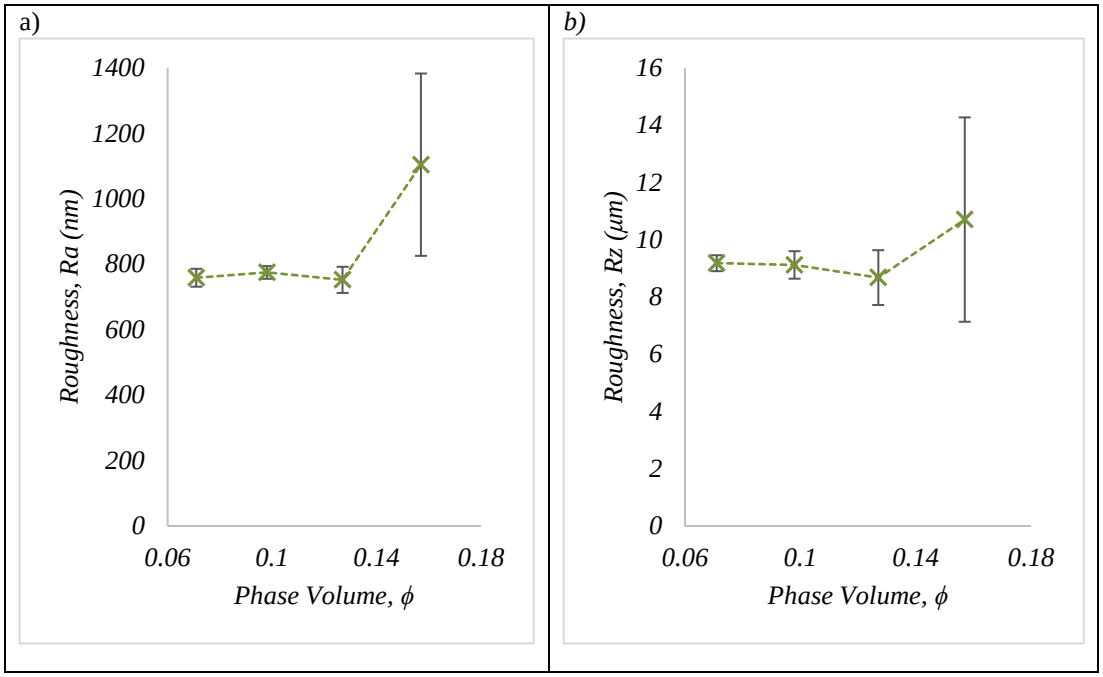

Figure 4.3.3.2- The effect of increasing phase volume on a) average surface roughness, Ra, b) Peak-to-peak roughness of GNP coatings

The flow of the ink through the mesh or the stencil is significant since it determines the uniformity of printed surface which is an important feature of conductive circuits [2]. Surface topography of the final coating impacts on the electrical properties of the film as the topological variations provide a significant barrier to efficient charge transfer [1][29]. The more viscous an ink, the less easily it flows through the screen and the more difficult it is for the ink to spread into an even film [30]. Jewell *et al (2013)* suggest that the reduced ability of higher solid content inks to "slump" following printing is related to increased ink viscosity [1]. At the lowest concentrations, $\phi \leq 0.098$, the GNPs are well dispersed, and the ink passes easily through the screen to form a smooth layer (Fig. 4.3.3.3a, b). There are thin areas at the edge of the squares where the low elasticity and viscosity of the GNP ink means the ink doesn't recover following the removal of shear and spreads outwards. At $\phi = 0.127$, the ink recovers structure following the removal of shear to give a sharper edge. At the highest concentration there is patterning in the surface of the prints as the increased viscosity and elasticity of the ink prevents it from relaxing to form a smooth layer (Fig.4.3.3.3d). Increased interparticle interaction at $\phi = 0.157$ caused increased viscosity, shear thinning behaviour, elasticity and a higher proportion of elastic behaviour at all shear rates and frequencies. The $\phi = 0.157$ ink also begins building structure at low shear rate shear thinning, and a yield stress associated with network formations. This higher resistance to flow and elasticity even at the highest

frequencies prevent the ink from relaxing to form a smooth coating, inducing mesh marking in the prints.

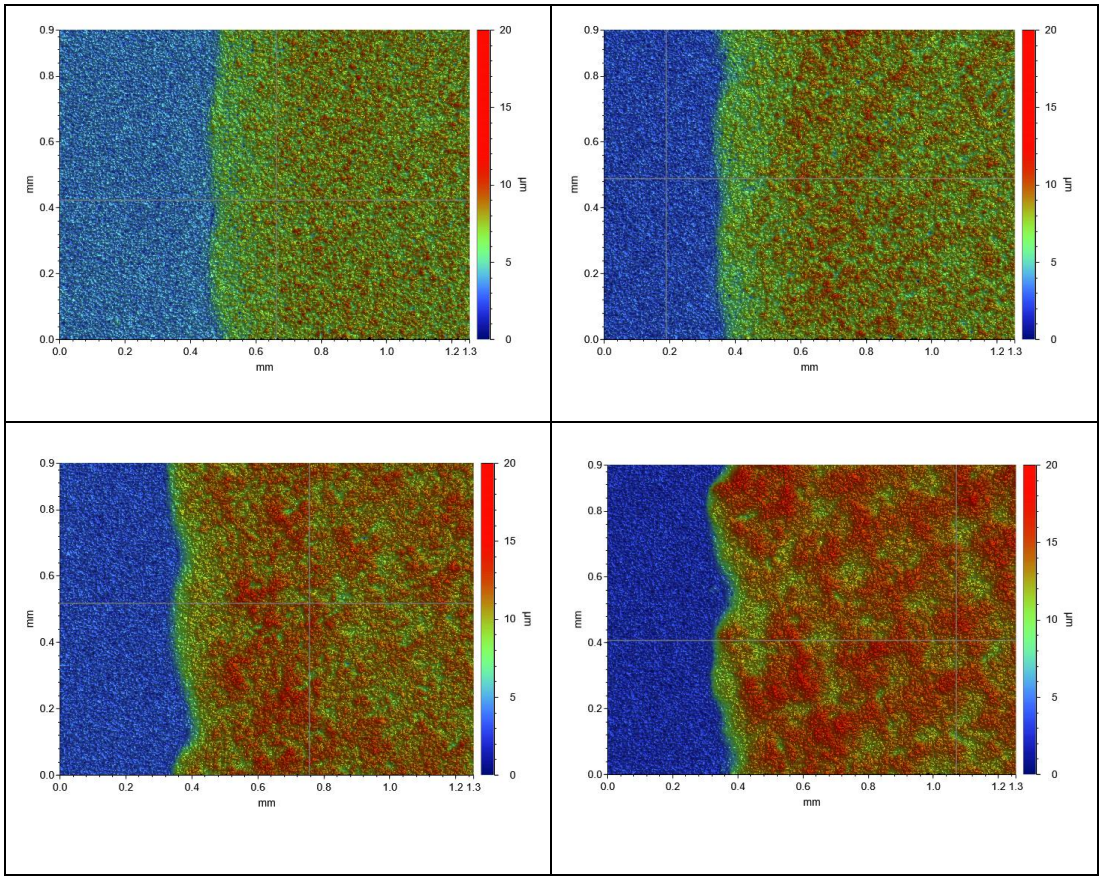

Figure 4.3.3.3- White light interferometry images showing the effect of increasing concentration GNP on print surface; a) ϕ=0.071, b) ϕ=0.098, c) ϕ=0.127, d) ϕ=0.157

GNPs were chosen as the functional component in the ink to improve the electrical conductivity of the ink. Increasing the volume of GNP decreased the measured sheet resistance exponentially as the higher GNP concentration leads to a thicker, better established conductive print with increased number of conductive particle-particle contact (Fig. 4.3.3.4). Bulk resistivity can be used to account for the effect of increased print thickness owing to increased solid content to give a better understanding of the material properties of the print.

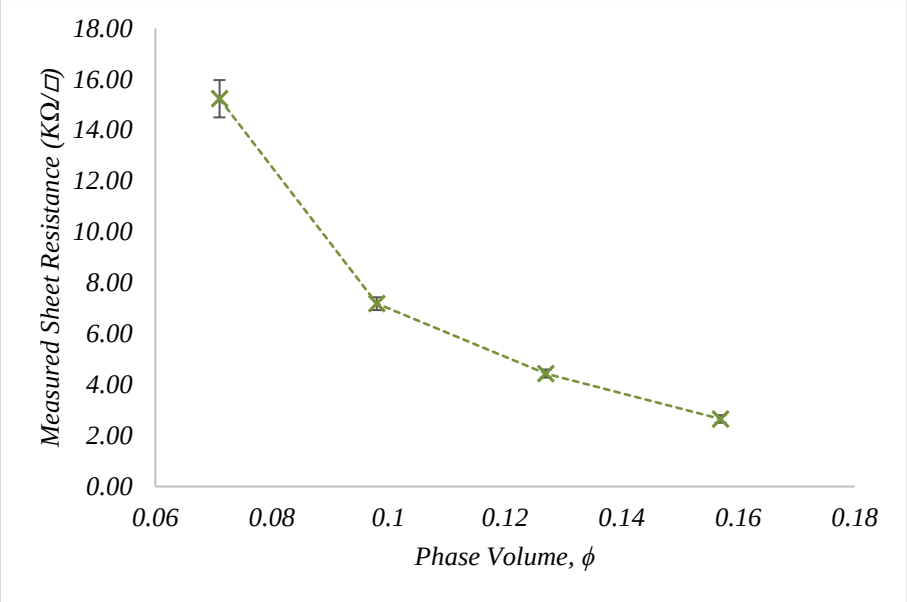

Figure 4.3.3.4 – The effect of increasing volume GNP on the sheet resistance of the NH_3 GNP coatings

There is a large decrease in the bulk resistivity between the ϕ=0.071 and ϕ=0.098 inks as a better-established conductive path is formed (Figure 4.3.3.5). Beyond this point there are more modest decreases in bulk resistivity as ϕ is increased beyond ϕ=0.098 suggesting a well-established conductive path has been formed.

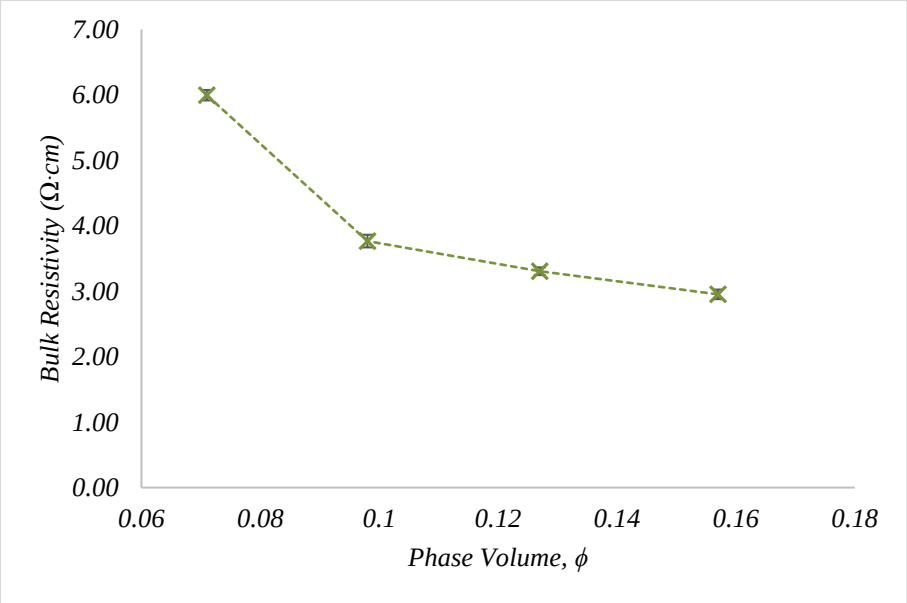

Figure 4.3.3.5- The effect of increasing phase volume on the bulk resistivity of NH_3 GNP coatings.

Line widths and conductivities were analysed to gain further insight into how the concentration of GNPs affected the shear and viscoelastic properties of the fluids and

their subsequent ink transfer through the screen. There was good correlation between viscosity and the elastic storage modulus and the minimum printed conductive line width, with the lower viscosity inks able to print finer conductive features (Figure 4.3.3.6) in good agreement with the literature [1]. This has been attributed to lower viscosity inks being able to more easily pass through the screen and then flow into the line to create a continuous feature [1]. All inks printed at 600 and 700um with the line resistance decreasing with increased solid loading up to ϕ=0.127 as would be expected with the lower bulk resistivity owing to the higher concentration conductive material. There is an increase in line resistance at ϕ=0.157 despite the ink having a lower bulk resistivity, this is likely due to poorer ink transfer owing to the higher ink viscosity and elasticity.

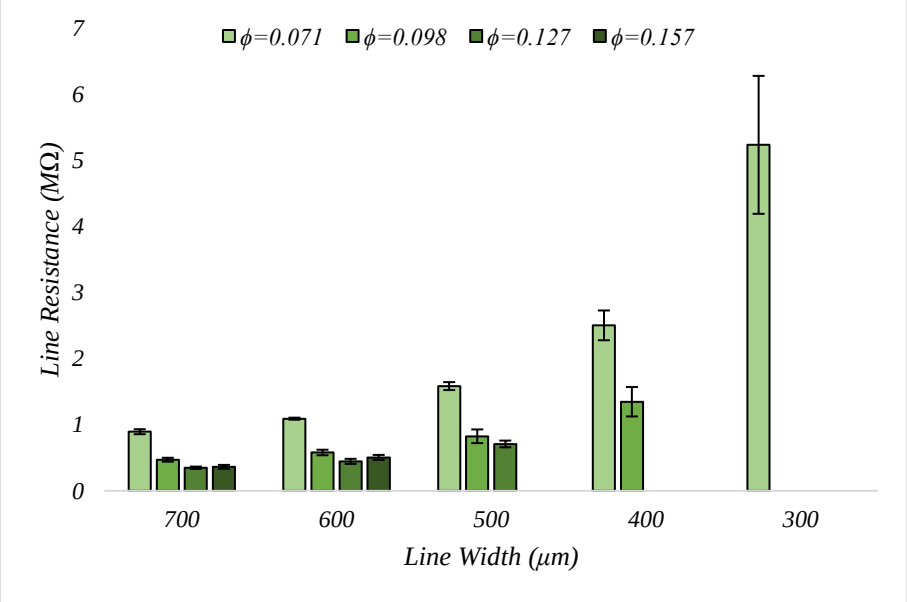

Figure 4.3.3.6) The effect of increasing concentration GNP on the resistance of printed lines of varying widths

Increasing concentration GNP increased the thickness of the printed lines and the printed line width (Fig. 4.3.3.7 a, b). At the lower concentrations $\phi \leq 0.098$ the width of the lines is greater than the target printed width as the ink continues to spread following the removal of shear (Fig. 4.3.3.7b). Above ϕ=0.098 the line width is less than the target width and the print is thicker and less consistent (Fig. 4.3.3.7a, b) as the ink is unable to relax following the removal of shear and the elastic nature of the ink means it is pulled vertically by the screen as it pulls away from the substrate to give a rough print.

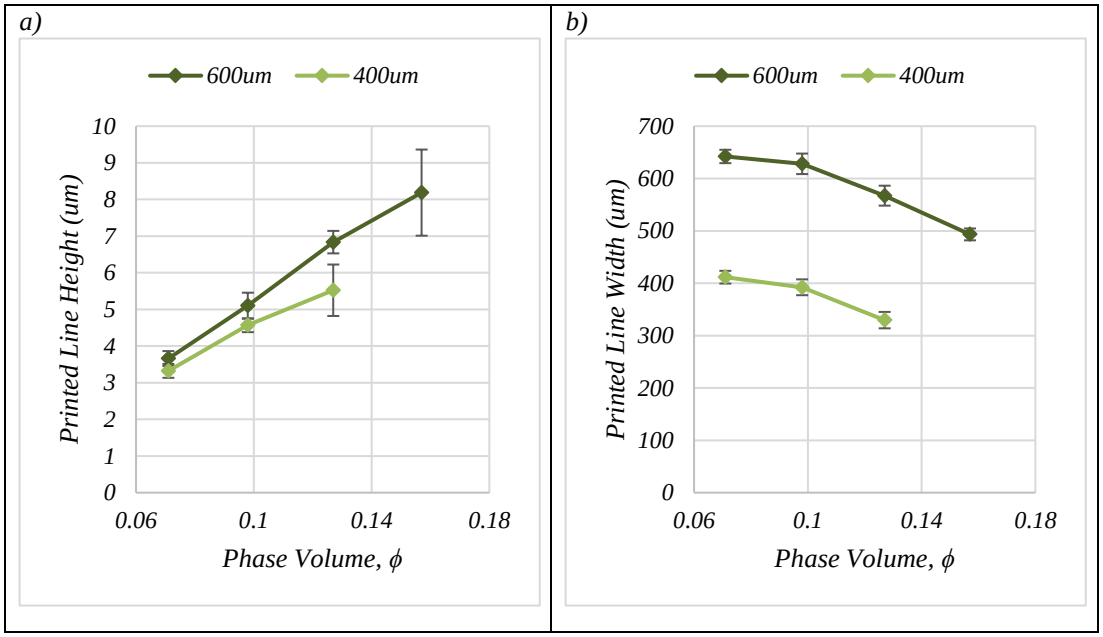

Figure. 4.3.3.7) The effect of concentration NH_3 GNP on the printed line morphology of a 600 and 400um printed line

4.4 Closure

The effects of phase volume of ammonia plasma functionalised GNPs, a high aspect ratio Nano-carbon, on a near Newtonian low viscosity thermoplastic polyurethane resin system has been studied using shear and quiescent oscillatory rheology.

SEM imaging showed the polydisperse nature of the GNPs following dispersion with a typical size of 1-8um and thickness 0.75-100nm. This would give the particles a range of aspect ratios between 10-100. The GNPs have dimensions within the Nanoscale shows they have been well dispersed following three roll milling.

At low concentrations, $\phi=0.071, 0.098, 0.127$ the GNPs were well dispersed with a similar shear profile and viscoelastic behaviour to the unfilled TPU resin, as viscous behaviour prevailed indicating the absence of any long-range order within the fluid. Particle interactions increased rapidly as $\phi \rightarrow \phi_m$ as indicated by rapid increases in the relative viscosity, increased low shear rate shear thinning, with G' becoming increasingly frequency independent, especially in the $\phi=0.157$ suspension. Interparticle distances decrease with increasing concentration and the nanoscale. High aspect ratio GNPs initially move out of one another's way to align with the flow before at the highest concentrations the GNPs form interactions that elastically store energy and trap matrix material, preventing it from deforming at the same rate as the rest of the matrix, to give a higher viscosity.

Established rheological models were fitted to the experimental data, to model the effect of high aspect ratio Nano-carbon on the viscosity of a low viscosity system. Using the intrinsic viscosity, $[\eta]$, and the maximum packing fraction, ϕ_m, as fitting parameters the Krieger-Dougherty (K-D) provided the best fit (RMSE=0.117) with values of $[\eta]$=6.33 and ϕ_m=0.184. From these parameters it was estimated that the GNPs had an aspect ratio of approximately 21.12. This gave good agreement between the estimates of aspect ratio from the SEM images, Ar=13-106 and the predictions of the aspect ratio from the rheological models, Ar=21.12. The fitting of the Krieger-Dougherty model to experimental viscosities at various phase volumes was shown to be an effective method of characterising the shape and dispersion of high aspect ratio nanocarbons, without the need for printing. Therefore, the fitting of the Krieger-Dougherty model to experimental data could be a time and cost-effective method for assessing dispersion.

Both Ammonia functionalised (NH_3 GNP) and un-functionalised (R1 GNP) Graphite Nanoplatelets were dispersed into a low viscosity resin system. Initial rheological measurements showed that the particles were of similar size, shape and dispersion following triple roll milling with both fitted to the curve developed in the previous work by the authors.

Over a twelve-week period the viscosity and viscoelasticity of the R1 GNP suspensions drops periodically in time with the rate fastest for the highest concentration. The unfunctionalized R1 GNPs approach each other under Brownian motion in the low viscosity fluid before agglomerating due to van der Waals forces. These larger, lower aspect ratio agglomerates occupy a smaller volume in the flow, increasing interparticle distance and reducing particle-particle and particle-polymer interactions. This causes a decrease in the viscosity, shear thinning behaviour and viscoelastic properties of the fluid.

The ammonia plasma functionalised NH_3 GNP suspensions maintain their rheological properties at all concentrations over the same period, with small increases in elasticity and viscosity attributed to solvent loss. Ammonia plasma functionalisation increases the Nitrogen content and surface polarity of the NH_3 GNPs, giving improved chemical compatibility with the thermoplastic polyurethane. This allows the TPU to better wet the particles to create a steric barrier that holds the

particles far enough apart to prevent agglomeration. Therefore, the NH_3 GNP suspensions maintain their rheological properties over the same twelve-week period.

This work shows that selecting an appropriate plasma functionalisation treatment, can lead to improved particle-polymer interactions that can create a steric barrier to help hold nanocarbons far enough apart to avoid agglomeration. The use of this work will be highly significant for highly filled Nano-carbon systems, such as those used in electrically conductive inks, where typically the binder is of lower viscosity than those used in melt polymers, and therefore interparticle forces play an increasingly significant role.

The effect of increasing concentration GNP on the printability and electrical conductivity of GNP based carbon conductive inks has been studies. As described in the first part of the chapter increasing the concentration of GNP caused increases in the viscosity and elasticity of the inks as particle interactions become increasingly prevalent.

Increasing the concentration of GNP increased the printed thickness due to the increased solid content within the inks. At $\phi<0.157$ the prints showed little change in surface roughness with increasing concentration, as increasing the concentration of GNP led to a more-dense layer of carbon material. At $\phi=0.157$ there is a large increase in surface roughness and the variance in the surface roughness with mesh marking appearing in the surface of the prints. This suggests that at the highest loading GNP the inks are suitably viscous and elastic that they are unable to relax having passed through the screen to form a smooth consistent layer.

Sheet resistance decreases exponentially with loading owing to increased volume of conductive material, therefore there is a larger conductive network available for the current to pass through. Bulk resistivity considers the increased thickness of the ink deposit to give a better understanding of materials. There is a large drop in bulk resistivity between $\phi=0.071$ and $\phi=0.098$ as substantially more GNP-GNP contacts are made to create a better-established conductive path. At $\phi>0.098$ there are modest decreases in the bulk resistivity as a well-established conductive path is already formed in the bulk material, with the increasing conductive material creating only a slightly better conductive path while causing significant increases in the viscosity

and elasticity of the fluids, causing increased surface roughness that negatively affects the electrical properties.

The lower concentration inks were able to print smaller features as the less viscous and elastic films could more easily flow through the screen and spread on the substrate, this can be seen in their lower feature height and having line widths greater than the attempted printed line width. At higher concentrations the elasticity of the ink and the inks inability to slump led to tall lines of low width as the ink grips onto the screen as it is pulled away from the substrate and can't wet upon the removal of shear to leave tall, narrow lines.

At $\phi > 0.127$ the roughness of the prints increased substantially, with only modest improvements in conductivity, therefore $\phi < 0.157$ GNPs should be used for optimum printability using the current print settings. Despite being well dispersed, and the high bulk conductivity properties the GNPs show significantly higher bulk resistivities, than commercially available carbon conductive inks. Like graphite this is likely due to the contact resistance between the high aspect ratio platelets, as they make limited direct physical contact. Investigation into the hybridization of the ink to improve interplatelet contact could provide improvements in the conductivity.

4.5 References

[1] E. Jewell, S. Hamblyn, T. Claypole and D. Gethin, "The impact of carbon content and mesh on the characteristics of screen printed structures," *Circuit World,* vol. 39, no. 1, pp. 13-21, 2013.

[2] T. S. Tran, N. K. Dutta and N. R. Choudry, "Graphene Inks for Printed Flexible Electronics: Graphene dispersions, ink formulations, printing techniques and applications," *Advances in colloid and interface science,* vol. 261, pp. 41-61, 2018.

[3] H. A. Barnes, J. F. Hutton and K. Walters, An Introduction to Rheology, Amsterdam: Elsevier Science Publishers, 1989.

[4] S. Chatterjee, J. Wang, W. T. N. Kuo, C. Salzmann, L. W.L, R. Hollertz, F. Nuesch and B. Chu, "Mechanical reinforcement and thermal conductivity in expanded graphene nanoplateles reinforced epoxy composites," *Chemical Physics Letters,* pp. 6-10, 2012.

[5] S. Kim, Y. Noh and J. Yu, "Thermal conductivity of graphene nanoplatelet filled composites fabricated by solvent free processing for the excellent filler dispersion and a theoretical approach for the composites containing the geometrized fillers," *Composites: Part A,* pp. 219-225, 2015.

[6] J. Williams, W. Broughton, T. Koukoulas and S. S. Rahatekar, “Plasma treatment as a method for functionalising and improving the dispersion of carbon nanotubes in epoxy resins,” *Journal of Materials Science,* pp. 1005-1013, 2013.

[7] A. Felten, C. Bittencourt, J. Pireaux, G. Van Lier and J. Charlier, “Radio-frequency plasma functionalisation of carbon nanotube surface O_2, NH_3, and CF4 treatments,” *Journal of Applied Physics,* vol. 98, 2005.

[8] C. Saka, “Overview on the Surface Functionalization Mechanism and Determination of Surface Functional Groups of Plasma Treated Carbon Nanotubes,” *Critical Reviews in Analytical Chemistry,* vol. 48, no. 1, pp. 1-14, 2018.

[9] M. R. Rueda, M.-C. Auscher, R. Fulchiron, T. Perie, G. Martin, P. Sonntag and P. Cassagnau, “Rheology and applications of highly filled polymers: A review of current understanding,” *Progress in Polymer Science,* pp. 22-53, 2017.

[10] H. A. Barnes, A Handbook of Elementary Rheology, Aberystwyth: University of Wales Institute of Non-Newtonian Fluid Mechanics, 2000.

[11] H. A. Barnes, “A Review of the Rheology of Filled Viscoelastic Systems,” *Rheology Review,* pp. 1-36, 2003.

[12] T. Amari, K. Uesugi and S. Hiroaki, “Viscoelastic properties of carbon black suspension as a flocculated percolation system,” *Progress in Organic Coatings,* vol. 31, pp. 171-178, 1997.

[13] D. Litchfield and D. Baird, “The rheology of high aspect ratio nano-particle liquids,” *Rheology Review,* pp. 1-60, 2006.

[14] P. Cassagnau, “Linear viscoelasticity and dynamics of suspensions and molten polymers filled with nanoparticles of different aspect ratios,” *Polymer,* vol. 54, pp. 4762-4775, 2013.

[15] N. Willenbacher and K. Georgieva, “Rheology of disperse systems,” in *Product Design and Engineering*, 2013, pp. 7-49.

[16] Haydale Graphene Industries, “HDPlas Technical Data Sheet,” [Online]. Available: https://www.graphene-info.com/files/graphene/HDPlas-GNP-Technical-Sheet-2.03.pdf. [Accessed 14 2 2018].

[17] Image J, “ImageJ,” [Online]. Available: https://imagej.nih.gov/ij/. [Accessed 05 02 2020].

[18] S.-J. Potts, Y. C. Lau, T. Dunlop, T. Claypole and C. Phillips, “Effect of photonic flash annealing with subsequent compression rolling on the topography, microstructure and electrical performance of carbon-based inks,” *Journal of Materials Science,* vol. 54, pp. 8163-8176, 2019.

[19] A. Kasgoz, D. Akin, A. I. Ayten and A. Durmus, “Effect of different types of carbon fillers on mechanical and rheological properties of cyclic olefin copolymer (COC) composites,” *Composites Part B: Engineering,* vol. 66, pp. 126-135, 2014.

[20] A. Metzner, “Rheology of Suspensions in Polymeric Liquids,” *Journal of Rheology,* vol. 29, pp. 739-775, 1985.

[21] S. Mueller, E. Llewellin and H. Mader, “The rheology of suspensions of solid particles,” *Proceedings of the Royal Society A,* vol. 466, pp. 1201-1228, 2010.

[22] J. King, M. Via, M. FA, K. Wiese, E. Beach, M. Cieslinski and G. Bogucki, “Characterization of exfoliated graphite nanoplatelets/ polycarbonate composites: Electrical and thermal conductivity, and tensile, flexural, and rheological properties,” *Journal of composite materials,* vol. 46, no. 9, pp. 1029-1039, 2011.

[23] J. Claypole, Application of advanced rheometric tecniques to printing fluids, Swansea University Thesis, 2015.

[24] V. Trappe and D. Weitz, “Scaling of the viscoelasticity of weakly attractive particles,” *Physical Review Letters,* vol. 85, no. 2, pp. 449-452, 2000.

[25] Y. H. Kim, S. H. Kwon, H. J. Choi, K. Choi, N. Kao, S. N. Bhattacharya and R. K. Gupta, “Thermal, Mechanical and Rheological Characterization of Polylactic Acid/Halloysite Nanotube Nanocomposites,” *Journal of Macromolecular Science, Part B,* vol. 55, no. 7, pp. 680-692, 2016.

[26] J. Xu, S. Chatterjee, K. W. Koelling, Y. Wang and S. E. Bechtel, “Shear and extensional rheology of carbon nanofibre suspensions,” *Rheological Acta,* vol. 44, pp. 537-562, 2005.

[27] T. F. Tadros, Colloids in Paints, Weinheim: WILEY-VCH Verlag GmbH & Co. KGaA, 2010.

[28] D. Jeffrey and A. Acrivos, “The rheological properties of suspensions of rigid particles,” *AIChE Journal,* vol. 22, no. 3, pp. 417-432, 1976.

[29] B. Phillip, E. Jewell, P. Greenwood and C. Weirman, “Material and process optimization screen-printing carbon graphite pastes for mass production of heating elements,” *Jornal of Manufacturing Processes,* vol. 22, pp. 185-191, 2016.

[30] H. Kipphan, Handbook of print media: Technologies and production methods, Springer Science & Business Media, 2001.

Chapter 5: Conductive Graphite Nano-platelet Hybrid Screen-printing inks for use in Multilayer Printed Devices

5.1 Introduction

Even at volume loadings close to the maximum packing fraction, GNP only inks have poor conductivity compared to commercially available conductive carbon screen-printing pastes. Hybridizing Carbon Nano-fillers has been shown to be an efficient method to improving the properties of composites [1][2][3]. Carbon conductive screen-printing inks typically use Graphite as the more conductive component and the relatively smaller Carbon Black (CB) particles to create denser films with enhanced interplatelet connectivity [1]. Planar graphite platelets typically tens of microns in length are therefore typically combined with smaller sub-micron spherical carbon black particles [3]. The spherical high aspect ratio CB particles improve electronic transport by improving the interparticle contact between graphite particles [3].

Hybridizing graphite nano-platelets with carbon black has been shown to also improve the electronic properties of composites [4][5]. The high structured Carbon Black particles were seen homogenously dispersed between the graphite nanoplatelets, to provide a physical bridge between the GNP stacks increasing the electrical conductivity [5]. The CB is far smaller and lower aspect ratio and as such can disperse in a more efficient manner [5]. However, this work was done on composite materials where the effect of hybridizing the composite on the rheological properties of the fluid is not as critical to processability. As material rheology impacts subsequent ink transfer to the film and the geometry and conductor density in the cured film [1], this work aims to examine the effect of CB on the rheological properties of the GNP inks and its subsequent effect on printability of inks.

This chapter examines whether the hybridization of GNP based inks to form GNP/Carbon Black (CB) hybrid inks is sufficient to improve the electrical properties of the inks to make them a realistic candidate as a carbon conductive ink system. The work in this chapter was carried out chronologically before the functionalisation experiments in Chapters 3&4. It was hypothesised that Oxygen plasma functionalisation would add polar functional groups to the edges and defects sites of the GNPs to promote interaction with the polar segments of the thermoplastic polyurethane, however, later experiments proved ammonia plasma treatment to be a

more optimal plasma treatment. The polymer content within the resin system is also higher at 15wt% instead of 12.5wt%. The wt% of the polymer was reduced to 12.5wt% for later experimentation to aid resin manufacture for the commercial production of the ink.

5.2 Materials and Methods

Two different formulation approaches were used to examine the effect of CB on the rheological, electrical and print properties of GNP inks. Different quantities of Oxygen functionalised GNPs (O_2-GNP) (Haydale Ltd) and Carbon Black (CB) (Conductex SC Ultra) were wet into a 15wt% TPU/DAA resin system.

Phillips *et al (2017)* noted that optimising the ratio of graphite to carbon black brought about significant changes to the rheological and electrical properties of graphite carbon black screen-printing inks [2]. It was hypothesised that similar improvements would be seen with the GNP based inks, however, the effect that the interaction between these two Nano-carbon particles would have on the ink properties were unknown. To examine this, four different ratios of GNP:CB were dispersed in the TPU resin in the quantities described in Table 5.2.1

Table 5.2.1- Composition of GNP:CB hybrid inks

(GNP:CB)	GNP (wt %)	CB (wt %)	TPU (wt %)	DAA (wt %)
1:0	22.5	0	11.625	65.875
3:1	16.875	5.625	11.625	65.875
2:1	15	7.5	11.625	65.875
1:1	11.25	11.25	11.625	65.875
TPU	0	0	15	85

Secondly, having noticed that the even the smallest replacement of GNP with CB brought about large changes to the rheological and electrical properties of the inks small amounts of CB were incrementally added to a 15wt% GNP suspension to try to gain insight into how much CB was required to improve the properties of these composites and the potential mechanisms behind these improvements. The inks were produced in the quantities displayed in Table 5.2.2.1. The inks were synthesised using the method described in Chapter 3.

Table 5.2.2 GNP + CB ink formulations

GNP (wt%)	CB (wt%)	Total Carbon (wt%)	TPU (wt%)	DAA (wt%)
15	0	15	12.75	72.25
15	2.5	17.5	12.375	70.125
15	5	20	12	68
15	7.5	22.5	11.625	65.875
15	10	25	11.25	63.75

The inks were then screen printed onto adhesion coated PET (Hi-Fi Films) using the method and screen described in chapter 3 to allow for the determination of their electrical and print performance using a four-point probe method and white light interferometry respectively.

The measured rheological properties represent measurement of a single sample. Analysis of three separate rheological measurements of the unfilled TPU resin put standard error of measurements at ±0.07Pa.s (1.58%) for the shear measurements at $1s^{-1}$ and at 0.62Pa (2.39%) for the complex shear moduli at 1Hz. Therefore, error bars are not used on the shear measurements as they are sufficiently small as not to be visible in the graphs. Error bars of 2.39% are used in all of the oscillatory rheology graphs.

5.3 Results

SEM images of three of the GNP + CB inks were taken (Fig. 5.3.1). Following three-roll milling the GNPs form a paved structure with the GNPs lying flat to the substrate with typical platelet diameter <<10um (Fig. 5.3.1a, b) in good agreement with the SEM images of the Chapter 4. Large, polymer-filled gaps are present between neighbouring GNPs within the coating as the high aspect ratio Nano-platelets pack poorly, giving few direct point contacts between the GNPs. At 15wt% GNP + 7.5wt% CB the submicron CB particles have coated the GNPs (Fig. 5.3.1 c, d). The spaces between neighbouring GNPs have been filled by the CB/TPU matrix to give a smoother surface, with these effects enhanced at highest concentration CB to give a very smooth coating (Fig. 5.3.1e, f).

During screen printing, pastes are run at various shear rates, therefore, to understand the effect of rheology on printing it is important to consider the rheology at various shear rates [6].

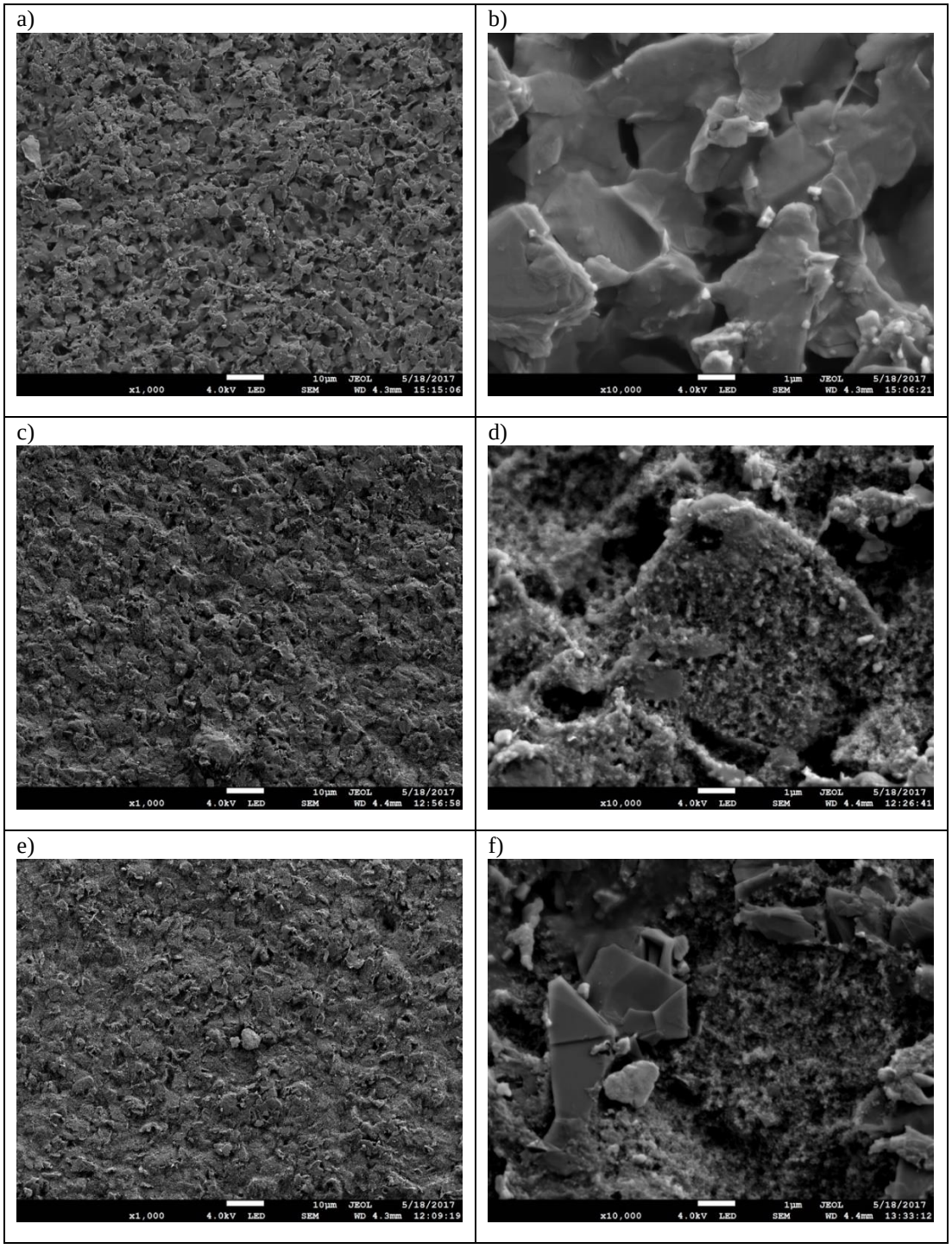

Figure 5.3.1 - SEM images at a),c),e) 1000x magnification, and b),d),f) 10,000x magnification for the a), b) 15wt% GNP ink, c), d) 15 wt% GNP + 7.5% CB ink, e), f) 15 wt% + 10% CB ink

Even at the higher concentration of 15wt% the unfilled TPU/DAA resin systems show near-Newtonian behaviour over all the measured shear rates in good agreement with Chapter 4 (Fig. 5.3.2a, b). The addition of both 15 and 22.5wt% GNP causes a vertical shift in the shear rate curve of the TPU resin with similar near-Newtonian behaviour to the unfilled resin system, with a low shear rate Newtonian plateau as

the addition of GNPs causes increased diversion of the flow lines in good agreement with the GNP only suspensions in Chapter 4.

The replacement of GNPs with a GNP/CB blend causes large increases in the low shear rate viscosity and a shear thinning behaviour. The increase in the low shear rate viscosity and low shear rate non-Newtonian behaviour is a result of the CB particles forming a weak 3D network of particles. This weak network traps part of the continuous phase, preventing it from deforming at the same rate as the rest of the continuous phase causing large increases in viscosity. Upon applying even modest shear these weak flocculates are broken down and the CB particles can move between the GNPs and align with the flow, reducing the viscosity of the ink [7]. This shows good agreement with the work on Graphite/CB inks by Phillips *et al (2017)* [2]. Increasing the GNP:CB ratio to 1:1 caused the greatest increase in the low shear rate viscosity as a stronger particle network is formed. Although this network is once more broken down by the flow, reducing its viscosity, it still has a higher viscosity even at the highest measured shear rate, indicating that the CB network is not fully broken down by the flow.

To examine the mechanism behind this increase in viscosity further, small incremental amounts of CB were added to a 15wt% GNP suspension (Figure 5.3.2b). The addition of 2.5wt% CB increases the viscosity although the shape of the flow curve is still near-Newtonian as the submicron CB particles freely flow between the larger GNPs. Increasing CB content above this point increases the shear thinning behaviour, with the largest effects seen at low shear, as the particles begin to form an increasingly dense 3D network, connecting the GNPs, to give large increases in viscosity, as this network traps the continuous phase preventing it from deforming at the same rate as the rest of the network. This weak network is broken down upon the application of even modest shear to allow the particles to align with the flow, reducing their effect on the viscosity. This suggests a critical concentration of CB particles in the fluid above which a network of CB particles starts to form, connecting the GNPs to form an increasingly dense network with increasing CB content.

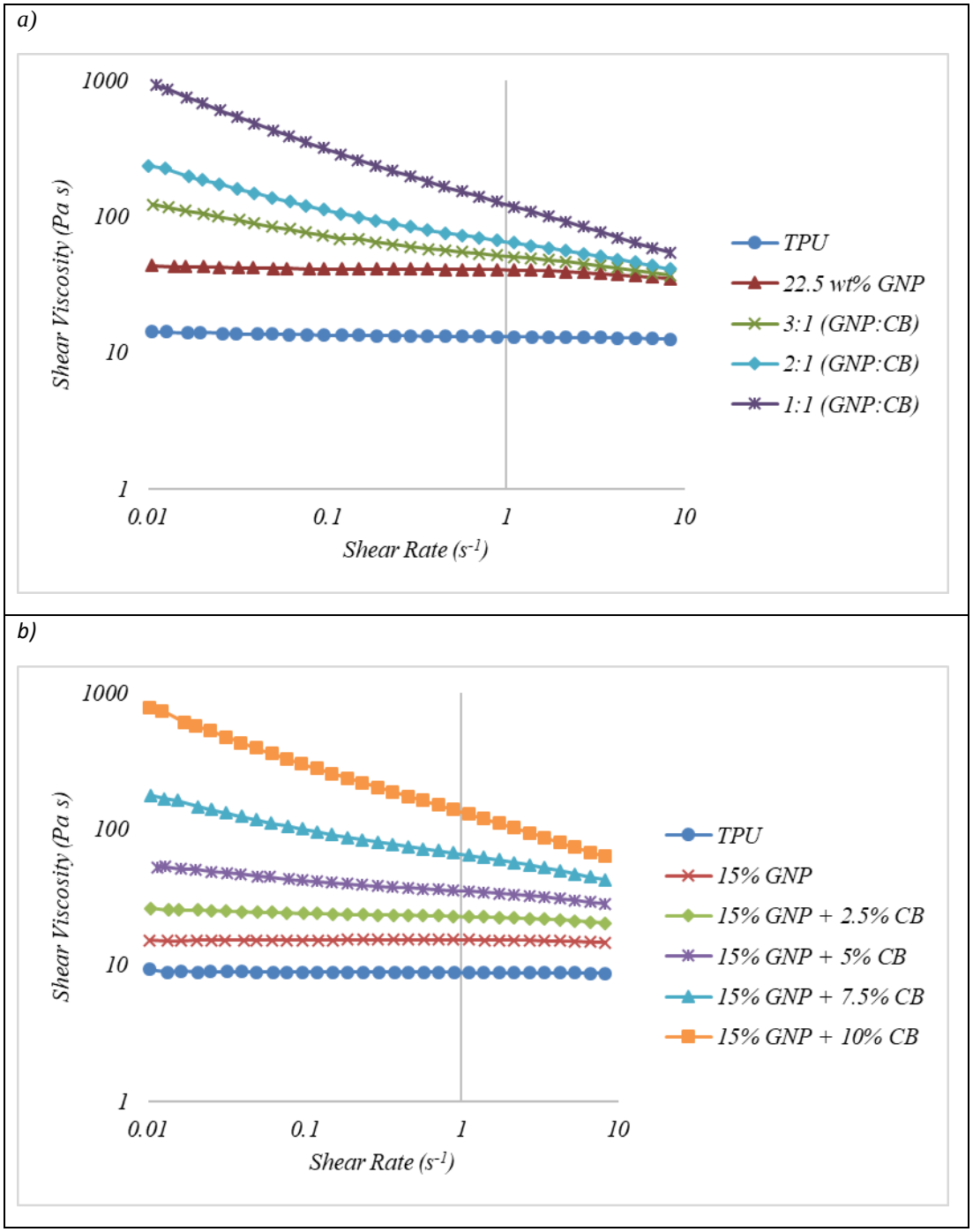

Figure 5.3.2 - a) The effect of shear rate on the instantaneous viscosity of GNP/CB composites with increasing content CB b) The effect of ratio GNP:CB on the viscosity-Shear Rate flow curve

The effect of shear rate on the shear stress of the inks is shown in Figure 5.3.3. The data is displayed at $<1s^{-1}$ and on a non-logarithmic scale to identify the intercept on the y-axis. The amount of force required to make a fluid flow is indicated by the value of the shear stress at zero shear rate. The unfilled TPU resin systems show an approximately zero intercept on the shear stress axis (Fig. 5.3.3a, b) indicating the absence of a yield stress. Yield stress has been attributed to the formation of a network of particles that deforms elastically in response to an applied stress with the

forces transmitted by direct particle to particle contact [8]. Increasing the CB content increases the intercept on the shear stress axis as the CB forms a network, which must be broken down to allow the particles to align with the flow. The inks with CB content greater than 10wt%, i.e 15wt% GNP + 10% CB and 1:1 GNP:CB, show a significant increase in the intercept on the y-axis with yield stresses >5 Pa.

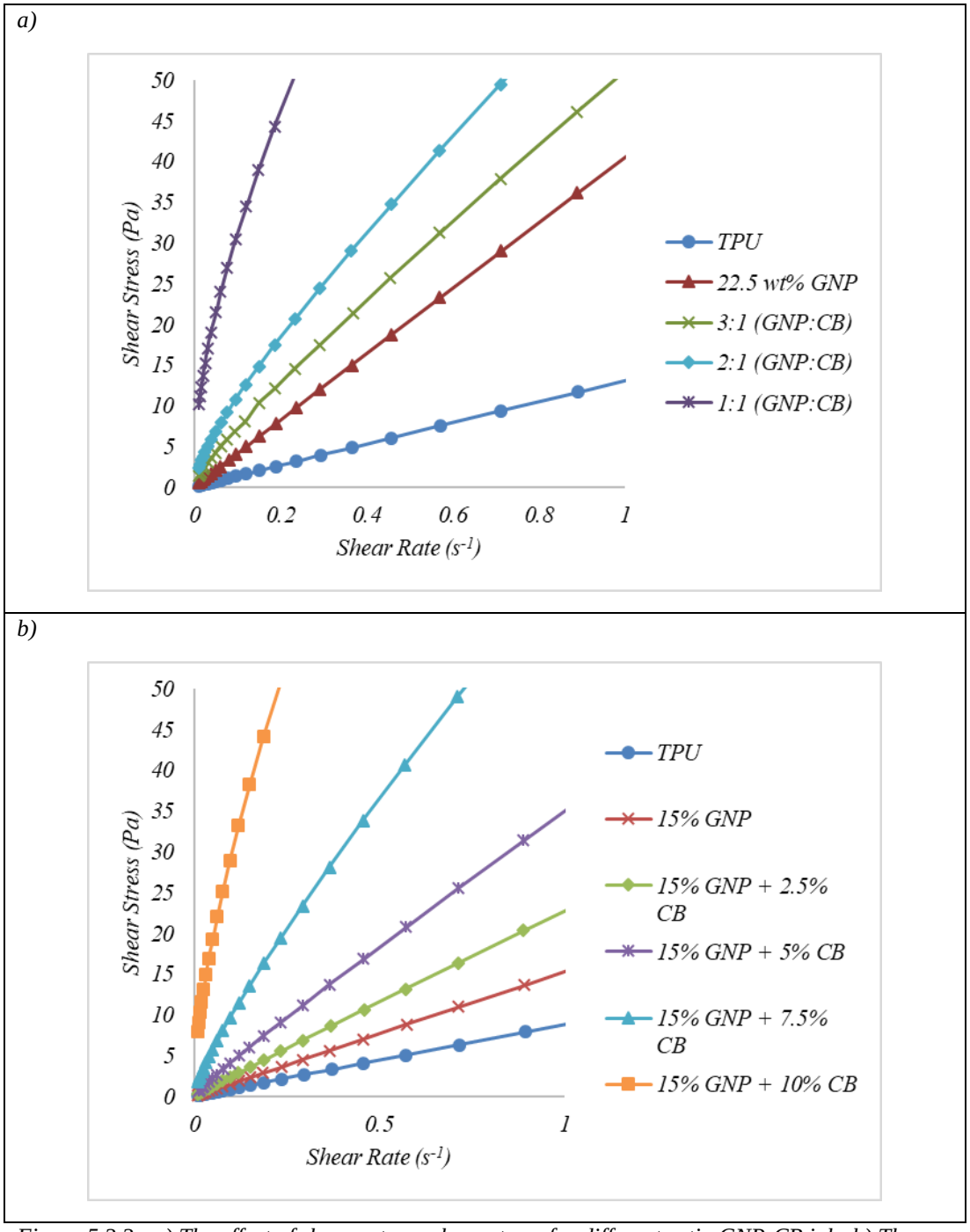

Figure 5.3.3 - a) The effect of shear rate on shear stress for different ratio GNP:CB inks b) The effect of shear rate on shear stress for GNP + CB inks

This suggest a critical concentration of CB at greater than 10wt% CB where a dense 3D network of particles is formed that must be broken down to allow the fluids to flow.

As seen in chapter 4, in the GNP only inks at 15wt% the GNPs are well dispersed within the fluid (Figure 5.3.4a). Small amounts of CB can flow with the fluid between the GNPs and will begin to coat the GNPs if the two particles are brought into direct contact (Figure 5.3.4b). At slightly higher wt% CB the CB begins to fully coat the GNPs and with increasing CB concentration, the CB begins to form connections between neighbouring GNP particles (Figure 5.3.4c). At the highest concentration CB, the surface of the GNPs is completely coated, and a dense interconnecting network of particles begins to form with the CB forming multiple connections between the GNPs (Figure 5.3.4d).

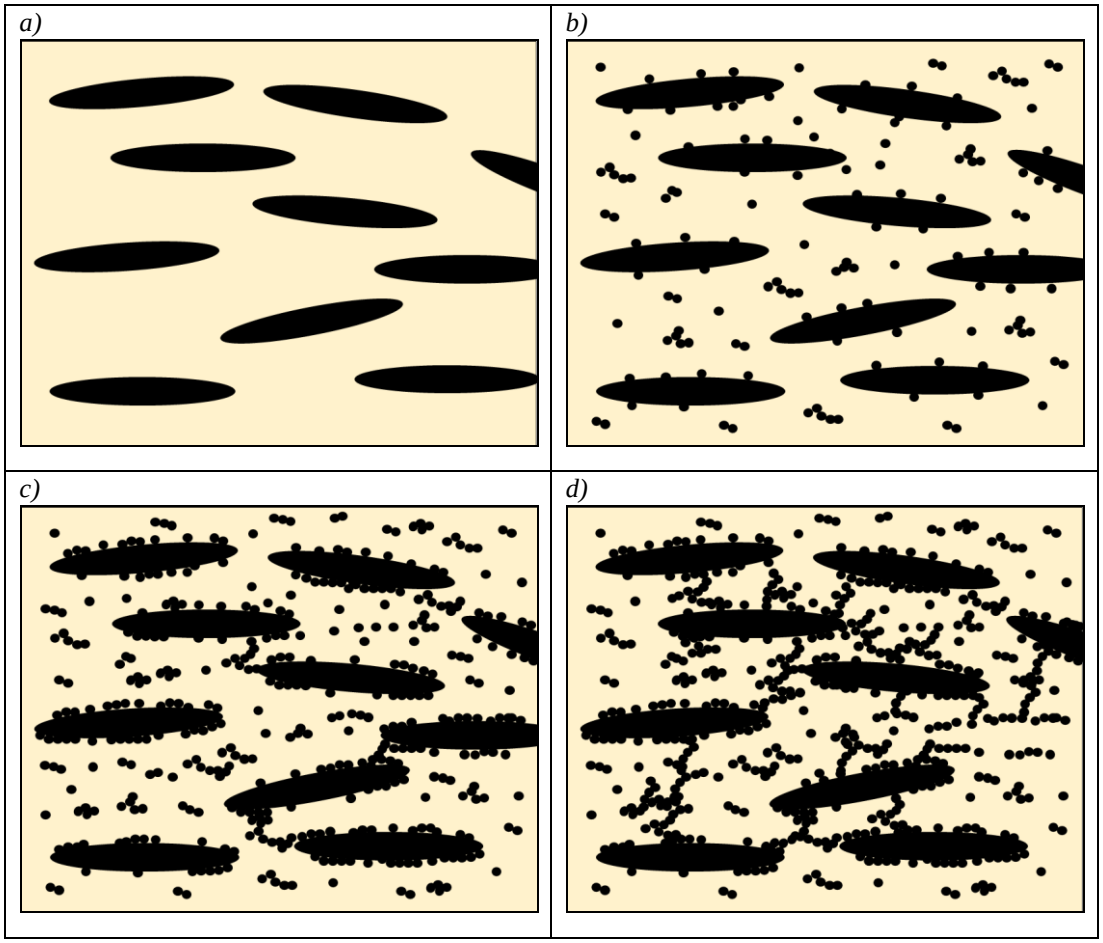

Figure 5.3.4 - Diagrams describing the effect of increasing CB content on the microstructure of GNP/CB inks at a) GNP only, b) Low CB content, c) Medium CB content d) High CB content

To simulate the effect of the ink relaxing following printing, the effect of time on the viscosity of the suspensions was measured at $0.1s^{-1}$. Thixotropy is a change in the

rheological properties with time of shearing [9]. The 1:1 (GNP:CB) ink increases in viscosity with time at a constant shear of $0.1s^{-1}$ with thixotropic nature decreasing with CB content (Fig. 5.3.5). The high concentration of the CB particles in the 1:1 (GNP:CB) ink could be beginning to form a network in time at low shear rates within the fluid, increasing the viscosity.

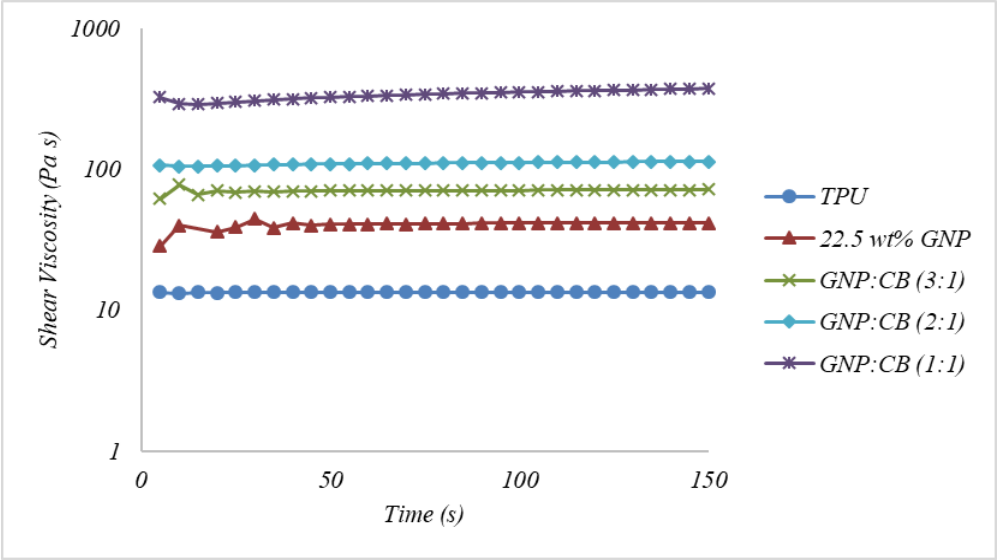

Figure 5.3.5 - Changes to the viscosity of GNP:CB inks with time of shearing at $0.1s^{-1}$

Using the method described in chapter 4 the viscoelastic properties of the fluids were measured using Small Amplitude Oscillatory Shear (SAOS). A Strain amplitude sweep was used to identify the linear viscoelastic range (LVR) (Fig. 5.3.6).

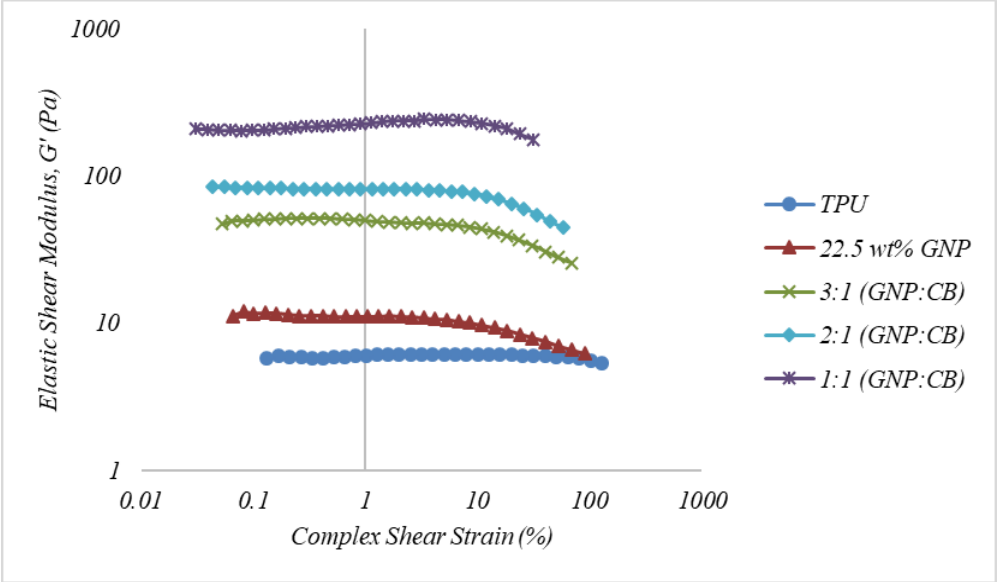

Figure 5.3.6 - Strain amplitude sweep of the GNP:CB inks at 1Hz

In the LVR *G'* and *G"* are independent of strain amplitude [7][10], indicating that there is no breakdown in the microstructure of the fluid. From this a complex shear strain of 1% was used as the amplitude of oscillation in the SAOS measurements.

Figure 5.3.7 shows the elastic (*G'*) and Viscous (*G"*) response of the materials at a frequency of 1Hz. In agreement with the work in chapter 4 the addition of 22.5wt% GNP to the TPU resin produced small increases in both *G'* and *G"*, due to increased particle-polymer and particle-particle interactions. Increasing the ratio of CB within the fluid increased both *G'* and *G"*. Increasing CB creates an increasingly dense CB network that bridges between the GNPs to create a dense 3D particle network capable of elastically storing energy. Increasing the CB ratio also increased the amount of viscous forces *G"* within the fluid although the increases are not as substantial, this could be due to the weak network of particles being easily broken down to allow the CB particles to flow to new equilibrium positions. At the highest CB content *G'* approaches *G"* as the ink begins to show more solid like behaviour as an increasingly dense 3D network of particles begins to form.

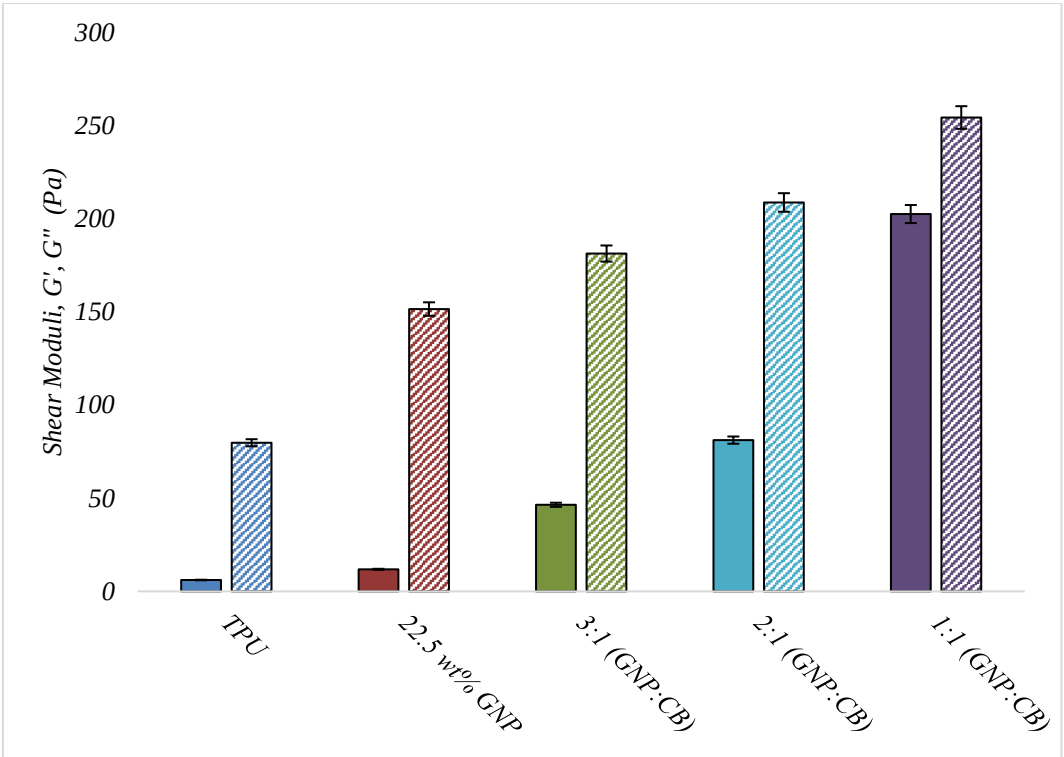

Figure 5.3.7 - The effect of GNP:CB ratio on the shear moduli at 1Hz, on the elastic storage moduli, G' (Filled), and the viscous storage moduli, G" (Patterned). Error bars of 2.39% represent the calculated rheometer measurement error for oscillatory

Figure 5.3.8 shows the phase angle of the materials at 1Hz. The TPU resin has a phase angle of 85.62 as viscous forces dominate, and the fluid has largely Newtonian behaviour (Fig. 5.3.7). In agreement with Chapter 4 the addition of 22.5wt% GNP had little effect upon the phase angle of the pure TPU resin, indicating proportional increases in both elastic and viscous forces, with Newtonian behaviour still dominating. Replacing GNP with CB causes the ink to show more elastic solid like behaviour. Increasing the ratio of CB decreases the phase angle, with phase angle is as low as 51.4 at 1:1 (GNP:CB) as *G'* tends to *G"*. This increasingly solid behaviour as CB content increases is indicative of the development of an increasingly dense CB network in the matrix bridging between the GNPs to form a dense 3D network.

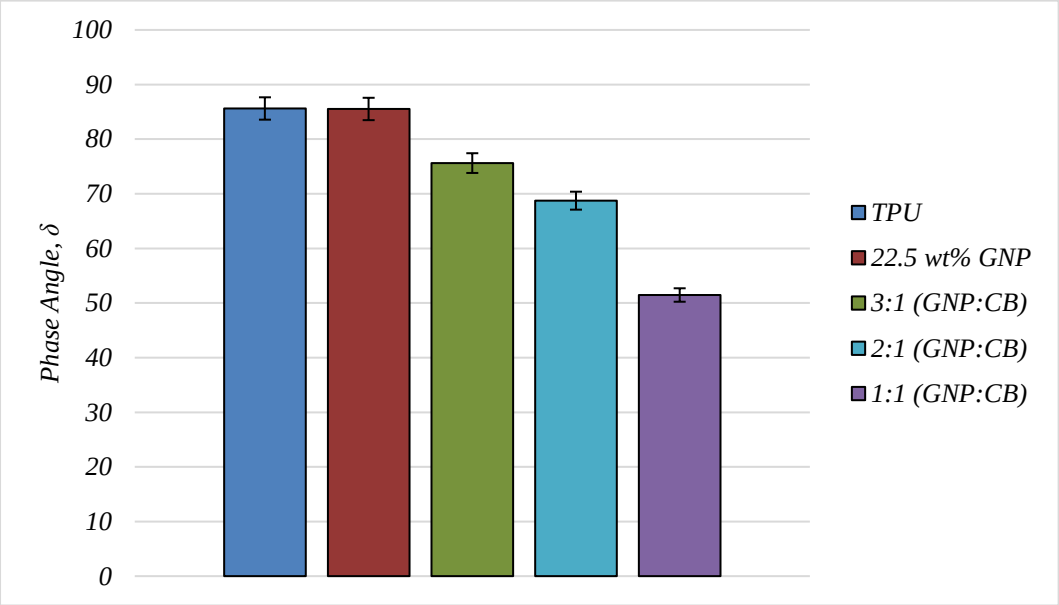

Figure 5.3.8 - The effect of ratio GNP:CB on the SAOS phase angle at 1Hz. Error bars of 2.5% represent the calculated rheometer measurement error for oscillatory

The 22.5wt% GNP only ink produced a significantly thicker print despite the same solids content as the flaked materials pack poorly to form a thick layer with spaces between the particles (Fig. 5.3.9). By replacing 25wt% of the GNPs in the 3:1 GNP:CB ink thickness reduced to ≈4um as the relatively smaller spherical CB particles pack between the GNPs to form a denser film. Further increases in CB caused increases in print thickness as the viscosity and elasticity of the ink increases, potentially causing more ink to be pulled from the screen to leave a thicker deposit.

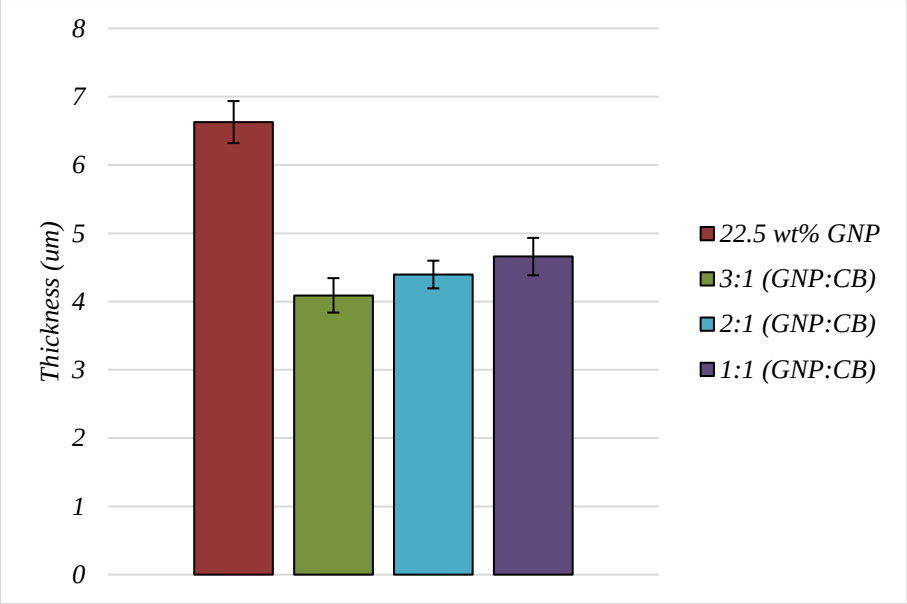

Figure 5.3.9 - The effect of GNP:CB ratio on the printed film thickness. Error bars represent the standard deviation of 15 measurements across 5 samples for each of the inks.

The addition of up to 5wt% CB to a 15wt% GNP ink has no significant effect on the printed thickness despite the increased viscosity and solid loading up to 15wt% GNP + 5wt% CB as the submicron CB particles can pack between the larger GNPs during drying to create a denser film (Fig. 5.3.10). At 10wt% CB there is a large increase in print thickness as the gaps between the particles have largely been filled and increasing the carbon content merely leads to an increased print thickness.

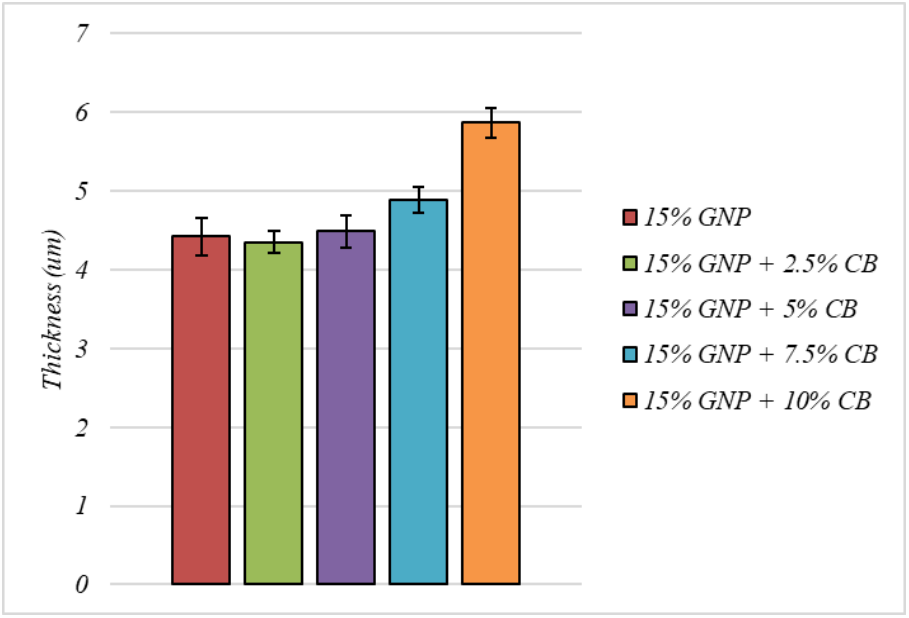

Figure 5.3.10 - The effect of CB content on print thickness. Error bars represent the standard deviation of 16 measurements across 4 samples for each of the inks.

Surface topography of the final coating impacts on the electrical properties of the film as the topological variations provide a significant barrier to efficient charge transfer [1] [11]. Two factors that contribute to the roughness of a printed feature are the underlying topography of the print and roughness due to particles [2].

The 22.5wt% GNP print showed the highest roughness producing an average surface roughness 1014nm (Fig. 5.3.11). As seen in Chapter 4 the flaked nature of GNP means they are unable to pack effectively during drying and leave a rough paved structure with GNPs at various angles to the substrates and gaps present in the surface [13][14]. Increasing the amount of CB to 3:1 (GNP:CB) produced a ≈40% decrease in the average roughness, creating a surface with roughness 602nm. This is because the significantly smaller, spherical carbon black particles can pack between the larger GNP flakes during drying to create a smooth flat layer [4][5] as can be seen in Figure 5.3.1.

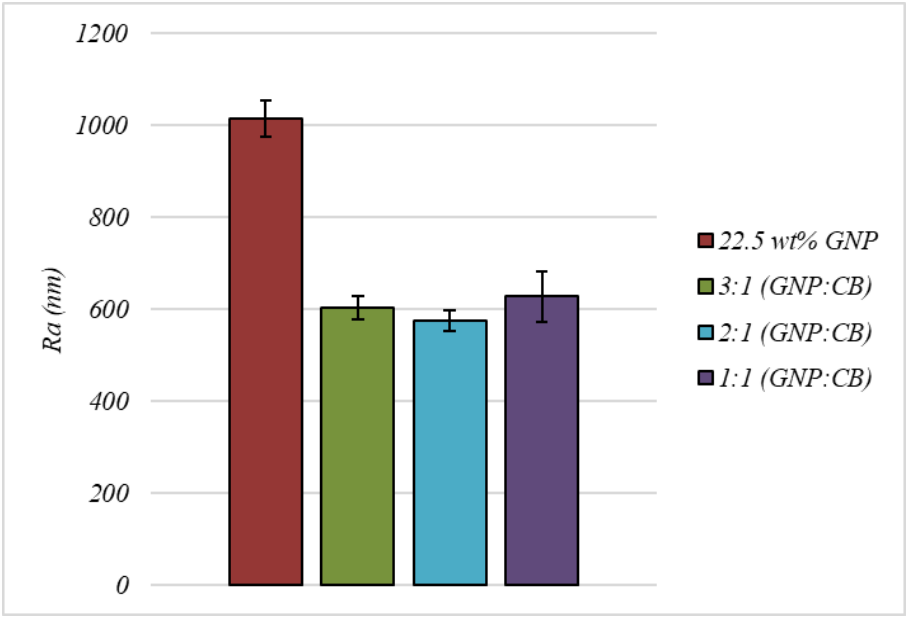

Figure 5.3.11 - The effect of ratio GNP:CB at 22.5wt% on print average surface roughness. Error bars represent the standard deviation of 15 measurements across 5 samples for each of the inks.

Increasing the amount of CB above this point to 1:1 (GNP:CB) leads to the introduction of print defects such as screen patterning. The 1:1 (GNP:CB) ink had the highest low shear viscosity and yield stress, the greatest amount of low shear rate shear thinning behaviour, the highest G' and the lowest phase angle, with all of these properties associated with the formation of an increasingly dense network of particles as CB content increased. The increasing development of elastic structure at low shear rates and prevent the 1:1 (GNP:CB) ink from slumping to form a smooth

continuous print following the removal of the shear forces associated with the squeegee to leave mesh markings (Fig. 5.3.12d) [2].

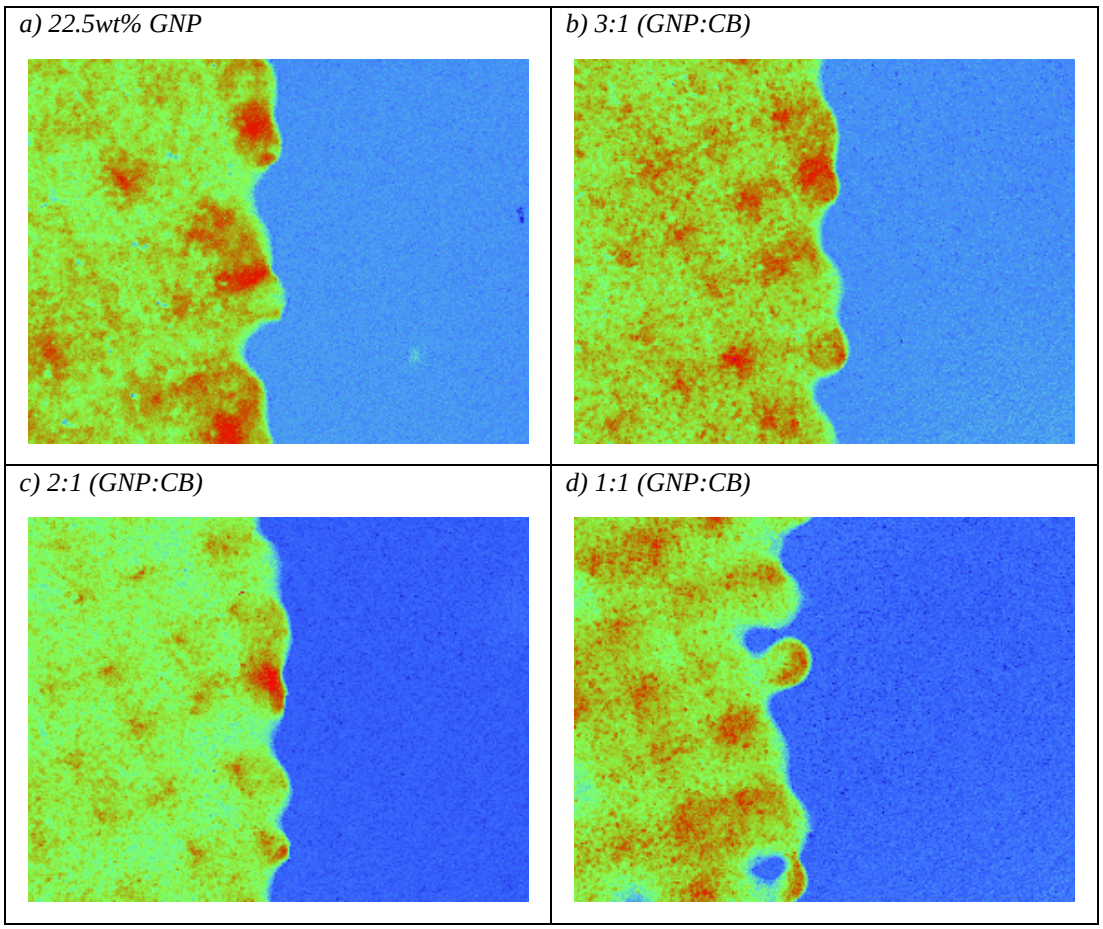

Figure 5.3.12 - Images from White Light Interferometry showing the effect of GNP:CB on the topography of the prints. a) 22.5wt% GNP, b) 3:1 (GNP:CB), c) 2:1 (GNP:CB), d) 1:1 (GNP:CB)

The addition of CB to the 15wt% GNP ink produced decreases in the average surface roughness, Ra, despite the increased ink viscosity and solids content as the CB/TPU matrix containing the submicron CB particles packed in the gaps between the GNPs to give a smoother, denser surface (Fig. 5.3.13).

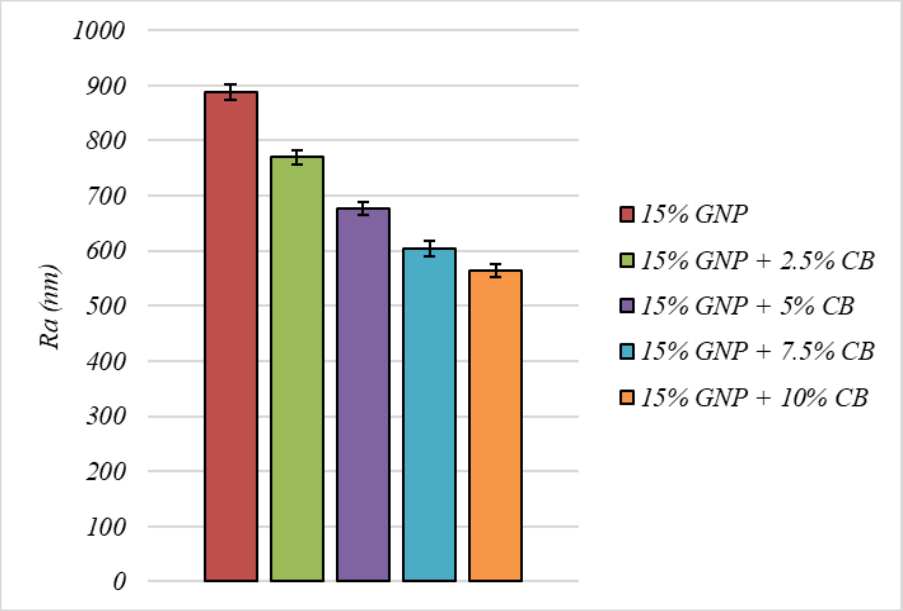

Figure 5.3.13 - The effect of increasing CB content on the average printed surface roughness, Ra (nm). Error bars represent the standard deviation of 16 measurements across 4 samples for each of the inks.

At the higher CB content inks, wt%>15wt% GNP + 7.5wt% CB, significant increases in the viscosity led to the introduction of print defects such as screen patterning as the higher CB content inks were unable to relax following the removal of shear to form a smooth, consistent layer (Fig. 5.3.14 d, e). The hybridization of GNPs with CB typically improves the surface roughness of the inks as the significantly smaller CB particles fills the voids between the GNPs to create a denser, smoother, surface. However, above a critical concentration of CB the increased viscosity, low shear rate shear thinning behaviours, yield stress and elastic shear moduli of the fluids arising from the formation of an increasingly dense network of particles prevents the inks from relaxing following in the release zone to form a smooth continuous print.

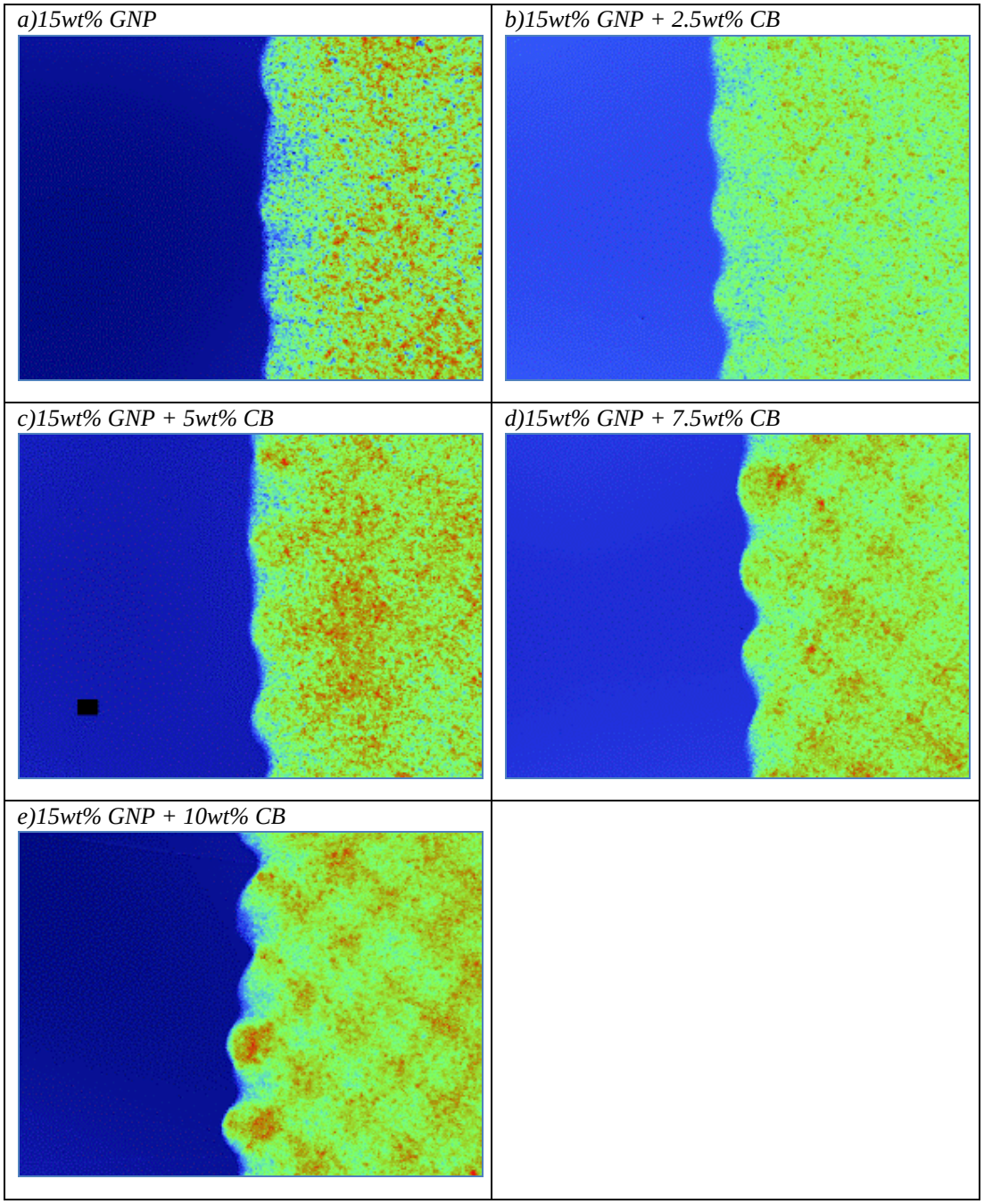

Figure 5.3.14 - White light images showing the effect of CB wt% on the surface roughness of GNP/CB hybrid screen-printing inks

Figure 5.3.15 shows the effect of CB of on the sheet resistance of the GNP/CB inks. Increasing the CB content to 3:1 (GNP: CB) decreased the sheet resistance of 22.5wt% GNP coatings by over an order of magnitude, from 5012 (Ω/□) to 323 (Ω/□) (Fig 5.3.15a). Further increases in CB content to 2:1 (GNP:CB) brought about further improvements in the electrical properties. The improvements with CB tail off at 1:1 GNP:CB. The decrease in resistance shows good correlation with the decrease in the surface roughness of the inks.

The addition of just 2.5wt% CB to the 15wt% GNP ink brought about significant improvements in the sheet resistance of the GNP only inks (Fig. 5.3.15b).

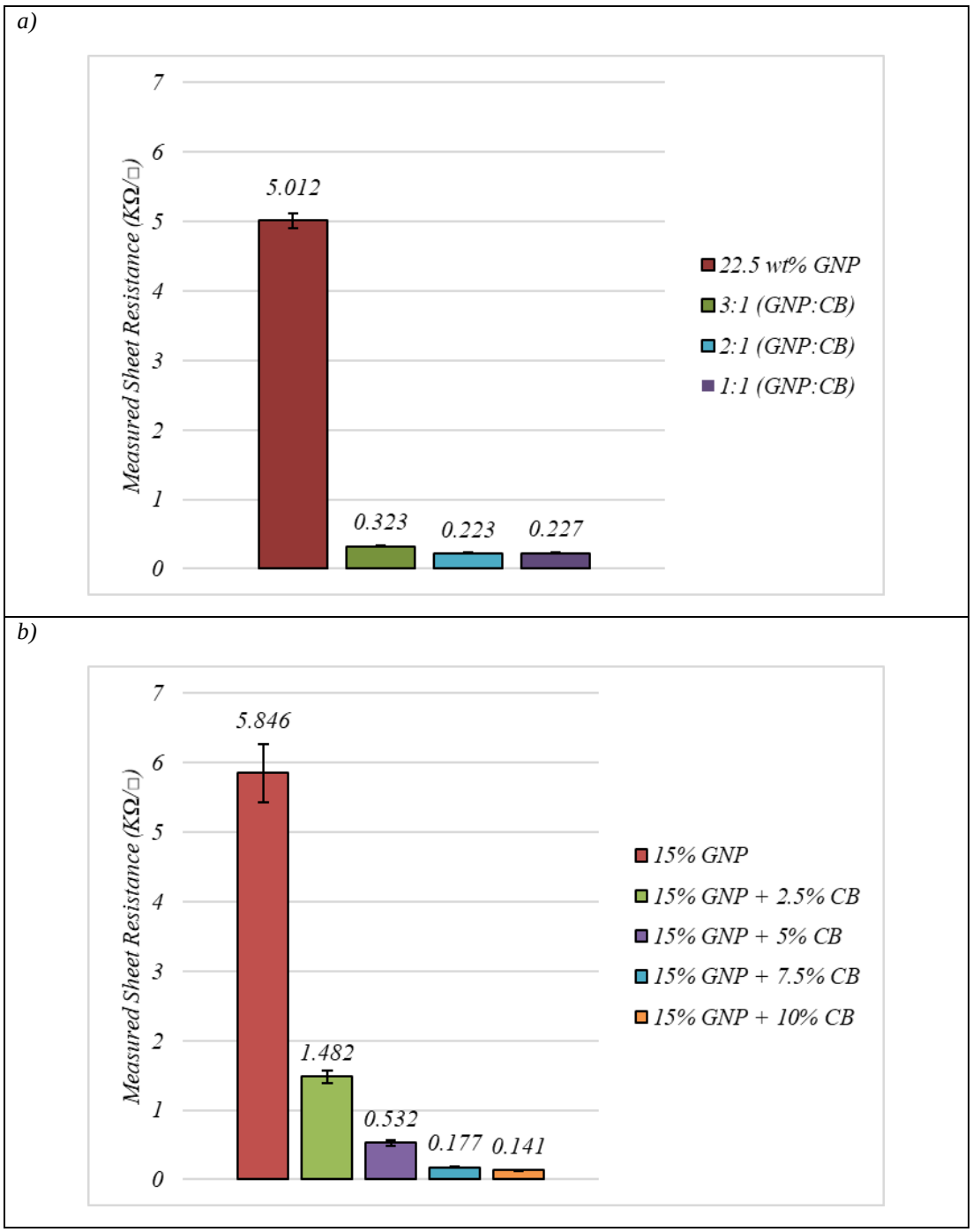

Figure 5.3.15 - a) The effect of GNP:CB ratio on the measured sheet resistance of the screen-printed coatings. Error bars represent the standard deviation of 20 measurements across 4 samples for each of the inks. b) The effect of increasing CB wt% on the measured sheet resistance of GNP inks. Error bars represent the standard deviation of 24 measurements across 4 samples for each of the inks.

Further improvements were seen in the electrical properties of the inks with increasing CB content with the improvements in the electrical properties again correlated with improvements seen in the average surface roughness.

The conductive GNPs are dispersed in an insulative TPU resin therefore the electrically conductive network of the print is dependent on the number of direct GNP-GNP contacts. For the poorly packed high aspect ratio GNPs the number of GNP-GNP contacts is low (Fig. 5.3.16a). The submicron, fractal CB is well dispersed throughout the TPU matrix to create a CB/TPU composite matrix. Even at loadings as low as 2.5wt% the CB coats the high specific surface area GNPs, increasing the areas of direct electrical contact between neighbouring GNPs (Fig. 5.3.16b). Increasing CB content further continues to increase the electrical conductivity of the coatings up to 7.5wt% CB as an increasingly dense conductive network develops between neighbouring GNPs (Fig. 5.3.16c), until at the highest concentration a dense network has formed between the GNPs (Fig. 5.3.16d)

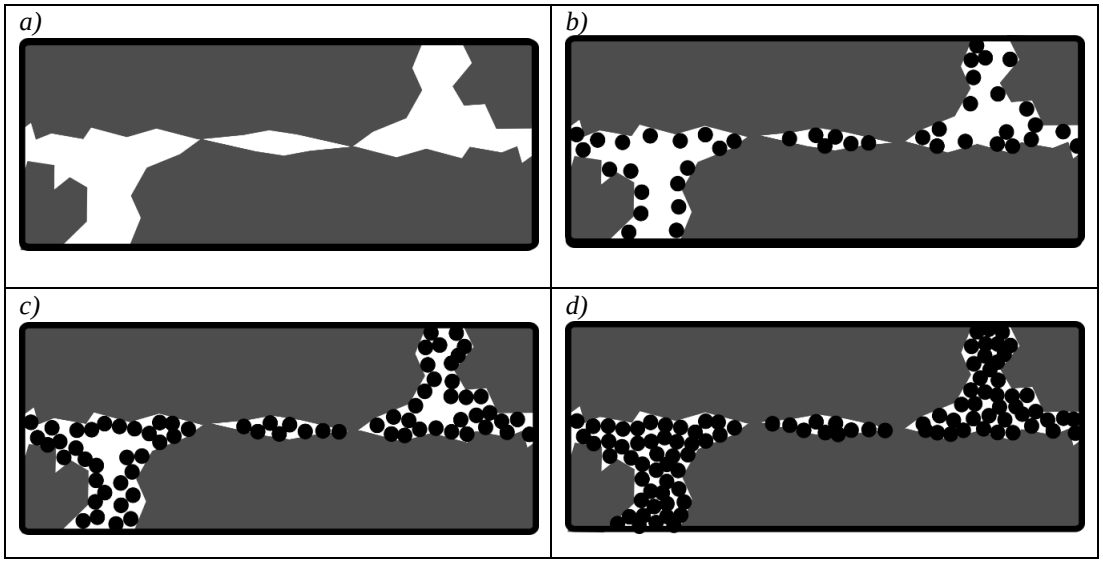

Figure 5.3.16) Diagrams representing the change in GNP-GNP contact with increasing concentration CB. a) GNP-GNP contact, b) The effect of low wt% CB on GNP-GNP contact c) The effect of intermediate CB wt % on GNP-GNP contact d) The effect of high wt% CB on GNP-GNP contact

Bulk resistivity can be used to gain a better understanding about the bulk electrical properties of the coating and allows for comparison with other materials. The two optimum inks with regards to electrical conductivity from the two different sets of ink were the 22.5wt% 2:1 GNP:CB and the 15wt% GNP + 10wt% CB inks with bulk resistivities of 0.1 and 0.08Ω·cm respectively. This is double the 0.04 Ω·cm of the optimised Graphite/CB ink used by Phillips et al [2] and the 0.037 Ω·cm of the Graphite/CB ink used by Potts et al [13]. This is likely due to the increased contacts with the matrix as the GNPs are significantly smaller particles than Graphite, increasing the number of contact points with the matrix. Industrially the resistivity is

often also displayed with regards to the sheet resistance normalised to 25.4um (Ω/□/mil). The 2:1 GNP:CB and the 15wt% GNP + 10wt% CB had normalised sheet resistances at 25.4um of 38.65±1.27 and 32.45±0.08 Ω/□/mil respectively.

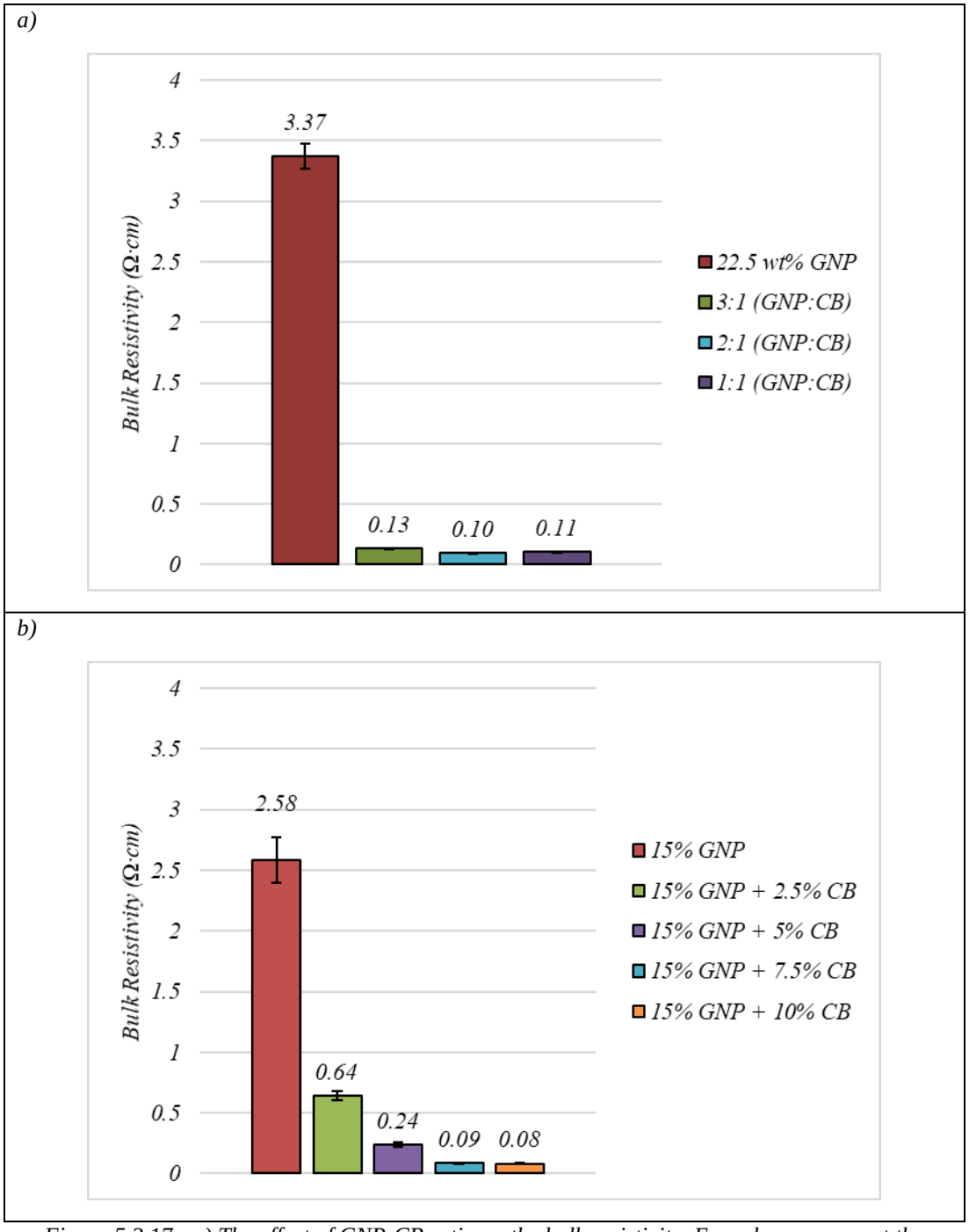

Figure 5.3.17 - a) The effect of GNP:CB ratio on the bulk resistivity. Error bars represent the standard deviation of 20 measurements across 4 samples for each of the inks. b) The effect of increasing CB wt% on the bulk resistivity of GNP inks. Error bars represent the standard deviation of 24 measurements across 4 samples for each of the inks.

This puts the conductivity of the materials at a competitive conductivity to the 12Ω/□/mil stated on the data sheet of the Haydale HDPlas IGSC02002 used in the original heater design.

The hybridization of GNP inks with CB brought about large decreases in the electrical properties and surface roughness of the inks despite increasing the viscosity, low shear rate shear thinning behaviours and elastic moduli of the inks. However, at the highest CB contents this increased viscosity and elastic moduli of the ink, prevented the ink from settling to form a smooth, consistent layer following screen printing which could have negative effects on the electrical properties of the ink, adhesion to the substrate and overall device performance in a multi-layer device. Therefore, going forward an ink formulation of 15wt% GNP and 7.5% CB (2:1 ratio GNP:CB) has been decided as an optimum formulation combining good electrical conductivity with good print surface roughness.

The O_2 GNPs used within this study were fitted to the model developed in Chapter 4 (Fig. 5.3.18).

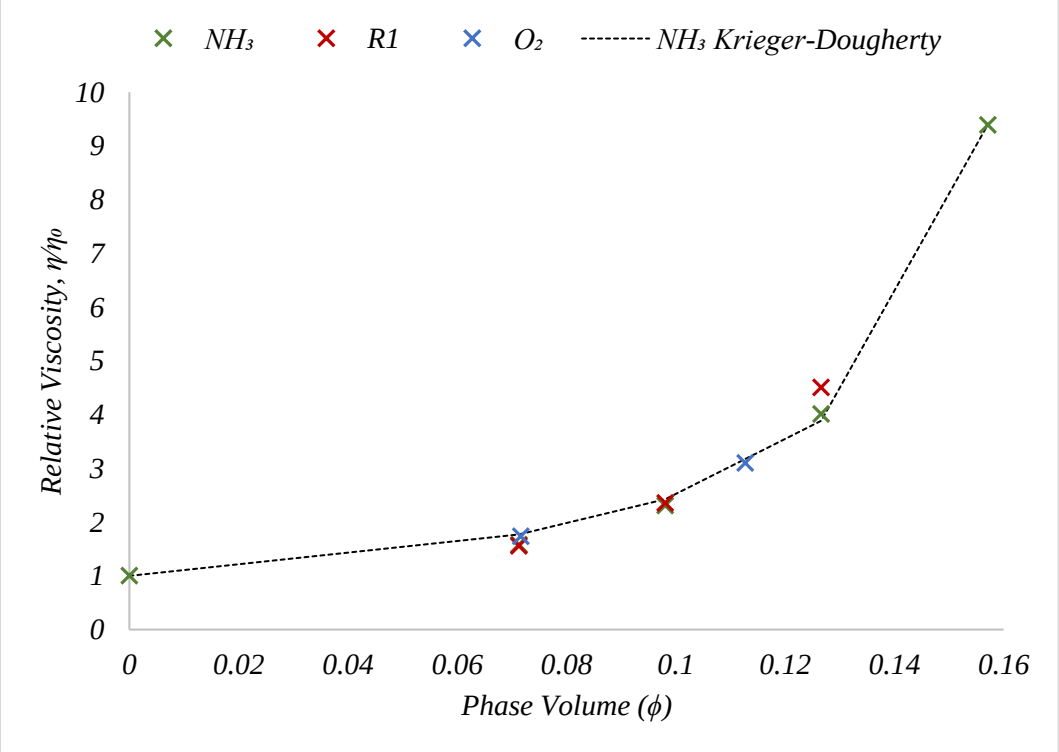

Figure 5.3.18 - Fitting experimental data for different f-GNPs to the model developed in Chapter 4

The GNPs show a good fit suggesting they are of a similar size, shape and dispersion quality and that the model can accurately predict the effect of phase volume GNP on

the suspension viscosity. The resin used in this study was of higher polymer concentration and as such was 10 Pa.s more viscous than that used in the previous study. That the O_2 GNPs can be fitted onto the same curve this demonstrates that the model is effective irrespective of plasma functionalisation and resin viscosity.

5.4 Closure

The effect of CB on improving the electrical properties of GNP based conductive inks was examined. Hybridization with CB brought about improvements in the electrical properties of the inks, but the addition of CB also affected the rheological properties, and therefore the print performance, of the inks.

Two different ink types were used to examine the effect of hybridizing GNP inks with CB. Firstly, the effect of changing the ratio of GNP:CB at a constant carbon content of 22.5wt% was examined. The second set of inks involved adding small incremental amounts of CB to a 15wt% GNP ink. Shear and oscillatory rheology were used to study the effect of increasing CB content on the rheological properties of inks. The addition GNPs to the TPU resin increased the viscosity and the viscoelasticity of the of the TPU resin. The GNP only ink showed similar shape flow curves and a similar phase angle to the TPU resin indicating the GNPs are well dispersed, and the liquid like properties of the resin properties dominate in good agreement with chapter 4.

In the 22.5wt% inks increasing the CB content led to increases in the increased low shear rate viscosity and shear thinning behaviour, increased yield stress, elasticity and solid like behaviour as the CB particles began to form a network between the GNPs. At the highest CB content, GNP:CB 1:1, the low shear viscosity was significantly higher than the other inks. This high elasticity and level of structure building prevents the ink from relaxing following the removal of shear to leave. The effect of CB on the rheological properties of the fluid was further examined by adding small 2.5wt% increments of CB to a 15wt% GNP ink. At low concentrations of CB the particles coated the GNPs and could flow between the larger GNP particles. As CB content increased an increasingly well-developed network of particles began to form, increasing viscosity, shear thinning behaviour and at the highest CB concentrations a yield stress >5Pa was visible.

GNP only ink showed high print thickness and roughness as the platelets were unable to pack effectively to form a smooth layer. Surface roughness decreased with the addition of the CB as the sub-micron CB particles coated the GNPs and filled the voids between the GNPs to form a smooth dense coating. Although at the highest CB contents, the increases in the ink viscosity and elastic properties prevented the ink from relaxing following the screen release to leave mesh marking and inconsistencies in the surface of the prints.

GNP only inks show poor electrical conductivity, as their poor packing leads voids between neighbouring GNP particles and a limited number of direct GNP-GNP contacts. Hybridizing GNPs with CB brought about significant improvements in the electrical properties of the Nano-composite coatings, as the CB particles coat the GNPs and fill the spaces between the GNPs to increase the number of electrical contacts between neighbouring GNPs, to create an increasingly dense conductive network. The addition of just 2.5wt% brought about significant improvements in the electrical properties of GNP only inks, while having a minimal effect on the rheological properties, as the well dispersed submicron CB particles were able to move between the larger GNPs in the fluid.

Optimum bulk resistivity of 0.082Ω·cm was achieved with the 15wt% GNP + 10wt% CB ink, however at this loading screen patterning began to become visible in the surface of the coatings. This is still double the resistivity found for optimised Graphite/CB inks by Phillips et al, however these coatings show significantly lower surface roughness with Ra<600nm. Bulk resistivity of 0.086Ω·cm was achieved with the 15wt% GNP + 7.5wt% CB, with this ink showing far lower viscosity and with this less evidence of mesh marking. The improved processability, and near equal electrical performance marks the 15wt% GNP + 7.5wt% CB the optimum ink. The combination of good electrical conductivity, good processability and low surface roughness makes GNP/CB inks a promising alternative to Graphite/CB inks for multi-layer electrical devices.

5.5 References

[1] E. Jewell, S. Hamblyn, T. Claypole and D. Gethin, “The impact of carbon content and mesh on the characteristics of screen printed structures,” *Circuit World,* vol. 39, no. 1, pp. 13-21, 2013.

[2] C. Phillips, A. Al-Ahmadi, S.-J. Potts, T. Claypole and D. Deganello, “The effect of graphite and carbon black ratios on conductive ink performance,” *Journal of Materials Science,* vol. 52, pp. 9520-9530, 2017.

[3] M. Hatala, P. Gemeiner, M. Hvojnik and M. Mikula, “The effect of ink composition on the performance of carbon-based conductive screen printing inks,” *Journal of Materials Science: Materials in Electronics,* vol. 30, pp. 1034-1044, 2019.

[4] Z. Fan, C. Zheng, T. Wei, Y. Zhang and G. Luo, “Effect of Carbon Black on the electrical property of Graphite Nanoplatelet/Epoxy resin composites,” *Polymer Engineering and Science,* pp. 2041-2045, 2009.

[5] H. Oxfall, G. Ariu, T. Gkourmpis, R. Rychwalski and M. Rigdahl, “Effect of carbon black on the electrical and rheological properties of graphite nanoplatelets/ poly(ethyl-butyl-acrylate) composites,” *eXPRESS Polymer Letters,* vol. 9, no. 1, pp. 66-76, 2015.

[6] C. Hua, X. Li, L. Shen, H. Lei, X. Guo, Z. Liu, Q. Kong, L. Xie and C.-M. Chen, “Influence of co-solvent hydroxyl group number on properties of water-based conductive carbon paste,” *Particuology,* vol. 33, pp. 35-41, 2017.

[7] H. A. Barnes, J. F. Hutton and K. Walters, An Introduction to Rheology, Amsterdam: Elsevier Science Publishers, 1989.

[8] S. Mueller, E. Llewellin and H. Mader, “The rheology of suspensions of solid particles,” *Proceedings of the Royal Society A,* vol. 466, pp. 1201-1228, 2010.

[9] H. A. Barnes, A Handbook of Elementary Rheology, Aberystwyth: University of Wales Institute of Non-Newtonian Fluid Mechanics, 2000.

[10] N. Willenbacher and K. Georgieva, “Rheology of disperse systems,” in *Product Design and Engineering*, 2013, pp. 7-49.

[11] B. Phillip, E. Jewell, P. Greenwood and C. Weirman, “Material and process optimization screen-printing carbon graphite pastes for mass production of heating elements,” *Jornal of Manufacturing Processes,* vol. 22, pp. 185-191, 2016.

[12] A. Claypole, J. Claypole, A. Holder, T. Claypole and L. Kilduff “Rheology of high-aspect-ratio nanocarbons dispersed in a low-viscosity fluid,” *Journal of Coatings Technology and Research, accepted for publication*

[13] S.-J. Potts, Y. C. Lau, T. Dunlop, T. Claypole and C. Phillips, “Effect of photonic flash annealing with subsequent compression rolling on the topography, microstructure and electrical performance of carbon-based inks,” *Journal of Materials Science,* vol. 54, pp. 8163-8176, 2019.

[14] A. Kasgoz, D. Akin, A. I. Ayten and A. Durmus, “Effect of different types of carbon fillers on mechanical and rheological properties of cyclic olefin copolymer (COC) composites,” *Composites Part B: Engineering,* vol. 66, pp. 126-135, 2014.

[15] J. Claypole, Application of advanced rheometric tecniques to printing fluids, Swansea University Thesis, 2015.

Chapter 6: Stretchable Conductive Inks for Wearable Heating Applications

6.1 Introduction

GNP/CB hybrid inks have been developed with electrical properties comparable to their commercially available Graphite/CB conductive carbon inks, but with the benefit of significantly lower surface roughness, making GNP/CB hybrid inks a promising material for thin, flexible multi-layer devices. Thermoplastic Polyurethane was selected as the binder for the stretchable inks used in this study as it offers unique properties such as excellent elongation, high impact strength, good elasticity and biocompatibility. These inks were printed onto a rigid, flexible PET substrate to assess their electrical and print properties, however as the aim of this thesis was to create stretchable inks for wearable technology it is important to assess the electro-mechanical performance of these inks under large tensile strain.

To allow for the characterisation of the performance of these GNP/CB/TPU inks under tensile strains, the inks were screen printed onto a stretchable TPU substrate. This substrate was selected for its thermoformability, high abrasion resistance and high surface energy, which, gives it significantly better adhesion to the conductive material than untreated PDMS [1]. Adhesion between the ink and the substrate is important for the mechanical properties of the finished device, with good adhesion previously seen between a TPU based silver ink and TPU substrates [2].

6.2 Characterising the Performance of Stretchable Inks

6.2.1 Introduction

The GNP/CB/TPU ink used in this paper was optimised for screen print quality and electrical performance in Chapter 5. The hybridization of GNP with CB caused significant improvements in the electrical properties and the surface roughness as the presence of CB improved interplatelet GNP contact, in good agreement with other works on GNP/CB composites [3][4] and Graphite/CB conductive pastes [5].

The construction of the printed heaters consists of a resistive heat-generating carbon coating with two silver busbars running along parallel sides of the heater (Fig. 6.2.1.1) with the electric current passing through the carbon coating to generate heat. The silver busbar is required to minimise potential drop along the width of the heater, ensuring a consistent voltage supply across the heater to give uniform heat across the coating. The performance of a stretchable GNP/CB/TPU ink is compared

with that of silver flake/TPU ink. The resistance of the carbon coating, and therefore the heat output, can be controlled by changing the number of printed layers. Therefore, the effect of printing multiple layers of intrinsically flexible inks is also examined. The characterisation of the inks will be aimed at their use in wearable technology.

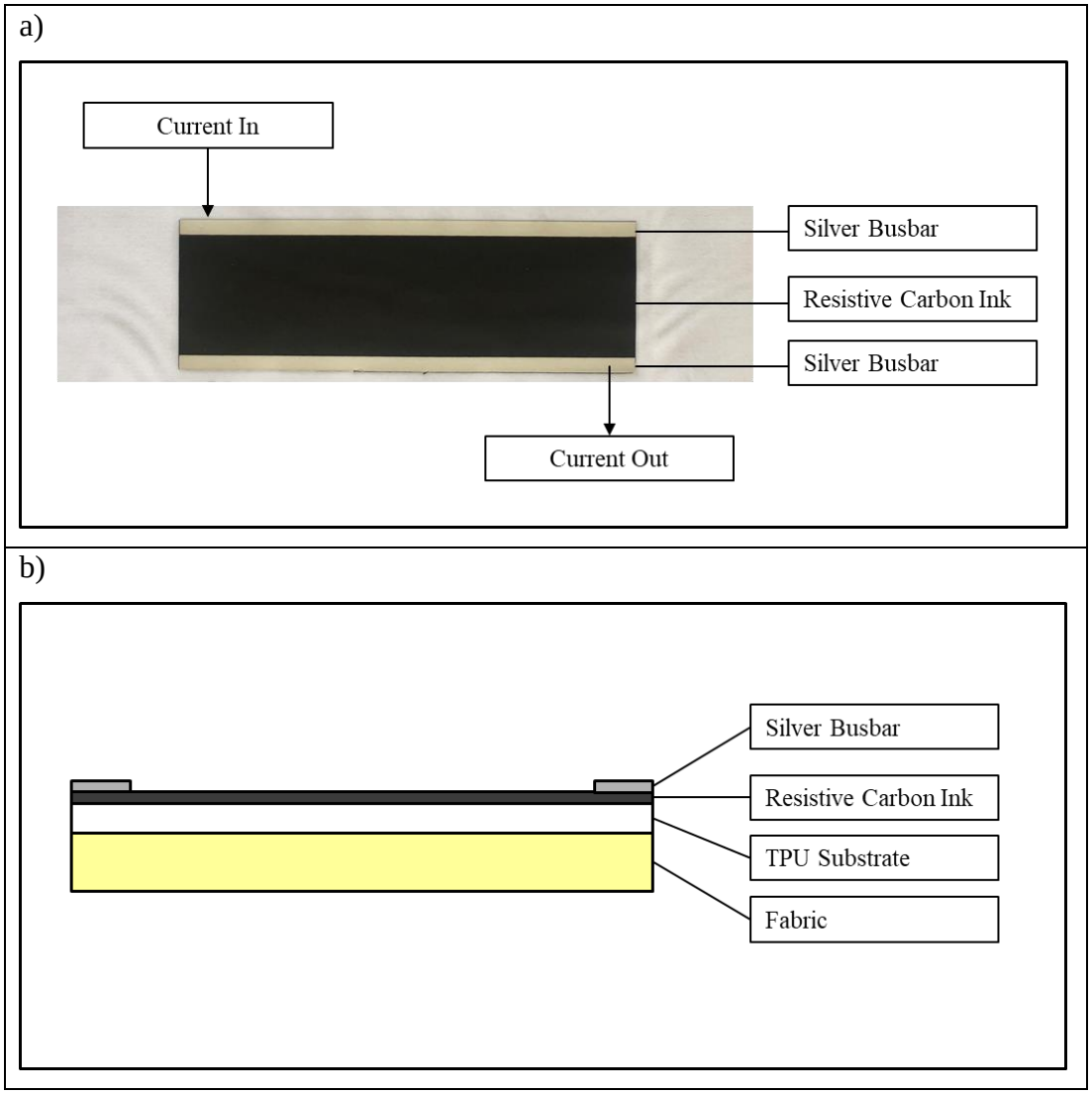

Figure 6.2.1 – The construction of the printed heater. a) Vertical photograph showing the construction of the printed heater. b) Cross-section diagram representing the construction of the printed heater

6.2.2 Materials & Methods

15wt% NH_3 GNP and 7.5wt% CB was dispersed into a 9.7wt% TPU Resin in a polar solvent. Using the density of GNPs as 2.2g/cm^3, and the density of thermoplastic polyurethane as 1.25g/cm^3, this gives a 1.32:1 ratio of particles to polymer in the dry ink. A 55wt% of 10um silver flake (Sigma Aldrich) was dispersed in the same 9.7wt% TPU resin in a polar solvent. Using the density of

silver as 10.49g/cm^3 this gives a conductive particle to polymer volume ratio in the dry coating of 0.68:1. Silver flake was selected over spherical particles to give greater particle overlap and particle contact.

The stretchable inks were screen-printed (DEK 248) using a 54-70 mesh consisting of 15x5 and 20x5cm block areas onto the stretchable TPU substrate. The TPU substrate (Poli-Tape Ultimate Print Soft 4030) has a thickness of 80±5um [6]. These inks were dried for 10 minutes at 70°C and left for >24 hours before testing to ensure all solvent had evaporated.

The electrical performance of the inks under tensile strain was then measured using the technique outlined in the Materials and Methods section 3.7. A labelled photograph of the electro-mechanical cyclic testing of carbon ink is displayed in Figure 6.2.2.

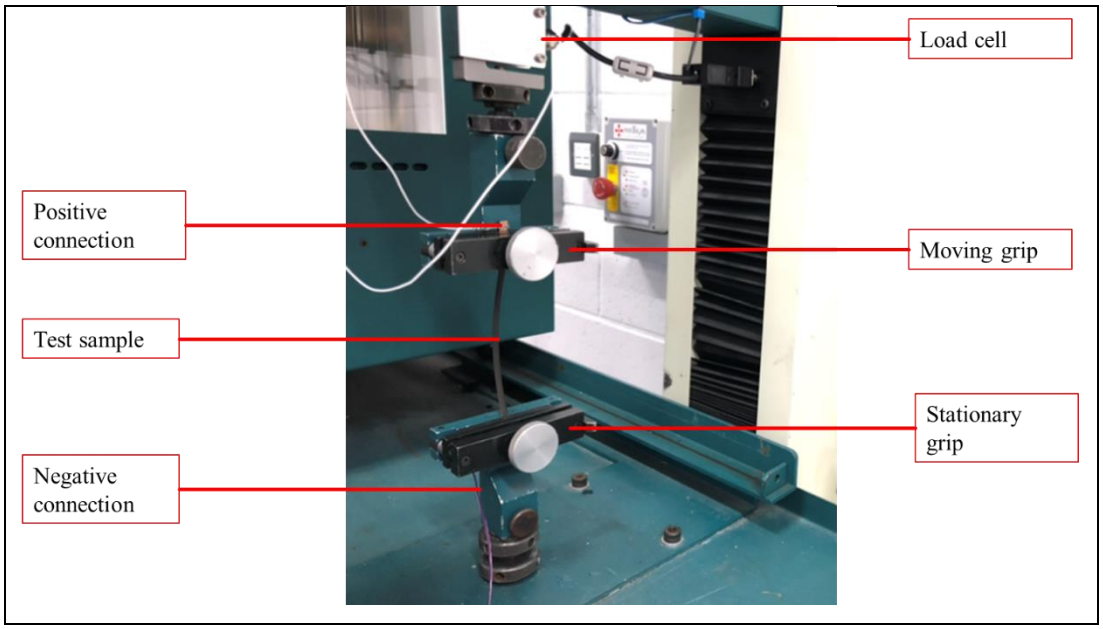

Figure 6.2.2 – Labelled photograph of the electro-mechanical testing procedure of a carbon ink sample during the cyclic testing to 10% nominal strain

6.2.3 Results

The addition of the conductive nanoparticles increased the viscosity of the unfilled TPU resin, especially at low shear rates, with the suspensions showing increased non-Newtonian behaviour over the measured shear rate (Fig. 6.2.3.1a). The silver flakes had the largest effect on the low shear rate viscosity of the pure resin, increasing the viscosity to 780.6 Pa s at 0.01s^{-1}, however, this ink readily shears at

close to 4.5 Pa s at 83 s^{-1} as the shear forces break down any interparticle reactions to allow the silver flakes to align with the flow, minimising their effect on viscosity. The addition of the GNP and CB increased the viscosity and amount of non-Newtonian behaviour of the unfilled TPU resin.

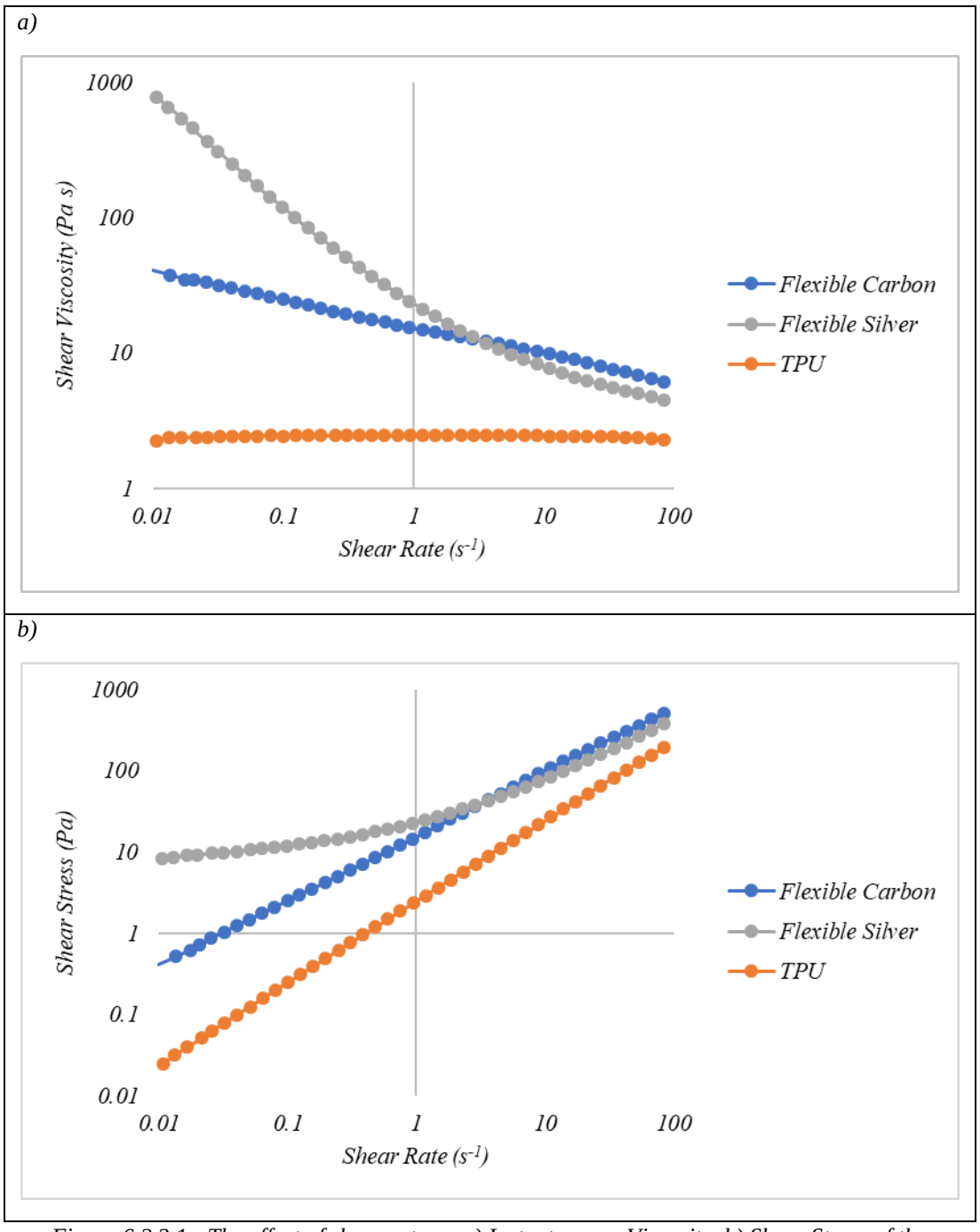

Figure 6.2.3.1 - The effect of shear rate on a) Instantaneous Viscosity, b) Shear Stress of the Carbon Ink, Silver Ink and TPU resin

The non-Newtonian behaviour of GNP/CB inks has been shown to be a consequence of the CB forming a network between the GNPs, trapping the resin and increasing the viscosity, however this weak network is easily broken down to allow the

particles to align with the flow. The effect of shear rate on the shear stress can be seen in Figure 6.2.3.1b. The Carbon ink and TPU show no signs of significant yield stresses indicates an intercept on the y-axis of >1Pa. The intercept is nearer to 10Pa for the Silver ink as the particles create a structure at low shear rates that must be broken down to allow the fluid to flow.

The carbon and silver inks had a similar print thickness with 7.96 and 8.73um respectively (Fig. 6.2.3.3a, c). Printing a second layer of carbon nearly doubled the print thickness to 14.76um (Fig. 6.2.3.3b).

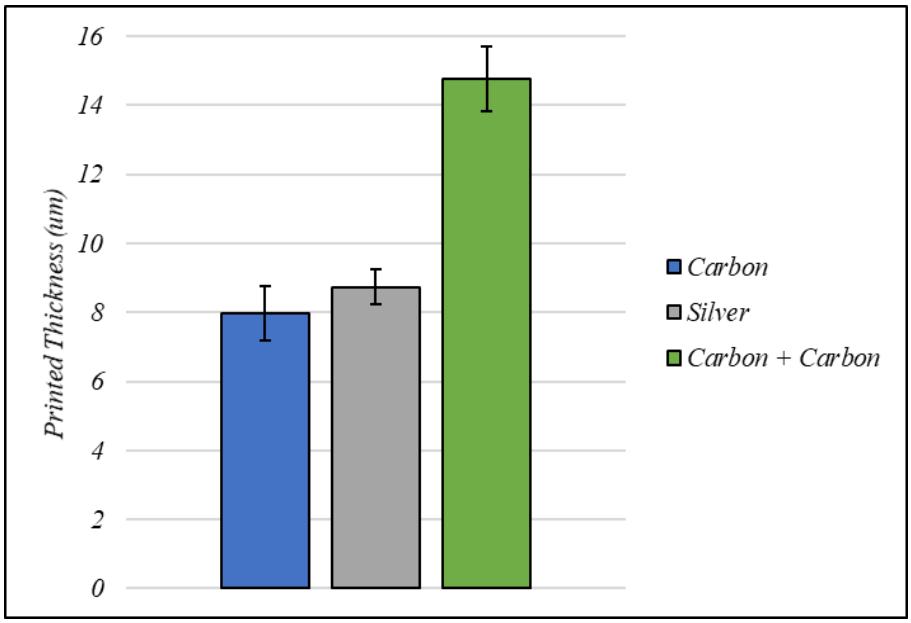

Figure 6.2.3.2 - The printed thickness of the coatings. Error bars represent the standard deviation from 10 measurements across 5 samples for each ink

The roughness of the surface of a printed feature are a consequence of the underlying topography of the print which is a function of the print process as well as the ink rheology, substrate roughness and the roughness due to the size and morphology particles [5][7][8]. The surface roughness from the centre of the prints for the inks and the uncoated substrate can be seen in Figure 6.2.3.3, with white light interferometry images in Figure 6.2.3.3.

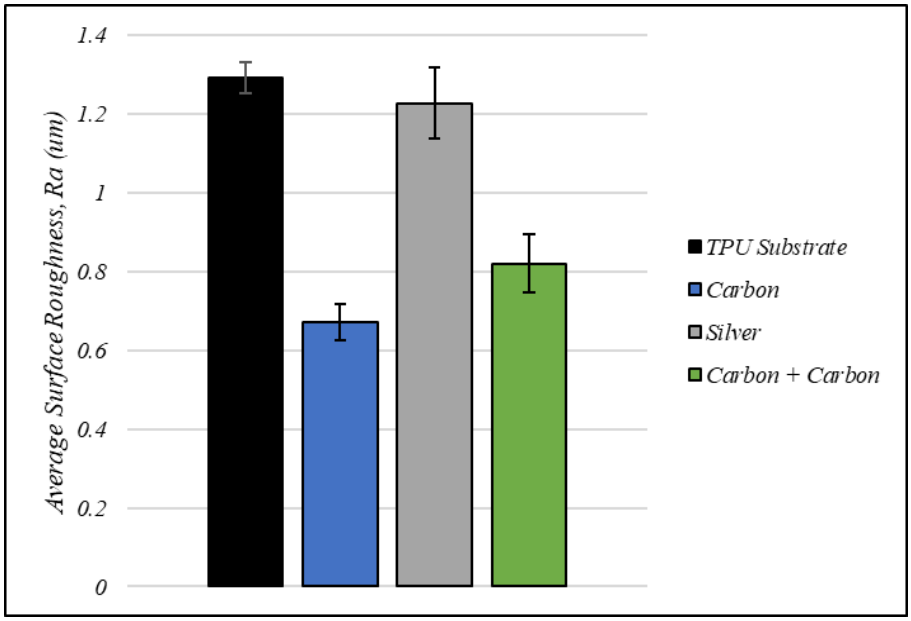

Figure 6.2.3.3 - The average surface roughness of the uncoated TPU substrate and the different printed inks from white light interferometry using 5x magnification. Error bars represent the standard deviation from 9 measurements across 3 samples

Printing the carbon coating onto the substrate approximately halved the surface roughness compared to the pure TPU substrate from 1.29 to 0.67um, as the ink spread to fill the roughness in the substrate (Fig. 6.2.3.3). The carbon prints had a relatively low average surface roughness of 0.671um. This shows good agreement with Chapter 5 where the hybrid GNP/CB was able to freely flow through the screen and relax following the screen pulling away from the substrate to create a smooth, uniform coatings (Fig. 6.2.3.4a, b) with average roughness's of ≈0.6um with the submicron CB decorating GNPs and filling any voids between neighbouring GNPs (Fig. 5.3.1d).

The silver prints were significantly rougher than the carbon with average surface roughness of 1.227um (Figure 6.2.3.5). Inspecting the white light images shows that the roughness of the silver print is likely a combination of both the topography of the surface of the prints and the particle size of the silver (Fig. 6.2.3.5). The high low shear viscosity and the presence of a yield stress in the silver ink were indicative of structure building within the ink at low shear rates (Fig 6.2.3.1a, b).

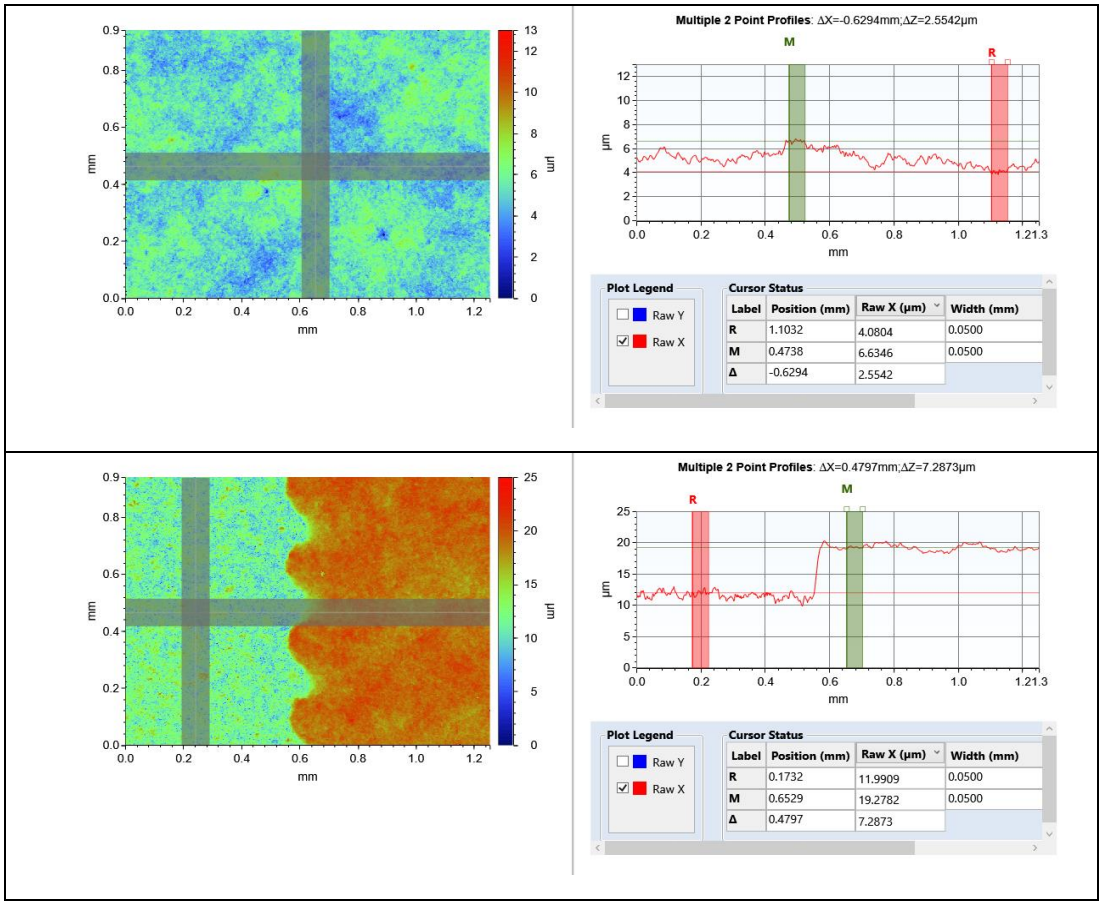

Figure 6.2.3.4 - White light images of the single layer carbon print at a) the centre of the print, b) the edge of the print.

Following the screen pulling away from the substrate the ink is unable to relax to form a consistent film, leaving mounds of conductive material, interspaced by valleys of thin coating with limited conductive material, with differences in print thickness up to 5um across the coating (Fig. 6.2.3.5a, b). The presence of small speckled red areas in the coating could be indicative of roughness due to particles. At 10um the silver flakes are significantly larger than the nanocarbons, resulting in increased surface roughness because of the increased particle size.

The carbon and silver prints onto the TPU substrate had measured sheet resistances of 230.102±12.40 and 0.078±0.0005Ω/□ respectively. The silver ink has a resistivity approximately 3 orders of magnitude lower than that of the carbon ink owing to bulk silver's considerably higher electrical conductivity. The resistivity of the samples calculated from the two-point measurement can be viewed in Table 6.2.3.1.

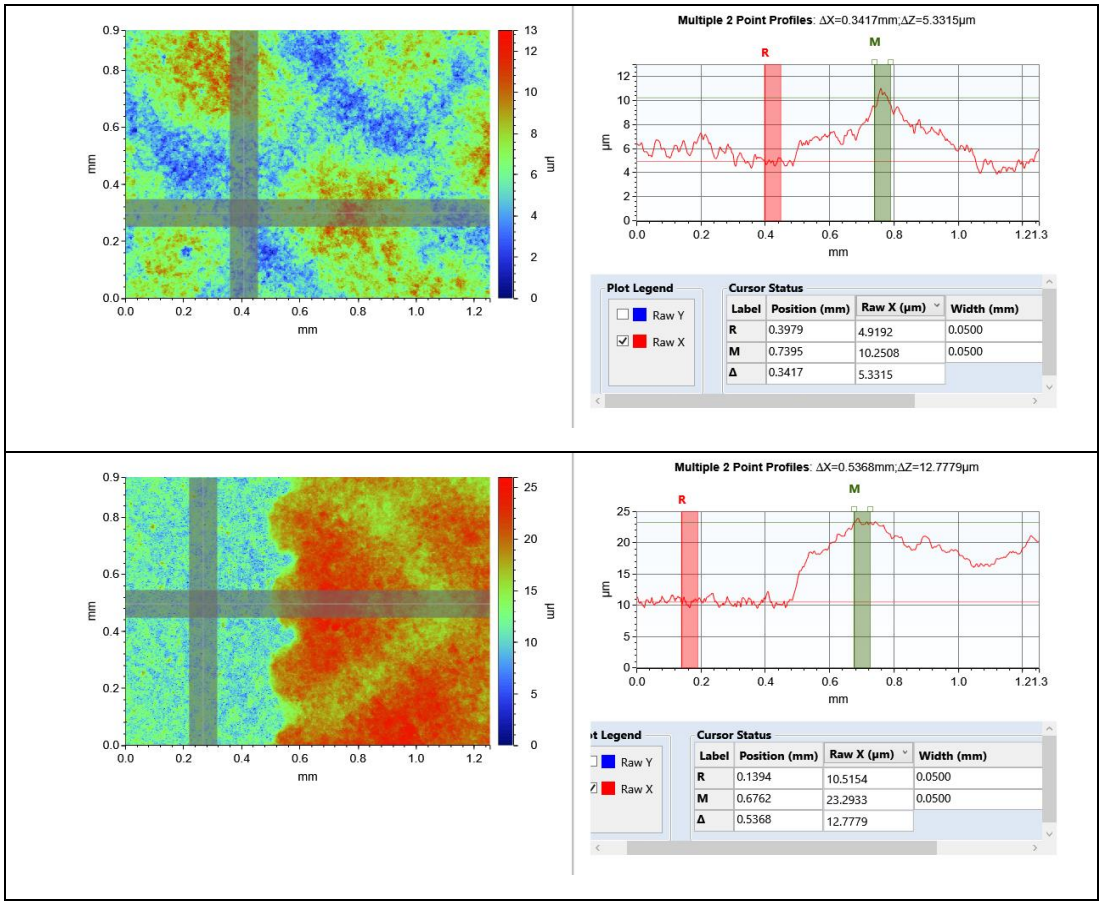

Figure 6.2.3.5 - White light images of the silver prints at a) the centre of the print, b) the edge of the print

Increasing the number of layers of carbon decreased the resistivity. The first layer of carbon was printed directly onto the relatively rough substrate whereas the second layer of carbon was printed onto the smoother first layer, enabling it to form a more uniform coating giving the coating improved bulk electrical properties. The two-layer carbon shows a similar bulk resistivity to the 0.1 $\Omega \cdot cm$ found for the optimised carbon found in the Chapter 5, with any differences likely to be due to the relatively rougher nature of the substrate and the coarser mesh used providing a rougher substrate.

Table 6.2.3.1 – Resistivity of samples pre-testing calculated using a two-point method

	Silver	Carbon	Carbon + Carbon
Thickness (um)	8.73	7.96	14.76
Width Sample (cm)	0.5	0.5	0.5
Length track (cm)	14	14	14
Resistivity (Ohm.cm)	0.000187	0.253512	0.179562429

6.2.4 Mechanical Testing

The stress-strain response of the substrate to an applied strain at 50mm/min can be seen in Figure 6.4.2.1. The uncoated TPU substrate shows a typical soft rubber-like material stress-strain response with a small linear elastic region at nominal strains of approximately <5%, followed by a plateau as the strain increases faster than the stress, before the substrates break at 330.17±27.2% nominal strain.

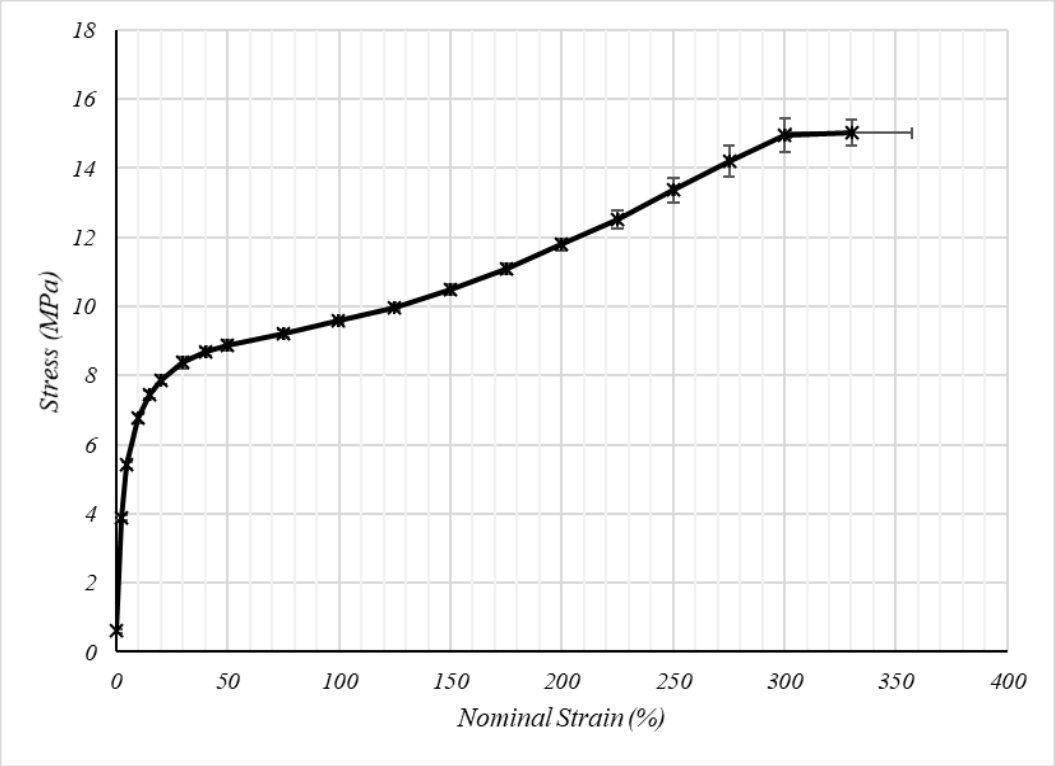

Figure 6.2.4.1 - Stress-Strain curve of the uncoated TPU substrate pulled to maximum extension at 50mm/min. Error bars represent the standard deviation across 3 samples.

The effect of the silver and carbon on the TPU substrate can be seen in Figure 6.2.4.2. The carbon coating increased the shear stress at nominal strains <50% but decreases the strain at break to 304.79±3.66% nominal strain. This increased stress at low nominal strains could be a result of the carbon coating stiffening the substrate and having a reinforcing effect. The difference in extension at break is within the standard deviation of the substrate therefore the sample break could be a result of substrate failure. The silver coated substrate showed a similar stress-strain curve to the uncoated substrate. This suggests that the silver coating does not have the same reinforcing effect as the carbon.

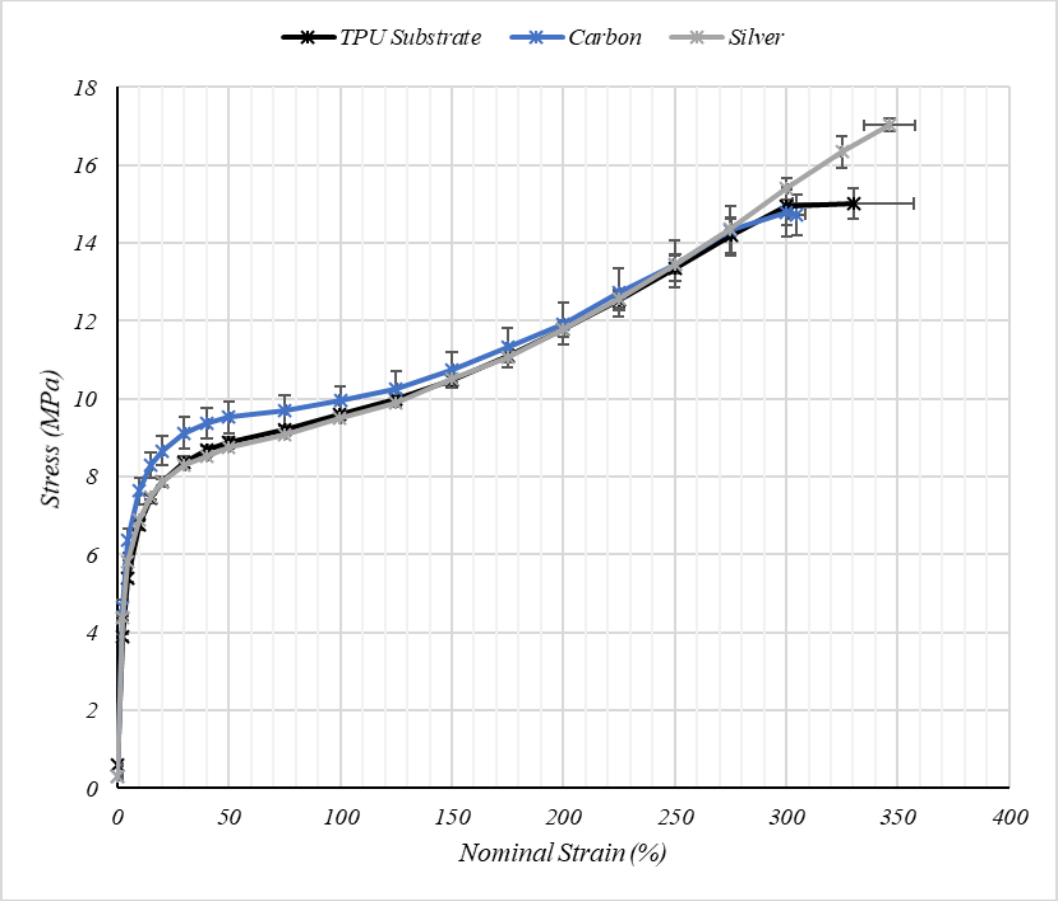

Figure 6.2.4.2 - The effect of carbon and silver ink coatings on the stress-strain curve of the TPU substrate during a maximum extension test at 50mm/min. Error bars represent the standard deviation across 3 samples

The effect of printing a second layer of carbon can be seen in Figure 6.2.4.3. Printing a second layer of carbon further increased the stress at low strains, followed by a plateau region where shear stress drops despite increasing strain, before the stress increases once more until break at 303.49±17.85%. Printing a second layer of carbon has increased the printed thickness has increased to 14.76um, with the coating now comprising 15.6% of the total substrate/coating composite further reinforcing the substrate to give greater increases at low strain rates as the mechanical properties of the coating becomes increasingly significant, as the coated thickness increases relative to the substrate.

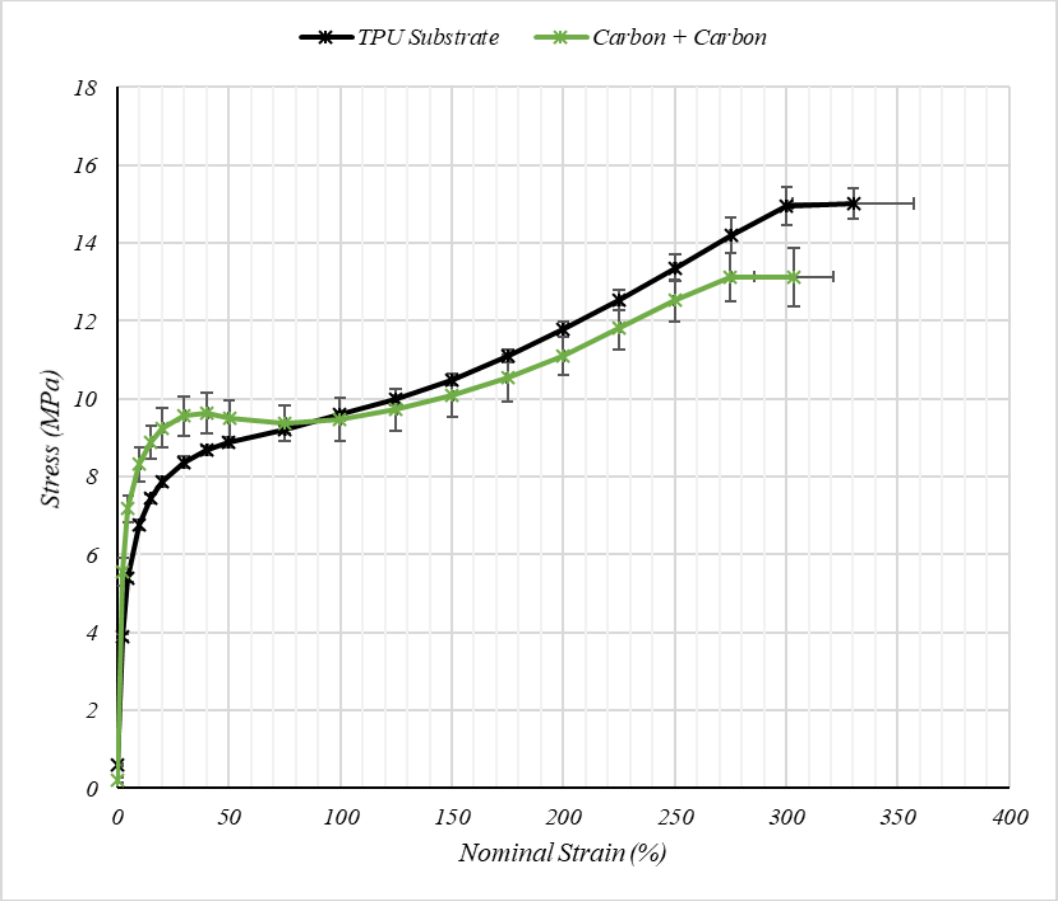

Figure 6.2.4.3 - The effect of printing two layers of carbon on the stress-strain curve of a TPU substrate when extended at 50mm/min. Error bars represent the standard deviation across 3 samples

The effect of strain on the electrical properties of the inks can be seen in Figure 6.2.4.4. The single- and double-layer carbon inks maintain electrical conductivity up to nominal strains of 304.79±3.66 and 294.34±5.52% respectively. The silver ink has a significantly lower initial resistance however it loses electrical conductivity at a significantly lower nominal strain of 166.43±1.79% suggesting the conductive network has been broken (Fig. 6.2.4.4) despite the coating being extended to mechanical break at nominal strains 346.34±11.52% (Fig. 6.2.4.2).

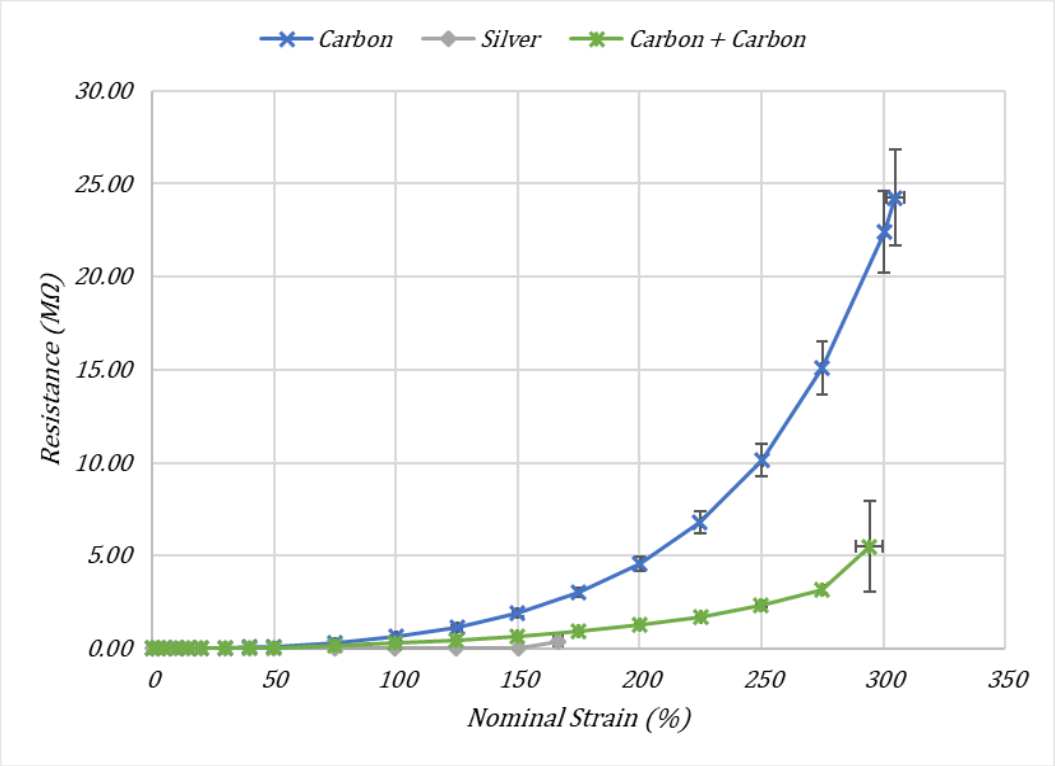

Figure 6.2.4.4 - The effect of nominal strain on the resistance of the screen-printed coatings. Error bars represent the standard deviation across 3 samples.

It is more informative to use the change in the electrical resistance from the initial value before testing to allow for better comparison of the two inks as carbon and silver have significantly different bulk electrical properties with these results displayed in Figure 6.2.4.5. The single and double layer carbon prints show a similar response up to 150% nominal strain however above this point the double layer carbon ink shows less sensitivity to strain, as with the increased print thickness the electrons have a greater number of potential conductive pathways to flow through, therefore, at the high strains where conductive networks begin to break down they can more easily find an electronic path. The silver prints showed a rapid change in resistance above 100% nominal strain until they lost electrical conductivity completely at 166.43%

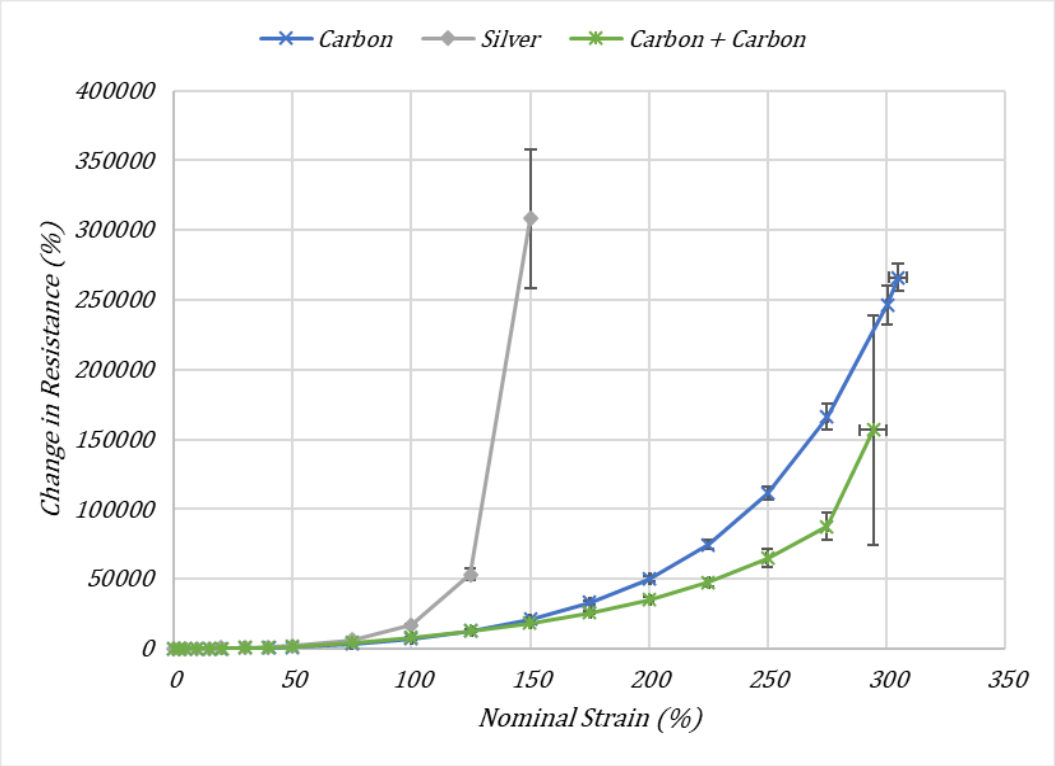

Figure 6.2.4.5 - The effect of nominal strain on the relative change in resistance of the coatings at a) 0-350% strain. Error bars represent the standard deviation across 3 samples.

The carbon ink maintained electrical conductivity up to substrate break while the silver ink lost conductivity at lower strains. This could be linked to the print surface topography and thickness. The high viscosity of the silver ink low at low shear rates led to patterning in the print surface, with mounds of conductive material and variance in print thicknesses of up to 5um across the coating (Figure 6.2.3.6a, b). Under tensile strains, these mounds of conductive material could be pulled away from each other, with higher stresses being experienced by the thinner areas between the mounds, until the conductive material was pulled far enough away from one another that the conductive network being broken. On a micro level the lower volume of the higher density silver flakes could be pulled away from one another at large strains leaving only insulative polymer between neighbouring flakes breaking the conductive network. The carbon better maintained conductivity up to substrate break suggests the volume of particles could be important in the electromechanical properties of conductive inks.

The carbon prints had significantly lower print roughness and variance in thickness. SEM images in Chapter 5 (Fig. 5.3.1.c, d) showed that the carbon ink consisted of multiple layers of GNPs coated in CB with CB filling the voids between

neighbouring particles to create a smooth but dense 3D interconnected coating consisting of multiple layers of GNP/CB. Due to the Nano-flake like nature of the CB coated GNPs, this 3D layered microstructure could facilitate strains by the higher volume of CB coated GNPs sliding past one another but maintaining direct contact to maintain the electrical network throughout the print. When direct contact failed, the current could travel through a conductive CB/TPU network. Further studies are required on a micro level, such as electro-mechanical testing of coatings with different ratios of GNP:CB including GNP only and CB only inks.

Printing a second carbon layer significantly reduced the resistivity of the composites with electrical contact maintained up until substrate failure at over 294% nominal strain. With good adhesion between layers, printing a second layer of an intrinsically flexible ink is an effective method for improving the conductivity of the printed composites.

Stretch-ability improves the conformity of electronics with the body as well as facilitating flexibility and thus improves the reliability of the measurement of several health parameters in wearable systems [9]. In textile applications about 15-20% strain occurs through the life cycle of the product [1]. The ability of the carbon ink to show consistent repeated resistance response to applied strain following initial deformation could be important in the utilisation of these inks in stretchable applications as following a pre-strain the devices would show consistent resistance within the range of the pre-strain. The carbon and silver inks could be strained to 304.79 and 166.43% nominal strain respectively while remaining electrically conductive (Fig. 6.2.4.2). The inks were cyclically strained to 10% nominal strain as this is close to the requirements for wearable textile applications when worn and was just beyond the elastic range of the materials. The carbon ink was then stretched repeatedly to 100% nominal strain to examine whether these strains were repeatable near to the yield strain of the material.

The effect of cyclically straining the TPU substrate can be seen in Figure 6.2.4.6. Following the first cycle to 10% there is initial plastic deformation of about 1.5%. The amount of stress required to strain the substrate to 10% nominal strain decreases with the number of cycles before stabilising at between 20-30 cycles, with between 2-4% of permanent plastic deformation in the substrate. The microstructure within

the TPU substrate become aligned in the direction of the force, reducing the amount of force required to move the substrate in the direction of the force. However, this movement creates a permanent, plastic change of 2-4% to the material which isn't fully recovered upon the removal of the force.

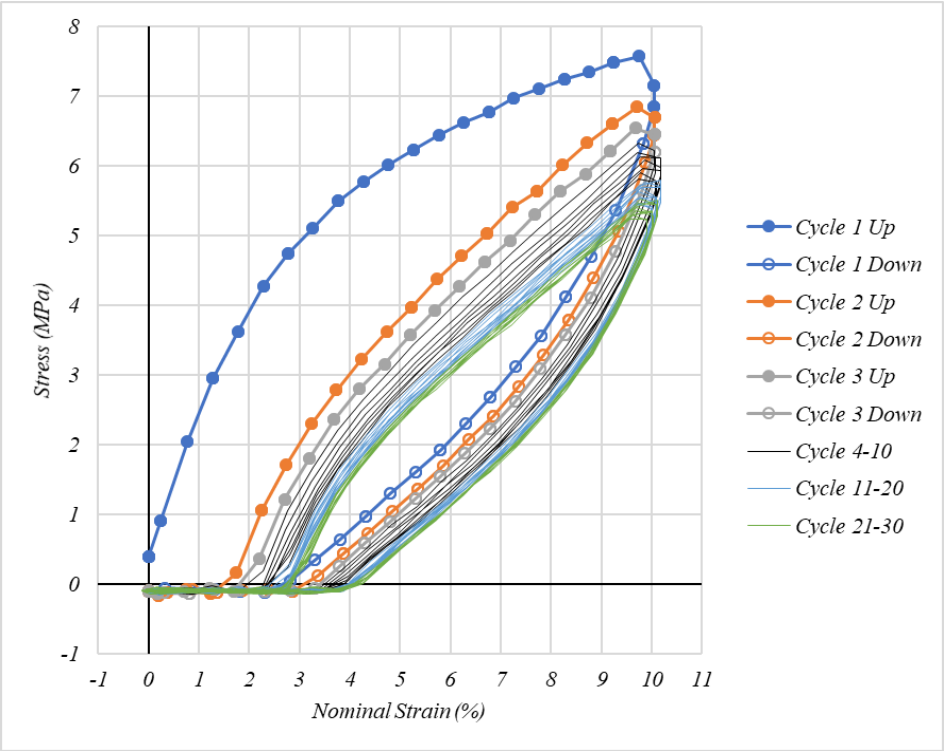

Figure 6.2.4.6 - The effect of 30 cyclic strains to 10% nominal strain at 50mm/min for the uncoated TPU substrate

The stress-strain curve of the carbon print (Figure 6.2.4.7) is in good agreement with the maximum extension curve, the single layer carbon coating shows a similar cyclic stress-strain response to the uncoated TPU substrate, with the stress required to strain to 10% decreasing with the number of cycles before stabilising at about 20-30 cycles with 2-4% of permanent strain. This indicates the tensile properties of the substrate dominate.

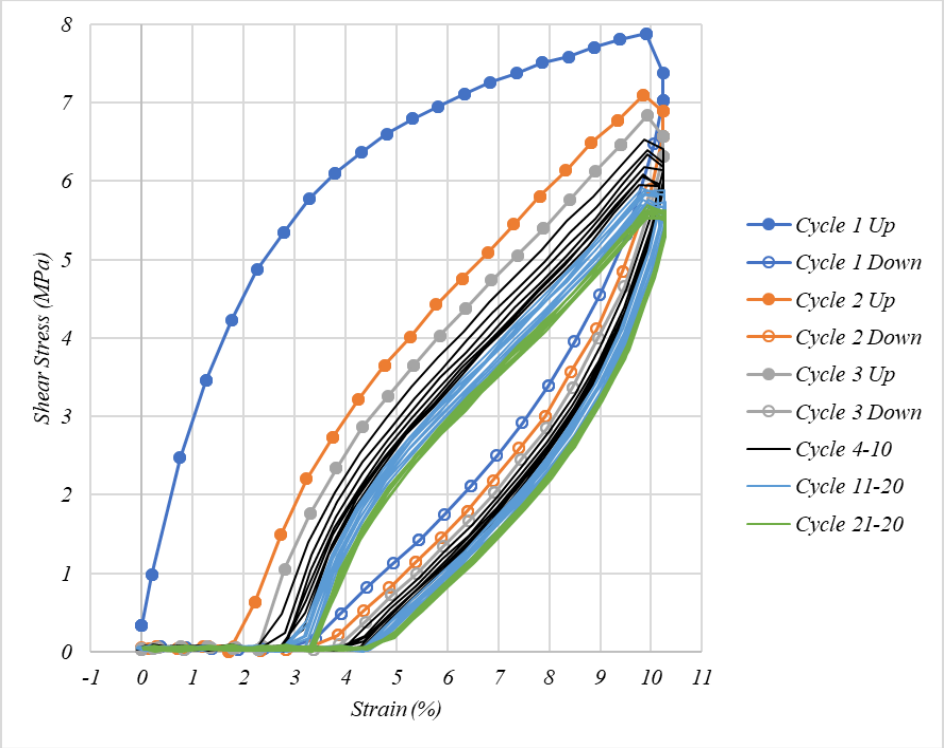

Figure 6.2.4.7 - The stress-strain curve of the carbon print onto the TPU substrate in tensile extension to 10% nominal strain at 50mm/min.

The electro-mechanical response of the carbon print onto the TPU substrate when being extended to 10% nominal strain can be seen in Figure 6.2.4.8. During the first cycle there is an increase in resistance of up to 100.61% when being strained to 10% nominal strain, with this returning to around a 51.01% increase once the strain is removed. This increase in the resistance at 0% nominal strain is likely a result of the permanent increase in the electronic pathlength as a result of permanent deformation to the substrate and the ink. Further cycles to 10% nominal strain reduce the change in resistance, before the change in resistance becomes consistent at an 73.62% increase in resistance at 10% nominal strain and recovering to 48.02% once the strain is removed. The area of constant resistance between 0-4% nominal strain in cycles 21-30 despite increasing strains (Fig. 6.2.4.8) correlates with the area of zero stress and therefore permanent strain in the mechanical tests (Fig. 6.2.4.7). This is as the coating and substrate have experienced a permanent deformation of approximately 4%, increasing the electronic path length. The decrease in the change in resistance and the increase in the consistency of the change in resistance to 10% nominal strain with increasing number of cycles suggests a permanent change in the microstructure of the print, orienting the particles in the direction of the strain to better facilitate strain in this direction. That the permanent change in resistance in

cycles 21-30 is lower than the change in resistance for the first extension in cycle 1 at strains >8% nominal strain suggests that the conductive microstructure has been optimally altered for strains up to 10%.

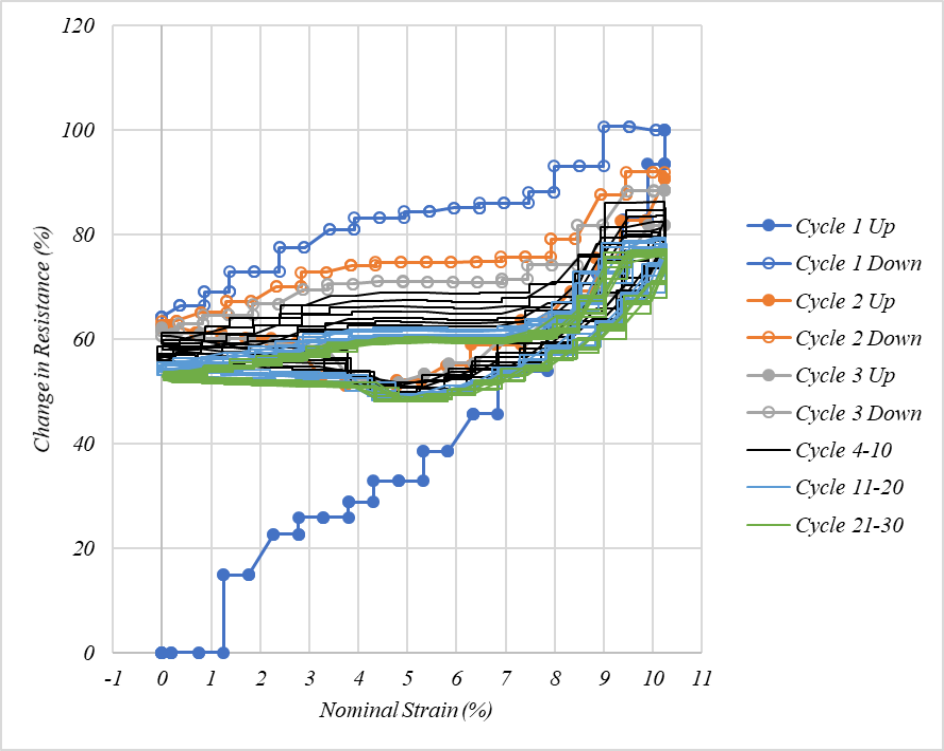

Figure 6.2.4.8 - The effect of cyclic strains to 10% nominal strain on the change in resistance of the carbon print on the TPU substrate at 50mm/min

The effect of cyclic nominal strains of 10% on the stress-strain response of the silver print on the TPU substrate can be seen in Figure 6.2.4.9. In good agreement with the maximum extension measurements, the cyclic properties are dominated by the properties of the substrate.

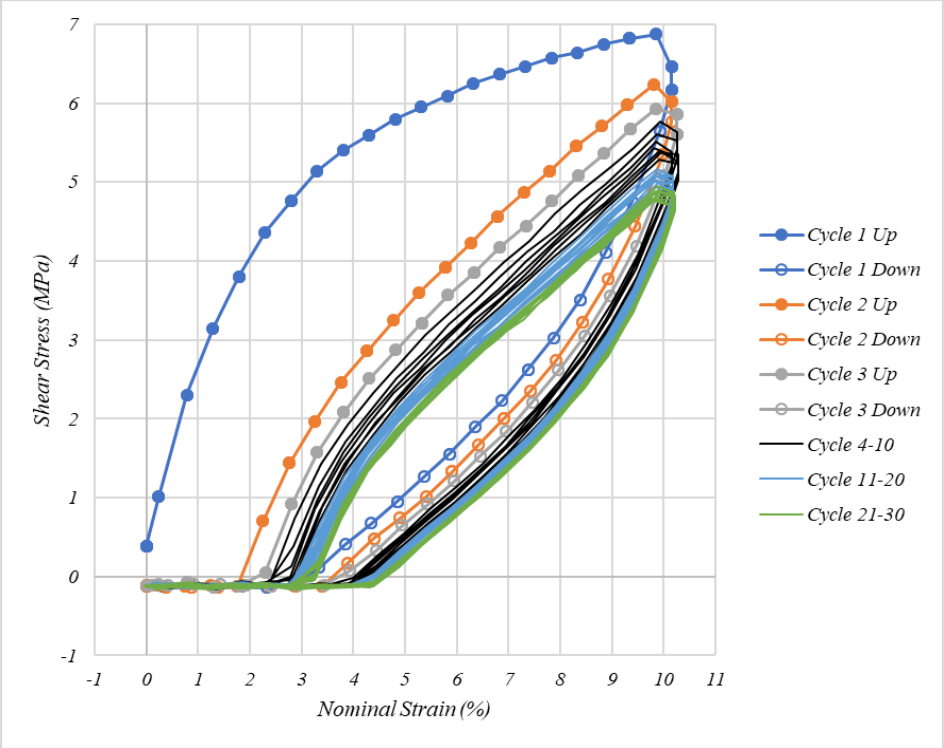

Figure 6.2.4.9 - The effect of cyclic strains to 10% nominal strain on the stress-strain response of the silver prints on the TPU substrate at 50mm/min.

The change in resistance of the silver prints on the TPU substrate with cyclic strains to 10% nominal strain can be seen in figure 6.2.4.10. Individual curves for cycle 10,20 and 30 are used to allow for easier interpretation of the data, with the stepped nature of the curves a result of the minimum data resolution of the data logger of one ohm. The change in resistance of the silver prints increases with the number of cycles, with the strain at 10% nominal strain increasing from 128.57% in the first cycle to 314.29% at cycle 30. In contrast the change in resistance at 10% nominal strain in the carbon ink was decreased from 99.96% in cycle 1 to 73.62% at cycle 30 (Fig. 6.2.4.8). This is despite the stress-strain properties of the carbon print, silver print and the uncoated TPU substrate when strained to 10% nominal strain being very similar (Fig 6.2.4.6, 7, 9). Therefore, this could indicate a change in the microstructure of the silver prints with every strain, that isn't fully recovered when the strain is removed that negatively affects the electronic properties of the print.

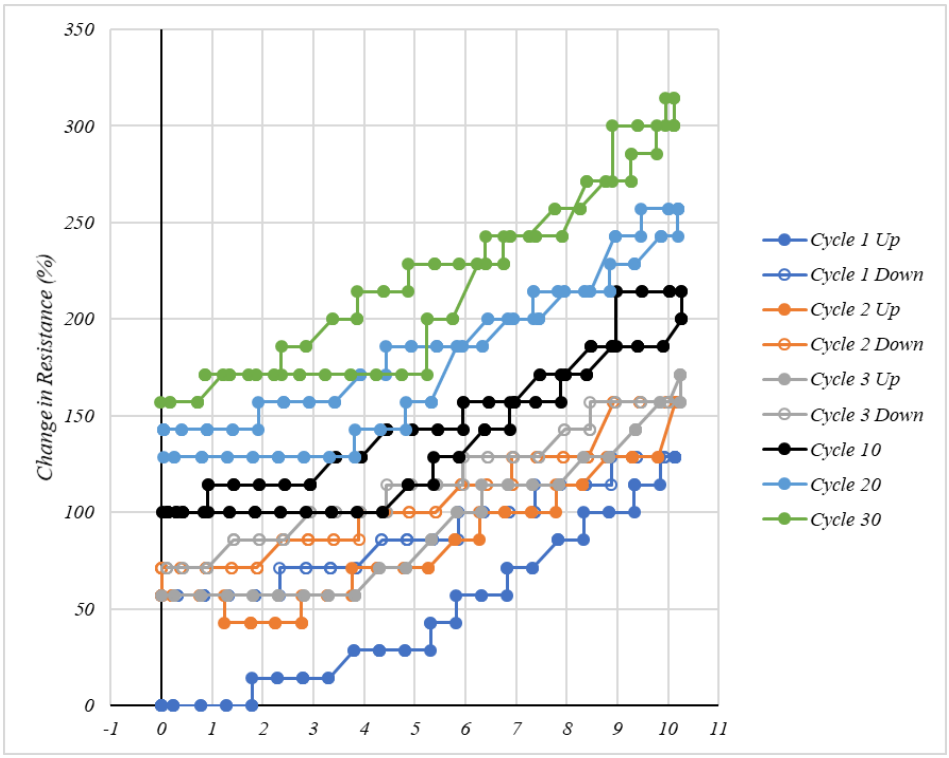

Figure 6.2.4.10 - The effect of cyclic strains to 10% nominal strain on the change in electrical resistance of silver prints on a TPU substrates when extended at strains of 50mm/min

A direct comparison between the Carbon and Silver inks between cycles 1-10 at 10% nominal strain can be seen in Figure 6.2.4.11. The silver print has significantly lower as a result of the significantly lower resistance of bulk silver.

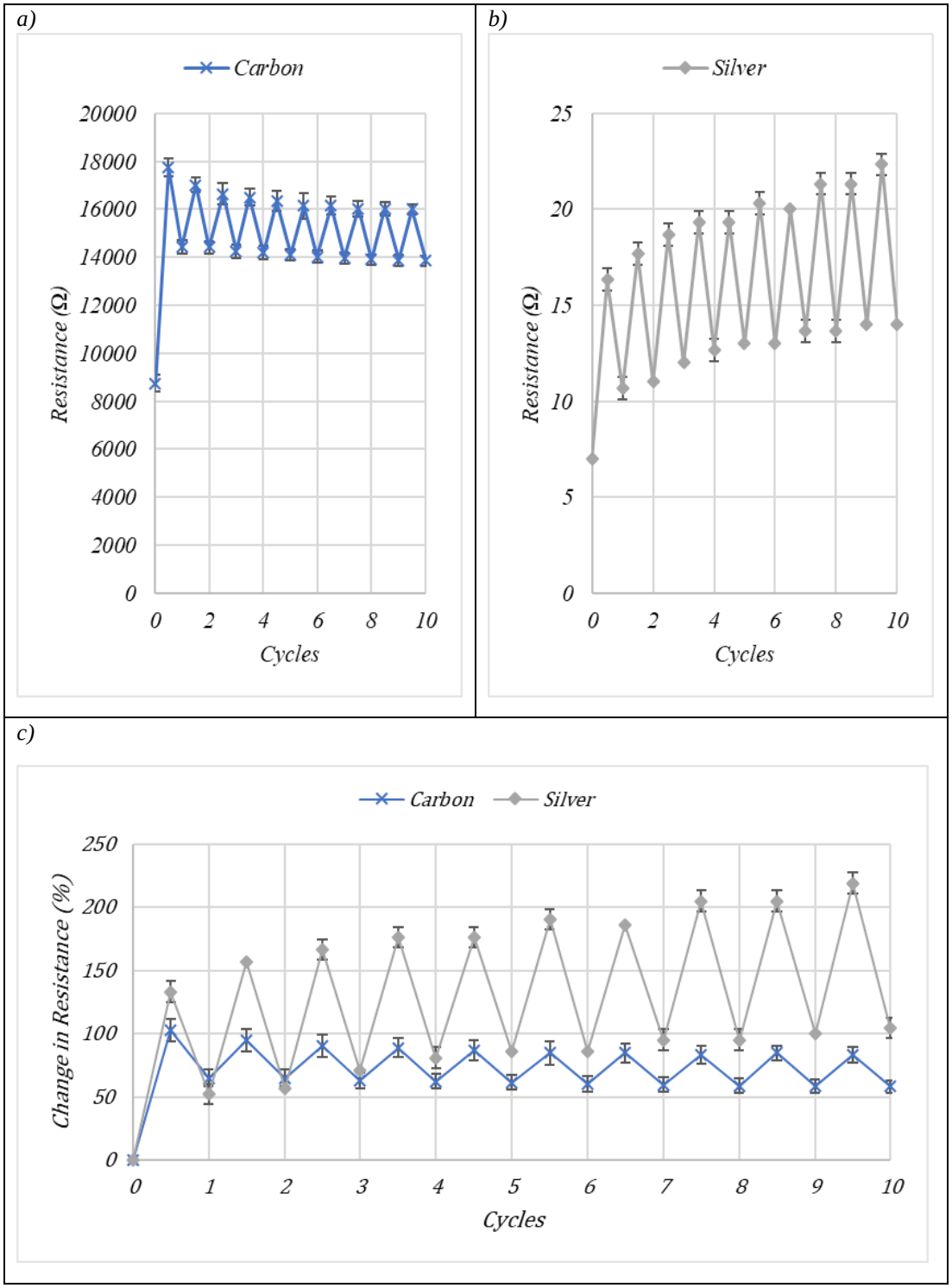

Figure 6.2.4.11 - The effect of cyclic strains to 10% nominal strain on; a) the resistance of the carbon ink, b) the resistance of the silver ink, c) the change in resistance of the silver and carbon ink. Error bars represent the standard deviation across 3 samples.

The effect of printing a second layer of carbon on the mechanical and electromechanical properties of the TPU substrate can be seen in Figures 6.2.4.12 and 6.2.4.13 respectively. In good agreement with the maximum extension tests (Fig. 6.2.4.3), printing a second layer of carbon increased the strain required to strain the

sample to 10% compared to the substrate alone (Fig. 6.2.4.12). This is likely due to the reinforcing effect of a thicker layer of the relatively stiffer carbon ink. In good agreement with the other prints and the unfilled substrate the amount of stress required to strain the print to 10% nominal strain decreased with the number of cycles, while there was a permanent deformation within the print of 3-4%.

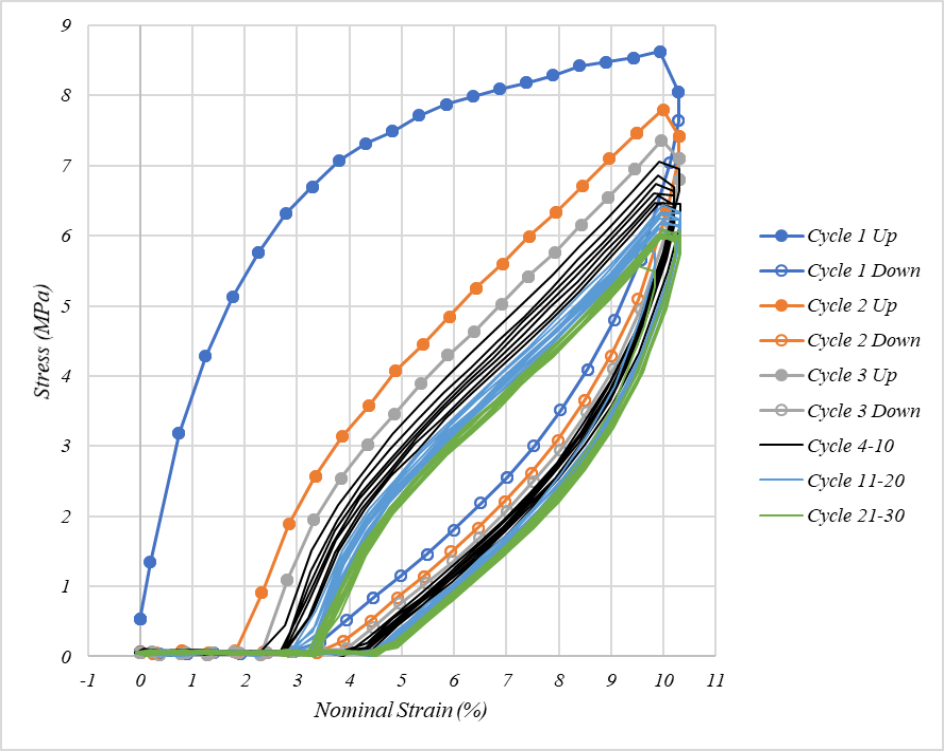

Figure 6.2.4.12 - The effect of cyclically straining on the stress-strain properties of the two-layer carbon print on TPU substrate to 10% nominal strain at 50mm/min

The effect of cyclically straining the two-layer carbon print to 10% nominal strain on the electrical properties of the print is shown in Figure 6.2.4.13. The first cycle to 10% nominal strain increased the resistance of the print by 122.57%, however in good agreement with the cyclic testing of the single layer carbon print (Fig. 6.2.4.8) this change in resistance at 10% nominal strain decreases with the number of cycles as the microstructure of the print becomes oriented with the direction of strain. Even after 30 cycles there is an increase in the 61.45% which isn't recovered when the strain is removed as a result of the permanent change to the microstructure.

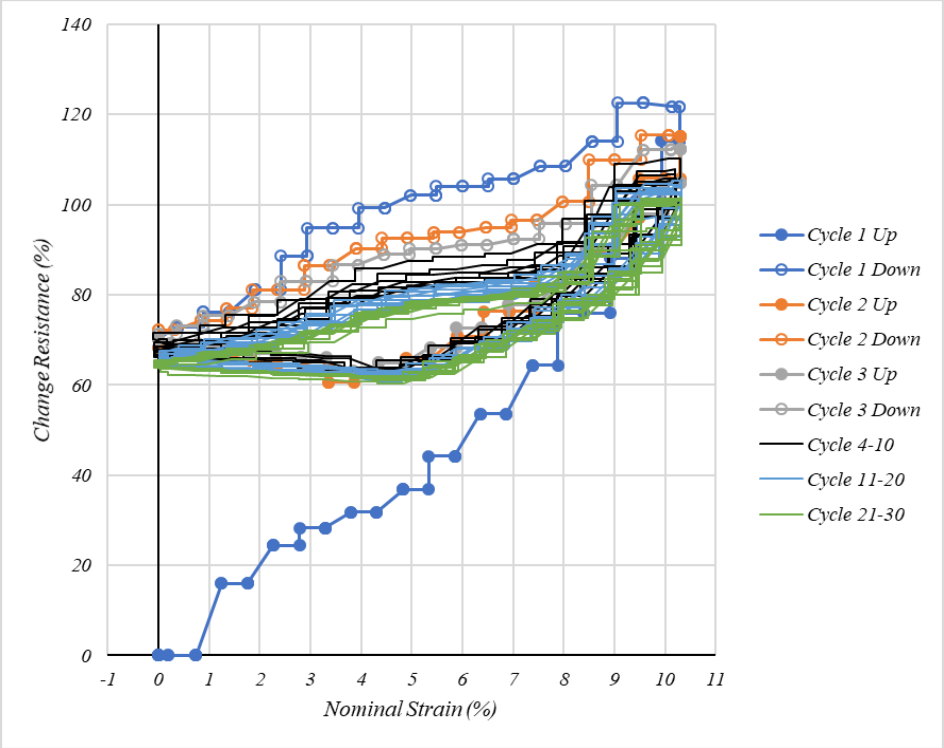

Figure 6.2.4.13 - The effect of cyclic strain to 10% nominal strain on the electrical properties of the two-layer carbon print at 50mm/min

Doubling the number of layers of carbon reduced the electrical resistance by 63%, as the thicker print gave a higher number of electronic pathways for electrical conductivity (Fig 6.2.4.14). The strain response of both the single and double-layer carbon inks to cyclic loading are similar. There is good interaction/bonding between the two printed layers of carbon allowing the two-layer carbon print to behave as a single composite layer. Therefore, increasing the number of printed layers is a good strategy for improving the conductivity of intrinsically stretchable conductive prints.

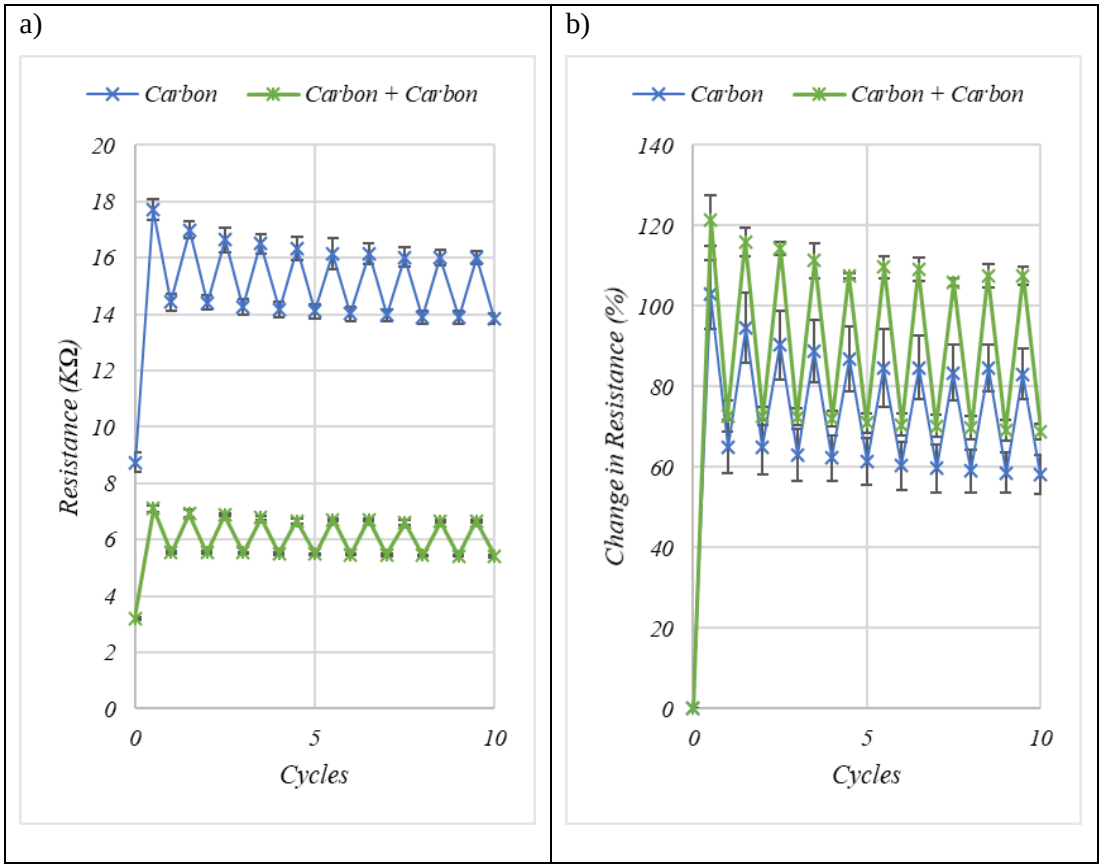

Figure 6.2.4.14 - The effect of cyclic strains to 10% nominal strain on a) the resistance of single layer and double layer carbon prints, b) the change in resistance of single- and double-layer carbon inks. Error bars represent the standard deviation across 3 samples.

To further examine the performance of the carbon ink, the ink was cyclically stretched to 100% nominal strain for 10 cycles to examine the very large strains that will likely be encountered in wearables, with the stress-strain response of the ink displayed in Figure 6.2.4.15. The poor cyclic performance of the silver meant it was excluded from this testing. The first cycle up to 100% nominal strain showed good agreement with the maximal extension test (Fig. 6.2.4.2) with a linear elastic region less <10% and a stress of 9.21 MPa required to stretch the composite to 100% nominal strain. Following this first strain cycle there is a permanent strain of approximately 30% nominal strain in the material. In good agreement with the cyclic strains to 10% nominal strain (Fig. 6.2.4.9), after this first cycle the stress required to reach 100% strain and the consistency of the stress-strain increases with a permanent strain of 40% in the printed composite.

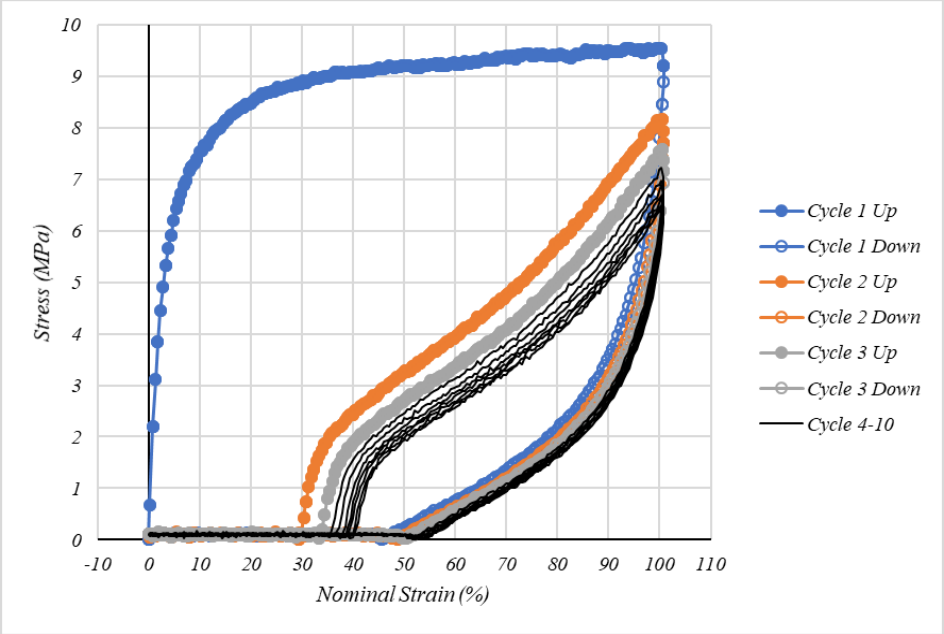

Figure 6.2.4.15 - The effect of cyclic extension to 100% nominal strains on the stress-strain response of carbon prints on a TPU substrate at 50mm/min

The effect of cyclically straining to 100% nominal strain on the electrical properties of the carbon prints on the TPU substrate is shown in Figure 6.2.4.16. The resistance of the prints at 0% strain increases after the first cycle as there is a permanent increase in the electronic path length owing to the permanent increase in the length of the print and the substrate. The change in resistance at 100% nominal strain decreases with the number of cycles from 6568% after the first cycle, to 5841% after the 10th cycle, again indicating the change in the microstructure of the prints as the conductive materials become aligned with the strain to optimise their resistance to strain. In contrast to the cyclic strains to 10% nominal strain (Fig, 6.2.4.8) there is an increase in the resistance at nominal strains <40% with the number of cycles despite the mechanical response to the strains being similar. This change in the electronic properties of the prints at low strains suggests a change to the microstructure of the carbon print bought about at strains up to 100% which isn't fully recovered once the stress is removed. The electronic properties are still recovering, indicated by a decrease in the change in resistance, before the strain is increased to 40% nominal strain, therefore whether these properties would recover with a longer time.

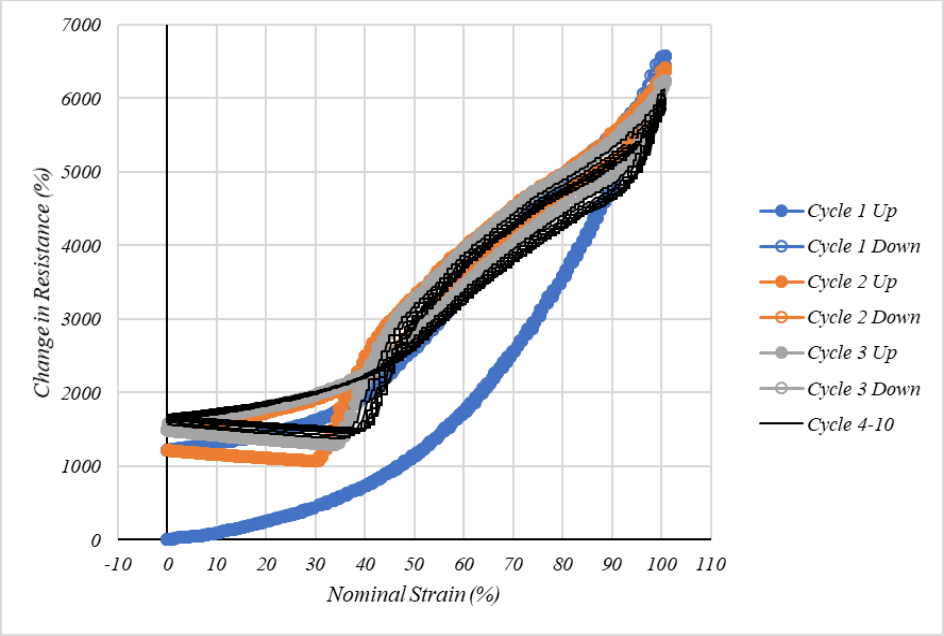

Figure 6.2.4.16 The effect of cyclic straining to 100% nominal strain on the electrical resistance of carbon prints on a TPU substrate at 50mm/min

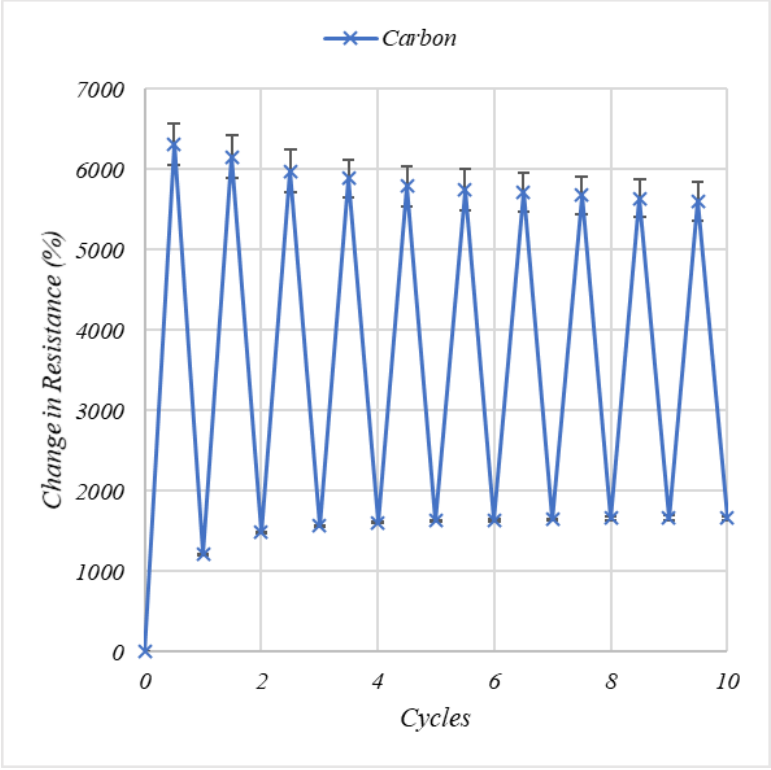

Fig 6.2.4.17 - The effect of cyclic strains to 100% on the change in resistance of the carbon ink. Error bars represent the standard deviation across 3 samples.

Strains locally during bending and compression can be very high, therefore a bend test was developed using 275N of force to compress a crease into the sample with the resistance change measured as displayed in Table 6.2.4.1. The printed side of the

sample was on the outside of the compression to maximise strains. This created a highly localised strain at the bend, with the remainder of the sample being relatively unaffected. During compression the resistance increased by 3.87% and following the removal of this compressive force the resistance of the sample instantly recovers to a 1.83% increased resistance. This permanent change in the resistance is likely a result of an increase in the electronic path length, visible as a crease in the sample.

Table 6.2.4.1) The effect of compressive loading on the resistance of the carbon ink

	Compressive Loading Force (N)	**Resistance (Ω)**	**Change in Resistance (%)**
Before	0	8476±150	0
Compression	-247±35	8809±150	3.87±0.06
Relaxation	0	8631±87	1.83±1.00

6.3 Utilising the Stretchable Inks in a Printed Stretchable Wearable Heater

6.3.1 Introduction

A heater was fabricated using the stretchable conductive inks characterised in Chapter 6.2 for use as a wearable heating device. This part of the chapter looks to initially characterise the temperature output of the heaters under different voltages to examine the power required to reach the 40°C required for passive heat maintenance. This chapter section then goes on to examine the temperature output of the heater under mechanical stresses including a maximum extension test, cyclic testing to 10% nominal strain and under compression.

Finally, the heater was built into a wearable proof-of-concept base-layer prototype in conjunction with the English Institute of Sport designed to help maintain the muscle temperature of Olympic Sprint Canoe athletes between sprint efforts while training on the water in winter. The performance of the heater in a 0°C cold chamber was examined to test the effectiveness of the garment.

6.3.2 Results

The heater consists of two stretchable silver busbars running parallel at either end of the heater, with connections at opposing corners to ensure consistent current flow through the stretchable conductive carbon coating (Fig 6.3.2.1a) to generates heat through electrical Joule Heating (Equation 6.3.2.1);

$$P = \frac{V^2}{R}$$

Equation 6.3.2.1. Joule Heating

The printed heaters had a total coating thickness of >21.29±0.39um with a total heater thickness including the 80um substrate of <125um. The two-point resistance of the printed heaters was 26.2±1.59Ω. Voltages between 10-20V were used to examine the temperature output of the printed heaters to replicate the low voltages that would be used in wearable heating applications.

a)

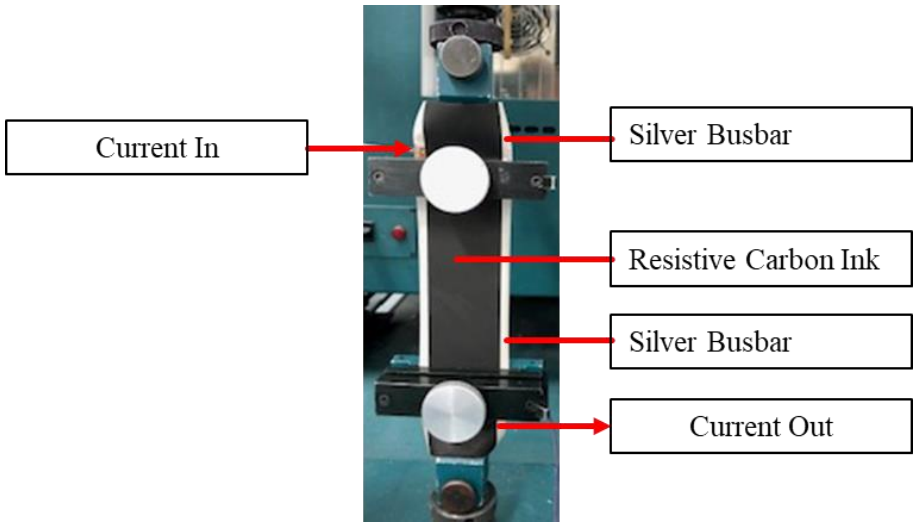

b)

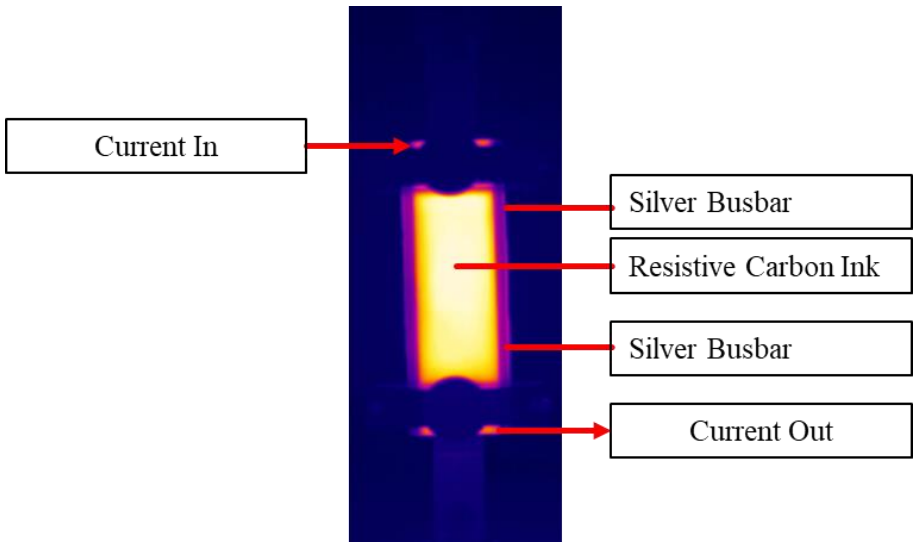

Figure 6.3.2.1 - Printed carbon heater a) Normal image, b) Thermal image

As the conductive silver coating is approximately three orders of magnitude more conductive than the carbon, this minimising the potential drop to ensure a near constant voltage across the heater. The heaters have excellent heat uniformity (Fig. 6.3.2.1b) with the current flowing evenly through the conductive carbon coating to give uniform heating across the 15x4cm carbon heater area. Chapter 6.2.3 demonstrated that screen-printing two-layer carbon ink produced a smooth surface with low average roughness of 0.82um and consistent thickness ensures that there is consistent resistance across the whole carbon layer coating leading to uniform current flow and therefore uniformity of temperature output across the carbon layer.

In agreement with the Joule heating principle, the maximum temperature achieved and the rate of increase in temperature is dependent on the applied voltage, and therefore the power of the heaters, with higher power leading to higher temperatures (Fig. 6.3.2.2). The heaters show a fast response to the application of power with heaters rapidly increasing in temperature up to a plateau value after 60s. This plateau is associated as the point where the power input into the heater is in equilibrium with the heat loss to the environment through conduction and convection. They also cool down equally quickly upon the removal of power. A power supply set at 15V was selected for further testing as it provides the most applicable temperature for wearable heating applications.

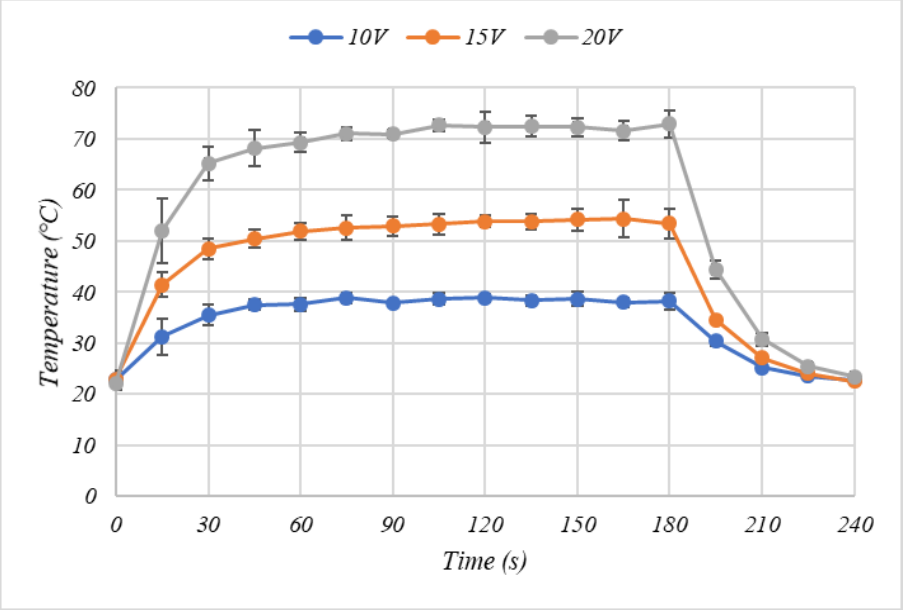

Figure 6.3.2.2 - The effect of applied voltage on the heat response of the printed carbon heaters. Error bars represent the standard deviation across 3 samples.

Upon the application of strain to 10% the temperature of the heaters decreases by 7.48°C from 58.42°C to 50.94°C (Fig. 6.3.2.3). The heaters continue to show good heat uniformity (Fig 6.3.2.4b). As seen from the conductive ink testing, applying even a modest strain of 10% increases the resistance of the coatings by up to 100%, and according to Joule heating this increase in resistance will decrease the power of the heaters, and with it a decrease in the temperature. Increasing the strain further to 20% sees a further decrease in the temperature to 43.8°C as the resistance of the coating increases further. Even at 20% strain there is still uniform heat distribution across the carbon coating however a 44.79°C hot spot begins to occur on the silver busbar as the relative resistance of the silver busbar increases at a faster rate than the rest of the heater, to create a mini-heater within the coating (Fig. 6.3.2.4c).

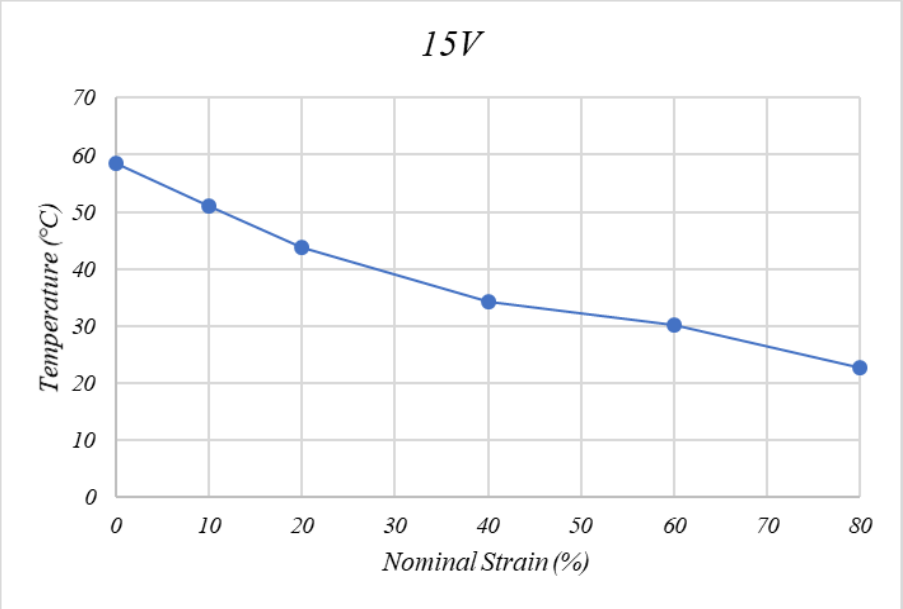

Figure 6.3.2.3 - The effect of nominal strain on the temperature output of the heaters

At 40% nominal strain the temperature of the heated carbon area drops further to 34.36°C while the temperature of the hot spot increases reaching 56.11°C as the silver busbar is damaged further (Fig 6.3.2.4d). At 80% nominal strain the increase in electrical resistance is sufficient to prevent the current flow and the heater returns to room temperature.

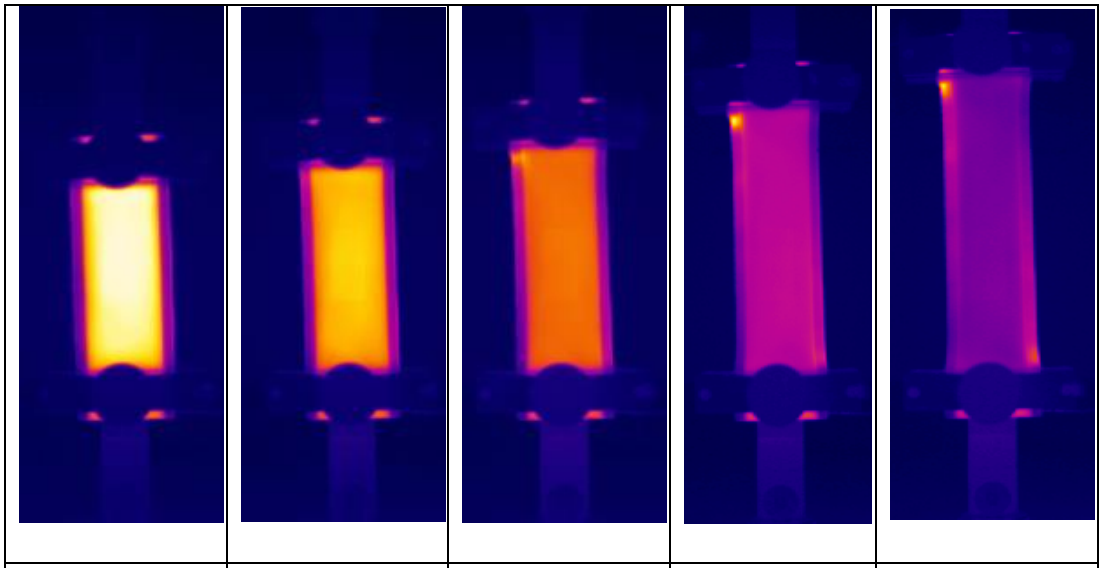

a) 0%	b) 10%	c) 20%	d) 40%	e) 60%

Figure 6.3.2.4 - The effect of nonimal strain on the uniformity of heat output

Cyclic testing of the prints in Chapter 6.2.4 showed that straining the prints to 10% nominal strain showed that the resistance of the inks increased 121.37 and 133.33% for the two-layer carbon and the silver prints respectively with permanent strains of 72.84% and 52.38% for the carbon and silver inks once the strain was removed.

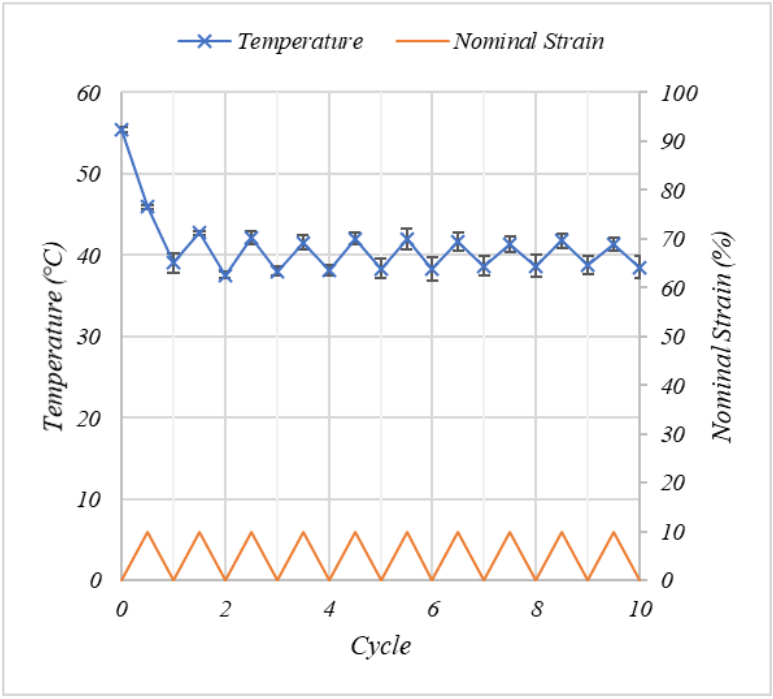

Figure 6.3.2.5 - The effect of cyclic straining to 10% nominal strain on heater performance. Error bars represent the standard deviation across 3 samples.

The resistance of the carbon inks then decreased further with the number of cycles to 10% nominal strain while in contrast the resistance of the silver inks continued to

increase at both 0 and 10% nominal strains. The increase in the resistance of both the carbon and silver ink is the likely cause of the decrease in the heat output of the heaters as at a constant heater voltage the heater power decreases. Following this initial deformation, the heaters show consistent temperature response to applied strain and can maintain a temperature of 40.09±1.73°C irrespective of strains up to 10%. This shows good agreement with the testing on the conductive inks where the response of the carbon ink was consistent when cyclically tested up to 100% nominal strain.

The heaters showed excellent heat uniformity even while creased (Fig. 6.3.2.6).

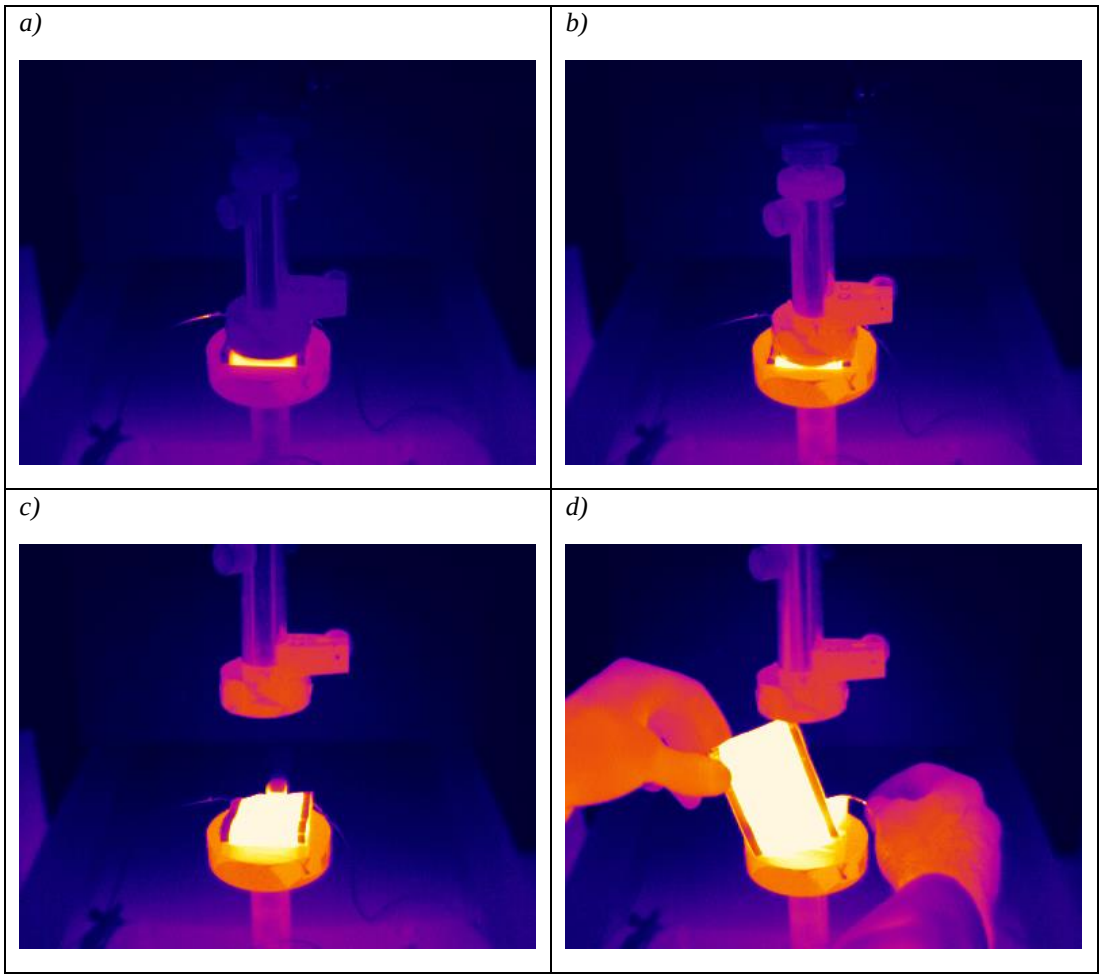

Figure 6.3.2.6 - The performance of the printed heater under a 20N compressive force. a) Before the compressive force is applied, b) Under 20N compressive force, c) 20N compressive force released, d) being flexed by hand

To test this one of the heaters was compressed with a 20N force using the Hounsfield mechanical tester. Before the compressive force was applied, the heater shows good uniformity even around the bent edge (Fig 6.3.2.6a). Then when the force is applied the heater continues to show good uniformity while also transferring heat to the

compressive loading platen (Fig 6.3.2.6b). Once the force is released the heater still shows good temperature output uniformity (Fig 6.3.2.6c) and continues to do so while being flexed by hand (Fig 6.3.2.6d). This heat uniformity even when bent is important in sports applications where the heaters would be expected to flex to conform to the muscles to achieve efficient conductive heat transfer through the fabric to the skin.

6.4 Development of Proof of Concept Heater for English Institute of Sport (EIS)

During training Sprint Canoe athletes often experience periods of inactivity on the water between sprint efforts, where body temperature can decrease and negatively affect performance, especially during winter training in the United Kingdom where temperatures can drop to below freezing. In conjunction with the Applied Sports Technology Exercise and Medicine (A-STEM) group at Swansea University and the Design Team at EIS a garment was designed using the printed heaters developed in this project to target key muscle groups.

As the garment was designed to be used in training, it was decided that the garment would be a close-fitting base-layer garment to improve heat transfer between the heaters and the athlete. This heated base-layer had to be lightweight and stretchable to minimise the impact on the athlete. As a multiple use garment, it had to be machine washable.

The heaters were screen-printed directly onto the stretchable TPU substrate using the 51-70 polyester mesh and the print settings described in the methods. The heater structure consisted of 3 layers of the GNP heater ink with 2 layers of silver used as the busbars. These heater panels were then heat pressed directly onto a stretchable Lycra base layer in the pattern described consisting of 4 20x5cm^2 panels to cover the back and shoulders and 6 10x5cm^2 panels to cover the biceps, triceps and pectorals (Fig. 6.4.1). Conventional wiring was then attached to the silver busbars of each heater using FFC/ FPC connectors (Amphenol ICC). The garment was split into two sides, left and right, with the heaters connected in parallel and with each side powered by an 11.1V Li-ion battery (Ansmann).

The electrical resistance of each side of the garment was 5.6Ω, therefore by applying the Joule heating law (Equation 6.4.1) each side of the garment produced 22.2W to give a total garment heating power of 44.4W. This is significantly higher than the

15W of the electrically heated and insulated trousers used in the study by Faulkner et al [10].

$$P = \frac{V^2}{R} = \frac{11.1^2}{5.6} = 22.2W$$

Equation 6.4.1 Joule Heating Law applied for one side of the heated garment

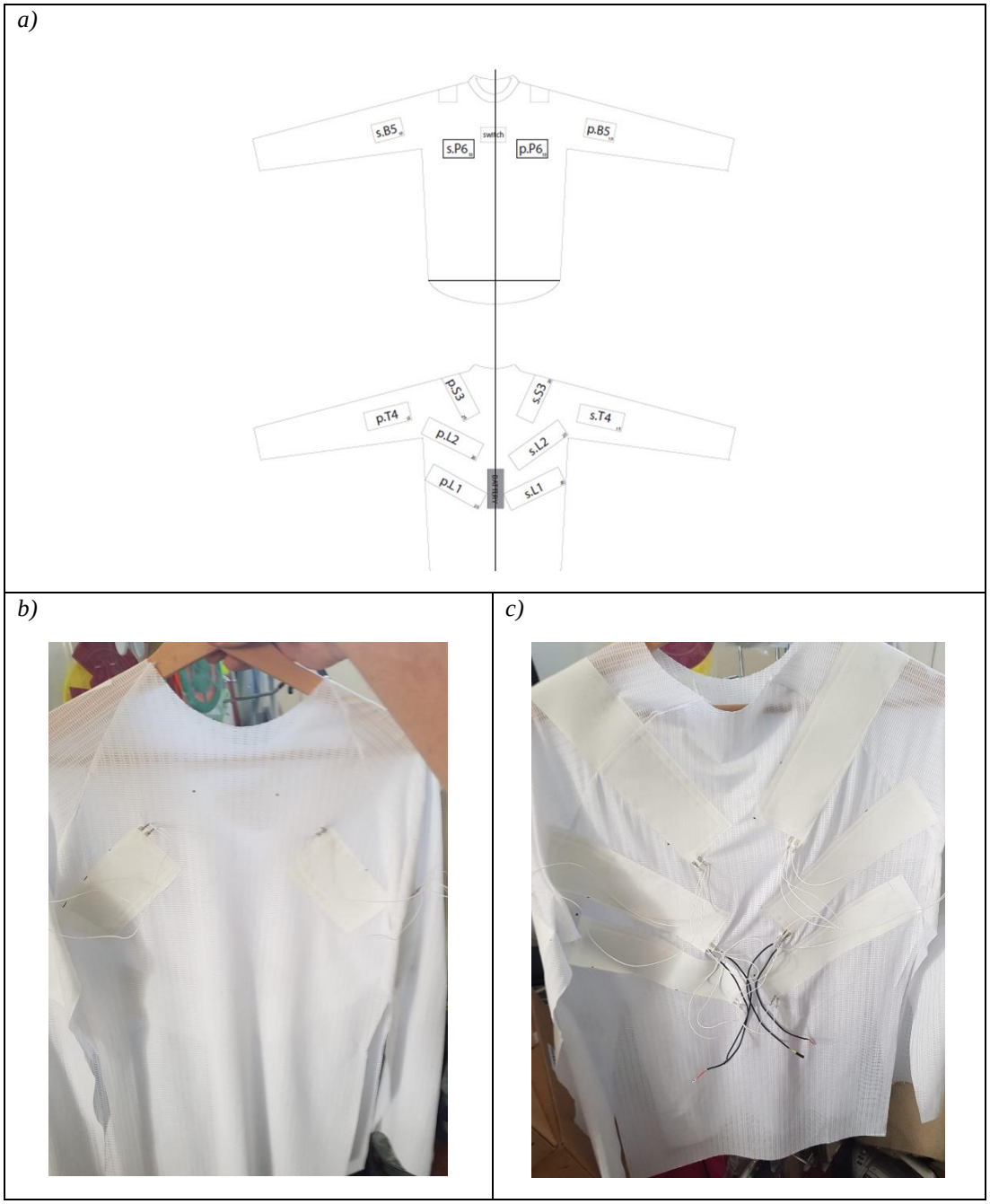

Figure 6.4.1 - a) The location of the heated panels on the garment designed to target identified important muscle groups for sprint canoe, b) The front of the test garment, c) the back of the test garment

Before on-athlete cold chamber testing a proof of concept garment was developed at the Welsh Centre for Printing and Coating (WCPC) using the above method. It was

found that even when attached to the stretchable Lycra base-layer the heaters still showed good heat uniformity and could reach temperatures in excess of 40°C as was specified in the EIS design brief.

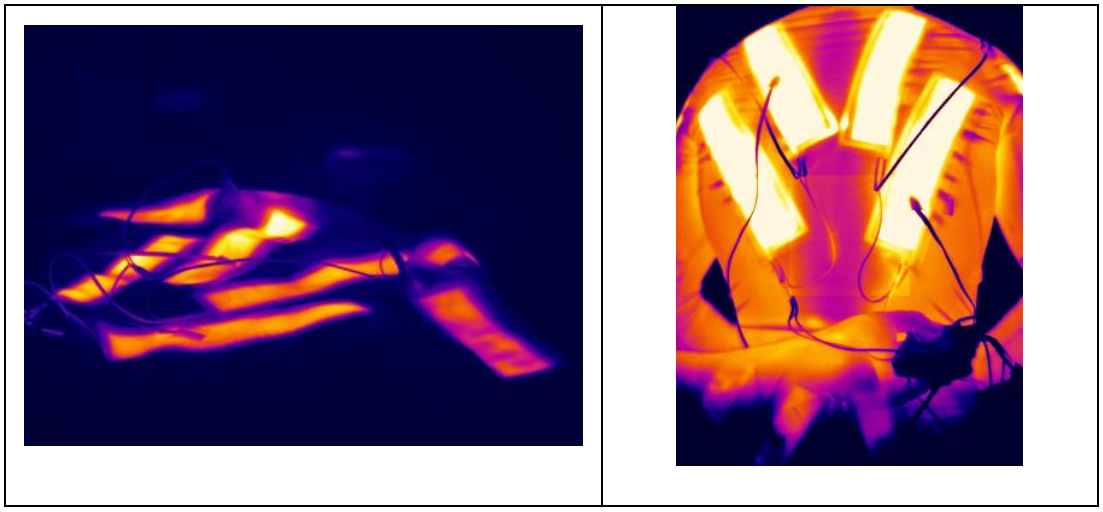

Figure 6.4.2 - Heat output of test garment for use in cold chamber testing

Cold chamber testing consisted of a former Olympic Gold Medal athlete performing two simulation sprint training sessions on an indoor ergonomic rower, in a 0°C environmental chamber at Nottingham Trent University (Fig. 6.4.3a), one wearing the garment with the heaters switched off and another wearing the garment with the heaters switched on (Fig. 6.4.3b).

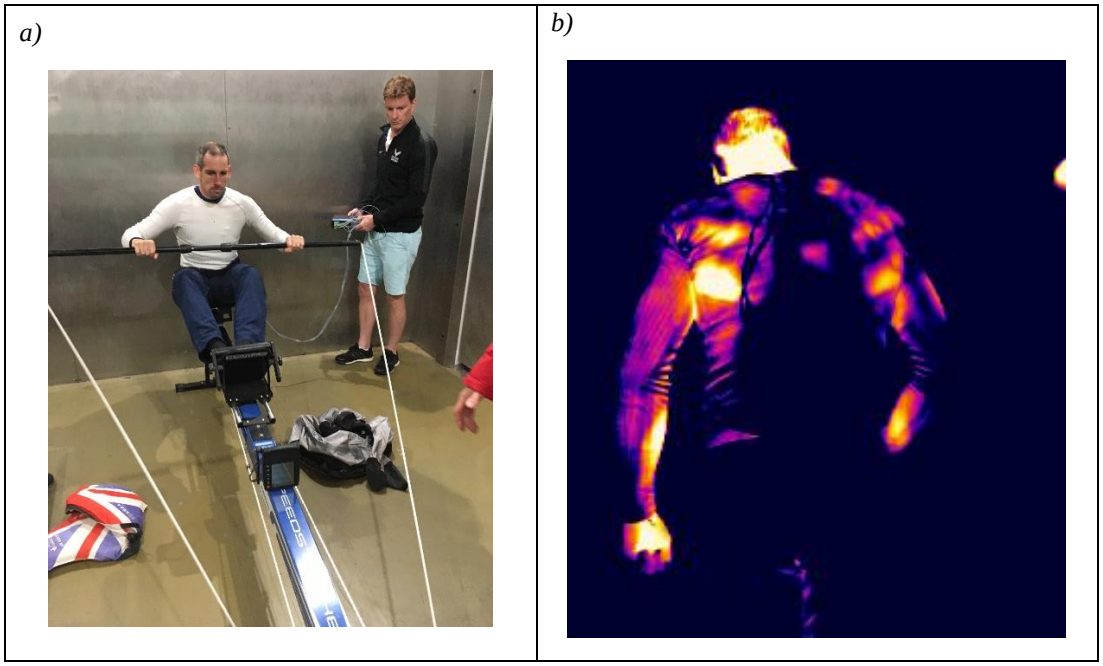

Figure 6.4.3 - a) Olympic athlete in the environmental chamber b) Thermal image showing the heated panels under the insulation within the environmental chamber

The athlete wore an extra base-layer on top of the heated garment as extra insulation.

The session consisted of a 15minute warm up, 15-minute rest period followed by 3 sets of sprint intervals. The changes to the skin temperature during the trial was monitored with the heaters switched off and with the heaters switched on for the Latissimus Dorsi (Fig. 6.4.4a), Triceps (Fig. 6.4.4b), Pectoral (Fig. 6.4.4c) and Abdominals (Fig. 6.4.4d). Despite skin temperature being higher in the non-heated garment following the warm up (WU6), during and following the rest period the skin temperature is significantly higher in the heated garments as the printed heaters help to reduce heat losses to the environment to better maintain the body temperature gained during the warm up.

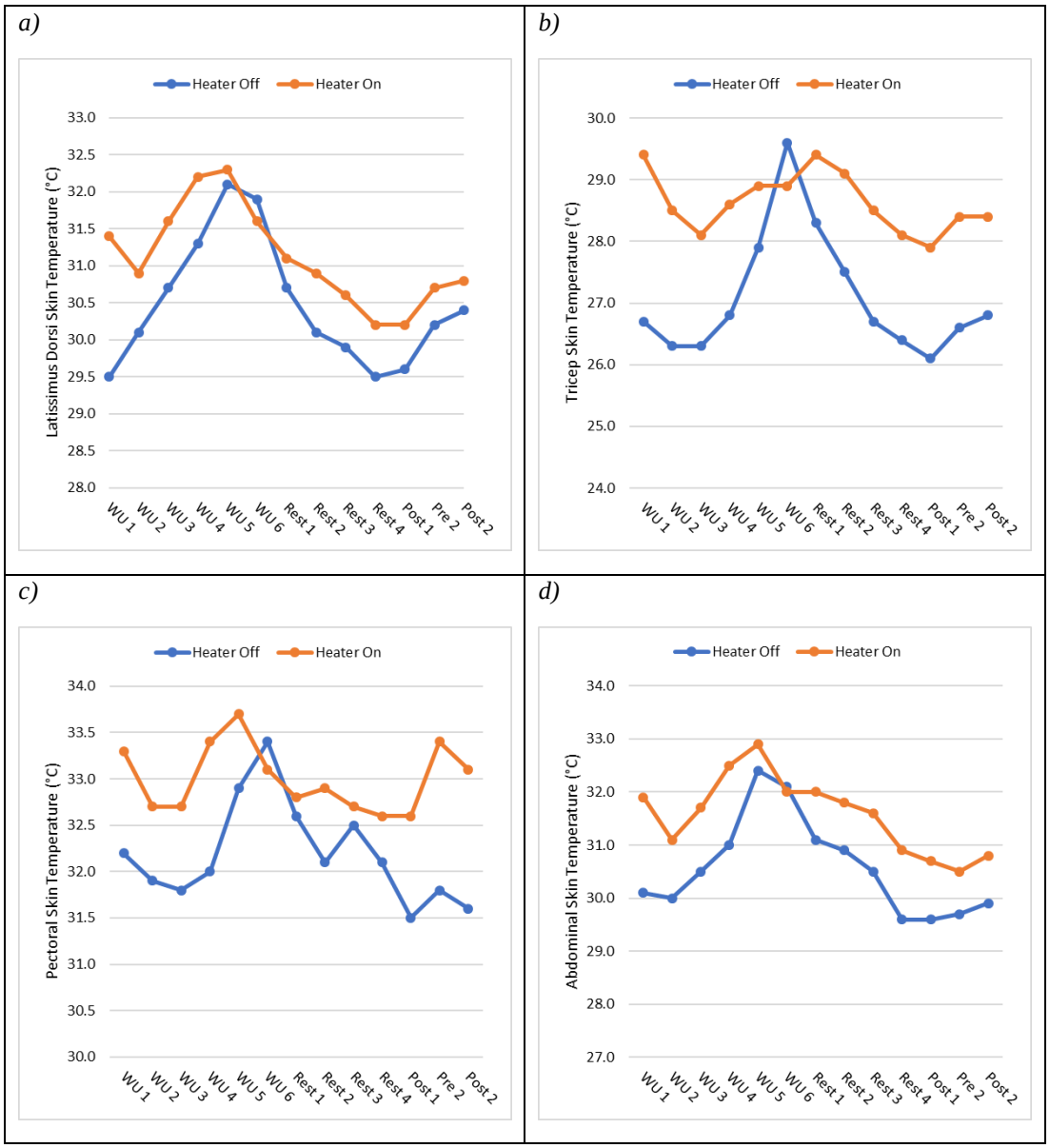

Figure 6.4.4 - Changes to the measured skin temperature (°C) over the warm-up (WU) 15-minute rest period (Rest) and before (Pre) and After (Post) the first two sprint efforts for the a) Latissimus Dorsi, b) Triceps, c) Pectorals, d) Abdominals

This performance is especially impressive given the environmental conditions in which testing took place.

This can be seen more clearly in the change in the athlete's skin temperature between the end of the warm-up and the end of the rest period (Figure 6.4.5). Turning the printed heater panels on reduced losses in the muscle temperature during the 15-minute rest period for all the measured skin temperatures with the benefits greatest in the Tricep, Latissimus Dorsi and Abdominal measure areas where the use of the printed heaters reduced losses in skin temperature by >1°C.

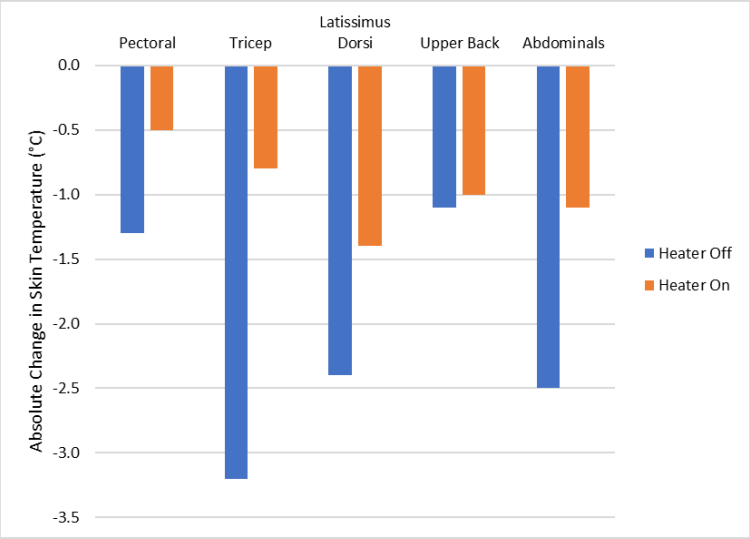

Figure 6.4.5 Absolute change in the athlete's skin temperature between the end of the warm-up and the end of the 15-minute rest period in a cold chamber set to 0°C

The athlete's perception of warmth was also measured throughout the trial on a scale of -4 to 4, with -4 indicating the athlete is feeling cold and 4 indicating the athlete is feeling warm with the results shown in Figure 6.4.6. In line with the skin temperature measurements the athlete felt warmer following the warm-up when the heaters were switched on, again with this most significant during the 15-minute period of inactivity during the warm-up.

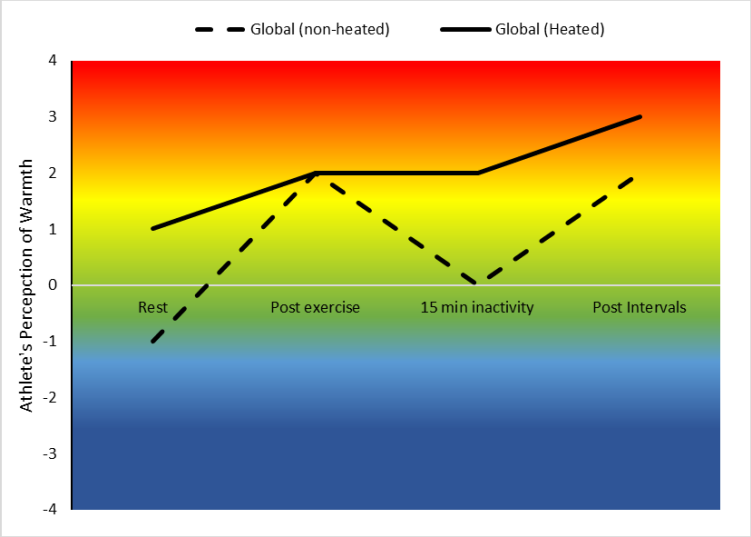

Figure 6.4.6 - Athlete's perception of warmth during the cold chamber testing, with a value of -4 indicating the athlete was feeling cold and a value of 4 indicating the athlete was feeling warm

6.5 Optimisation and in-use testing of EIS garments

Following the success of the cold chamber trial the design was optimised to focus on heating the lateral muscles that are key in sprint canoe and to reduce the heated area and therefore, the required power supply size, to create a more lightweight garment

The substrate was changed from the soft TPU to a more rigid PET/TPU substrate, allowing the heaters to still flex and bend but increasing the force required to exert large strains. This was done to allow printed wires to be used to connect the heated panels and therefore reduce the amount of conventional wiring and the number of connections from the printed electronics to the conventional electronics to improve the wear-ability of the garments.

Changing to a different substrate can affect the properties of the coated layer as it affects adhesion and the inks film forming ability. Changing from the TPU to the PET/TPU substrate had negligible effect on the sheet resistance of the coatings with the sheet resistance on the PET/TPU and the TPU substrates 226±4 and 230±12 respectively. To confirm the required voltage to reach the 40°C required in passive heat maintenance devices the heat output of the printed heaters with two carbon layers and two silver layers was measured at voltages between 6 and 15V after 150s (Fig. 6.5.1). As joule resistive heating elements, the temperature output increased with increasing voltage from a minimum of 32.07°C at 6V to a maximum of 69.95°C at 15V. Voltages greater than 9V could achieve temperatures in excess of 42.26°C. All the heaters showed excellent heat uniformity across the surface of the heaters.

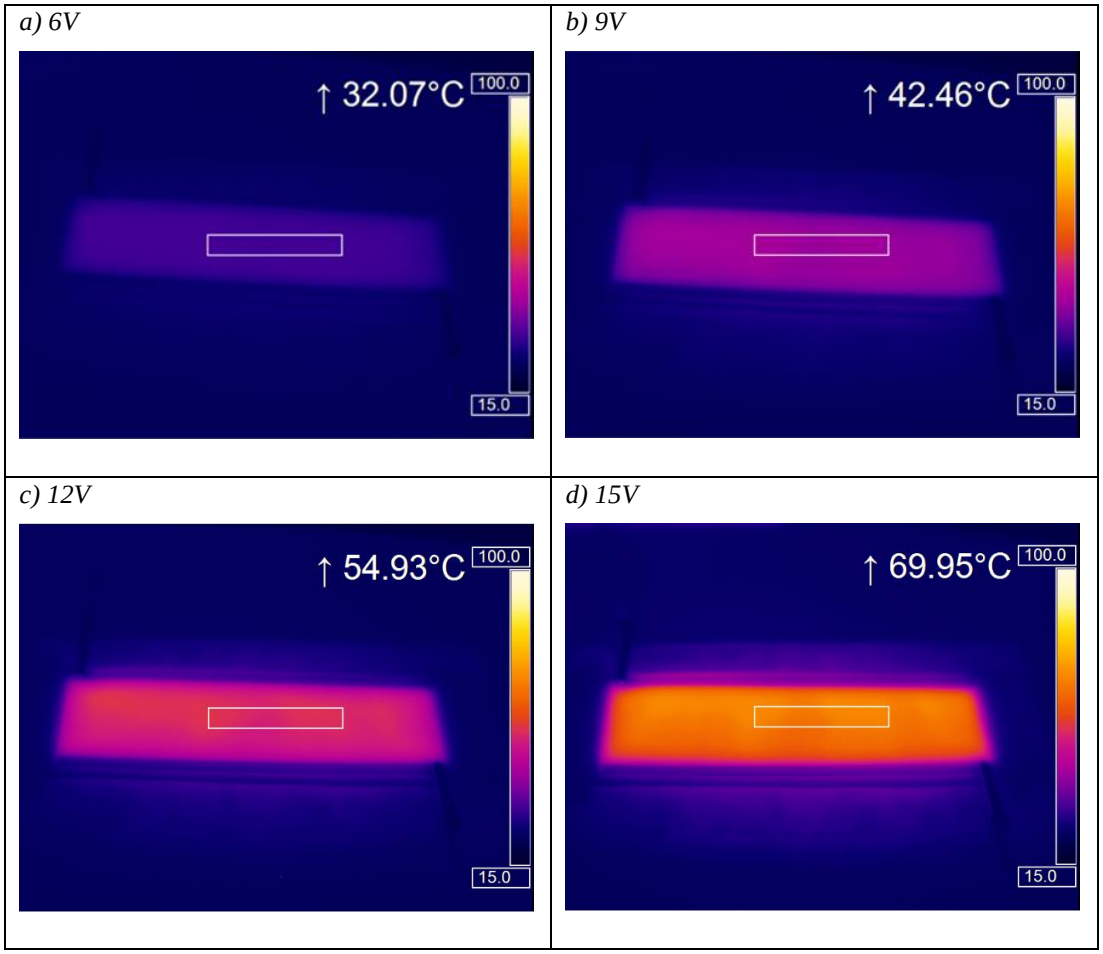

Figure 6.5.1 - The effect of voltage on the temperature of a two-layer carbon, two-layer silver heater after 150s

The power, and therefore the temperature output, of electrical heating devices is inversely proportional to the resistance of the heater. The resistance of a composite print is a function of the print thickness and the print uniformity, as well as the material properties of the coating, and therefore, the resistance of the heater can be controlled by varying the number of printed layers, and hence the printed thickness, of the heat generating carbon resistive layer. The effect of the number of printed layers of carbon on the resistance, temperature and heat uniformity at 12V can be seen in Figure 6.5.2. The resistance across the carbon and the corner to corner resistance is identical at 66.6Ω as the significantly more conductive silver busbar is minimises voltage drop across the heater. Printing a second layer of carbon decreased the sheet resistance of the carbon prints from 226 to 97Ω/□. This halved the resistance across the carbon layer by more than half from 66.6 to 30Ω. This was associated with the temperature output of the two-layer carbon heater at 150s at 50.42°C being 12.81°C hotter than the 37.61°C achieved by the single layer carbon

print. Printing a second layer of carbon also decreased the variance between heaters leading to a more consistent temperature output across the three heaters. Therefore, printing a second layer of ink could be useful in reducing print variance.

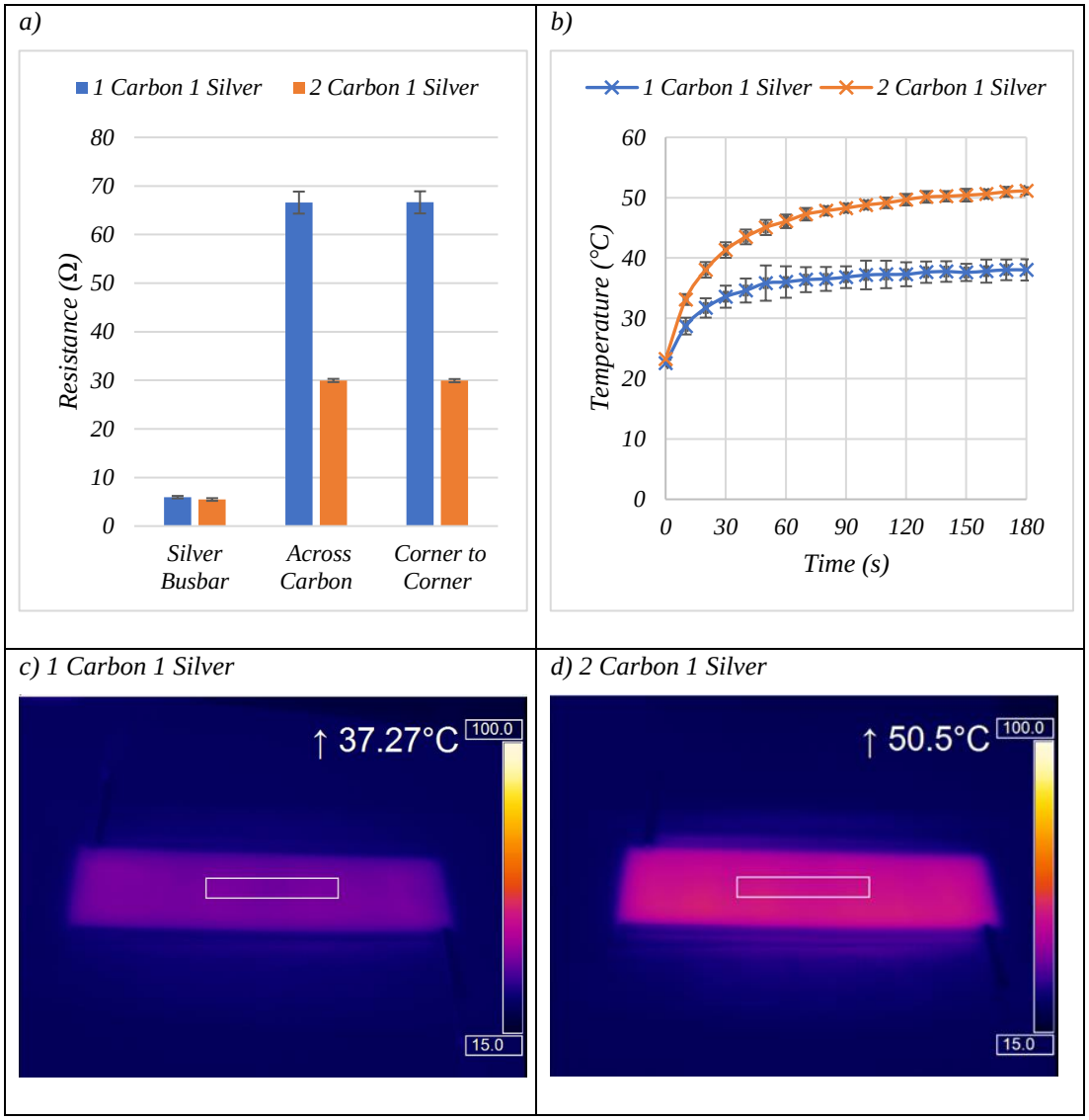

Figure 6.5.2 - The effect of printing a second carbon on a) The resistance of the heaters, b) the temperature time response at 12V. The temperature output of c) one-layer carbon, d) 2- layer carbon at 12V after 150s

Decreasing the distance between the two silver busbars, will decrease the resistance of the heaters and therefore, increase their power. The effect of halving the path length between the two silver busbars can be seen in Figure 6.5.3. Halving the path length approximately halved the resistance across the heaters from 30 to 15.5Ω. This was associated with an increase in heater temperature of 48.5°C to 98.9°C at 150s and 12V. This large increase in temperature can be associated with halving the resistance, and therefore doubling the heater power, while, as the carbon is the only

area that heats up, by decreasing the path length the heated area also halves, increasing the watts/cm^2.

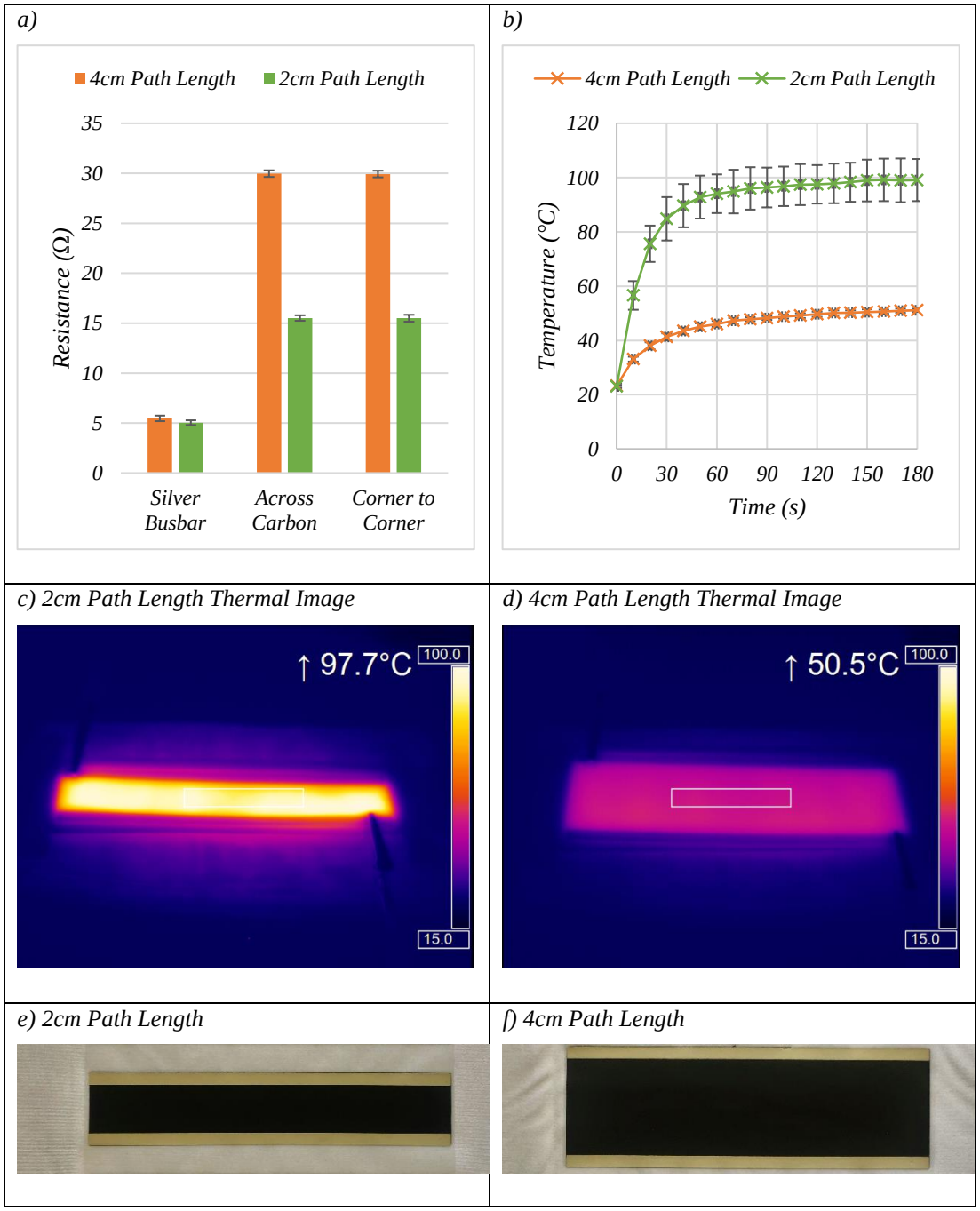

Figure 6.5.3 – The effect of reducing the heater path length on a) Resistance of the heaters, b) temperature-time response. Thermal images of the c) 2cm path length, d) 4cm path length heaters at 12V after 150s. Photographs of, e) 2cm path length heater, f) 4cm path length heater

The silver busbar is required to reduce voltage drop across the heater to ensure a constant current flow through the resistive carbon ink. To do this the silver is required to be more conductive than the carbon. The effect of printing a second layer of silver for the busbar can be seen in Figure 6.5.4. Printing a second silver layer for

the busbar, more than halved the resistance along the busbar, reducing the resistance from 5.5 to 1.6Ω, however, this resulted in only a moderate decrease in the resistance across the heater from 30 to 26.1Ω. This decreases in resistance across the heater panel resulted in a 2.5°C higher output temperature of 52.9°C for the 2 layer silver prints, however, given the high cost associated with silver ink and the additional time costs of printing a second layer of silver ink printing a single layer of carbon ink may be a more prudent option.

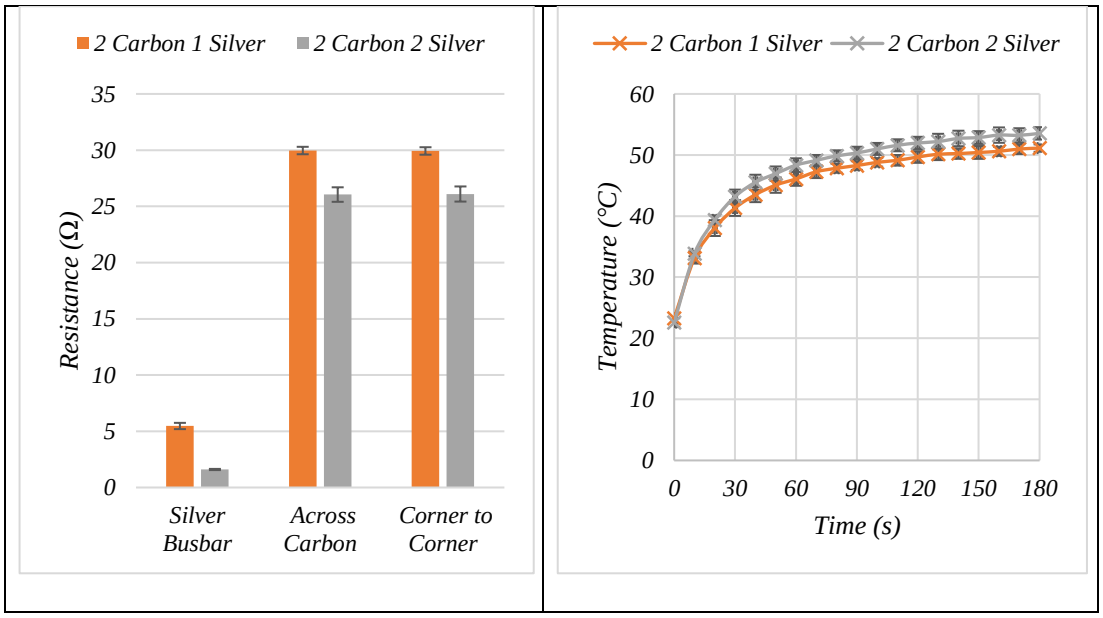

Figure 6.5.4 – The effect of printing a second layer of silver on the busbar on a) the resistance of the heaters, b) the temperature-time response of the heaters at 12V

Following the optimisation of the structure of the printed heaters, a design constructed of six 15x5cm heater panels connected by printed wiring, targeted to heat the latissimus dorsi muscle groups was developed. For this the two-layer carbon, two-layer silver construction was printed onto the TPU/PET substrate to achieve >40°C from a single 14.8V li-ion battery. Despite only having a small effect on the temperature output of the printed heaters, two-layers of silvers was used to minimise the voltage drop in the wiring connecting the heaters. Although all voltages >9V could achieve >40°C in a thermo-neutral environment a 14.8V battery combined with control electronics designed to maintain heater temperature at 40°C was used in the final heated garments. This was done to ensure that the heaters had the capacity to reach 40°C even in cold environments where losses to the environment would be expected to be greater.

As the heated garments were to be used during on-water training the garments had to be water resistant. To test the water resistance of the heaters, the resistance of the heaters was measured, then the heaters were submerged in water for two minutes, before their resistance was measured once more. The printed heaters on both the TPU and the TPU/PET substrate showed negligible changes in resistance following two minutes submersion. The batteries and control electronics had to be encapsulated within custom casings to ensure they were waterproof and shockproof enough to enable them to be used during training on water.

As the heaters to be used on a base-layer that would be worn next to the skin during training it was imperative for athlete hygiene that the garments could be machine washed. To test the wash resistance of the heaters, both the TPU and TPU/PET heaters were passed through a domestic washing machine 5 times before being air dried, with their electrical resistance compared before and after washing. Once more the TPU and the TPU/PET showed negligible change in their resistance following machine washing.

Having verified the benefits of the printed wearable heater and optimised the structure of the printed heaters the heaters were ironed onto a stretchable base-layer fabric with V1 prototypes sent out for in-use testing for 2018-2019 winter training. These garments survived the full winter training season, including machine washing, with the athlete's giving positive feedback on the garment's benefits.

Following this minor optimisation was made to the garments to create a V2 prototype. These garments were independently wash tested at Manchester University, with the garments surviving 15 washes, with their performance verified using a thermal imaging camera. Thirty V2 garments were then delivered to the sport and used during the 2019-2020 winter training season in preparation for the Tokyo Olympic Games (Fig. 6.5.5).

a)

b)

c)

Figure 6.5.5 – Photographs of the final V2 prototype upper body heated garment. a) Front view, b) Rear View, c) Garment and electronics

6.6 Closure

The performance of stretchable screen-printed silver and carbon inks has been tested. The carbon ink showed good printability with surface roughness's <0.8um, whereas the Silver Flake coatings had increased surface roughness due to the larger particle size and the topographical features of the print arising from higher ink viscosity. Despite having higher surface roughness, the silver flake coatings were significantly more electrically conductive owing to the superior bulk electrical properties of silver compared to carbon.

The mechanical properties of the coated samples were dominated by the substrate as a result of the substrates substantially higher thickness, 80um, compared to the thickness of the prints, 8um. The GNP/CB coatings maintained electrical conductivity until sample break at approximately 300% nominal strain whereas the Silver flake coating lost electrical conductivity at around 150% despite the sample being stretched to 300% before break. The GNP/CB ink consists of the larger more conductive GNP flakes dispersed in a CB/TPU matrix. When this matrix is strained although the larger GNP flakes are pulled further apart a less conductive path is still available through the CB/TPU matrix, enabling the current to continue to pass through the matrix despite large strains. In contrast at strains >100% the relatively large conductive silver flakes are pulled sufficiently far apart that they no longer are in direct contact and an electrical pathway is lost.

During cyclic strain testing to 10% after an initial permanent deformation during the first strain the GNP/CB coatings showed repeated electrical response to applied strain, whereas the resistance of the silver ink increased with every cycle as the sample continued to undertake permanent damage. Straining the coatings to 10% nominal strain produced permanent plastic deformation as the conductive traces, as 10% nominal strain is outside of the elastic region of the substrate causing a permanent increase in the electrical path length, and therefore the resistance. Therefore, the mechanical response of the substrate and characterising its elastic regions is a critical design consideration to produce truly elastic stretchable printed electronics. Following this initial deformation, the GNP/CB coating can be repeatedly deformed up to 10% nominal strain with consistent electrical response as the particles and polymer are aligned to the direction of strain and stretching within this region provide no further damage to the substrate. This repeated electrical response to strain performance was shown up to 100% nominal strain. The silver coatings displayed increased electrical resistance with increasing number of cycles as the coating underwent permanent deformation with every strain as the particles moved to new equilibrium positions, further away from one another, reducing direct particle contact and increasing the electrical resistance. The GNP/CB coatings showed less than 5% increase in electrical resistance under a compressive strain of 250N, showing good resistance to compression and creasing, making them a

promising material for use in electrically conductive coatings for wearable technology.

Printing a second layer of carbon decreased the resistance of the coating by >50%. Both single and double-layer GNP/CB coatings showed a similar electrical response to both cyclic and maximal strains demonstrating that there is good interaction between the two layers and therefore the double layer coating acts as a single composite layer of greater thickness. At the highest maximal strains of greater than 150% the two-layer carbon showed less sensitivity to strain as the thicker print gave more potential conductive networks for the current to pass through. This suggests that printing multiple layers is a good way to enhance the electrical conductivity of intrinsically stretchable printed structures making it a promising method for incorporating less conductive carbon-based inks into stretchable applications where higher electrical conductivity is required.

A large area GNP/CB/TPU heater with excellent heat uniformity, capable of reaching up to 50°C in within 45 seconds of voltage being applied, was manufactured using established screen-printing techniques before being pressed onto a stretchable fabric and its performance measured under strain. The temperature response of the heater was studied under applied nominal strains. The heater continued to show good heat uniformity up to 20% nominal strain, however beyond this point a hot spot became increasingly developed within the silver busbar as the applied strain caused large local increases in the resistance of the silver ink to create a high-power low area mini heater. The cyclic performance of the heater to 10% nominal strain was tested with the heater capable of maintaining temperatures of 40.09±1.73°C over a 10% strain range. The heaters showed uniform heat output even while under compression. This study suggests that GNP/CB /TPU are a promising candidate for wearable heating applications.

The printed heaters were built into a stretchable base-layer garment to be used during training in cold environments. The ability of the heaters to maintain muscle temperature was evaluated during a simulated training session inside a 0°C environmental chamber and compared to a non-heated control. The heated garment better maintained muscle temperature and gave the athlete higher perceptions of warmth than the unheated control. Prototype garments were developed from this test

in collaboration with English Institute of Sports for 2018/2019 and 2019/2020 winter training for the canoe team in preparation for the Olympic games in Tokyo 2020.

6.6 References

[1] J. Suikkola, T. Bjorninen, M. Mosallaei, T. Kankkunen, P. Iso-Ketola, L. Ukkonen, J. Vanhal and M. Mantysalo, "Screen-Printing Fabrication and Characterisation of Stretchable Electronics," *Scientific Reports,* vol. 6, pp. 1-8, 2016.

[2] T. Araki and Nogi, "Printable and Stretchable Conductive Wirings Comprising Silver Flakes and Elastomers," *IEEE Electron Device Letters,* vol. 32, no. 10, pp. 1424-1426, 2011.

[3] Z. Fan, C. Zheng, T. Wei, Y. Zhang and G. Luo, "Effect of Carbon Black on the electrical property of Graphite Nanoplatelet/Epoxy resin composites," *Polymer Engineering and Science,* pp. 2041-2045, 2009.

[4] H. Oxfall, G. Ariu, T. Gkourmpis, R. Rychwalski and M. Rigdahl, "Effect of carbon black on the electrical and rheological properties of graphite nanoplatelets/ poly(ethyl-butyl-acrylate) composites," *eXPRESS Polymer Letters,* vol. 9, no. 1, pp. 66-76, 2015.

[5] C. Phillips, A. Al-Ahmadi, S.-J. Potts, T. Claypole and D. Deganello, "The effect of graphite and carbon black ratios on conductive ink performance," *Journal of Materials Science,* vol. 52, pp. 9520-9530, 2017.

[6] Poli-Tape, "Poli-Tape ultimate print soft 4030 matt datasheet," Poli-Tape, 2019. [Online]. Available: https://www.politape.us/wp-content/uploads/2019/01/TD_ULTIMATE_PRINT_SOFT_4030_MATT_us.pdf. [Accessed 31 01 2020].

[7] E. Jewell, S. Hamblyn, T. Claypole and D. Gethin, "The impact of carbon content and mesh on the characteristics of screen printed structures," *Circuit World,* vol. 39, no. 1, pp. 13-21, 2013.

[8] B. Phillip, E. Jewell, P. Greenwood and C. Weirman, "Material and process optimization screen-printing carbon graphite pastes for mass production of heating elements," *Jornal of Manufacturing Processes,* vol. 22, pp. 185-191, 2016.

[9] W. Dang, V. Vinciguerra, L. Lorenzelli and R. Dahiya, "Printable Stretchable Interconnects," *Flexible and Printed Electronics* , vol. 2, 2017.

[10] S. Faulkner, R. Ferguson, S. Hodder and G. Havenith, "External muscle heating during warm-up does not provide added performance benefit above external heating in the recovery period alone," *Eur J Appl Physio,* pp. 2713-2721, 2013b.

[11] H. K. Park, S. M. Kim, J. S. Lee, J.-H. Park, Y.-k. Hong, C. H. Hong, Kim and K. Kang, "Flexible plane heater: Graphite and carbon nanotube hybrid composite heater," *Synthetuc Metals,* vol. 203, pp. 127-134, 2015.

[12] L. Pahalagedara, I. Siriwardane, N. Tissera, R. Wijesena and N. d. Silva, "Carbon black functionalised stretchable conductive fabrics for wearable heating applications," *RSC Advances,* vol. 7, pp. 19174-19180, 2017.

Chapter 7: Conclusions and Future Work

7.1 Conclusions

A plasma functionalised GNP enabled flexible printed heater has been developed to maintain muscles temperature for elite athletes and hence provide a competitive advantage. The heaters have to be attached to soft, stretchable substrates to allow them to conform to the body to maximise heat transfer whilst minimising disruption to athletic effort. The heat output had to remain uniform even while being flexed and stretched. This required the development of improved flexible and stretchable conductive inks.

There has been limited previous studies on conductive inks of the effect of:

- high concentrations GNPs on the rheological, electrical and print properties
- plasma functionalisation on the performance
- hybridizing GNPs with CB on the rheology and print performance

All of which are key to understanding the impact of formulation on the ink performance. The following are the key findings from the investigations.

The effect of up to 30wt% ($\phi=0.157$) of GNP concentration on the shear and viscoelastic properties of a low viscosity TPU resin/solvent system was studied. The work modelled the effect of the Nanoscale, high aspect ratio GNPs using established suspension rheology methods. From this, values for the intrinsic viscosity ($[\eta]$) and maximum packing fraction (ϕ_m) of GNPs were derived and used to gain insight into the morphology of GNPs in the low viscosity suspension. This novel modelling of GNPs could be used in the future formulation of inks containing GNPs as a component to predict their effect on the rheology of the inks. As the work aimed to create a highly, conductive stretchable carbon ink the effect of GNP concentration on the electrical conductivity and print thickness and topography was studied.

The effect of Ammonia plasma functionalisation (NH_3 GNP) on the rheological properties, print performance and time stability of GNP inks was compared to that of an un-functionalised control (R1 GNP). The print and rheological properties of both the NH_3 and R1 GNPs were similar following initial dispersion, suggesting the particles were of a similar size, shape and morphology. The viscosity and elastic modulus, *G'*, of the R1 GNP inks decreased in time, as the particles agglomerated to

form particles of a new shape. These effects were exaggerated by concentration suggesting that this decreases in concentration was related to a particle effect. Ammonia (NH_3) plasma functionalisation was identified as an optimal plasma functionalisation to improve the suspension stability as the NH_3 GNP suspensions showed consistent rheological properties over a 12-week period suggesting that particles maintained their, size, shape and morphology.

Even at 30wt% the bulk resistivity of the GNP only coatings, 2.95Ω·cm, sheet resistance 2660 Ω/□, was too high to be used in wearable heating applications. The effect of hybridising GNP with Carbon Black (CB) on the rheological, electrical, print and electromechanical properties of a screen-printing ink was studied. The CB was shown to coat the surface of the GNPs and fill gaps between neighbouring GNPs to improve GNP-GNP contact. This created highly smooth coatings, with low electrical resistance. The addition of just 2.5wt% CB to a 15wt% GNP ink dramatically decreased the electrical resistance and surface roughness. At large concentrations CB a CB network formed in the fluid to form a dense 3D GNP-CB network, causing large increases in viscosity and elasticity that led to print defects as the ink couldn't relax during printing. Although the addition of CB can bring about decreases in the electrical resistance and surface roughness of coatings, the addition of CB also effects the processability of the fluids, therefore, when developing an ink a balance must be struck between the material properties and the processability. An optimum ink formulation of 15wt% GNP + 7.5wt% CB produced coatings with bulk resistivity 0.09 Ω·cm, sheet resistance 177 Ω/□, and average surface roughness 603nm.

As the devices were designed to be used in wearable applications, electromechanical testing of the optimum GNP/CB/TPU ink to be used as the resistive element of the heater, the silver flake/TPU ink to be used as busbars and the uncoated substrate was examined. The Carbon ink maintained electrical conductivity up to substrate break of 305% nominal strain, while the silver ink lost electrical conductivity at 166% nominal strain despite the substrate being extended to 346% nominal strain at break. After an initial increase in relative resistance of the carbon ink during the first cycle, the resistance change at 100% nominal strain decreased and became increasingly consistent as the conductive network became aligned with in the direction of the

strain. In contrast the resistance of the silver ink increased with number of cycles suggesting damage to the microstructure.

A heater consisting of the optimised GNP/CB/TPU ink was screen printed onto a stretchable TPU substrate and thermoformed to a stretchable lycra garment. The heater could reach uniform temperatures of >50°C from a 15V power supply, demonstrating that the GNP/CB/TPU coating was of high enough conductivity to be used in low voltage wearable heating applications. To conform to the body to give optimal fit and heat transfer, while minimising disruption to athletic technique, the garments should be able to stretch to 15-20%. Therefore, the performance of the heater under tensile strains was examined. The temperature output of the heaters decreased with increasing tensile strain as a result of the increasing electrical resistance of the printed heaters. The heater continued to show uniform heat output and temperature output of >40°C up to 20% strain. At nominal strains greater than 40% the resistance had increased locally on the silver busbar to create a hot spot, which disrupted the ability of the busbar to minimise voltage drop across the heater, causing large decreases in the temperature output and eventual heater failure. The heater showed good response to 10% cyclic nominal strains. After an initial decrease in temperature output during the first strain cycle, the heater could produce a consistent heat output of 40.09±1.73°C irrespective of strains up to 10%. Strains during compression can be very large, however, the printed heater showed good resistance to being creased and flexed, maintaining a consistent, uniform, heat output.

In conjunction with the English Institute of Sport a stretchable base-layer garment with printed heater panels was designed to be worn during on water training during winter for Olympic Sprint Canoe athletes. The viability of printed heaters as a passive heat maintenance device was assessed by comparing the performance of the printed heater garment versus a non-heated control during a simulated sprint canoe session, performed by an Olympic gold medal athlete in 0°C environmental chamber. The printed heater garment better maintained muscle temperature and the athlete's perception of warmth during a 15-minute post-warm-up recovery period than the unheated control. Following this the design was optimised, with 30 base-layer garments delivered to sprint canoe to be used during winter training 2019-2020 in preparation for Tokyo 2020.

7.2 Future Work

The GNP inks in this study were three-roll milled to break apart agglomerations to disperse the GNPs throughout the fluid. In this work the Krieger-Dougherty model was fitted to the experimental data to gain insight into the particle morphology, which may provide a method for assessing dispersion. By comparing the viscosity of both milled and un-milled GNP suspensions and fitting the Krieger-Dougherty model to the experimental data, the effect of three roll milling on dispersion could be studied. Comparing the fitting parameters to images of the surface of prints, would show whether fitting of with suspension rheology models could provide a potential method to assess dispersion without the need for printing.

The NH_3 GNPs were shown to be stable in a 4 Pa.s near-Newtonian TPU resin system even up to 25wt% NH_3 GNP. Repeating the study in a lower viscosity system, such as those used in flexography inks, where particle interactions and sedimentation effects would be expected to be greater, may further emphasize the benefits of plasma functionalisation.

Plasma functionalisation has the potential to functionalise smaller nanocarbons such as few layer graphene (FLG). Levels of surface functionalisation would be expected to be greater on these smaller particles, as there are a higher number of edges and defect sites to functionalise. However, the effects of particle interaction would be expected to be greater as interparticle distance reduces with particle size. The stabilisation and agglomeration effects described in Chapter 4 for GNPs would therefore be expected to be amplified with FLGs, therefore a similar study with FLGs would build on the conclusions of chapter 4.

The carbon ink showed improved electromechanical performance to the silver ink with these improvements hypothesised to be a consequence of the dense layered microstructure of the carbon compared to the lower volume of silver flakes. To further examine the effects of particle morphology on the electromechanical properties of conductive inks, a study comparing the rheological, print and electromechanical properties of different carbon including, graphite, GNPs, CB, FLGs and hybrids of these materials in the same TPU resin system should be performed. At a constant wt%, as the particles are all carbon materials of approximately the same density, they would be expected to have approximately

equal volumes in the final composite, allowing for comparison of the effect of particle morphology on the electromechanical properties.